NTN

Make the world **NAMERAKA**

TECHNICAL REVIEW
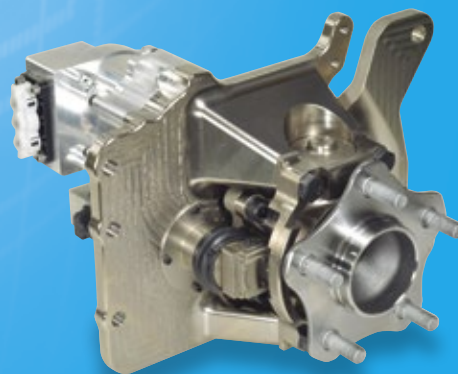
Completely Revised "Ball and Roller Bearings" Catalog

NTN has completely revised the "Ball and Roller Bearings" catalog that provides comprehensive coverage of technical explanations and our product lineup for roller bearings.

Roller bearings are used in various types of machinery and devices as an important machine element. Performance requirements are becoming increasingly sophisticated and diversified in terms of they need to have a long operating life, be compact, be lightweight, and support high speeds and specific environmental conditions. Particularly in recent years, there is a need for applicable technology that increases the performance of bearings as well as peripheral technology that includes bearings. **NTN** is working hard to help improve the overall performance of machinery by advancing development and improvements to respond to these needs.

The new ball and roller bearings catalog, which has now been completely revised, was edited to enable customers to select the best type and size of bearing based on technical content backed by the results of our development and improvements.

The main revised content is shown below.

○ The latest content for ISO and JIS standards are included, and general commentaries such as bearing selection, bearing periphery design, and handling have been substantially increased.

○ From the results of continuous improvements in material, product and production technology, the current bearing operating life is longer than previously published. Therefore, the basic dynamic load ratings have been revised and increased in many cases based on actual bearing performance data.

○ "ULTAGE" is the newest and highest performing **NTN** product line. Expanded ULTAGE product offerings can be found in the revised catalog which now features bearings newly added to the ULTAGE series in addition to the ones previously established.

We encourage you to use this revised "Ball and Roller Bearings" catalog, and hope that we can work and grow together with our customers "to realize a NAMERAKA society". Thank you for your continued support.
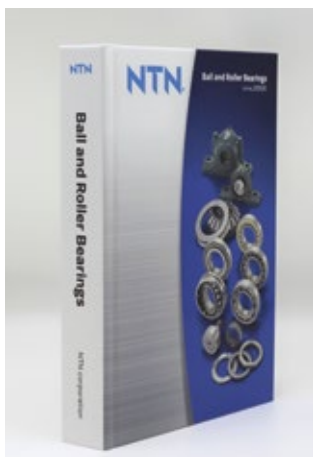
Ball and Roller Bearings catalog

The catalog is now easier to use with the addition of a stepped index on the edge of the page and bookmark strings

NTN

TECHNICAL REVIEW

NTN TECHNICAL REVIEW No.88

CONTENTS

The affiliations and titles of the authors mentioned in the text are as of March 2021.

For Industrial Machinery/Automotive Products, Fundamental Technology, and New Business Areas

Executive Officer, CTO (Chief Technology Officer)

Masaki EGAMI

NTN has been issuing the NTN Technical Review, which is a technical information magazine for the general public, every year in the fall. Over the past 15 years, we have featured automotive products and industrial machinery products alternately every other year, as aligned with the Tokyo Motor Show and Japan International Machine Tool Fair (JIMTOF). However, due to the global pandemic caused by COVID-19, many events which attract large groups of people such as the Olympics, have been put off or canceled; including JIMTOF 2020 where we had planned to participate as an exhibitor. As you are aware, tremendous efforts are being made to change the formats of these events to, for example, online exhibitions and webinars, to communicate new information to the public and prevent an economic slowdown.

We have a keen interest to provide information regarding new products and technologies, even under these circumstances, as much and as soon as possible to you. Therefore, we decided to publish our Technical Review No. 88 in a new format, not focusing on specific areas as we once did, but featuring the details of both industrial machinery products, which we exhibited in JIMTOF 2020 Online, and new automotive products, ahead of time, as a special issue of "Industry Machinery/Automotive Products, Fundamental Technology, and New Business Areas."

From the title you may have an impression that it is a mixture of everything, but we will introduce you to recent progress of rolling bearings and module products for wind turbines, rolling stock, robots and machine tools that we focus on in the industrial machinery area, and discuss the most recent technology of data analysis through sensing and AI algorithms, leveraging the biggest feature of rolling bearings, which is their ubiquitous nature of "being used in each and every product," as our initiative for advancing IoT. This includes achievements from the "NTN Next Generation Research Alliance Laboratory" established in Osaka University in September, 2017.

In the automotive area, one important challenge is how to deal with CASE, which is perceived as a "once-in-a-century transformation." Specifically, in this issue, we are introducing newly developed products such as: refined rolling bearings for a smaller and lighter form factor contributing to lower fuel consumption and drive shafts, module products which offer new functions and value, as well as the fundamental technologies of rolling bearings which preserve adequate bearing life with new lubricant with lower viscosity that the automotive manufacturers are developing to reduce fuel consumption.

It is always best to see the actual products because "seeing is believing," however, we hope this magazine will be helpful for you, under the current situation where a real exhibition is impossible due to COVID-19. NTN has been working on "DRIVE NTN 100," which is our mid-term management plan with the basic policy of accelerating business transformation for the next 100 years since April, 2018, when we celebrated our 100th year of foundation. We are starting a new mid-term management plan "DRIVE NTN 100" Phase 2 in April, 2021. We strive for further development of the industry as a whole, enhancing our R&D activities under our corporate philosophy:

"We shall contribute to international society through creating new technologies and developing new products (For New Technology Network: Networking the World with New Technology)."

The Past and Present of AI and Prospects in Manufacture

Ken-ichi FUKUI

Associate Professor Division of Information and Quantum Sciences/SANKEN (The Institute of Scientific and Industrial Research)/Osaka University

AI is now said to be in the third boom. In this article, the author first gives an overview of the history of AI up to the present Deep Learning. Next, Deep Learning, which is currently undergoing rapid development, focusing on the expansion of that area is introduced. Then, the author introduces new issues and hot topics arisen with the significant development of Deep Learning, such as ethical issues, explanations and safety issues. In addition, the problems of human resources for AI development with the expansion of application areas is discussed. Lastly, based on the above, the author will state the prospects of AI in the manufacturing industry.

1. Introduction

AI (Artificial intelligence) has been a topic of discussion in the general public and mass media since around 2015. In 2016, the AI software for the game of Go "AlphaGo," developed by Google DeepMind beat the top human Go player, which became a bit of a sensation at the time[1]. That software uses a technology called deep learning. While the excessive hype of media coverage has calmed down, today, AI is steadily making strides into various industrial sectors with expectation of increasing productivity.

2. History of AI: 3 booms and "winter times"[1]

2.1 What is an AI?

In general, AI is described as a research and technology field with the objective of realizing computer programs with the "ability to recognize the external world, learn from the experience, think with acquired knowledge and behave or have a conversation just as humans do." However, the exact definition of AI is controversial among researchers, because there is no clear answer to the fundamental question of "what is an intelligence?" In addition, "what is an AI?" changes over time, too. For example, in the late 1960s, when adoption of character recognition in commercial use started, automatic recognition for postal codes was called an AI.

Research of AI can be categorized broadly into two directions:

1) Engineering technology development to realize the intelligent processing functions in the computer
2) Research for gaining insight in human intelligent behavior and brain functions by realizing the intelligent processing function in the computer

What the public at large talks about and expects most is the AI of the above 1) Engineering achievement of intelligent functions. Among different areas of AI, deep learning has proven to achieve high accuracy especially in recognition and identification.

2.2 History of AI

(1) Dawn of AI (-1956)

When the world's first computer ENIAC was developed in 1946, research for a "machine to perform human intelligent activities" started. In this period, artificial neuron (mathematical model on transmission of electrical signal of nervous cells) was proposed by W. McCullouch and W. Pitts and a program playing chess was developed by C. Shannon and A. Turing. In 1956, the research area on computers performing intelligent activities was named "Artificial Intelligence" in the "Dartmouth Conference" organized by J. McCarthy and others.

(2) Search/reasoning: The first boom (1957-1960s)

It was an extraordinary accomplishment, during this period, that a computer could deal with even the slightest intelligent activity as it had only been able to do calculations before. At that time, AI was converting objects into explicit symbols, then used logic for search and reasoning. Automatic mathematical theorem proving was one of the research areas. However, in 1969, the "Frame Problem," the largest technical difficulty, was raised by J. McCarthy and J. Hayes. The frame problem describes an issue that a computer cannot deal with all the possibilities that potentially arise in real life since it only has limited information processing capability (actually, current deep learning has not fundamentally resolved the "Frame Problem," yet).

(3) Winter time ① (1970s)

It became clear that the approach of search and reasoning based on the symbols in the 60s was only effective in toy problems (toy problems such as a building block puzzle called Tower of Hanoi) with clear rules and small magnitude but not with real-life problems. One of the reasons was that the AI programs did not have knowledge of the objects and the second reason was that the computers were still not powerful enough to solve large-scale problems within a practical time frame. Therefore, the fervor of research was gradually diminished.

(4) Time of knowledge: The second boom (1980s)

During this period, researchers were focusing on handling real-life problems by incorporating knowledge of the objects into computers. They were called "expert systems" as they were dedicated systems for individual problems. Many commercial expert systems were developed. In Japan, with the leadership of the Ministry of International Trade and Industry (currently, Ministry of Economy, Trade and Industry) the fifth-generation computer development project (ICOT) started in 1982 with different development projects of expert systems and reasoning systems using symbols based on them.

The principal player of the second boom was the expert system. However, research of artificial neurons, which was one of the areas that opened the field of artificial intelligence research also made good progress with the introduction of Multi-Layer Perceptron. Character recognition through neural network also developed in the late 1980s to the 1990s. This was the period when the foundation of the current deep learning was built.

The former approach of knowledge processing based on the symbols represented by the expert system is called "symbolism" and the latter approach of computing mechanism based on the multi-layer perceptron and the numerical values of neural network is called "connectionism." Both of these contrasting approaches led their respective times.

(5) Winter time ② (1990s-2000s)

The boom of the expert system gradually dwindled down due to its limitation of describing knowledge base and complexity of maintaining and updating extensive data. On the other hand, in Japan, the internet was connected for the first time in 1984 and the www (World-wide web) and communication environment drastically evolved in the 1990s. As massive information crossed over the web, research of data mining (technology to discover (mining) useful knowledge from a large amount of data) and image/information retrieval was very heavily conducted. In addition, statistical machine learning based on mathematical and statistical theories such as probability/statistics and mathematical optimization developed.

(6) Period of data and learning: The third boom (2013-present)

The period from 2013 to present is called the time of "Learning" by deep learning based on big data. Deep learning is being achieved from the integration of connectionism that has been inherited from the continuing research and mathematical foundation of statistical machine learning being developed in the 1990s and 2000s, as well as availability of storage with the capability of storing and processing massive data and high-speed computing capability leveraged by a GPU (Graphic Processing Unit).

2.3 Overview of AI field

Fig. 1 is an extract of the Overview of AI research for beginners and interdisciplinary researchers "AI Map β 2.0"[2] which was published in June 2020 by the Japanese Society for Artificial Intelligence. The website of the Japanese Society for Artificial Intelligence shows 4 detailed maps from different perspectives, so please review them if you are interested.

The first layer in **Fig. 1**, foundation, shows that AI is built on the broad foundational scientific studies such as mathematics, logic, cognitive science, brain science and psychology. Then, AI's own foundation includes logic, inference and knowledge engineering. In the second layer, on top of the first layer, machine learning including deep learning as the foundational technology related more tightly with applications, language and image/voice media processing are found. The research areas located in the upper side within the second layer are the foundational areas closer to applications. Then the most upper layer, the third layer is the application area and shows robots and real world, medical/biology, education, etc. however, the application fields of AI is, recently, drastically expanding.
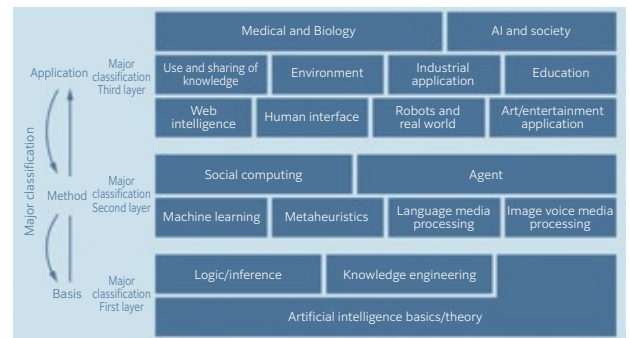
(Source: The Japanese Society for Artificial Intelligence "AI Map β 2.0 (June, 2020)"[2]
This figure is an English translation of the Japanese version of AI Map β 2.0.)

Fig. 1 Development from basic research to methods and applications

3. Present status of AI: period of big data and learning[1)]

3.1 What is machine learning?

Machine learning refers to the overall technologies to have computers acquire learning ability. Learning is, simply put, the ability to handle various tasks well based on past experience and data. For example, becoming proficient at catching a ball by predicting the trajectory after playing catch many times. Therefore, machine learning is a technology for inference and prediction by studying principles from experience and observation. Machine learning is broadly used today, in medical diagnosis, recommendation systems, spam filters, prediction of financial markets, classification of DNA sequences, pattern recognition such as voice recognition and character recognition, games such as shogi (Japanese chess) and most recently, automated driving **(Fig. 2)**.

Today, the mainstream machine learning acquired functions to conduct tasks such as identification and prediction from data. If the desired output is y for the input x, then machine learning acquires the mapping function $c:x \longmapsto y$ from the training data. Since acquiring a true mapping function from the limited amount of training data is impossible, in practice, parameters of such function are adjusted to obtain the desired output by, for example, limiting the form of function or placing certain assumptions. This parameter adjustment of functions is called "learning." Parameter adjustment for the training data which was used to acquire functions is relatively easy if the degree of freedom of function is increased; however, for new unknown data, this adjustment does not work well and is likely to fall into overfitting. One of the challenges of machine learning is how to reduce overfitting and increase generalization performance for unknown data and various technologies are being developed.
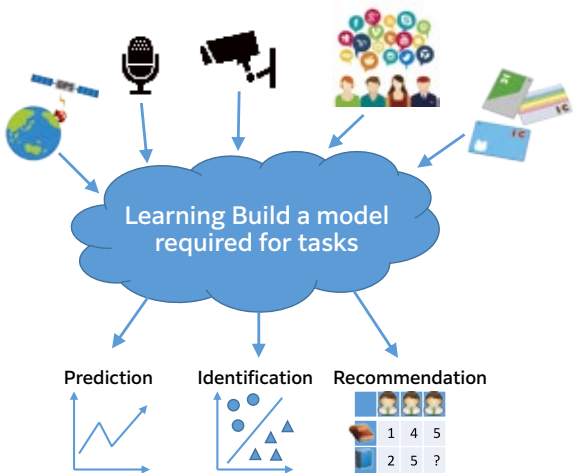
3.2 What is deep learning?

Deep learning is a general name for a neural network with many layers. Originally, the neural network was a model of transmission of electrical signals of neural cells. However, today it is used as a type of machine learning to learn mapping functions corresponding to various tasks. **Fig. 3** is an example of a typical neural network of a task to identify an animal in an image. In the learning stage, many images of various animals are used and the weight between neurons in the hidden layer is adjusted so that only the neuron in the output layer corresponding to cats (gray dot) responds strongly when an image of a cat is input. Conventionally, learning of a neural network with a deep hidden layer was difficult, however, with the recent evolution of various mathematical optimization techniques and development of computers, learning of the network in deeper layers is now possible.

With deeper layers, various expressions can be acquired inside the network. Before deep learning, experts in different fields had to design input features well, however, with deep learning, it is possible for the network to learn features even when raw data is directly input into the neural network. This technology of learning features of the object problems from data is called "feature learning." When training data can be massively collected, this high feature learning ability can be maximized, so deep learning currently shows extraordinary accuracy in identifying images and voices.

In addition, **Fig. 3** depicts a simple overlay of networks of full connectivity, however, various network structures have been recently created by configuring neurons with various functions and exploring different connectivity of networks. For example, there are Convolutional Neural Networks (CNN) which leverage space information such as images and Recurrent Neural Networks (RNN) which learn change in temporal sequence.
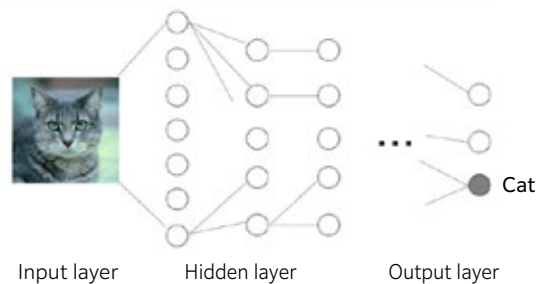
(Source: Introduction to learning how to use AI through Python[1)])

Fig. 3 Typical pattern of image recognition by deep learning

(Source: Introduction to learning how to use AI through Python[1)])

Fig. 2 Machine learning used in various applications

3.3 Development of deep learning

Deep learning started to attract attention when it broke the record of the conventional classification performance with a significant margin at international competitions of image recognition in 2012 and 2013. **Fig. 4** shows the championship records of ImageNet Large Scale Visual Recognition Challenge (ILSVRC)[3] held from 2010 to 2017. ILSVRC is a large-scale problem of classifying around 14 million images into 20,000 classes. Until 2011, a method combining the conventional image processing and machine learning was winning, however, since the appearance of deep learning in 2012, classification errors have been drastically decreased year over year. A classification error of a human being for classification by visual identification is said to be around 5 %. Deep learning has been exceeding the average human classification since 2015.
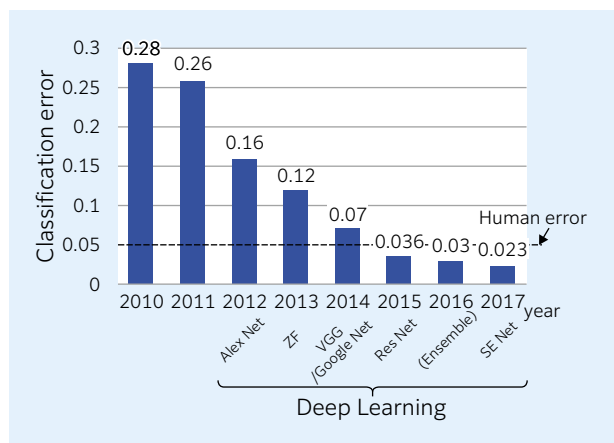

Fig. 4 Championship Record of ImageNet Large Scale Visual Recognition Challenge (ILSVRC)

Deep learning initially attracted attention in the field of image recognition. Then from 2014 to 2016, its application range expanded into "action" from "recognition," such as general game playing, AI go and automated driving through Deep Q-Network (DQN), which combines deep learning with Reinforcement Learning. In 2016, when "AlphaGo" developed by Google DeepMind beat the go champion, that news grabbed headlines. From 2016 to 2018, natural language processing (field of processing languages) also made significant progress thanks to deep learning. Conventional automated translation that used statistical model with bilingual corpus was replaced with deep learning, which drastically improved translation accuracy.

In addition, the invention of the network called Generative Adversarial Network (GAN), with which two networks learn from each other, enabled "generation" and "imitation" and its application range has been recently expanding to creative fields such as art. A famous example is the successful generation of a masterpiece of the famous Dutch artist of the 17th century, Rembrandt, by learning his painting style through "The Next Rembrandt"[4], a project led by

Microsoft. In Japan, the singing voice of Hibari Misora, who passed away 30 years ago, was recreated and featured on a TV program, NHK's Kohaku Utagassen[5] in 2019 and a new manga (comic book) production of Osamu Tezuka (also passed away over 30 years ago), "Phaedo" was published as a result of collaboration between AI and human artists in February 2020, through a project called "TEZUKA 2020."[6] [7]

4. Future of AI: a thought on the outlook in the manufacturing industry from the front line of research

4.1 Issue of ethics

The evolution of AI, especially that of deep learning is tremendous as we have seen in Chapter 3. Those technologies are put into practice in many industrial fields. In order to prevent unforeseen circumstances, discussions on the ethical aspect of R&D and utilization of AI are taking place throughout the world.

In Japan, the Ethics Committee was established in the Japanese Society for Artificial Intelligence in 2014 and the "Japanese Society for Artificial Intelligence Ethical Guidelines" was released in 2017.[8] It lists 9 articles, namely, 1. Contribution to humanity, 2. Abidance of laws and regulations, 3. Respect for the privacy of others, 4. Fairness, 5. Security, 6. Act with integrity, 7. Accountability and Social Responsibility, 8. Communication with society and self-development, and 9. Abidance of ethics guidelines by AI. In addition, "AI R&D Guidelines"[9] was released in July, 2017 by the Ministry of Internal Affairs and Communications for developers, "Social Principles of Human-Centric AI"[10] was released in March, 2019 by the Cabinet Office for users and policy makers, and "AI Utilization Guidelines" [11] was released in August, 2019 by the Ministry of Internal Affairs and Communications for all parties including consumers.

Among those guidelines, technical research on fairness has recently been picking up steam. In 2018, AI conducted the hiring process, after learning past resumes and the successful/unsuccessful results of applicants. As a result, AI rejected female applicants for engineering positions through the review process, as the engineering positions are mainly occupied by male workers. This happened because the training data was biased. Therefore, research on technologies to fairly handle the socially sensitive attributes are now being conducted.

4.2 Issue of explainability

Importance of the ability to explain the "basis of decision" is increasing as AI is being introduced in various fields. Current mainstream deep learning consists of several millions and tens of millions of parameters making it impossible for human beings to explore the basis of decision by manually analyzing the model that AI used for learning. Explainability is one of the challenges critical for introduction of AI, as a lack of explanation for the decision-making process can often be a barrier of introduction.

The research area to add explainability to AI is called XAI (eXplainable AI) and it is very active in the field of image recognition[12]. For example, **Fig. 5** (a) shows a dog and a cat and **Fig. 5** (b) highlights the area when a "dog" is focused on in the trained deep learning model. Accordingly, **Fig. 5** (c) highlights the area when a "cat" is focused on. In principle, gradation is applied on the image based on the calculation of the gradient of output response when input pixels are slightly manipulated.

(a) Original image   (b) Focused area for dog   (c) Focused area for cat
(Source: International Journal of Computer Vision[13])

Fig. 5 Visualization example of attractive areas in deep learning with Grad-CAM

4.3 Issue of security

In 2013, it was pointed out that the identified result of the trained deep learning model could intentionally be altered. This leads to the risk of misinterpretation of traffic signs and "impersonation" in face recognition. This is called an Adversarial example, Adversarial attack and Adversarial perturbation. For example, **Fig. 6** shows that when a special perturbation (in the middle) is added to the image input to the trained deep learning model (left side), all the images (right side) are identified as an "ostrich" even if they look the same as the input images. Defense technologies against adversarial attacks are also being researched/suggested, however, they are only symptomatic treatment for each case, not fundamental solutions. It is expected that fundamental defense technologies will be developed.

Original image   Perturbation   Ostrich   Original image   Perturbation   Ostrich

(Source: Cornell University arXiv[14])

Fig. 6 Example of adversarial attack

4.4 Limitation of current AI

In 2016, an automated driving vehicle had an accident colliding with a trailer. It was explained that AI could not recognize the trailer as the sunlight reflected on its white body. In addition, from 2008 to 2015, a service to estimate the outbreak of influenza from search words was provided, however, it overestimated the actual outbreak by more than 50 %. These problems were caused by the fundamental issue that the current machine learning is based on the inductive approach where laws are obtained from past data. It works well for the "interpolated" cases closer to the past data, but not at all for the "extrapolated" cases not present in the past data.

Research of refinement in operation is being pursued but another direction is to incorporate existing theories into machine learning. Collaboration with physics which has a robust theory background is gradually increasing under the names of Theory-guided Data Science and Physics-informed Machine Learning. Our group is also looking into this area, collaborating with experts of meteorology, to forecast the wind in the upper troposphere. We are proposing deep learning for outputting the forecast by decomposing the components based on the equation and the residual components[15] **(Fig. 7)**.
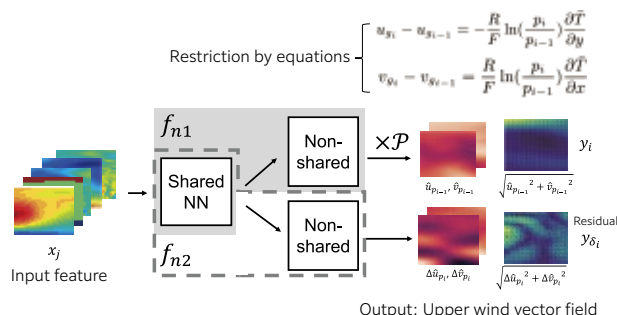

Fig. 7 Deep learning in consideration of physical models[15]

4.5 Issue of AI human resource

Recently, the shortage of human resources that can understand and utilize AI has become a serious issue, as AI is being introduced in various fields. In view of this, the Japanese government established the Strategic Council for AI Technology in 2016 to study and discuss the human resource issues with the Human Resource Development Task Force[16)17)]. The task force summarized that the development of AI human resource with the following capabilities is critical:

① Problem solving with AI technology

Ability to understand foundational technologies of AI such as machine learning and natural language processing and to indicate a roadmap for problem solving from the AI standpoint

② Implementation of AI technology

Ability to implement AI by programming capability and knowledge of computer science such as algorithm and data structure

③ Utilization of AI technology

Ability to capture the challenges of the respective target fields as the AI problems

Based on the discussion at the Strategic Council for AI Technology, education program for fostering immediately effective players, "Learning AI through the Real Data", was held at Osaka University, where the author belongs, and the University of Tokyo from 2017 to 2019 as a commissioned R&D project of NEDO (New Energy and Industrial Technology Development Organization)[18)]. This course assumes engineers (all fields) with a few years to 10 years of experience after graduation as the audience with objectives of learning AI foundational technologies including machine learning, deep learning and computer vision and putting the knowledge into practice through exercises using real data. This NEDO project has now completed but the lecture of Osaka University still continues having established a non-profit organization[19)].

4.6 Prospects in Manufacturing

Fig. 8 is an extract from "Study Report on Utilization of AI Technology in Manufacturing Area"[20)] by the Ministry of Economy, Trade and Industry published in March, 2018, which summarizes manufacturing areas where AI can be introduced by field and objective/accomplishment. Areas of introduction span not only the manufacturing process but also upper stream and downstream, as well as business management.

Currently, the area that AI fits the most is the application of images where big data can be easily collected. Inspection through image recognition is the most favorable area. AI is also introduced in the area where relatively organized data can be collected such as fault detection and design support. On the other hand, replacement and/or succession support of craftsmen's skills which involves tacit knowledge is still a difficult area even if some advancement can be observed. The issue here is sensing rather than the technical issue of AI.

The current AI is completely based on data. Therefore, it is important to identify and collect/extract "useful data" for utilizing AI. Field knowledge is indispensable and certain know-how is also required for collecting valuable data. When the know-how of data collection is established and useful AI systems are completed, the next important phase seems to be the creation of an ecosystem where "humans and AI collaborate" and complement each other for the operation in the field. Increasing individuals who correctly understand AI's characteristics and "are able to successfully operate AI systems" will be required. The methodology of AI (machine learning) system operation is called "machine learning systems engineering." In 2018, the Special Interest Group on Machine Learning Systems Engineering[21)] was launched within the Japan Society for Software Science and Technology, to promote discussions and know-how sharing.

How AI can be utilized in manufacturing				
Area | Objective/Accomplishment	Improvement of production process (Automation/improvement → energy saving/cost reduction)		Improvement of quality/service (Increase value to the customers)	Creation of new values (What was impossible becomes possible)
Upper stream of manufacturing	■ Design of production system/ Development of production plan	■ Inventory control ■ Inspection of parts/materials (efficiency improvement)	■ R&D/material design support ■ Inspection of parts/materials (improvement of accuracy)	■ R&D/material design support (AI supporting experts)
Manufacturing process	■ Optimization of traffic line ■ Automation of assembly work/ picking	■ Analysis and implementation of energy saving ■ Improvement of yield/availability	■ Replacement/succession of craftsman's skills(Succession of skills, machining conditions, optimization of manufacturing conditions, management and control of reaction/fermenting process)	■ Manufacturing evolution support (AI supporting experts)
Downstream of manufacturing	■ Image recognition inspection (efficiency improvement) ■ Maintenance/follow-up service	■ Efficiency in packaging process ■ Improvement of logistics → energy saving	■ Image recognition inspection (improvement of accuracy) ■ Maintenance/follow-up service (improvement of service)	■ Provision of new follow-up service
Support activities for manufacturing	■ Development of estimate ■ Facility management	■ Production line management/ maintenance (Maintenance, fault prediction, energy saving)	■ Support for succession of skills/ skills training ■ Production line management (stable operation)	
Business/Management	■ Development of business strategy ■ Demand forecasting	■ Marketing	■ Labor management/human resource management ■ Marketing ■ Customer relation	■ New business/new product development expenses ■ Expansion of business scope

(Source: Ministry of Economy, Trade and Industry "Study Report on Utilization of AI Technology in Manufacturing Area"[20)])

Fig. 8 AI-applicable fields in manufacturing

5. Summary

The public hype of AI in the past seems to have calmed down, however, introduction of AI is steadily advancing. As mentioned in this paper, significant progress of deep learning expanded the utilization of AI, however, at the same time, new issues such as ethics, explainability and security have emerged. On the other hand, the current AI, which is based on training, depends very much on advanced data collection and preprocessing. Therefore, it has significant potential for the Japanese manufacturing industry to use its strength of "front line skills." In order for useful AI systems to become firmly established in society, not as a temporary "boom," we expect to build a system that is operated effectively where AI and humans work together, with correct understanding of AI's strengths and weaknesses.

References

1) Ken-ichi Fukui (author), "Introduction to learning how to use AI through Python," Japan Technical Education Development Center (2020)
2) Japanese Society for Artificial Intelligence, "AI Map β 2.0" (June, 2020), Japanese Society for Artificial Intelligence HP
   https://www.ai-gakkai.or.jp/resource/aimap/
3) ImageNet Large Scale Visual Recognition Challenge (ILSVRC) HP
   http://www.image-net.org/challenges/LSVRC/
4) The Next Rembrandt HP
   https://www.nextrembrandt.com
5) YAMAHA Corp., "Hibari Misora Vocaloid AI" YAMAHA HP
   https://www.yamaha.com/ja/about/ai/vocaloid_ai/
6) KIOXIA Corporation, "TEZUKA 2020," Kioxia HP
   https://tezuka2020.kioxia.com/ja-jp/
7) Special issue "Revival of Osamu Tezuka by AI," Artificial Intelligence, Vol. 35, (May, 2020), 390-429.
8) Ethics Committee of the Japanese Society for Artificial Intelligence, "Japanese Society for Artificial Intelligence Ethical Guidelines," (February, 2017).
   http://ai-elsi.org/report/ethical_guidlines
9) Ministry of Internal Affairs and Communications, "AI Development Guidelines," Promotion Council for AI Network Society Report 2017, (July, 2017)
   https://www.soumu.go.jp/menu_news/s-news/01iicp01_02000067. html
10) Cabinet Office, "Social Principles of Human-Centric AI," Council for Social Principles of Human-Centric AI, (March, 2019).
    https://www.cas.go.jp/jp/seisaku/jinkouchinou/pdf/aigensoku.pdf
11) Ministry of Internal Affairs and Communications, "AI Utilization Guidelines," Promotion Council for AI Network Society Report 2019 Annex 1, (August, 2019).
    https://www.soumu.go.jp/menu_news/s-news/01iicp01_02000081.html
12) Satoshi, Hara, "Interpretability in Machine Learning," The Japanese Society for Artificial Intelligence HP, My Bookmark (May, 2018)
    https://www.ai-gakkai.or.jp/my-bookmark_vol33-no3/
13) Ramprasaath R. Selvaraju, Michael Cogswell, Abhishek Das, Ramakrishna Vedantam, Devi Parikh, and Dhruv Batra, "Grad-CAM: Visual Explanations from Deep Networks via Gradient-Based Localization", International Journal of Computer Vision, 128, (2020), 336-359.
    https://link.springer.com/article/10.1007%2Fs11263-019-01228-7
14) Christian Szegedy, Wojciech Zaremba, Ilya Sutskever, Joan Bruna, Dumitru Erhan, Ian Goodfellow, and Rob Fergus, "Intriguing properties of neural networks", Cornell University arXiv, last revised 19 Feb 2014.
    https://arxiv. org/abs/1312.6199
15) Ken-ichi Fukui, Junya Tanaka, Tomohiko Tomita, and Masayuki Numao, "Physics guided Neural Network with Model Discrepancy Based on Upper Troposphere Wind Prediction", Proc. IEEE 18th International Conference on Machine Learning and Applications (ICMLA 2019) , (2020) , 414-419.
16) Yasushi Yagi, "Educational program for fostering AI human resources: Discussion at the Strategic Council for AI Technology," Artificial Intelligence, Vol. 33, (May, 2018), 259-264.
17) Ministry of Education, Culture, Sports, Science and Technology, NEDO, "Human Resource Development Task Force Final Report," Reference Material 1-1, for the Fifth Strategic Council for AI Technology (March, 2017).
    https://www.nedo.go.jp/content/100862415.pdf
18) NEDO, "Fostering an Industry-Ready Workforce in the AI Field—NEDO to hold series of special lectures at Osaka University and the University of Tokyo —" NEDO HP News Release, (July, 2017).
    https://www.nedo.go.jp/news/press/AA5_100809.html
19) Datability Consortium "Learning AI through the real data"
    https://www.cds.or.jp/jinzai/course01/index.html
20) Ministry of Economy, Trade and Industry "Study Report on Utilization of AI Technology in Manufacturing Area" Ministry of Economy, Trade and Industry Commissioned Study Report, (March, 2018).
    https://www.meti.go.jp/meti_lib/report/H29FY/000119.pdf
21) Special Interest Group on Machine Learning Systems Engineering, Japan Society for Software Science and Technology
    https://sites.google.com/view/sig-mlse/

<Author Biography>

Ken-ichi FUKUI

Associate Professor Division of Information and Quantum Sciences/SANKEN (The Institute of Scientific and Industrial Research)/Osaka University

2003	Completed Materials/Life Information Engineering Course (Master's Program), Graduate School of Human Informatics, Nagoya University
2005-2010	Specially appointed Assistant Professor, Materials Science & Technology Research Center for Industrial Creation, Institute of Scientific and Industrial Research, Osaka University
2010	Received Ph.D. from Osaka University
2010-2015	Assistant Professor, Division of Information and Quantum Sciences, Institute of Scientific and Industrial Research, Osaka University
2015-Present	Associate Professor, Division of Information and Quantum Sciences, Institute of Scientific and Industrial Research, Osaka University
2020-Present	Trustee, Japanese Society for Artificial Intelligence

[Specialty]
・Machine learning, data mining and its applications
・Knowledge discovery, prediction, fault detection especially from event series data
・Scope of application includes sleep, meteorology, earthquake, fuel cell, etc.

[Affiliated academic societies]
IEEE Computer Society, Japanese Society for Artificial Intelligence, Information Processing Society of Japan, The Japanese Society for Evolutionary Computation and The Institute of Electronics, Information and Communication Engineers

[Awards]

2008	IEEE 8th International Conference on Computer & Information Technology (CIT), Best Paper Award
2011	25th Annual Conference Best Presentation (oral presentation), Japanese Society for Artificial Intelligence
2013	President Award, Osaka University
2013	Encouragement Prize, Research Area, President of Osaka University
2013	Incentive Award in 2012, Japanese Society for Artificial Intelligence
2016	FAN Best Paper, 26th Intelligent System Symposium
2016	The Workshops at the 14th Pacific Rim International Conference on Artificial Intelligence (PRICAI-2016), Best Workshop Paper Award
2017	Incentive Award in 2016, Japanese Society for Artificial Intelligence
2018	Encouragement Prize, Research Area, Artificial Intelligence and Knowledge Processing Research, The Institute of Electronics, Information and Communication Engineers
2018	Elsevier, Knowledge-Based Systems, Outstanding Reviewer
2020	34th Annual Conference Best Presentation (international session oral presentation), Japanese Society for Artificial Intelligence

[Publication]
"Understanding Machine Learning by Python and Real Data - identification/prediction/fault detection," Ohmsha, 2018, etc.

Rolling Bearing Development for the Future of Industrial Machinery

Etsu HARIMA*

NTN supplies many bearing sizes based on the needs of various applications in the industrial machinery market. These range from ultra-small bearings with outer diameters of a few millimeters for electronic devices, to ultra-large bearings with outer diameters of several meters for wind turbines and large mining machinery. In addition to existing customers for "core" industrial markets such as construction machinery, agricultural machinery, and machine tools, business from customers relating to social infrastructure is increasing. Activity with customers in the aircraft, railway vehicle, and wind turbine markets is growing with changes in social structure and increased awareness of environmental issues. Therefore, **NTN** has developed related engineering and production systems accordingly. Due to advancements in Internet of Things (IoT) and development of artificial intelligence (AI) technology, it is expected that the current environment will change significantly. This report introduces advancements in **NTN**'s analysis and evaluation technology, as well as **NTN**'s approach to higher bearing performance and reliability.

1. Introduction

In Egyptian pictures drawn thousands of years ago, people are transporting rocks by pulling them on rollers placed underneath the rocks. This is the origin of rolling bearings (hereafter, "bearings").

It is also believed that Leonardo da Vinci, an artist in the Renaissance era, invented the basic principle and structure of modern day bearings. Da Vinci had drawings of bearings with almost the same structure as the ones used today.

It has been about 100 years since **NTN** started manufacturing bearings. The appearance and components are almost the same as back then. However, the performance of the components has significantly improved thanks to the progress of materials, lubricants, and processing technologies. Bearings are now indispensable machine components for equipment.

In this paper, the evolution of bearings in areas such as steel manufacturing methods, manufacturing technologies, and design technologies is reviewed. Additionally, **NTN**'s progress of analytical technologies and evaluation technologies, as well as its initiatives for improvement of reliability are introduced.

This paper also introduces an approach for modular and intelligent components by integrating forward-looking bearing technology, sensing technology, and precise control technology, as well as new products and services leveraged by fault detection, condition monitoring system (CMS), and IoT.

2. Past technology development[1]

Looking at the **NTN** company history, there are numberous revolutionary years showing excellence in technology.

In 1934, **NTN** developed bearings for aircrafts and its products were adopted in the engine and body of 100% domestically-produced aircraft, "Kamikaze." This aircraft set a world record of 94 hours 17 minutes and 56 seconds of flight between Tokyo and London.

Double-row cylindrical roller bearings and single-row deep groove ball bearings were adopted in 1964 as journal bearings of the 0-series Shinkansen (bullet train), which made its debut on the newly opened Tokaido Shinkansen line. Components of the materials, heat treatment, and inspection conditions were rigorously examined and standardized by the then Japan National Railways (currently, Japan Railways) and only **NTN** and other designated companies were allowed to deliver the products.

Later, the H-1 rocket, which made a successful launch of its first test vehicle in 1986, was the first rocket with 100% domestically-produced liquid oxygen/liquid hydrogen engine in the second stage. Almost all of the bearings[2] used in the rocket were produced by **NTN**. In 2002, **NTN** developed bearings capable of ultra-high-speed rotation of 3 million in dn[*1] value in liquid hydrogen (-253 ℃) for the first time in the world together with the National Aerospace Laboratory of Japan (currently, JAXA)[3].

*1 dn value: d=ID (mm) × n= shaft rotation speed (min⁻¹)
In general, dn value exceeding 1 million is called "high-speed" and a dn value exceeding 2 million is called "ultra-high-speed".

---

* Operating Officer, Corporate General Manager, Industrial Business Headquarters

As such, **NTN** has been accumulating product technologies and manufacturing technologies so that **NTN** can respond to the needs of its customers such as "long operating life" and "high speed." These features are required by all industrial machines.

2.1 Long operating life

The evolution of the steel making method has significantly contributed to "long operating life." As cleanliness of modern bearings has increased, internal origin flaking due to rolling contact fatigue caused by non-metallic inclusions is reduced under proper lubricating conditions. Operating life of bearings made of bearing steel with standard heat treatment (immersion quenching) are said to be semi-permanent if used under the fatigue limit load[4]. Conversely, since operating conditions of the actual bearings are severe and they are used under higher temperature, higher speed, and higher load, the expectation of the market is longer life with thinner lubrication and contamination.

Past research achievements[5] revealed that improvement of steel chemical components (alloy element) and heat treatment characteristics (toughness, hardness, etc.) can increase bearing life. As such, **NTN** has provided many long-life bearings on the market using these technologies. **NTN** has recently developed the "ETFA bearing."[6] This bearing provides twice the bearing life of the conventional long-life "ETA bearing" and 6 times longer than the **NTN** standard "4 Top" series with contaminated lubrication. Resistance to foreign objects was increased thanks to special heat treatment technology (enhanced grain refinement) of case-hardened steel (carburized steel) **(Fig. 1)**.
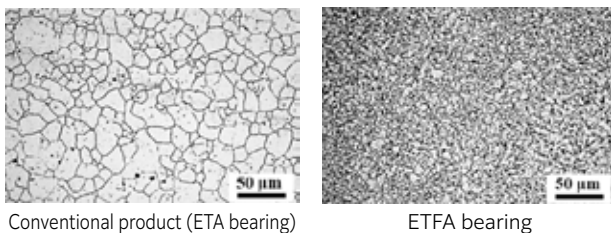

Conventional product (ETA bearing)   ETFA bearing

Fig. 1 Prior austenite grain under surface of bearing raceway

2.2 High speed

Another critical performance characteristic required for the bearings is "high speed." Particularly, main shafts of machine tools, such as machining centers, are operated at significantly higher speed to improve machining efficiency and accuracy. **NTN** has been working on development and improvement of its products to respond to the requirement of high-speed operation[7].

As a result, **NTN** has achieved ultra-high-speed operation by adoption of ceramic balls which are lighter than steel balls and adapt well to high-speed operation with high contact pressure, adoption of smaller roller elements to reduce centrifugal force of high-speed operation, and adoption of air-oil lubrication and air-cooling technology[8]. The last two developments increase lubrication reliability by reducing heat caused by agitating resistance of lubricant **(Fig. 2)**.
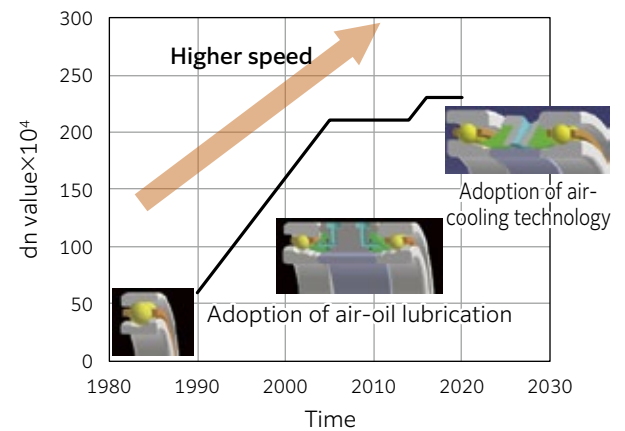
Fig. 2 Transition into higher speed machine tool bearings

Recently, demand for bearings for main shafts that use grease lubrication has increased for ease of use and reduced environmental impact. With grease lubrication, heat can cause degradation of the grease, and have a significant impact on bearing life. Therefore, reduction of heat during operation is an important factor. **NTN** developed "Machine Tool Spindle Bearing with Air Cooling Space for Grease Lubrication"[8] with its unique air-cooling technology. This technology introduces bearing cooling through air-cooling nozzles on outer ring spacers between bearings to cool the inner rings via inner ring spacers **(Fig. 3)**.

Fig. 3 Machine Tool Spindle Bearing with Air Cooling Spacer for Grease Lubrication

3. Evolution of rolling bearings

As mentioned earlier, the required function for bearings was to rotate smoothly under a large load for a long time. However, current bearings are not limited to that and **NTN** is now putting bearings with several more functions on the market.

New products are being developed to respond to demand, such as wind turbines and railway vehicles in growing markets, robots, aircrafts and machine tools. All of these industries require state-of-the-art technology.
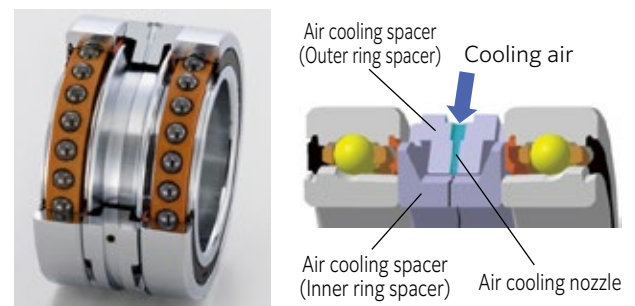
3.1 Bearings for large wind turbines and CAE[*2] analysis technology

Large wind turbines have rapidly evolved as an application area of bearings over the last 20 years. In addition to the requirement of a design life of over 20 years, highly reliable large-scale bearings are in high demand for offshore wind turbines. These bearing have outer diameters of over 2 m.

The magnitude and direction of load on bearings can vary depending on the wind conditions, and there are up to several millions of directional load combinations. Also, because of the size of the bearings, tests using the actual products are extremely difficult. Therefore, CAE analysis technology for deformation of bearings and their mating shafts and housings is indispensable **(Fig. 4)**.

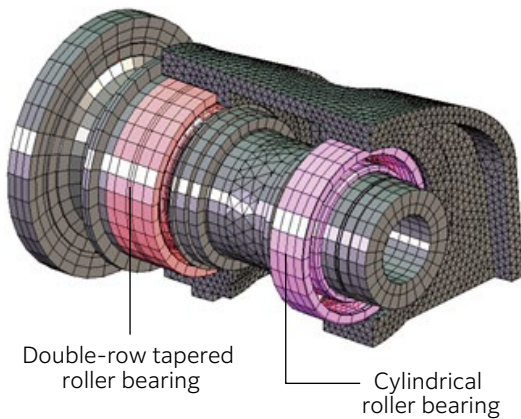*2 Abbreviation of Computer Aided Engineering

Double-row tapered roller bearing
Cylindrical roller bearing

Fig. 4 Analysis model of wind turbine main shaft system

NTN also develops unique products contributing to long operating life. For main bearings, self-aligning roller bearings have been used which allow installation errors and may lead to early failure due to wear on the raceway.

Noting that a larger load is applied to the rear row (farther row from the blade) of bearings than the front row (closer row to the blade), **NTN** unveiled the "asymmetric self-aligning roller bearing"[9] adopting **NTN**'s unique design of different roller lengths and contact angles on rows in 2017 **(Fig. 5)**.

Front row (Close to the blade)   Rear row (Far from the blade)   Front row   Rear row

Wind load
Axial load
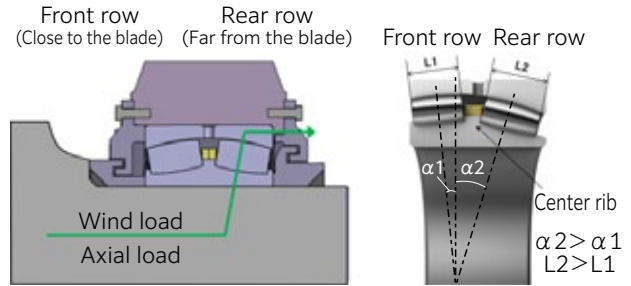
Center rib
$\alpha 2 > \alpha 1$
$L2 > L1$

Fig. 5 Left: Loading condition, Right: Asymmetrical design

3.2 Bearings for machine tools and IoT

Bearings for main spindles of machine tools are required to offer ultra-high-speed operation with ultra-high accuracy. However, the new trends of integration and combination of machining processes require a single tool to handle deep cutting with medium to low speed rotation with high load resistance and fine cutting with high speed rotation. **NTN** developed the "Angular Contact Ball Bearing for High-Speed and Heavy-Cutting Machine Tools" in 2018 by optimizing the internal design of the conventional high-speed angular contact ball bearing "HSE type" achieving 30 % higher load carrying capacity and permissible axial load while maintaining high speed performance[10].

In addition, there is high demand for condition monitoring and IoT functions for reliability. **NTN** has newly added load detection and wireless functions to the unit "Sensor Integrated Bearing Unit"[11] which had been announced previously with integrated sensors in the outer ring spacer adjacent to bearing for realizing advanced condition monitoring **(Fig. 6)**.

<Integrated in outer ring spacer>
· Sensor (load, vibration, temperature)
· Electromagnetic generator
· Wireless module
Wireless

Fig. 6 Sensor Integrated Bearing Unit for Machine Tool Spindles

3.3 Rolling bearings for railway vehicles and insulation technology

Bearings are used in the journal, driving mechanism, and main electric motor locations of railway vehicles. Bearing performance and quality directly affect the safety of railway vehicles. Therefore, particularly high reliability is required among industrial machine bearings.

NTN is also working on technology development to respond to recent demand of high-speed operation and extension of maintenance intervals. Stray current corrosion can occur in the journal and main traction motor bearings. Usually, measures are taken on vehicles and its carriages, however, insulating bearings themselves can be a very effective measure. **NTN** has developed the "MEGAOHM™ Series"[12] with ceramic spray or resin coating on the bearing outer diameter. This development has been was received very well **(Fig. 7)**.

Ceramic spray insulation coating

Cylindrical roller bearing

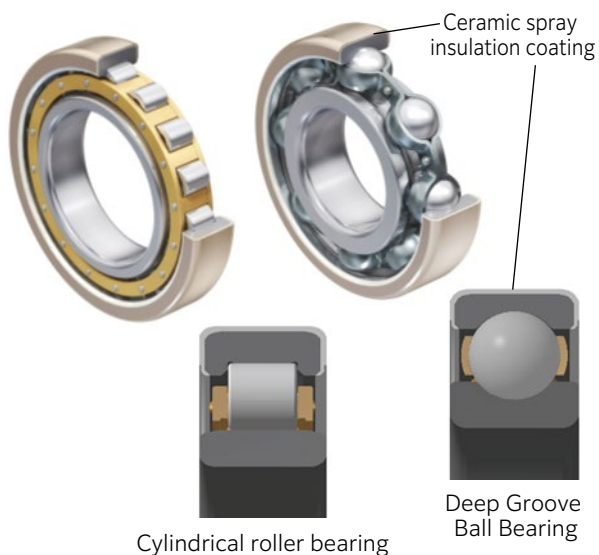Deep Groove Ball Bearing

Fig. 7 Ceramic insulated MEGAOHM™ series

3.4 Condition monitoring service of bearings

NTN is currently developing a condition monitoring service (hereafter, "CMS"[*3]) for predictive maintenance by IoT and **NTN** sensing technologies in order to respond to the demand of energy saving, long and stable operation, and reduction of life cycle cost.

*3 Abbreviation of Condition Monitoring System

In the wind turbine area, **NTN** has already developed the condition monitoring system "Wind Doctor™." This development has been implemented in wind turbine systems with very favorable feedback **(Fig. 8)**.

For CMS to contribute to reduction of maintenance cost and improvement of equipment availability in the wind power generation business, highly accurate prediction and fault detection technology are required so that repair work can be scheduled at the right time with the remaining life of the components known.

For improved accuracy, data analysis technology and diagnosis algorithms must be developed, which integrate different kinds of information, such as operation and management of facilities, not only measurement data from sensors.

From these perspectives, **NTN** is promoting development of the CMS technology, effective for supporting maintenance activities, and intends to make specific proposals in the areas of railway vehicles, machine tools, and machinery equipment.

① Data collection system

② Data management software

③ Monitoring/analysis software

Sensors for measurement (vibration, etc.)

Information of operation (rotational speed, generated power)

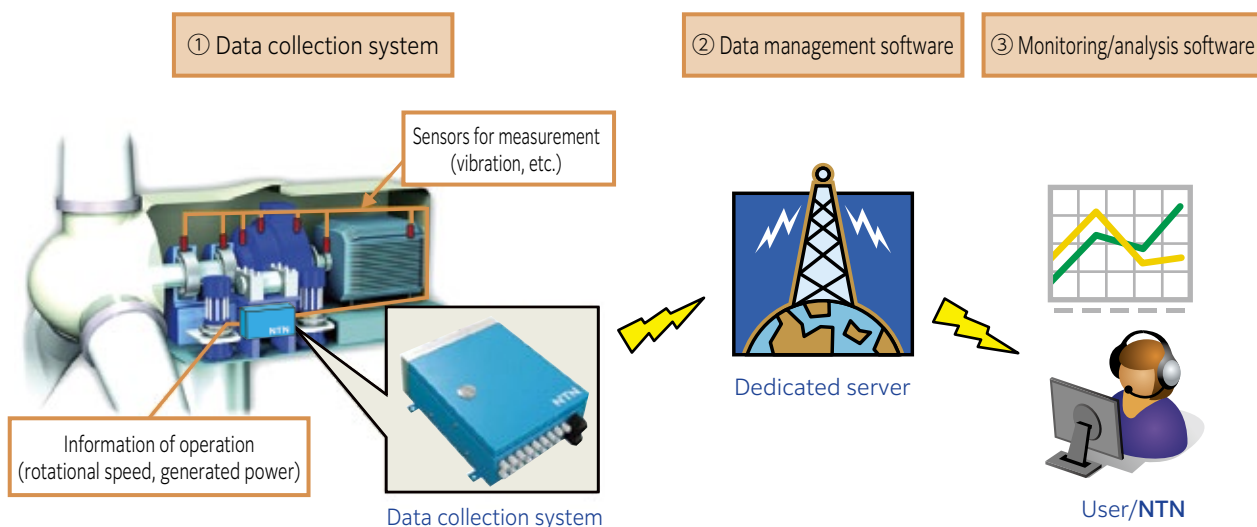Data collection system

Dedicated server

User/**NTN**

Fig. 8 System configuration of Wind Doctor™

4. Future Development

Changes in the market environment are about to occur.

・Carbon neutral
・DX(Digital transformation), IoT(Internet of Things)
・Reduction of productive population ratio

Challenges for rolling bearings are also changing in the midst of these changes. "Carbon neutral" raises expectations of renewable energy, especially wind turbines. The wind turbine facility will become increasingly larger and include offshore installations. Companies who can design and produce bearings that support rotors and blades of these turbines are few and far between, however, **NTN** can.

As mentioned previously, **NTN** is increasing the reliability of its bearings and contributing to the reduction of maintenance cost and increase of equipment availability in the wind turbine business through utilization of CMS.

NTN will also work on making bearings intelligent in the backdrop of "DX (digital transformation) and IoT (Internet of Things)." Moving forward, leveraging **NTN**'s sensing and analysis technologies, as well as AI (Artificial Intelligence), **NTN** will offer services to support efforts by users on fault prediction and predictive maintenance of bearings.

Adoption of automation and robots will accelerate due to the "reduction of productive population ratio." In the area of industrial robots, high rigidity bearings are required for precise positioning. **NTN** is focused on development of bearings with higher rigidity within limited space. **NTN** is also marketing the "i-WRIST™" Wrist Joint Module, which leverages **NTN**'s base technology of bearings[13].

Bearings are also becoming a commodity due to the fierce competition of low-cost products. **NTN** is tackling the challenge of cost reduction as an important task by optimizing procurement of materials and components.

5. Summary

The rolling bearing will continue to be a critical machine element. **NTN** must strive to lead the world in technology development on the eternal objectives of "long operating life," "ultra-high-speed," "high rigidity" and "high reliability." **NTN** is focusing on bearings that leverage IoT, condition monitoring and data collection of rotating machines, peripheral machines that utilize data, and development of applications, so that after 10 or 20 years, everyone will be amazed how rolling bearings have changed.

The **NTN** industrial machinery business remains indispensable, supporting development of world industry based on bearing technology and leveraging digital technology.

References

1) The history of NTN: 100 years (2019)
2) Masataka Nosaka, Satoshi Takada, Makoto Yoshida, Research and development of cryogenic tribology of turbopumps for rocket engines, Aeronautical and Space Sciences Japan, Vol. 58, Issue 681, (2010) 303-313.
3) NTN press release "Receives the Japanese Society of Tribologists, Technology Award" NTN website, https://www.ntn.co.jp/japan/news/press/news20030530_3.html
4) NTN Ball and roller bearings' catalog, CAT. No.2203/J, A-19-21.
5) Kikuo Maeda, Hirokazu Nakashima, Hiroshi Kashimura, Development of Long Life TAB and ETA Bearings and Their Automotive Applications, NTN TECHNICAL REVIEW, No.65, (1996) 17-22.
6) Masahiro Yamada, Naota Yamamoto, Chikara Ohki, "ETFA" Bearings Strengthened by Fine Microstructure Design, NTN TECHNICAL REVIEW, No.88, (2020-2021) 99-104.
7) Keiichi Ueda, Technical Trend of the Precision Bearings for Machine Tools, Tool Engineer, Vol. 60 No. 16, (2019) 41-43.
8) Kazuki Sonoda, Tomohiko Obata, High Speed Machine Tool Main Spindle Bearings with Air Cooling Spacer for Grease Lubrication, Japanese Society of Tribologists, Proceedings for Tribology Conference 2020 Fall (2020) B-11 95-96.
9) Kazumasa Seko, Takashi Yamamoto, Asymmetrical Spherical Roller Bearings for Wind Turbine Main Shafts, NTN TECHNICAL REVIEW, No.86, (2018) 96-101.
10) Jin Takegahana, Mineo Koyama, Kouji Jinno, Yuya Tanaka, Angular Contact Ball Bearings for High-Speed and Heavy-Cutting Machine Tools, NTN TECHNICAL REVIEW, No.86, (2018) 56-61.
11) Shohei Hashizume, Yasuyuki Fukushima, Yusuke Shibuya, Yohei Yamamoto, Development of Sensor Integrated Bearing Unit for Machine Tool Spindles, NTN TECHNICAL REVIEW, No.86, (2018) 50-55.
12) Hideji Ito, Insulated bearing "MEGAOHM" series, NTN TECHNICAL REVIEW, No.71, (2003) 48-51.
13) Keisuke Kazuno, Hiroshi Isobe, Masaki Kagami, Jun Midomae, Yuki Shimura, Seigo Sakata, Yukihiro Nishio, Naoki Marui, Application Examples and Function Improvements of the Wrist Joint Module "i-WRIST™", NTN TECHNICAL REVIEW, No.88, (2020-2021) 105-110.

Photo of authors

Etsu HARIMA

Operating Officer,
Corporate General Manager,
Industrial Business Headquarters

New Products and Improved Reliability of Main Bearings for Wind Turbine Generators

Michio HORI*
Yusuke YAMADA*

Wind turbine generators, which are becoming an increasingly more mainstream source of renewable energy, are becoming larger. Furthermore, bearings used in these wind turbines are required to be reliable. This section introduces **NTN**'s latest products and design approach for spherical roller bearings used in many onshore turbines and single-row tapered roller bearings that are used in offshore turbines more and more.

1. Introduction

Adoption of renewable energy is being promoted worldwide to address global warming, as exemplified by the Paris Agreement, an international accord for reducing greenhouse gas emissions. Last year, renewable energy, excluding hydropower, exceeded nuclear power in global share of power generated - wind power accounted for about 5 % of the total[1].

To broaden adoption of renewable energy, it will be important to reduce the LCOE (Levelized Cost of Energy) which is calculated by dividing costs of power generation, including construction, operation, and maintenance costs, by the projected amount of power generated during the operating period. Turbines have improved utilization as a result of increased tower heights, lengthening of blades, and improved blade shape. Off-shore wind power has been increasingly adopted in recent years. Since construction costs are higher than on-shore wind power, there is a need to develop ultra-large turbines, often exceeding 10 MW, extend service life, and improve maintenance efficiency.

In wind turbines, bearings are used at the support section for the rotor shaft (main shaft), gearbox, and generator as shown in **Fig. 1**. Additionally bearings are used to allow pitch control of each blade, yaw control of the machine head, and within the pitch and yaw reducers which drives them. This article describes efforts by **NTN** to improve reliability and achieve optimization of the main bearing used at the main shaft support section.
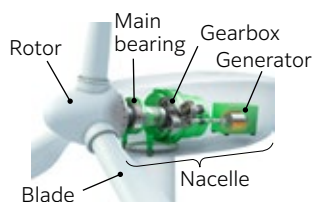

Fig. 1 Internal Wind Turbine construction

2. Composition of main bearing

The main bearing is the most important part for supporting the wind load received by the blades and transmitting driving power to the generator. The bearing type used varies depending on the composition of the drivetrain. As shown in **Fig. 2**, there are two basic categories: the gearbox type, and the 'direct drive' type with no gearbox.
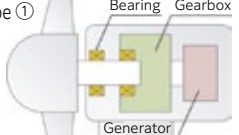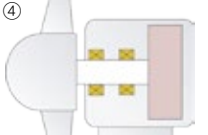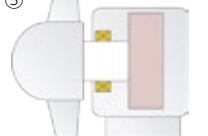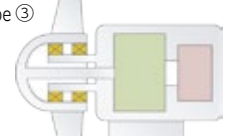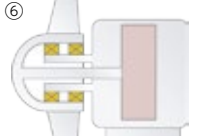
Type ① in **Fig. 2** has traditionally been the most common choice for the gearbox type installed on-shore. In this type, the main shaft is typically supported by a single main bearing within a pillowblock housing and a bearing inside the gearbox. Spherical roller bearings tolerant of mounting error are used. Type ②, in which support is provided using two spherical roller bearings, is also used in many on-shore turbines. However, with type ②, sliding must be allowed at the outer ring outer diameter surface on the free side to cope with thermal expansion and contraction of the main shaft. To ensure reliability over the long term, there are also structures which use inward-facing (direct mount) double row tapered roller bearings in the fixed position, and cylindrical roller bearings capable of accommodating thermal expansion and contraction by sliding in the axial direction in the floating position.

With the direct drive type, on the other hand, reliability is better due to the reduced number of parts. A directly-linked generator enables power generation at a low rotational speed by making permanent magnets multipolar, however, this increases the size of the generator rotor. Therefore, the main shaft must have a large diameter and loading is supported by a compact double row tapered roller bearing with a large contact angle (Type ⑤).

In addition to the direct drive type, a multi-pole synchronous generator of the "gearbox + medium speed type" balances reliability and cost and is also used in off-shore turbines. Due to the increased size of

* Application Engineering Dept., Industrial Business Headquarters

wind turbines, there is increased use of back-to-back single row tapered roller bearings instead of double row tapered roller bearings with a large contact angle which have a large impact on productivity and cost (type ② , ③). With this bearing type, it is possible to optimize service life and system rigidity through the use of preload. Bearing setting must be done by the wind turbine manufacturer, but at **NTN**, we support users through analysis to determine the setting range.

Gearbox type		Direct Drive type	
Type ①	Bearing Gearbox	Type ④	
Main bearing + bearing in gearbox Bearing type: SRB		Main bearing ×2 Bearing type: TRB×2 or DRTRB+CRB	
Type ②		Type ⑤	
Main bearing ×2 Bearing type: SRB×2 or TRB×2 or DRTRB+CRB		Main bearing ×1 Bearing type: MBRG	
Type ③		Type ⑥	
Main bearing ×2 (in rotor) Bearing type: TRB×2 or DRTRB+CRB		Main bearing ×2 (in rotor) Bearing type: TRB×2 or DRTRB+CRB	

SRB: Spherical roller bearing   TRB: Tapered roller bearing
DRTRB: Double row tapered roller bearing （face-to-face)
MBRG (moment bearing): Double row tapered roller bearing (back-to-back)
CRB: Cylindrical roller bearing

Fig. 2 Relationship between drive train and bearing type

The following will introduce **NTN**'s efforts with a focus on spherical roller bearings, which are the mainstream choice for on-shore turbines, and single row tapered roller bearings, which are increasingly used in off-shore turbines.

3. Extending life of spherical roller bearings

The aforementioned spherical roller bearings are advantageous due to their tolerance for mounting error, and the ability to use independent housings for each bearing. However, there are cases where premature damage occurs due to operational wear of the raceway surface. **NTN** is helping to extend the life of these types of bearings and minimize turbine size by using unique technology which accounts for the application conditions particular to main bearings.

3.1 Asymmetrical design of different rows

The main bearing is subjected to a radial load acting vertically on the shaft due to the weight of the rotor and blade, and axial loading acting horizontally on the

shaft due to the wind load. If we assume an upwind wind turbine, i.e., the mainstream type with the rotor receiving the wind located on the upwind side, then a larger load acts on the rear bearing row away from the blade than on the front bearing row near to the blade **(Fig. 3)**.
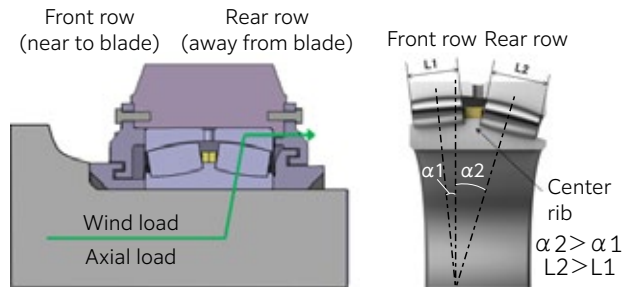

Fig. 3 Loading condition   **Fig. 4** Asymmetrical design

At **NTN**, we noticed these characteristics of the applied load, and in 2017 we issued a press release on an asymmetrical spherical roller bearing. This bearing has a unique design featuring different roller lengths and contact angles among the different rows[2] **(Fig. 4)**. These changes increase calculated life by about 2.5 times, and enable reduction of inner diameter by about 10 % and weight by about 30 % in a bearing with life comparable to the conventional product. If this bearing is used in a wind turbine, bearing downsizing can be achieved, which can contribute to reducing size, weight, and cost of the entire wind turbine **(Fig. 5)**.
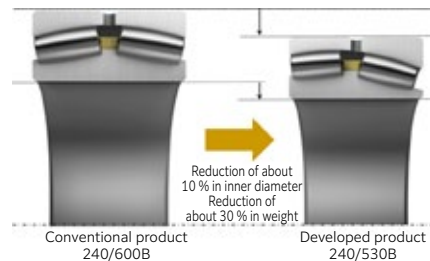
Fig. 5 Example of design for downsizing

3.2 DLC coating

(1) Structure

The rollers of spherical roller bearings are barrel shaped. Within the spherical roller bearing, differential slippage[*1] occurs, where the bearing rotates with slippage at the contact points between the roller contact surface and raceway surface. Also, rotation repeatedly stops and starts due to wind conditions, and the bearing is lubricated with grease. If poor lubrication (insufficient oil film) is experienced during operation, wear may occur at the raceway surface due to metal contact, starting from points with a high PV value (i.e., the product of the contact stress (P) and sliding velocity (V)) and progressing into a two-peaked form. As a result, stress is then concentrated at the lines of pure rolling contact where no wear occurs, and this may cause flaking and cracking of the raceway surface **(Fig. 6)**.

*1 Differential slippage: Slippage attributable to differences in speed in the rotation direction between the roller and raceway

Fig. 6 Damage mechanism

The rotating inner ring experiences loading about the entire circumference of the raceway surface, but the outer ring is fixed in the housing, and thus the load zone is concentrated in a specific range, and damage occurs due to repetitive loading.

With the aforementioned asymmetrical design, the PV value can be reduced by about 30 %, so the design is effective to some degree in reducing wear. On the o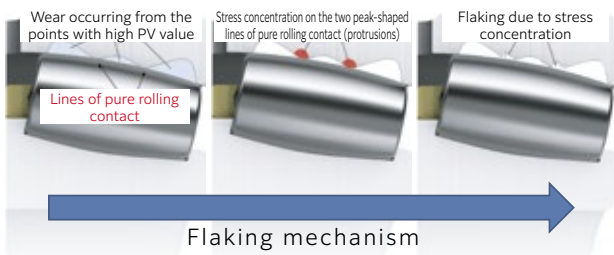ther hand, it is difficult to avoid metal contact in a state with insufficient oil film, and other approaches were needed to further improve reliability. Thus we developed a bearing with a DLC (diamond-like carbon) coating applied to the roller contact surface **(Fig. 7)**. The DLC coating used by **NTN** employs a three-layer structure: ① a metal sub-layer to increase adhesion to the base material, ② an intermediate layer to act as a hardness gradient between the metal sub-layer and the top layer, and ③ a high hardness top layer of DLC coating. The coating has outstanding adhesion and wear-resistance given the differential slippage particular to spherical roller bearings and lubrication conditions where oil film formation is inadequate **(Fig. 8)**.

Fig. 7 DLC coating spherical roller bearing
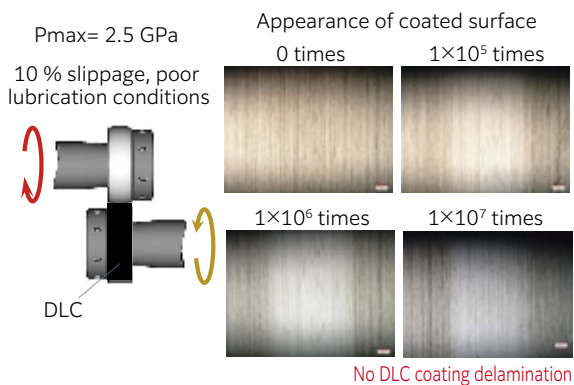
Fig. 8 DLC coating delamination test

(2) Verification of effectiveness

Verification testing was carried out to confirm the superiority of the DLC coating. Testing was done with two types of bearings: a small model bearing and a full scale test bearing.

① Evaluation using a small model bearing
(φ 120 × φ 180 × 60)

A combined radial and axial load was applied, similar to an actual turbine, and wear status of the outer ring load region was compared every 50 hours, under accelerated conditions where the outer ring raceway surface of a standard product flakes at 300 hours **(Fig. 9)**.

Fig. 9 Outer ring raceway after 300 hours

Fig. 10 shows the test results. The wear progression speed of the asymmetrical product was about 2/3 that of the standard product. On the other hand, about 5 μm of wear occurred initially with the DLC coating product, but after that wear did not progress and the results were extremely good.
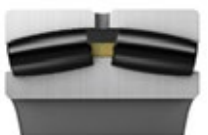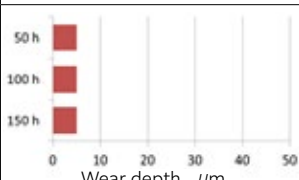
Fig. 10 Test results with model size bearings

② Evaluation using actual-size bearing
(φ 600 × φ 870 × 272)

To accelerate testing, as with the small model bearing, evaluation was done under conditions where the standard product flakes at 720 hours.

Fig. 11 shows the condition of the outer ring raceway surface load region after testing. Flaking is evident on the standard product, but not on the DLC coating product, where the results were extremely good with only 2 μm of wear.
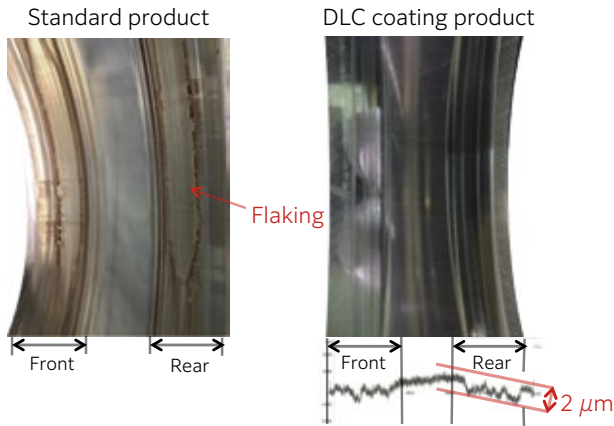
Fig. 11 Test results with full scale bearings

3.3 Proposed specifications of spherical roller bearings

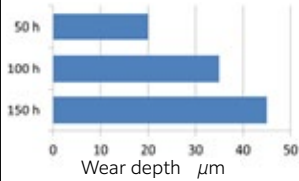In light of the above, **NTN** proposes the following for spherical roller bearings used as the main bearings in wind turbines **(Fig. 12)**.
① Standard design: This type employs asymmetrical rollers, and has a center rib on the inner ring. Structurally, rollers are supported at three points: the inner/outer ring raceway surfaces, and a center rib on the inner ring. This prevents skew[*2] of the rollers, and suppresses slippage between the raceway and rollers.
② DLC coating: This type is based on the standard design, and is used when wear damage needs to be suppressed.
③ Asymmetrical design: This is used when there is a need to extend life (through flaking countermeasures) and reduce turbine size (bearing size reduction).
④ DLC coating + asymmetrical design: This type lowers initial cost by reducing overall size and weight of wind turbines, and can potentially improve reliability and reduce generation costs through more stable operation.
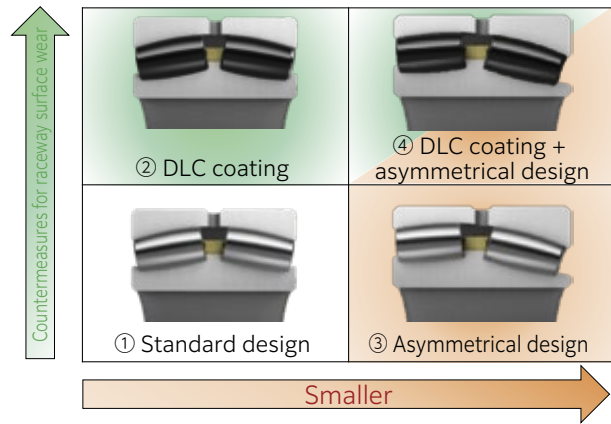
Fig. 12 Lineup of spherical roller bearings for wind turbine main shaft

*2 Skew: Roller inclination over its normal axis of rotation in roller bearings

4. Size reduction of tapered roller bearings

Here we introduce the characteristics and design approaches for size reduction of the back-to-back single row tapered roller bearings **(Fig. 13)** that are being increasingly used in off-shore turbines.

Fig. 13 Single row tapered roller bearing

4.1. Design parameters

Wind loads act on the blades and the weight of the rotor itself act on the main bearing as moment loads **(Fig. 14)**, thus maintaining a large distance between the load centers of the two main bearings in the system is key for reducing the resultant bearing load. By using single row tapered roller bearings in a back-to-back arrangement, the distance between load acting points can be kept large, which enables reduction of bearing size and weight.
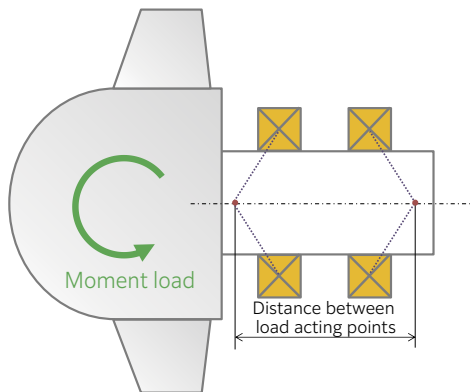
Fig. 14 Relationship between applied load and bearing span

In determining the contact angle and distance between load centers, optimal values must be considered in light of use conditions. Characteristics based on differences in contact angles are presented next.

4.2 Verifying effects due to differences in contact angle

(1) Effects on life

In Example 1, considered in **Fig. 15**, we confirmed the effects when the contact angle was varied only for the axially loaded row. As the contact angle increased, both the equivalent load and bearing capacity decreased, but the capacity decreased less, so life increased.

In Example 2, considered in **Fig. 16**, we verified the effects of the axially loaded row when the contact angle was varied only for the non-axially loaded row. In this case, the results showed that life decreased regardless of the fact that the distance between load centers increased due to the increased contact angle. This is because the induced axial load increased when the contact angle of the non-axially loaded row was increased. This shows that increasing the distance between load centers does not necessarily lead to longer life directly, and that the induced axial load must also be taken into account. That is, increasing the distance between load centers by maximizing the contact angle of the axially loaded row is related to longer life of both bearings.
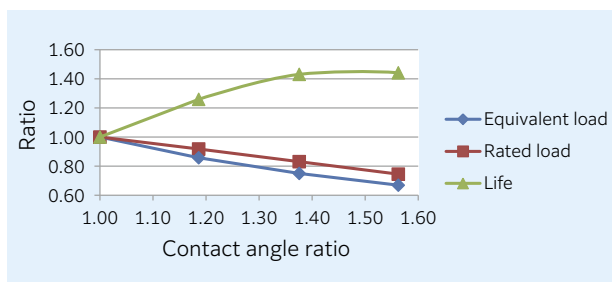
Fig. 15 Example 1 Relationship between contact angle and bearing life for axial load side row
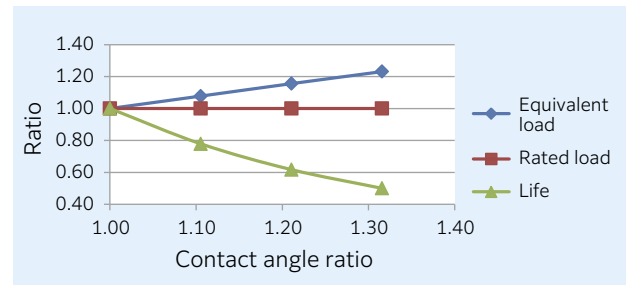
Fig. 16 Example 2 Effect on the axial load side row due to the change in contact angle of non-axial load side row

(2) Relationship of axial setting and life

When the axial setting is 0, as indicated in **Fig. 17**, the larger the contact angle, the longer the bearing life. However, the rate of decrease in life increases as the axial gap decreases (i.e., when preload is increased), and there is a reversal at more than 1,050 μm preload. This is because axial rigidity and resultant applied axial load increases with a larger contact angle.
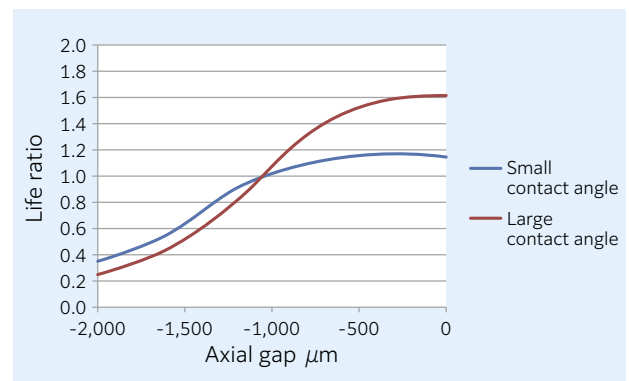
Fig. 17 Effect of axial clearance and bearing life for differing contact angles

(3) Effects of temperature variation on life

With back-to-back single row tapered roller bearings, radial expansion and contraction of the bearing, as well as axial elongation and contraction of the shaft and housing, both affect the axial setting. However, the effect of axial elongation/contraction of the shaft and housing is small, and the effect of axial expansion/contraction of the bearing is dominant. Variation in the axial setting was calculated by taking -1,050 μm where life reverses as a basis, as shown in **Fig. 17**, and assuming the inner ring operating +5 ℃ hotter than the outer ring **(Fig. 18)**. If the contact angle is small, then the rate of decrease in life becomes smaller, as shown in (2), but the amount of change in the axial setting increases, so caution is necessary.
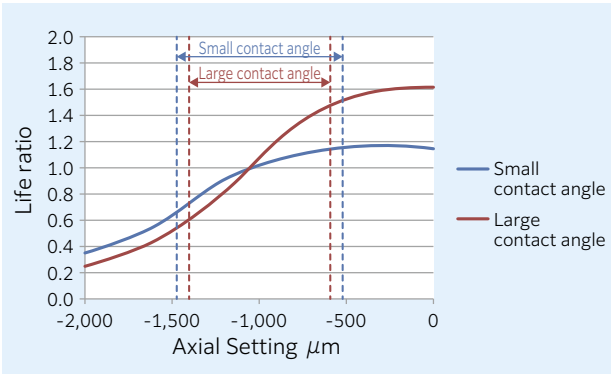
Fig. 18 Effect to bearing life for temperature change

(4) Relationship of aspect ratio and capacity to bearing cross section

As shown in Example 1 considered in **Fig. 15**, life changes with variation in the contact angle, but the aspect ratio[*3] of the bearing cross section may have an effect. As shown in **Fig. 19**, with an aspect ratio of 1.1, that is a cross section that is larger in the radial direction, it is evident that the rate of decrease in bearing capacity when the contact angle is increased from $\alpha 1$ to $\alpha 2$ is smaller than the aspect ratio 0.9. This is because it is easier to achieve increased roller diameter and roller length within the smaller aspect ratio even when the contact angle is increased. On the other hand, if the contact angle is reduced, then decreasing the aspect ratio also makes it easier to achieve increased bearing capacity.

*3 Aspect ratio: Bearing cross section height / Bearing group width

Larger radial cross section (aspect ratio 1.1)
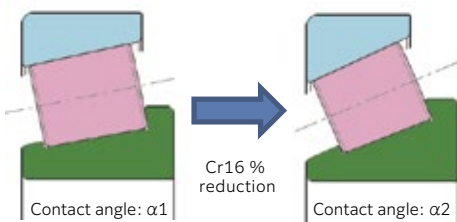
Wider axial cross section (aspect ratio 0.9)
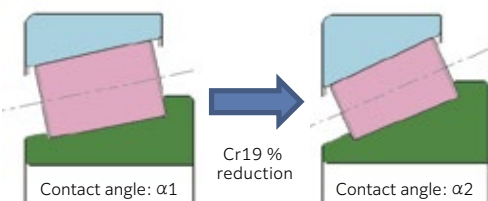
Fig. 19 Relationship between aspect ratio of cross section and load rating

4.3 Summary of effect verification

By increasing the contact angle, it is possible to reduce the radial reaction load, but there is also an increase in the induced axial load, and it is necessary to check effects on life and contact stress. Furthermore, main bearings are initially set into preload, but care must be given to the fact that the applied axial load increases under preload to the extent that axial rigidity increases. Another point for caution is that, when the contact angle is reduced, increased variation in axial setting may result in response to temperature changes.

Design with single row tapered roller bearings must be based on a good understanding of the above characteristics, but in actual practice, selection of the contact angle also varies depending on the permissible bearing size. Therefore, at **NTN**, we will utilize analysis tools and know-how we have acquired through our extensive experience to collaborate with wind turbine manufacturers from an early stage, to provide support to establish drivetrain designs.

5. Summary

This article has introduced the efforts of **NTN** to improve reliability and achieve optimization of main bearings used in wind turbines.

As the size of bearings continue to increase, we will respond by proposing new technologies and new products to help optimize designs and improve reliability, including manufacturing methods, and thereby help broaden adoption of renewable energy in collaboration with wind turbine designers.

References
1) P:Statistical Review of World Energy 2020.
2) Kazumasa Seko, Takashi Yamamoto, "Asymmetrical Spherical Roller Bearings" for Wind Turbine Main Shafts, NTN TECHNICAL REVIEW. No.86, (2018) 96-101.

Photo of authors

Michio HORI
Application Engineering Dept., Industrial Business Headquarters

Yusuke YAMADA
Application Engineering Dept., Industrial Business Headquarters

Product Development of Rolling Bearings for Railway Vehicles

Takashi NISHIKAWA*   Kengo SUZUKI*
Wataru ORITO*   Tsukasa TOYODA**

In order to ensure the safety of railway transportation, it is required to develop bearings for railway vehicles with respect for high reliability of products. Providing bearings to public transportation services such as railway transportation service and contributing to society is significant as corporate activity. **NTN** has been working on development of bearings for railway vehicles for many years. This article introduces our product development activity of bearings for railway vehicles.

1. Introduction

Bearings used in the axles, drive units, and traction motors of railway machinery **(Fig. 1)** are crucial to the overall safety of the vehicle. They are therefore required to meet particularly high quality and reliability standards for an industrial application.

These bearings must have the strength and performance to withstand not only large static loads, but also the elevated dynamic loads associated with operation of the vehicle. The bearings must also withstand continued exposure to extreme temperature environments, humidity, and dust.
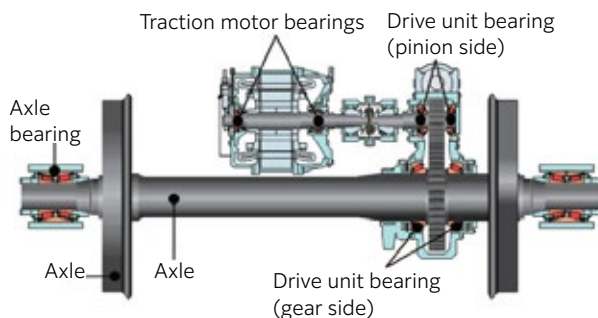
Fig. 1 Railway Bearing Application

To meet these reliability requirements, we at **NTN** have worked for many years to develop high quality bearings for axle, drive unit and traction motor applications. **NTN** is also a leading supplier of railway bearings both inside and outside the country of Japan.

In 2010, **NTN** acquired the International Railway Industry Standard (IRIS)[Note 1] certification, further establishing **NTN** as a leader among Japanese companies in ensuring quality management systems that conform to international standards for manufacturers of railway vehicles bearings.

This article introduces efforts to develop bearings for railway vehicles.

Note 1) The specifics of these provisions were inherited by the International Standard Technical Specification ISO/TS22163 (Railway Quality Management System (RQMS)) in 2017.

2. Technology trends in bearings for railway vehicles and development efforts

2.1 More compact and highly functional axle bearings

Axle bearings for railway applications need to support both the static weight of the vehicle and the dynamic loading created during operation. Double row tapered roller bearings and double row cylindrical roller bearings with outer diameter dimensions of φ 210– φ 250 mm are commonly used for this application and double row tapered roller bearings with grease lubrication are more common today.

To meet the need for higher speeds and longer maintenance cycles, **NTN** has developed and improved special-purpose bearings that employ oil seals to reduce heat generation during operation. Reinforced resin cages and measures to suppress fretting between the inner ring and backing ring[Note 2] are also used.

Note 2) Fretting occurs at the contact surface due to repetitive minute relative displacement of the inner ring and rear cap during axle bearing use. Our patented technology (patent no.: 4060232) suppresses fretting and prevents ingress of wear debris into the bearing by mounting a metal plate with gasket.

*   Application Engineering Dept., Industrial Business Headquarters
**   Product Design Dept., Industrial Business Headquarters

In addition to development aiming at improving basic performance, **NTN** has also developed products to meet the need for compactness and increased functionality in recent years. Examples of these developments include the short-type sealed axle bearing unit and the ceramic coated insulated axle bearing.

2.1.1 Development of short-type sealed axle bearing unit

(1) Background

Shortening the axial dimension of the axle bearing unit makes the structure around the axle box more compact and improves rigidity, making for an effective solution at preventing fretting wear. However, there have been limitations to this approach due to constraints with the oil seal size.

Occasionally this issue is resolved by using a shield plate instead of an oil seal. However, the simpler design of the shield plate often introduces issues with sealing performance.

NTN developed the short-type sealed axle bearing unit to simultaneously achieve good sealing performance while also minimizing the axial dimension of the axle bearing unit for increased fretting resistance. **(Table 1, Fig. 2)**.

(2) Features and specifications
  - More compact, lighter weight
  - Fretting resistance
  - Improved reliability, reduced maintenance costs

Table 1 Specification of short-type sealed axle bearing unit

Item	Specifications
Bearing type	Sealed double row tapered roller bearing
Bearing main dimensions	ϕ 130 × ϕ 240 × 160/160 mm
Basic dynamic load rating	1,040 kN
Basic static load rating	1,870 kN
Axial dimension of bearing unit	Compared with our conventional product　−15 %
Bearing unit weight	Compared with our conventional product　−10 %

Conventional oil seal

Conventional product

15 % reduction

Oil seal with shorter axial direction dimension

Developed product
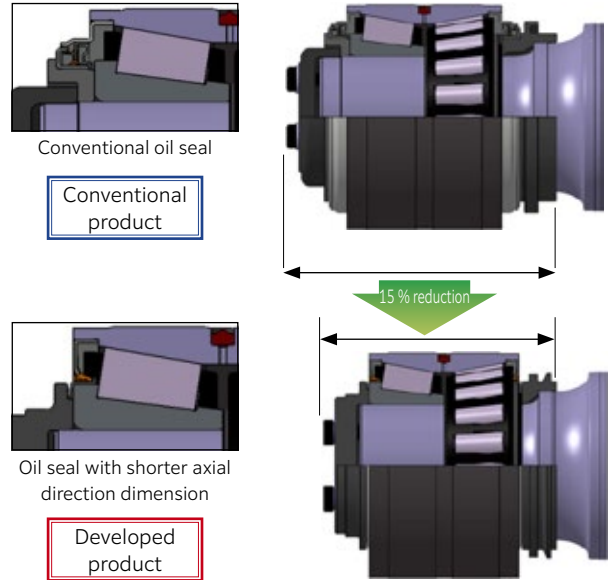
Fig. 2 Short-type sealed axle bearing unit

(3) Evaluation test

(3-1) Bearing rotating test

A durability test was carried out equivalent to running 1.2 million km at 420 km/h. There was no abnormal rise in temperature during testing, and no problems were evident in the bearing or grease condition after testing **(Table 2, Fig. 3)**.

Table 2 Test condition

Item	Conditions
Radial load	91.4 kN (fixed)
Axial load	16.7 kN (5 s load, 25 s no load)
Rotational speed	Max. 2,685 min^{-1} (equivalent to 420 km/h) Forward/reverse rotation (4 h cycle)
Wind cooling speed	10 m/s
Test time	3,429 h (equivalent to 1.2 million km)
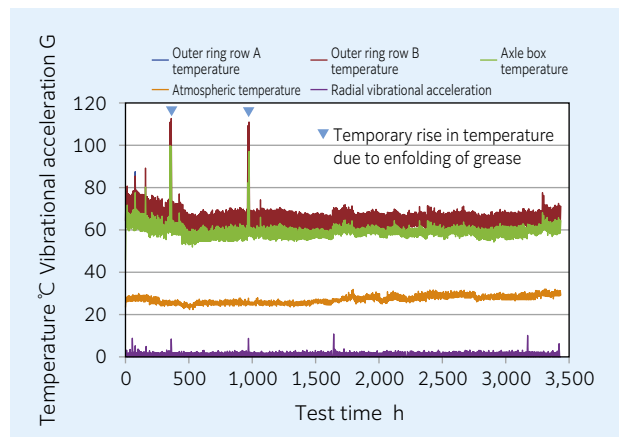
Fig. 3 Bearing rotating test result

(3-2) Test to check sealing performance

A rotational vibration test confirmed that grease sealing performance of the short-type sealed axle unit bearing is superior to the shield plate specifications, and comparable to the conventional product **(Table 3, Fig. 4)**.

Table 3 Test condition

Item	Conditions
Rotational speed	Max. 2,685 min^{-1} (equivalent to 420 km/h)
Vibration frequency	50 Hz
Acceleration	50 – 200 m/s^2 Increased in 50 m/s^2 increments every 24 h

Developed product:
No grease leakage

Conventional product:
No grease leakage

Grease leakage

Shield plate:
Grease leakage occurs

Vertical vibration

Rotation and vibration test
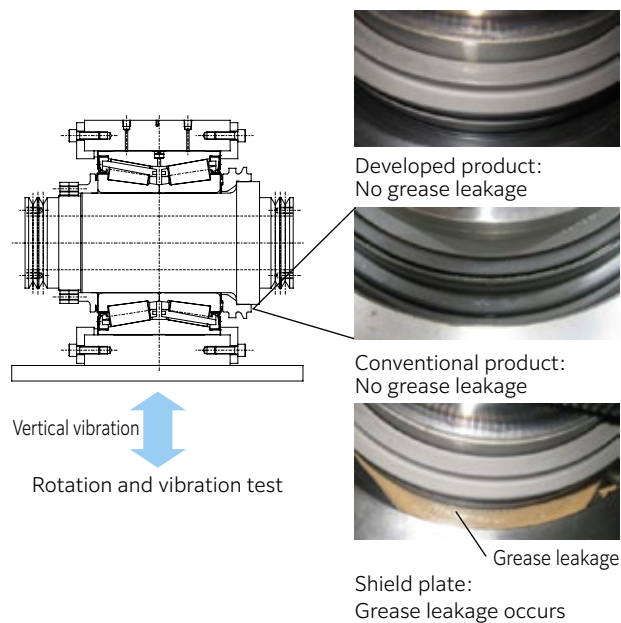
Fig. 4 Sealing test result

2.1.2 Development of ceramic coated insulated axle bearing

(1) Background

Insulation is often employed around the axle bearings in railway vehicles to prevent electrical corrosion, which can cause a multitude of performance issues depending on the specific operating condition. However, the most effective measure for countering electrical corrosion is to insulate the bearing itself. To optimize electrical corrosion prevention in railway applications, **NTN** has worked to develop a ceramic coated insulated axle bearing. **(Table 4, Fig. 5)**

(2) Features and specifications
- Ceramic coating on outer ring
- Prevention of electrical corrosion
- Improved reliability and reduced maintenance cost

Table 4 Specification of ceramic-insulated axle bearing

Item	Specifications
Bearing type	Sealed double row tapered roller bearing
Insulation specifications	Ceramic coating on outer ring
Bearing dimensions	ϕ 135 × ϕ 240 × 140/130 mm
Basic dynamic load rating	770 kN
Basic static load rating	1,270 kN
Insulation resistance	10 M Ω min. (DC500 V)

Ceramic coated insulated outer ring

Thermal sprayed ceramic coating

To counter electrical corrosion:
Prevents passage of current

Oil seal
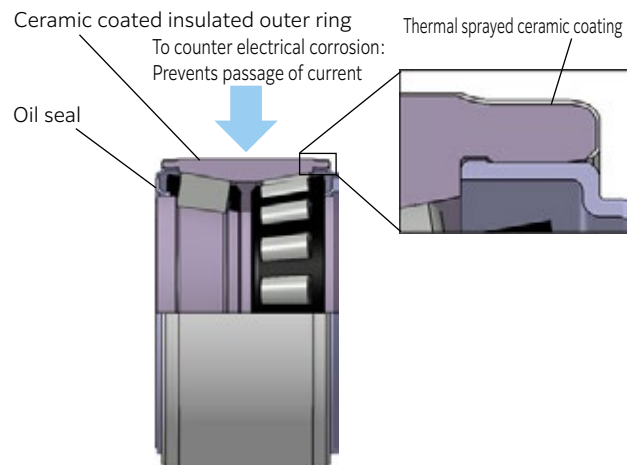
Fig. 5 Ceramic-insulated axle bearing

(3) Evaluation test

A strength evaluation was carried out of the ceramic coating under load conditions equivalent to actual use conditions. No cracking, chipping or other damage to the coating was evident after testing, and there were confirmed to be no problems with insulation resistance **(Table 5, Fig. 6)**.

Table 5 Test condition

Item	Conditions
Static strength test	Radial load: Max. 110 kN
Fatigue strength test	Radial load: 28.6 – 54.3 kN Number of loading cycles: 10^7

Load

Housing

Bearing

Axle

Test method

Outer surface of ceramic coated insulated outer ring (Photo taken with ring placed in the vertical axis direction)

Result of post-test coating penetrant inspection

Fig. 6 Strength test result of ceramic-insulation coating

2.2 Improved reliability of resin-insulated bearing for traction motor

In the traction motor, NU type cylindrical roller bearings are used on the drive side, and deep groove ball bearings are used on the counter-drive side. These bearings support the rotor.

The drive and counter-drive side bearings are both typically grease lubricated with an outer diameter of φ 120 – φ 170 mm.

To prevent electrical corrosion within these induction motors, **NTN** has developed a ceramic-insulated bearing in which the ceramic is plasma sprayed on the outer ring. **NTN** has also developed a resin-insulated bearing made with injection molded reinforced resin **(Table 6, Fig. 7)**. The former is mainly used in Shinkansen (bullet train) vehicles, while the latter is mainly used for conventional railroad lines.

To better manage changes in the environmental conditions of traction motor bearings which have occurred in recent years, **NTN** has also been working to develop resin-insulated bearings with improved heat dissipation.

2.2.1 Development of resin-insulated bearings

(1) Background

To reduce lifecycle cost, railway manufacturers are increasingly looking for methods to lengthen the maintenance cycle of traction motors. The maintenance cycle of a traction motor is determined mainly by the lubrication life of the bearing. To extend the lubrication life, it is essential to limit heat generation within the bearing during operation. Railway manufacturers are also increasingly adopting fully-closed traction motors[1], which typically expose the traction motor bearings to more severe temperatures than the standard open motor type.

In extending the maintenance cycle and developing applications for fully-closed traction motors, improving the heat dissipation of resin coatings is vital to achieve higher reliability.

(2) Features and specifications
  - Improvement of heat dissipation of injection molded resin coating for outer rings
  - Improved reliability and reduced maintenance costs

Table 6 Specification of resin-insulated bearing

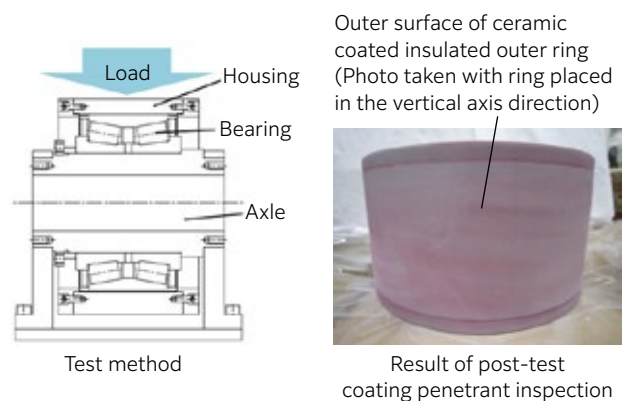| Item	Specifications	
Bearing type	Cylindrical roller bearing	Deep groove ball bearing
Insulation specifications	Injection molded resin coating of outer ring	
Bearing dimensions	NU214 φ 70 × φ 125 mm	6311 φ 55 × φ 120 mm
Basic dynamic load rating	83.5 kN	71.5 kN
Basic static load rating	95 kN	45 kN
Insulation resistance	100 M Ω min. (DC500 V)	

Cylindrical roller bearing Deep groove ball bearing

Injection molded resin coating
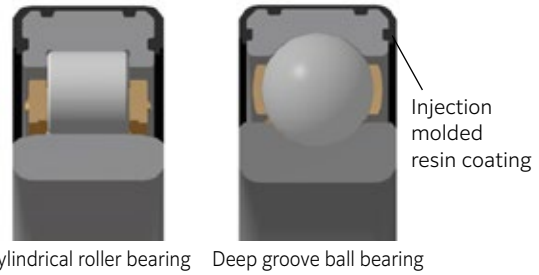
Fig. 7 Resin-insulated bearing

(3) Evaluation test

(3-1) Outer ring temperature

Evaluation was carried out by heating the raceway of the resin-insulated outer ring with a heater to simulate elevated temperatures during bearing use, and then measuring the outer ring base material outer surface temperature **(Table 7)**.

The test results showed that changes in the material of the resin coating resulted in a drop of about 5 ℃ in the outer ring base material outer surface temperature when compared to the conventional product **(Fig. 8)**.

Table 7 Test condition

Item	Conditions
Prototype	Resin-insulated outer ring (NU214)
Heating method	Heating of outer ring raceway using special-purpose jig with cartridge heater
Heating temperature	120 ℃ (special-purpose jig part)

(3-2) Change in bolt fastening force

The outer ring of the resin-insulated bearing is compressed in the axial direction due to the bolt fastening force of the traction motor's bearing box and end cap. Therefore, a drop in bolt fastening force occurs due to deformation in the film thickness of the resin coating on the outer ring.

We incorporated the developed resin-insulated outer ring and conventional product into a test jig, fastened the bolt of the test jig with the specified fastening force, and applied compressive force in the thickness direction to the resin coating width surface. The raceway was heated to 120 ℃ × 100 h, and cooled to room temperature, and the drop in bolt fastening force was evaluated **(Table 8)**.

The test results showed that the developed product was more effective at reducing change in bolt fastening force by roughly 20 % compared to the conventional product **(Fig. 9)**.

Table 8 Test condition

Item	Conditions
Prototype	Resin-insulated outer ring (NU214)
Bolt fastening	4-M10, axial force 18 kN/bolt
Heating method	Heating of outer ring raceway using special-purpose jig with cartridge heater
Heating temperature	120 ℃ (special-purpose jig part)
Test time	100 h
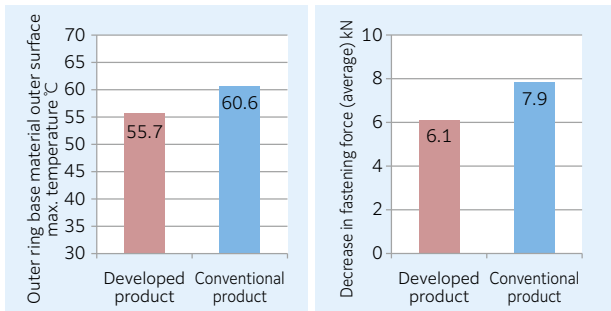
Fig. 8 Temperature of outer ring

Fig. 9 Change in bolt fastening force

2.3 Improved seizure resistance performance of drive unit bearings

It is typical for tapered roller bearings to be arranged face-to-face in a parallel Cardan drive unit **(Fig. 10)**.

The pinion-side bearing supports the pinion axle weight, part of the coupler weight, and the gear engagement load. The gear bearing supports part of the gearbox weight and the gear engagement load.

In terms of main bearing dimensions, the outer diameters of the pinion bearing and gear bearing are, respectively, φ 150 – φ 180 mm and φ 280 – φ 330 mm, and lubricating oil is supplied to the bearing by gear rotation.

In recent years, drive units using cylindrical roller bearings have also been developed[2)-4)], but the major bearing type is still tapered roller bearings. With this type, an axial load acts on the tapered roller bearing, and seizure resistance performance of the pinion-side bearing is especially important.

The next section introduces efforts to improve the seizure resistance performance of the pinion-side tapered roller bearing in low temperature environments.

2.3.1 Improved seizure resistance performance of tapered roller bearings for drive units in low temperature environments

(1) Background

While some research has been done on the effects of the bearing axial clearance and surrounding temperature have on the rise in bearing temperature in connection with seizure of the pinion-side bearing in low temperature environments[5)], there have been no examples of observing the status inside a drive unit and measuring bearing load under low temperature conditions. Thus, we improved the product by observing the state inside the drive unit, and measuring the bearing load.

(2) Internal observation of drive unit

The upper cap of the drive unit was switched to one made of acrylic resin, and we took a video in order to observe the situation inside the drive unit at low temperature up to seizure of the pinion-side bearing **(Table 9)**.
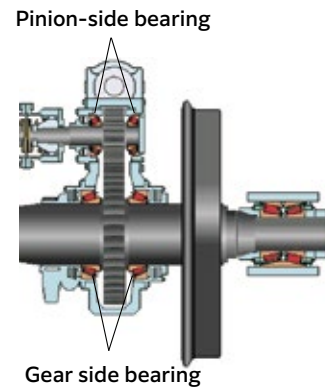
Fig. 10 Bearing arrangement in driving-unit

Table 9 Test condition

Item	Conditions
Test bearing	Drive unit pinion-side tapered roller bearing
Atmospheric temperature	-15 ℃
Maximum rotational speed	5,772 min⁻¹
Lubricating oil	Lubricating oil for drive unit
Axial gap	60 % of design value (to reproduce seizure)

[Results of observing situation inside the drive unit in a low-temperature environment **(Fig. 11)**]

① At startup, high-viscosity lubricating oil brought up by the gear is supplied to the pinion engagement section, and some of that is supplied to the pinion-side bearing.

② After that, viscosity of the lubricating oil decreases with rising temperature, and the lubricating oil deposited on the walls inside the drive unit flows along the inner walls due to the flow of air inside the unit.

③ Immediately before the pinion-side bearing seizes, the inside of the drive unit gradually clouds up due to lubricating oil and the pinion momentarily gives off sparks.
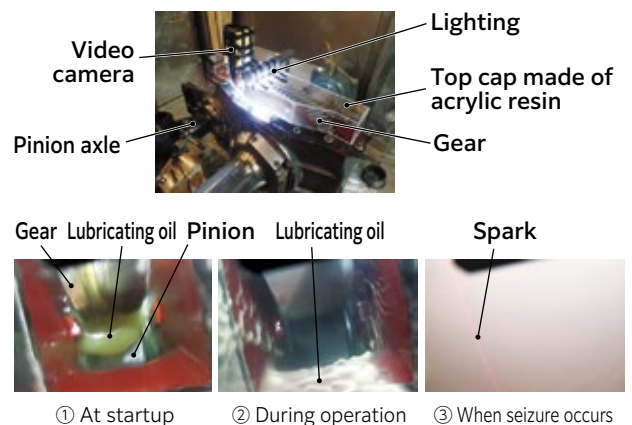
① At startup ② During operation ③ When seizure occurs

Fig. 11 Internal state of driving-unit in low-temp. environment

(3) Results of measuring axial load

The axial load of the pinion-side bearing was measured in order to understand the process up to seizure of the pinion-side bearing. The measurement results **(Fig. 12)** revealed a mechanism where, after starting from a low-temperature condition, the axial clearance disappeared before long due to the difference in thermal expansion of the bearing inner ring, pinion axle, and gearbox. After a few minutes of operation, the axial load increased, resulting in seizure. It was also confirmed that an axial load as high as 150–200 kN acts on the pinion-side gear when seizure occurs.
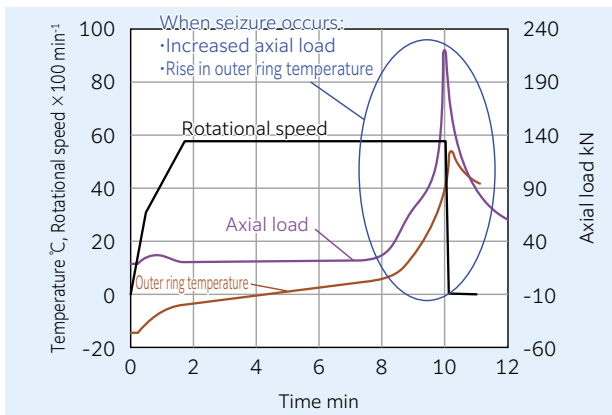
Fig. 12 Bearing temperature and axial load

(4) Effectiveness of countermeasure design

To improve seizure resistance performance of the tapered roller bearing for drive units in low-temperature environments, it is effective to improve seizure resistance strength of the roller large end face and the inner ring rib surface. Suppressing the rise in temperature is also important to limit the reduction in the axial clearance. An improvement effect was evident in comparative testing of the conventional product and the improved product by incorporating these countermeasures **(Fig. 13)**.
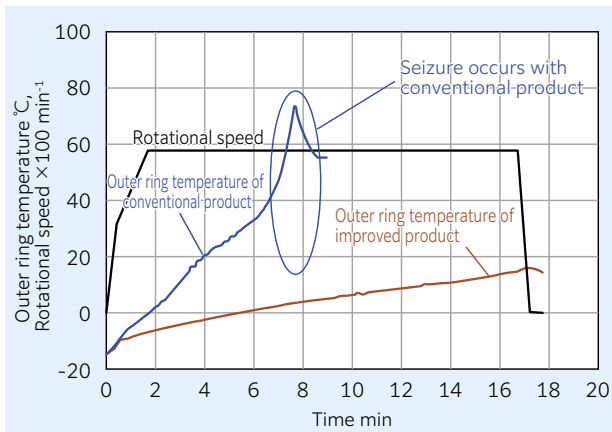
Fig. 13 Start-up test result in low-temp. environment

3. Summary

This article has introduced efforts to develop bearings for railway vehicles at **NTN**. Development of bearings for railway vehicles often proceeds in close collaboration with development of vehicles and equipment. The examples presented in this article are some of **NTN**'s development activities for railway vehicle bearings.

Contributing to society by developing and providing bearings for public transportation services such as railway transportation is significant as a corporate activity. Going forward, we will continue active efforts to develop technology and products.

References

1) Toyo Denki Seizo 100-Year History Editorial Committee, A One-Hundred Year History of Toyo Denki Seizo, Toyo Denki Seizo K.K. (2018) 234-235.
2) Emiko Cho, Ken Iwanami, Fumihiko Suzuki, Ryohei Shimamune, Development of Double Helical Gear Driving Device, JR EAST Technical Review, No.53 (2015) 29-32.
3) Hiroshi Ono, Satoshi Hayashi, Technology Trends in Gearing for High-Speed Railways, THE TRIBOLOGY, 2017.5, (2017) 40-42.
4) Takafumi Nagatomo, Railway Vehicle Bearings and Related Technology Trends, Tribologist, Vol. 63, No. 2 (2018) 100-105.
5) Ken Takahashi, Takafumi Nagatomo, Behavior of Bearing Clearance in Starting Gear Units of Railway Vehicles, Japan Society of Mechanical Engineers, 2019 Conference Proceedings, S11320.

Photo of authors

Takashi NISHIKAWA

Application Engineering Dept.,
Industrial Business
Headquarters

Kengo SUZUKI

Application Engineering Dept.,
Industrial Business
Headquarters

Wataru ORITO

Application Engineering Dept.,
Industrial Business
Headquarters

Tsukasa TOYODA

Product Design Dept.,
Industrial Business
Headquarters

Approach to Development of Robotic Joint-Related Products

Hiromichi KOKUMAI*   Hideaki TANAKA**
Kosuke SUZUKI***   Yuichiro KAWAKAMI***

In recent years, the robot industry has been expanding due to the market demand for improved productivity and labor savings. In particular, those represented by smaller size robots, typically collaborative robots, are expected to grow rapidly in the future. For various devices incorporated into robot's joints, such as reduction gears and rotary encoders, many bearings are used. This paper outlines **NTN**'s latest developments for these applications.

1. Introduction

In recent years, robot replacements for human workers have become popular worldwide as a way to resolve labor shortages and stabilize product quality. There has been particularly active capital investment in the automotive and electronic components markets due to increased demand relating to IoT (Internet of Things). The robot market is also expanding in Japan due to further growth in demand, due to labor shortages brought on by the decreasing birthrate and aging population, and labor-saving driven by surging personnel costs in developing countries.

Typical examples of robots include: industrial robots installed on manufacturing lines for welding, painting, transfer, and other tasks; field robots that work outdoors at locations such as farms, at sea, and disaster sites; and service robots that interact with people in medical and nursing care settings, and the home and workplace. There is expected to be particularly rapid dissemination of compact robots such as collaborative robots that work with human workers, and service robots to cope with diversification of services.

NTN has developed numerous bearing and sensor related products as mechanical components for use in robotic joints[1)-5)]. Here we will introduce our efforts to develop products for compact robots that will see market growth going forward.

2. Robot market needs

In addition to the basic function of robots—grasping objects at determined positions and working accurately—recently, market needs have been growing in the following areas:

① Increasing productivity by reducing tact time (higher speed)
② Improved positioning accuracy and repeatability during work transfer (higher precision)
③ Simplification of teaching (improved operability)
④ Securing work space by reducing the footprint of robots (greater compactness)
⑤ Improved line operation rate by lengthening maintenance intervals (improved reliability and maintainability)

3. Robot structure and joint mechanisms

Vertical articulating robots which perform the same movements as the human arm, from the shoulder to the wrist, are one typical type of robot **(Fig. 1)**. These robots need to transfer heavy objects at high speed to a determined position with high accuracy. This requires not only driving force and rigidity of each joint, but also accurate positioning control. Therefore, high-rigidity precision reduction gears with high torque density are used at joint locations, and positioning is performed through feedback control using angle detection by rotary encoders **(Fig. 2)**.

In compact robots, it is essential to reduce the size and weight of these joint mechanisms, and strain wave gearing and lightweight, compact rotary encoders are used as compact precision reducers (outer diameter φ 100 mm or less).

NTN is working to develop products such as bearings for use in rotational supports of strain wave gearing and multi-track magnetic rings enabling detection of absolute angle and rotation speed.

*   Application Engineering Dept., Industrial Business Headquarters
**   Robotics Sensing Engineering Dept., Industrial Business Headquarters
*** Product Design Dept., Industrial Business Headquarters
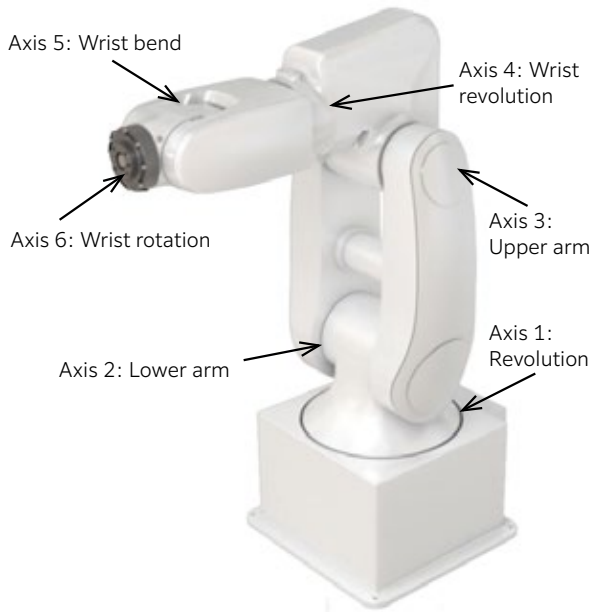
Fig. 1 6 axes articulating robot
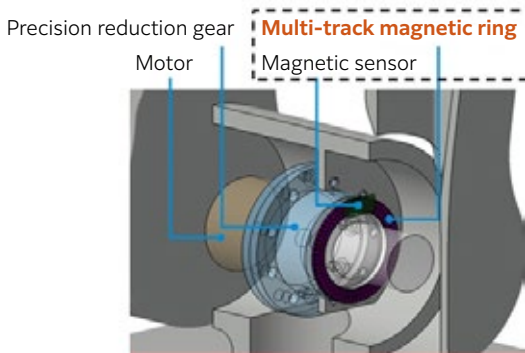
Fig. 2 Structure of robotic joint part
(2nd axis: Lower arm)

4. Development of bearings for strain wave gearing

4.1 Points where bearings are used in strain wave gearing

Fig. 3 shows a sample schematic diagram of the structure of strain wave gearing (unit type) that can amplify output torque of a servomotor (reduce speed) and apply a moment load. A thin section elastic ball bearing (which plays the role of the wave generating mechanism) and cross roller bearing (which supports the moment load on the output side) are used in this reducer.

Now the operating principle of this reduction gear will be explained. It consists of a thin section elastic toothed gear (external gear) made of a thin, elastic metal ring with gear teeth. It incorporates a thin, elastic ball bearing into which an oval shaft is inserted. The elastic toothed gear is in contact with the thick, rigid internal gear and the major axis of the oval. This provides a unique reducing mechanism cleverly utilizing the elastic deformation of the

external gear. The operating principle is shown in **Fig. 4**. If the internal gear is fixed while the oval shaft rotates clockwise once, the external gear rotates counterclockwise by the difference in the number of teeth between the external gear and the internal gear (e.g. the external gear has two less teeth) which is extracted as the output. Here, the diagram at right in **Fig. 4** shows the situation where the oval shaft has rotated through half a turn and the external gear has moved counterclockwise by one tooth. This reducer has a concentric and simple structure with compact form factor and provides a significant reduction ratio of 1/30 to 1/320. Since both teeth are simultaneously engaged like wedges, providing a high contact ratio without backlash, the reducer is characterized by averaged gear errors, high angle transmission accuracy, and high torque capacity. Also, a cross roller bearing is used for the main bearing supporting output rotation of the external gear, and since this bearing is compact and has high moment stiffness, it also ensures the positioning accuracy, which is the most important characteristic for a robot.

Fig. 3 Structure of strain wave gearing (Unit type)

Fig. 4 Operating principle of strain wave gearing

The highly-robust, specialized design of the thin section elastic ball bearing and cross roller bearing is essential to maintain stable performance and operation of the reducer and achieve high reliability.

4.2 Thin section elastic ball bearing

The engaging reaction force from the gear is supported in the oval deformed state so that the thin section elastic ball bearing used in strain wave gearing provides torque transmission as a wave generating mechanism. At this time, the inner ring engages tightly with the oval shaft, and rotates while being deformed into an oval, and the deformed state of the outer ring repeatedly changes via the rolling element. In addition to the preload due to this oval deformation, reaction from the gear during torque transmission also acts on the inside of the bearing. In other words, a thin section elastic ball bearing needs to have the following characteristics to accurately transmit high torque over the long term.

① Longer life through high load capacity design (improved rolling fatigue life)
② Flexibility in response to elastic deformation of the inner/outer raceway
③ Improved fatigue strength against cracking of the outer ring

To satisfy these conditions, the basic design uses a larger rolling element, thinner inner and outer rings, and an increased rolling element filling rate. **Table 1** shows a comparison of cross-section form with the 68-series standard product, a typical thin section bearing series. The thin section elastic ball bearing has thinner inner and outer rings than the 68-series. The rolling element ratio with respect to the cross section (cross section ratio) is roughly 1.2 times larger, and the load capacity is about 1.4 times larger. This design allows realization of both elastic deformation and higher load capacity of the inner and outer raceway.

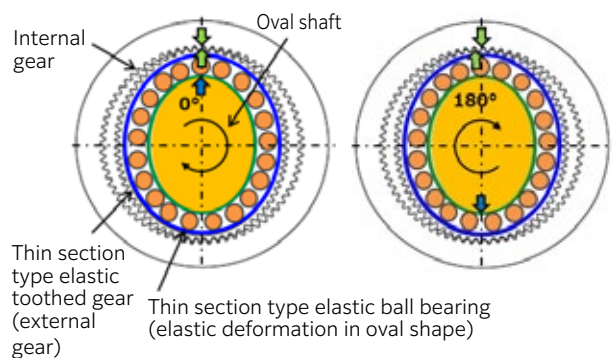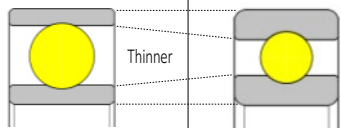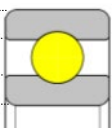**Table 1** Features of thin section elastic ball bearing

Schematic diagram	Thin section elastic ball bearing	68-series
Cross section ratio	1.2	1
Load capacity ratio	1.4	1

* Cross section ratio, load capacity ratio: Ratio taking 68-series to be 1

Here, we strive for ① "Longer life through high load capacity design (improved rolling fatigue life)" and to ensure tensile and compressive stress amplitude are applied due to repeated elastic deformation of the outer ring via the rolling element during operation. We must take into account not only rolling fatigue life, but also fatigue strength against cracking of the outer ring. **Fig. 5** shows an example of outer ring stress analysis. Analysis was done using a 1/4 cut model of the outer ring, while taking into account elliptical deformation and external load. On the major axis side, the outer ring is pushed to the diameter expansion side via the rolling element, and thus tensile stress is produced at the outer ring outer diameter. On the minor axis side, the rolling

element is unloaded and contracts in diameter, and thus compressive stress is produced at the outer ring outer diameter. Furthermore, during operation the deformed inner ring rotates, and the stress distribution of the outer ring changes moment to moment in the rotation direction. The major and minor axes are alternately interchanged, and thus it is evident that repeated tensile and compressive stress are applied to the outer ring outer diameter. **NTN** has achieved ① Longer life through high load capacity design (improved rolling fatigue life), ② Flexibility in response to elastic deformation of the inner/outer raceway, and ③ Improved fatigue strength against cracking of the outer ring, by developing an understanding of the correct stress situation through this type of stress analysis, and thereby selecting the optimal thickness for suppressing stress amplitude, and optimizing the corner shape design to prevent stress concentration.
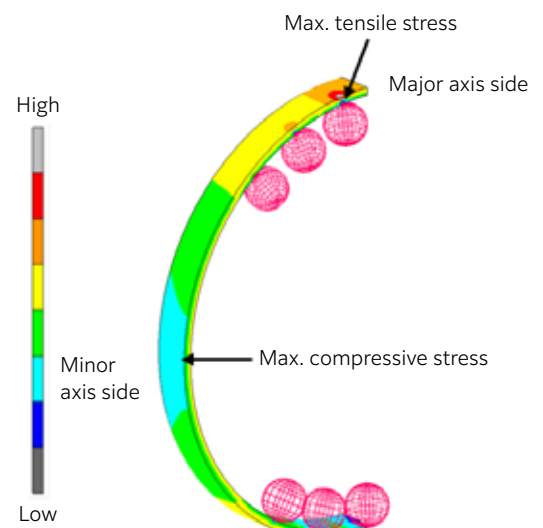
Fig. 5 Outer race stress analysis of thin section elastic ball bearing

Also, in a thin section elastic ball bearing, the inner and outer rings are extremely thin, and thus one issue for manufacturing is how to suppress deformation during machining and heat treatment. However, we have commercialized a thin section type elastic ball bearing through thin machining technology previously cultivated by **NTN** and optimization of heat treatment conditions **(Fig. 6)**.

Fig. 6 Cut model of thin section elastic ball bearing

4.3 Cross roller bearing

Main bearings used in strain wave gearing must directly support the moment load acting on a robotic joint, and, even when holding a large moment load, they must have high moment stiffness and support rotation with long-term stability while suppressing axis inclination and bearing internal stress (contact stress). Therefore, the bearing must have ① greater compactness, ② higher moment stiffness, and ③ longer life. To achieve these functions, a cross roller bearing is used which has no cage, and a larger number of rollers arranged with alternating contact angles **(Fig. 7)**.
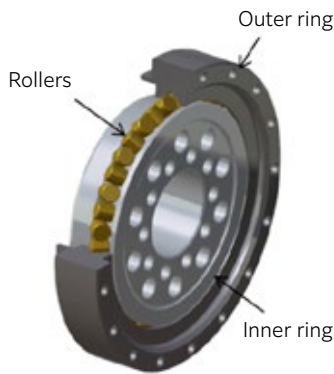
Fig. 7 Structure of cross roller bearing

Table 2 shows a comparison when tapered roller bearings and deep groove ball bearings are used, as typical bearing types other than a cross roller bearing, for the main bearing of strain wave gearing. Tapered roller bearings have outstanding moment stiffness and load capacity, but use of two rows is a reqirement for supporting a moment load in both directions. This results in issues in terms of compactness. Deep groove ball bearings are compact, but there are issues in terms of moment stiffness and load capacity. Thus, the cross roller bearing is the most functional for this application.

Table 2 Comparison of bearing types for strain wave gearing main shafts

Type	Cross roller bearing	Tapered roller bearing	Deep groove ball bearing
① Compact	◯	×	◯
② High moment stiffness	◯	◯	×
③ High load capacity (long life)	◯	◯	×

To achieve ② "high moment stiffness" with a cross roller bearing, the design must increase internal preload, and thus the bearing internal gap is set to a negative gap (preload). On the other hand, increasing preload involves an increase in contact stress, and thus reduction in service life must be considered. **Fig. 8**

shows the relationship of moment stiffness and life to preload. With increasing preload, there is also an increase in moment stiffness. Life, on the other hand, tends to increase in the low preload region due to suppression of preload loss in response to an external load. In the high preload region, life tends to decrease due to an increase in contact stress. **NTN** has achieved: ① greater compactness while simultaneously realizing ② higher moment stiffness and ③ longer service life by setting the optimal preload range.
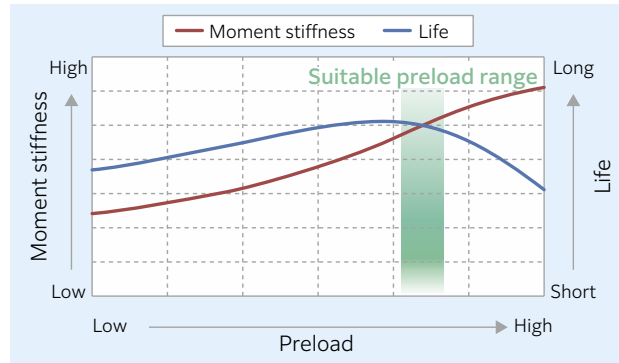
Fig. 8 Moment stiffness and lifetime at preload for cross roller bearing

5. Development of multi-track magnetic ring for rotary encoders

5.1 Application of multi-track magnetic rings to robotic joints

To achieve accurate positioning control of robots, it is necessary to detect the rotation angle, rotation direction, and rotation speed on the output side of the motor which drives the joint with high accuracy. That output is used for feedback control.

Rotary encoders are broadly divided into two types: optical and magnetic. The optical type has high position detection accuracy and resolution, but has low environmental resistance because it is affected by aspects of the ambient environment, such as temperature variation, dust, and oil. The magnetic type, on the other hand, is highly resistant to environmental aspects, and can be used in ordinary work environments.

NTN has developed a multi-track magnetic ring for use with absolute angle detection type rotary encoders[3] **(Fig. 9)**.

Fig. 9 Multi Track Magnetic Ring

This multi-track magnetic ring uses thin, press-formed core metal, and is hollow with a large diameter. Therefore, it is ideal for robots whose wiring passes through hollow shafts such as joints, and helps to save space. **Fig. 10** shows an example using multi-track magnetic rings and iC-MU[6] series sensor ICs at robotic joints.
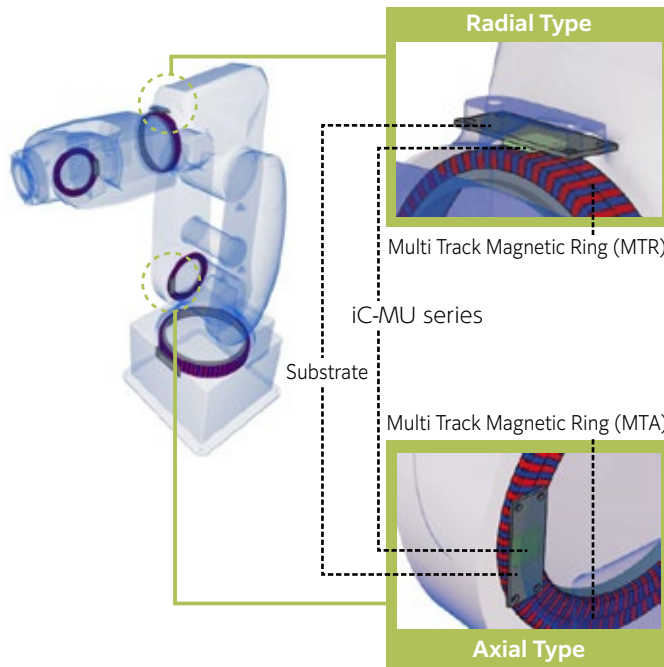
Fig. 10 Application example of Multi Track Magnetic Ring in robotic joint

5.2 Multi-track magnetic rings

The multi-track magnetic rings developed at **NTN** consist of different numbers of magnetic poles arranged in two tracks, and we have realized high-accuracy magnetization by accumulating magnetizing technology for the magnetic rings used in bearings with rotational sensors.

The iC-MU **(Fig. 11)** used in a set with a multi-track magnetic ring provides a Hall element and signal processing circuit in a single package. It reads the phase difference of the magnetic poles in the two tracks with different numbers of magnetic poles, and can detect the absolute angle by internally calculating. Using parameter setting inside the iC-MU, it is also possible to generate highly-divided output up to a maximum of 20 bits (resolution: approx. 0.00034°). **Fig. 12** shows the results of measuring absolute angle error under ideal conditions, where the relative positional deviation between the multi-track magnetic ring and iC-MU is minimal. An angle error of ± 0.025° is achieved, although this is only a reference measuring result.

The multi-track magnetic ring introduced in this article is the OFF-AXIS type, in which the inner diameter part is fixed to the axis outer diameter part. **NTN** has also commercialized an ON-AXIS type angle sensor unit, in which a magnet is fastened to the axis end[4]. Also, as rotation detection technology and application products, **NTN** has commercialized bearings with rotational sensors[5] **(Fig. 13)**, hub bearings with sensors, and other products.

Fig. 11 Image of Combination of iC-MU and Multi Track Magnetic Ring
(Conceptual illustration, provided by: iC-Haus GmbH)

Fig. 13 Integrated Rotation Sensor Bearing
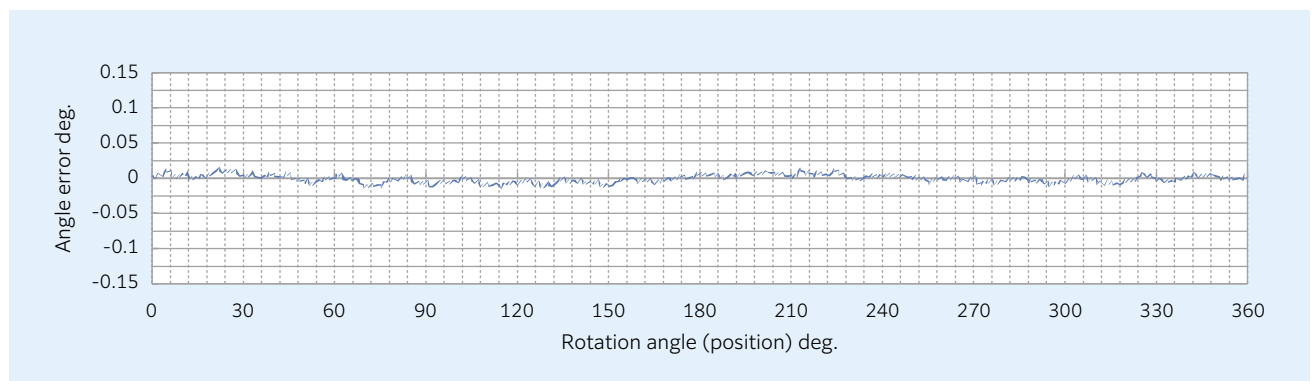
Fig. 12 Angular accuracy measurement result when combining the Multi Track Magnetic Ring and dedicated iC-MU

5.3 Developing a multi-track magnetic ring series

After starting mass production of multi-track magnetic rings, first of the radial type with 64/63 polar pairs (inner diameter 44 mm, outer diameter 51.5 mm, width 8.2 mm, weight 10.7 g), an axial type was added with 64/63 polar pairs. **NTN** has also developed a compact type with 32/31 polar pairs (MTR32 and MTA32) **(Fig. 14)** with an eye toward non-robot applications, such as electric tools and compact motors to support self-driving automobiles. To meet market needs, **NTN** is developing a series of multi-track magnetic rings with the model names shown in **Table 3**.

Going forward, we will consider marketing an ultra-compact type with 16/15 polar pairs and a large type with 128/127 polar pairs to meet user needs.
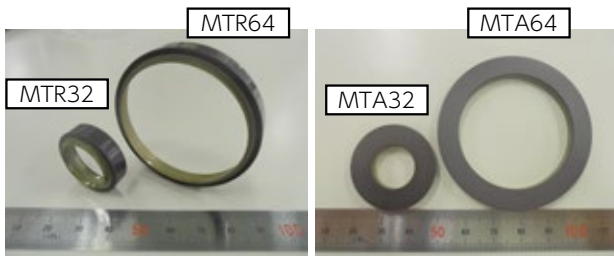
Fig. 14 Comparison of 64/63 pole pairs and small size 32/31 pole pairs

6. Summary

NTN is developing products applicable to robotic joints, and this article has introduced those efforts. Going forward, needs for compact robots are expected to diversify due to expansion of the service field and diversification of collaborative work with people, and product development will be needed to cover these new needs.

NTN will keep a close eye on industry trends, and continually move forward with product development suited to market needs.

References

1) Makoto Oebisu, Hiromichi Kokumai, Yasuyoshi Hayashi, Masato Tsujihashi, Technical Trend and Features of the Bearing for Robot, NTN TECHNICAL REVIEW, No.86, (2018) 34- 39.
2) Hiromichi Kokumai, Technology Trends in Robot Bearings, THE TRIBOLOGY, No.11, (2019.11) 12-14.
3) Takashi Koike, Yasuyuki Fukushima, Yusuke Shibuya, Hiroyoshi Itou, Development of Multi Track Magnetic Ring for High Accuracy Absolute Angle Detection, NTN TECHNICAL REVIEW, No.86, (2018) 45-49.
4) Shoji Itomi, Hiroyoshi Itou, NTN Sensor Units for Construction Machine, NTN TECHNICAL REVIEW, No. 76, (2008) 118-125.
5) Hiroyoshi Itou, Takashi Koike, Bearings with Rotational Sensors, NTN TECHNICAL REVIEW, No. 69, (2001) 108-116.
6) iC-Haus GmbH, iC-MU off-axis nonius encoder with integrated hall sensors.

Table 3 NTN Multi Track Magnetic Ring corresponding to sensor IC (iC-MU series) of iC-Haus

	Pole Pair Number (Main Track / Sub Track)	Pole Pitch of Main Track (mm)		
		1.28	1.50	2.00
Multi Track Magnetic Ring	32/31	MTR32 MTA32	MTR32-1 MTA32-1	MTR32-2 MTA32-2
	64/63	MTR64 MTA64	MTR64-1 MTA64-1	MTR64-2 MTA64-2
Magnetic Sensor made by iC-Haus		iC-MU	iC-MU150	iC-MU200

Photo of authors

Hiromichi KOKUMAI

Application Engineering Dept., Industrial Business Headquarters

Hideaki TANAKA

Robotics Sensing Engineering Dept., Industrial Business Headquarters

Kosuke SUZUKI

Product Design Dept., Industrial Business Headquarters

Yuichiro KAWAKAMI

Product Design Dept., Industrial Business Headquarters

Development of Sensor Integrated Bearing Unit for Machine Tool Spindles

Shohei HASHIZUME* Yusuke SHIBUYA**
Daichi KONDO** Yohei YAMAMOTO***
Hiroyuki IWANAGA****

Machine tools require not only fundamental features like high speed, high rigidity and super precision capabilities, but also condition monitoring and "Connected Industries" related technology. **NTN** developed the "Sensor Integrated Bearing Unit for Machine Tool Spindles" in 2018 and secured many positive responses from the manufacturing industry. **NTN** has recently added load detection function and wireless system to the unit, based on the additional requirements. This report introduces the features, structure, and performance of the unit.

1. Introduction

Machine tools support monozukuri in various types of industry, including automotive, aircraft, medical equipment and IT, and the market demand for them is becoming increasingly sophisticated and diversified[1)2)]. Particularly in recent years, the diminishing working population has created a need to improve production efficiency. There is an increased need to detect abnormalities at an early stage to prevent damage to the spindle and spindle bearing, which are key components within machine tools, and to prevent such factors as downtime and spindle replacement associated with this damage. Generally, a sensor is installed on the outer diameter surface of the spindle to detect any abnormalities as a method to measure the temperature and vibration. However, there is a problem with this method in that the sensor is easy to install but the measuring position is far from the bearing raceway surface, which makes it difficult to detect any abnormalities at an early stage such as sudden temperature rises in the bearing.

To solve this problem **NTN** has integrated sensors in the spacer, a bearing unit component, to perform sensing around the bearing raceway surface. This has allowed us to develop a "Sensor Integrated Bearing Unit" for Machine Tool Spindles[3)] that enables advanced condition monitoring. This product was displayed as a reference exhibit at the 29th Japan International Machine Tool Fair (JIMTOF2018) held in 2018. As a result, we received a great deal of praise from the market for this product and also received many requests to add a load inspection function and wireless technology, and so proceeded with developing these items. The developed product

(hereafter, this bearing unit) can be applied to lathes and machining centers as shown in **Fig. 1**, and this bearing unit's features, structure, and performance test results are introduced below.
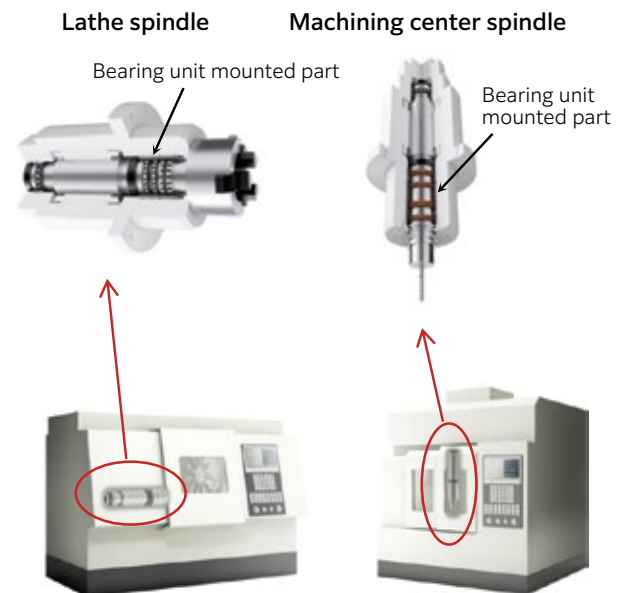

Fig. 1 Machine tools and spindles
(Left : Lathe, Right : Machining center)

*   Application Engineering Dept., Industrial Business Headquarters
**   New Product Development R&D Center
***   Product Design Dept., Industrial Business Headquarters
**** Robotics Sensing Engineering Dept., Industrial Business Headquarters

2. Structure and Function of the Sensor Integrated Bearing Unit

This bearing unit monitors the condition and detects abnormalities at the spindle on machines tools, and the spindle bearing. To achieve this, the bearing unit has 3 types of sensors for load, temperature and vibration built into the outer ring spacer, which is arranged between two rows of back-to-back angular contact ball bearings. Furthermore, the unit has a built-in generator as an independent power source and a wireless module to provide wireless technology. **Fig. 2** shows this bearing unit's structure, **Fig. 3** shows an example of application on a machine tool spindle, and **Table 1** shows the function and purpose.

In addition, when this bearing unit was announced in 2018, it was integrated with 3 types of sensors for temperature, heat flow and vibration. Among these sensors, the heat flow sensor has been replaced with a load sensor.
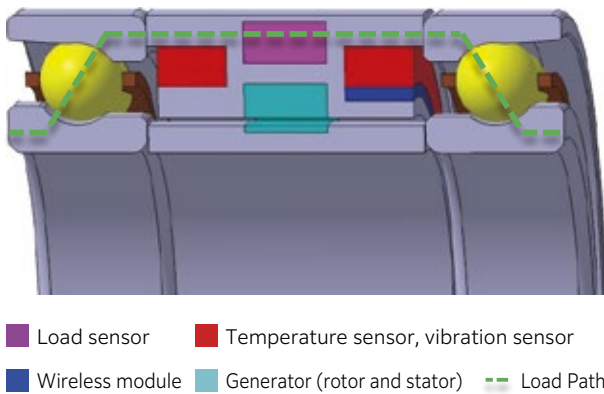

■ Load sensor   ■ Temperature sensor, vibration sensor
■ Wireless module ■ Generator (rotor and stator) -- Load Path

Fig. 2 The sensor integrated bearing unit

Outer ring spacer   Housing outer diameter surface of spindle
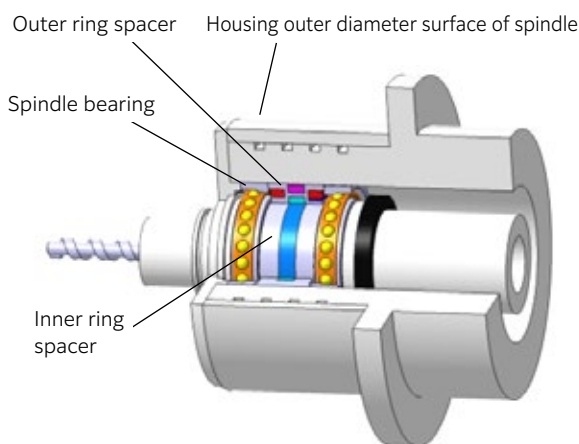
Spindle bearing

Inner ring spacer

Fig. 3 Application example of the sensor integrated bearing unit to the machine tool spindle

2.1 Sensors
2.1.1 Load Sensor

The load sensor detects loads applied on the bearing, such as bearing pre-load and external loads applied to the spindle.

This bearing unit has a newly developed, compact and high-sensitivity load sensor built into the load path that can detect sudden increases in pre-load that occurs prior to bearing seizure. This contributes to the prevention of such seizure. Furthermore, detecting pre-load for bearings after spindle installation makes it easier to manage the pre-load for such bearings and is expected to reduce the number of man-hours required for assembly in comparison with the conventional method of calculations based on spindle rigidity and the method of calculations based on the spindle's natural vibration frequency. It is also possible to detect the external load applied to the spindle and this can be used to monitor the machining conditions in terms of changes in the cutting load to contribute towards improving the machining quality and productivity. Additionally, there is the potential to also use this to detect collisions between the tool and the workpiece.

2.1.2 Temperature Sensor

The temperature sensor detects heat generated from the bearing as a result of spindle rotation and the cutting load. Generally, when measuring the bearing temperature during operation, the temperature is measured at the housing outer diameter surface of the spindle where the sensor is easy to install, and then the bearing temperature is estimated based on this value. However, fluid cooling channels are provided for the bearing and motor between the bearing and housing outer diameter surface, which means the temperature is lower than when the bearing temperature is measured directly. Furthermore, the housing's heat capacity is large and the sensor requires some time to detect temperature changes. Due to this fact, it was difficult to accurately know the temperature of the bearing.

This bearing unit measures the temperature of the outer ring spacer in close proximity to the bearing. When compared to measuring at the housing outer diameter surface, it provides a more accurate measurement of the bearing temperature and can increase the reliability of condition monitoring.

2.1.3 Vibration Sensor

A vibration sensor is used to detect roughness, peeling, and seizure on the bearing raceway surface due to insufficient lubrication that commonly occurs in machine tool spindle bearings, and to detect abnormal indentations due to collisions between the spindle and the workpiece. Generally, when measuring bearing vibration during operation, the vibration is often measured at the housing outer diameter surface of the spindle because this makes it easier to install the sensor; the same as for the temperature sensor. However, any vibration originating from the bearing is dampened when measured through the housing.

This bearing unit has a vibration sensor built into the outer ring spacer in close proximity to the bearing. Since the vibration is measured at a position close to the bearing raceway surface it is possible to measure the initial stage of an abnormality and even the smallest level of vibration with good sensitivity. Furthermore, there is the potential to also use this to detect collisions between the tool and the workpiece; the same as for the load sensor.

Table 1 Functions & purpose examples of the sensor integrated bearing unit

Function		Purpose
① Load sensor	Detects pre-load for spindle bearing (While spindle is rotating and after spindle installation)	・Early detection for signs of bearing seizure ・Reduces man-hours for spindle assembly
	Detects external loads applied to the spindle	・Detects the machining load applied to the spindle, and monitors machining (Contributes to improving the machining quality and productivity) ・Detects collisions between the tool and the workpiece(Used to reduce spindle damage and investigate the cause of any damage)
② Temperature sensor	Detects temperature changes in the spindle and spindle bearing	・Monitors the condition of the bearing raceway surface
③ Vibration sensor	Detects vibration changes in the spindle and spindle bearing	・Monitors the condition of the bearing raceway surface ・Detects collisions between the tool and the workpiece(Used to reduce spindle damage and investigate the cause of any damage)
④ Independent power source	Supplies power required for the sensors and wireless module	・No need for an externally connected cable or wiring space ・Reduces man-hours to assemble the spindle ・No need to change the spindle structure
⑤ Wireless module	Provides wireless communication to a location outside the spindle for detected data	

2.2 Wireless Technology

This bearing unit has a built-in independent power source and wireless module. This means that there is no need for an externally connected cable and wiring space used to transmit data and to supply power, achieving the same level in handling properties as conventional bearings with spacers that do not have sensor integration. The following sections describe the independent power source and wireless module.

2.2.1 Independent Power Source

The bearing unit uses a compact and high output electromagnetic generator that generates power using the rotation of the spindle. A power-generating rotor is arranged at the inner ring spacer while a power-generating stator is arranged opposing it at the outer ring spacer. This setup supplies the power required for the sensors and wireless module by generating power from the relative rotation of the inner and outer ring.

2.2.2 Wireless Module

A wireless module is built into the outer ring spacer to enable data detected by the sensors to be transmitted wirelessly to a location outside the spindle. The wireless module is compact and consumes only a small amount of power to ensure it can operate using power from the above mentioned independent power source with consideration for communication standards, the frequency used, signal strength, and safety, and to maintain sufficient space required for its antenna even when integrated in the spacer.

3.Evaluation Test

This section introduces the measurement results taken using wireless technology with the load sensor that was newly added to this bearing unit. Evaluation test results are shown for "Detects pre-load for spindle bearing (While spindle is rotating)" and "Detects external loads applied to the spindle" in section ① of **Table 1**.

The test machine used to simulate the machine tool spindle is shown in **Fig. 4.** This bearing unit was set up on this test machine and the evaluation test was performed. A high speed angular contact ball bearing with ceramic balls (HSE type) was used for the test bearing. A two-row back-to-back arrangement was chosen for the bearing to simulate a machine tool spindle. This bearing unit wirelessly transmits data detected by the sensors using the wireless module to a receiver set up at a location external to the test machine.
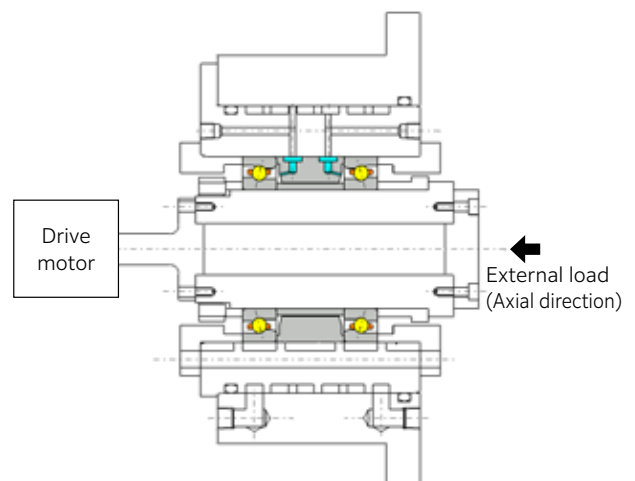
Fig. 4 Structure of test spindle

3.1 Bearing Pre-load Detection Test

A performance test was conducted to detect the pre-load of the bearing while the spindle is rotating. **Table 2** shows the test conditions. **Fig. 5** shows the measurement results from the load sensor using wireless technology that was newly added to this bearing unit. For comparison, the graph also shows the bearing pre-load (theoretical value) obtained from the spindle's rotational speed and the bearing's inner and outer ring temperature which were measured separately form this bearing unit. From the test results we confirmed that it is possible to estimate the pre-load of the bearing while the spindle is rotating using the load sensor on this bearing unit.

Table 2 Test condition of the bearing preload detection

Test bearing	φ 70 × φ 110 × 20 Part equivalent to 5S-2LA-HSE014 (high speed angular contact ball bearing with ceramic balls)
Pre-load method	Fixed position pre-load (pre-load of 750 N after spindle installation)
Rotational speed	0 - 14,000 min^{-1}
Lubrication method	Air oil lubrication
Lubricating amount	0.03 mL/10 min
Lubricating oil	ISO VG32
Lubricating air flow rate	30 NL/min
Fluid cooling channel	Yes, room temperature tuning
Axis position	Horizontal axis
External load	None

Fig. 5 Test result of the bearing preload detection

3.2 External Load Detection Test

An external load test was conducted to detect the external load applied to the spindle. **Table 3** shows the test conditions. During this test the spindle was rotated at 5,000 min^{-1} and an external load was applied in the axial direction. **Fig. 6** shows the measurement results. From the test results we confirmed that the load

sensor on this bearing unit can estimate the external load in the axial direction while the spindle is rotating.

Table 3 Test conditions of the external load detection

Test bearing	φ 70 × φ 110 × 20 Part equivalent to 5S-2LA-HSE014 (high speed angular contact ball bearing with ceramic balls)
Pre-load method	Fixed position pre-load (pre-load of 750 N after spindle installation)
Rotational speed	5,000 min^{-1}
Lubrication method	Air oil lubrication
Lubricating amount	0.03 mL/10 min
Lubricating oil	ISO VG32
Lubricating air flow rate	30 NL/min
Fluid cooling channel	Yes, room temperature tuning
Axis position	Horizontal axis
External load	(Axial direction) 0 - 3 kN
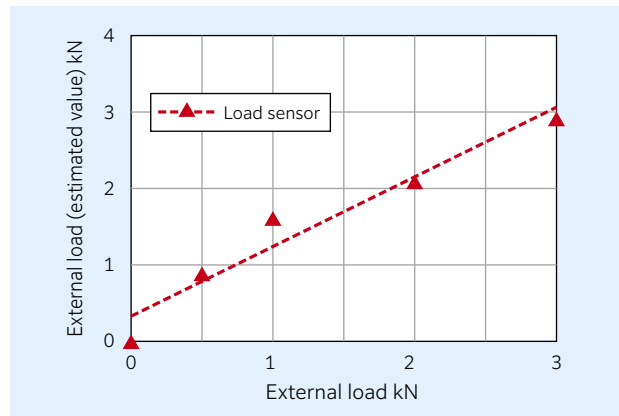
Fig. 6 Test result of the external load detection

4.Collaboration with Industrial IoT Platform

In order to use the data detected by this bearing unit, this bearing unit must be connected to a machine tool and an industrial IoT platform **(Fig. 7)**. When used for machine control that requires high responsiveness, the bearing unit should be connected to the machine tool (data transmission target ①). It is often necessary to develop a dedicated connection program or similar such program in this case. Meanwhile, when monitoring the condition and conducting predictive maintenance that uses measurement data, it is more common to connect to a management system in the form of an industrial IoT platform (data transmission target ②). Since the connection program is provided, the connection can be relatively easily established in this case.

For example, connecting this bearing unit to an industrial IoT platform such as Edgecross[*1] enables

information for the load, temperature and vibration to be imported. Utilizing the various measurement data imported into the industrial IoT platform not only enables condition monitoring of the bearing, but it also enables monitoring of the machining conditions. The data can also be stored on a server, which also enables the use of big data.
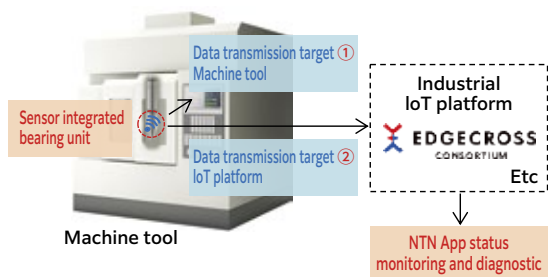
Fig. 7 Communication examples of the sensor integrated bearing unit

This bearing unit uses an independent power source to supply power and send data wirelessly, which can reduce the man-hours required to install sensors and also simplify the move to an IoT environment.

NTN has developed Wind Doctor™, a Condition Monitoring System for wind turbines that fully utilizes bearing analysis and our diagnostic expertise, and provides a monitoring service for power generation companies[4].

Additionally, we are also currently developing a diagnostic application for industrial IoT platforms that incorporates the knowledge and expertise we gained from Wind Doctor™ and plan to propose solutions employing this bearing unit.

*1 : A Japanese-developed open software platform in the field of edge computing to enable FA and IT collaboration. (From Edgecross Consortium official website https://www.edgecross.org/en/)

5.Summary

Further enhancement of condition monitoring functions is required for machine tools against such factors as the backdrop of a diminishing working population.

NTN has developed the "Sensor Integrated Bearing Unit" for Machine Tool Spindles and announced this product at 2018 JIMTOF2018 in response to this need. While promoting proposals to customers, we have received many requests to add a load detection function and wireless technology so have developed a new unit to achieve this purpose.

We will continue to make further improvements in performance and in the practical use of this product into the future. We are also aiming to improve technology for predictive maintenance using AI technology to continue contributing towards more efficient maintenance and operation of equipment, including machine tools.

References

1) Naoki Matsumori, Keiichi Ueda, Technical Trend of the Precision Bearings for Machine Tools, NTN TECHNICAL REVIEW, No.84, (2016) 40-45.
2) Keiichi Ueda, Technical Trend of the Precision Bearings for Machine Tools, Bearing & Motion Tech, No.002, (2016) 33-35.
3) Shohei Hashizume, Yasuyuki Fukushima, Yusuke Shibuya, Yohei Yamamoto, Development of Sensor Integrated Bearing Unit for Machine Tool Spindles, NTN TECHNICAL REVIEW, No.86, (2018) 50-55.
4) Makoto Miyazaki, Wataru Hatakeyama, Application of Condition Monitoring System for wind turbines, NTN TECHNICAL REVIEW, No.86, (2018) 40-44.

Photo of authors

Shohei HASHIZUME

Application Engineering Dept., Industrial Business Headquarters

Yusuke SHIBUYA

New Product Development R&D Center

Daichi KONDO

New Product Development R&D Center

Yohei YAMAMOTO

Product Design Dept., Industrial Business Headquarters

Hiroyuki IWANAGA

Robotics Sensing Engineering Dept., Industrial Business Headquarters

Development of a Low Contamination Generation Bearing for Servo Motors

Araki TANAKA*   Naoaki TSUJI**
Hideyuki MITANI**   Takayuki KAWAMURA***

NTN has developed low contamination generation bearings for servo motors and has experienced increased demand for these bearings in recent years. This bearing type generates 90 % less contamination and requires 50 % less torque than conventional bearings; this allows the servo motor to be downsized and increases the motor's power output. This report introduces the features and performance of the low contamination generation bearing.

1.Introduction

With increasing demand for improved productivity and reduced labor costs against the backdrop of a diminishing working population, performance improvement is required for FA devices and motors **(Fig. 1)**, the power sources of devices such as machine tools and industrial robots[1].

NTN has recently developed a low contamination[*1] generation bearing to decrease the size and increase the power output of servo motors for industrial robots.

In addition to technical trends for servo motor bearings **(Fig. 2)**, this developed product's features and evaluation test results are introduced below.

Fig. 1 Motor

Fig. 2 Servo motor bearings

2.Development Background

In recent years, demand for servo motors for use in machine tools and industrial robots has increased. A servo motor features a rotation detector and brake, or control device, that enable it to control rotation with a high level of precision. Generally, a sealed and greased deep groove ball bearing with cost advantages is used in a servo motor to support high speed rotation. **Table 1** shows the characteristics required for servo motors and their supporting bearings.

Table 1 Requirements of Servo Motor Bearings

Application	Required Servo Motor Characteristics	Required Bearing Characteristics	Other Bearing Characteristics
Machine tool	High speed rotation	High speed rotation	Plastic ribbon cage
		Long grease life	ME-1 Grease
Industrial robot	Compact	Low contamination generation	Low contamination generating grease
	High power output	Low torque	Contact seal

Servo motors used for machine tools rotate at high speeds and are often used to drive a spindle. Therefore, the bearing must have good high speed rotational performance and a long grease life. **NTN** has historically used "ME-1"[3] high temperature, long-life grease and its proprietary "plastic ribbon cage" **(Fig. 3)**. This cage has the advantage of extending the grease life and prevents centrifugal expansion that inhibits high speed rotation. **NTN** also offers its commercialized[4] "ULTAGE[*2] Deep Groove Ball Bearings for High-Speed Servo Motors" **(Fig. 4)** that combine long operating life with high speed rotation at a d_mn value[*3] of 1 million.

ULTAGE

Fig. 3 Plastic ribbon cage[2]

Fig. 4 ULTAGE deep groove bearings for high-speed servo motors[4]

*1 Throughout this report, contamination refers to lubrication emitted by the bearing.
*2 ULTAGE is the name for **NTN**'s new generation of bearings that is noted for its industry-leading performance. The name is created by combining "ultimate", signifying refinement, and "stage", signifying **NTN**'s intention for this product to be used for a variety of applications.
*3 d_mn is a value that represents the bearing's rotational performance.
 d_mn=d_m(bearing rolling element pitch diameter, mm) $\times$ n(rotational speed, min^{-1})

* Application Engineering Dept., Industrial Business Headquarters
** Product Design Dept., Industrial Business Headquarters
*** Advanced Technology R&D Center

Servo motors used in industrial robots are often used to drive joints and, like those used in machine tools, are required to be compact. These bearings must also generate a high power output to increase the axis speed and acceleration/deceleration rates of the joints they support. A control device is typically mounted near the bearings of industrial robots. However, bearing lubrication can splash onto and stick to these control devices which causes a drop in detection accuracy and braking performance. To prevent this, sealed device could be used to protect the control device, but this increases the size of servo motor and results in a less compact system. A low contamination generation bearing is required to prevent lubrication from exiting the bearing and sticking to the control device when a servo motor does not equip sealed device between its bearing and control device. Furthermore, low torque generation is required to achieve high power output from the servo motor. **NTN** has therefore commercialized a low contamination generation bearing[1] that utilizes a seal arrangement that prevents pressure from increasing inside the bearing, the main cause of contamination generation, and requires low torque. This bearing also uses "EP-1" grease, a low contamination-generating grease. Each year the requirements for low contamination generation and low torque become more stringent, and further performance improvement is required.

3.Product Structure and Features

The "Low Contamination Generation Bearing for Servo Motors" **(Fig. 5)** is a deep groove ball bearing with a newly developed low contamination-generating grease and a newly developed contact seal on both sides of the bearing. In comparison with conventional **NTN** products, this bearing both reduces the amount of contamination generated by the bearing by approximately 90 % and the rotational torque by approximately 50 %.
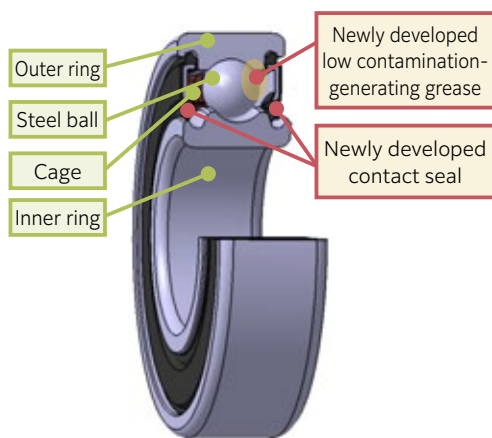
Fig. 5 Low Contamination Generation Bearing for Servo Motors

3.1 Low Contamination Generating Grease

When bearings rotate, compressive and shearing forces are applied to the grease within the bearing. This causes the base oil to separate from the thickener. Furthermore, fine particles are released.

As explained in section 2, lubrication can exit the bearing and splash onto the servo motor control device. After collecting and analyzing this contamination, **NTN** found it to be a component of the base oil. However, the grease thickening agent was not detected. It is therefore necessary to prevent the base oil in the grease from separating and evaporating **(Fig. 6)**. More specifically, increasing the surface tension of the base oil[5] and decreasing the grease consistency is considered to be effective for low contamination generation. The following pages show the test results that confirm this effect.

Furthermore, since contamination generated by the bearing is caused by heat generated by bearing rotation and internal bearing pressure increase, it is also necessary to devise a means to stop the internal bearing pressure from rising.
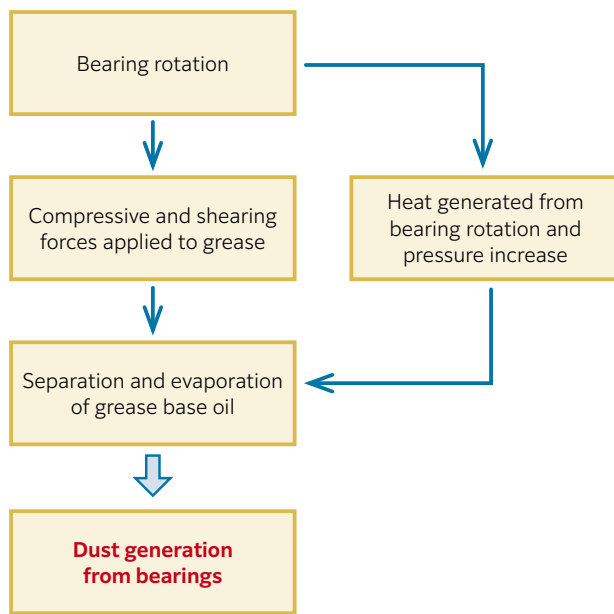
Fig. 6 Dust generation from bearings

1) Relationship Between Base Oil Surface Tension and Contamination Generation[5]

16 types of bearing lubrication with different base oil surface tensions were applied onto test bearing part number 608 with an average thickness of 1 μm. The amount of contamination generated was then investigated while rotating the test bearing inner rings at a speed of 1,000 min^{-1} with an axial load (Fa) of 10 N. A light scattering particle counter with a total volume of 9 L was used to count particles of contamination with sizes of 0.1 μm or larger for 30 minutes. The trial was then continued for 8 total hours. **Fig. 7** shows the results.

A distinct trend was observed: the higher the base oil surface tension, the smaller the amount of contamination generation at both the initial stage of rotation and after 8 hours had elapsed. This means that selecting a base oil with a high surface tension can be effective for low contamination generation.
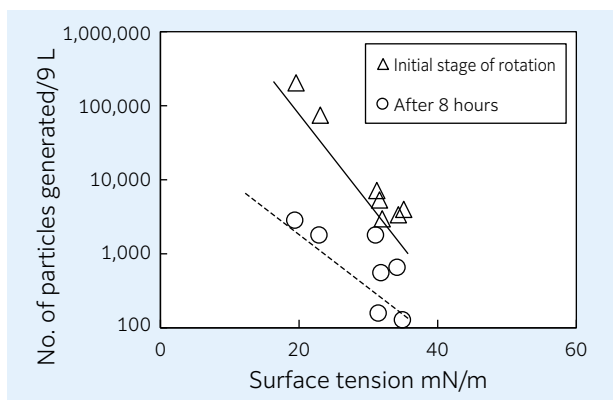
Fig. 7 Relationship between base oil surface tension and contamination generation

2) Relationship Between Consistency and Contamination Generation

After adjusting the type and amount of thickening agent, 16 test grease types, 8 with thickening agent A and 8 with thickening agent B and all with different trial consistencies, were applied on test bearing part number 608 with a total weight of 0.1 g. The same test method used in section 1) above was used to calculate the amount of contamination generated after 8 hours of testing had elapsed. **Fig. 8** shows the results.
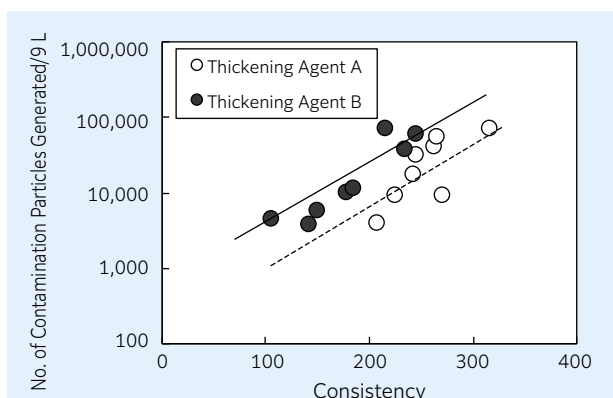
Fig. 8 Relationship between grease consistency and contamination generation

Another distinct trend was observed: the lower the consistency of the grease, the smaller the amount of contamination generation for both of the tested thickening agents. This means that optimizing the type and amount of thickening agent to achieve low grease consistency can be effective for low contamination generation.

Selecting a base oil with a high surface tension and optimizing the type and amount of thickening agent **(Table 2)** reduces the contamination generated by approximately 60 % compared to "EP-1", the current low contamination generation grease **(Table 3, Fig. 9)**.

In addition, this developed grease satisfies the requirements for high temperature durability and wear resistance for servo motor applications. An appropriate additive was selected that has no adverse effect on the base oil's surface tension and consistency.

Table 2 Characteristic of the developed grease

	Developed low contamination generation grease	Current grease EP-1
Thickening agent	Urea	Urea
Base oil	Synthetic oil	PAO
Base oil viscosity, mm^2/s (40 ℃)	130	47
Mix consistency, 60 W (25 ℃)	220	220

Table 3 Condition for contamination generation test

Test bearing	6900	Axis orientation	Vertical
Load condition	Fa = 30 N	Test temperature	Constant 120 ℃
Rotation speed	Constant 6,000 min^{-1}	Test time	200 hours
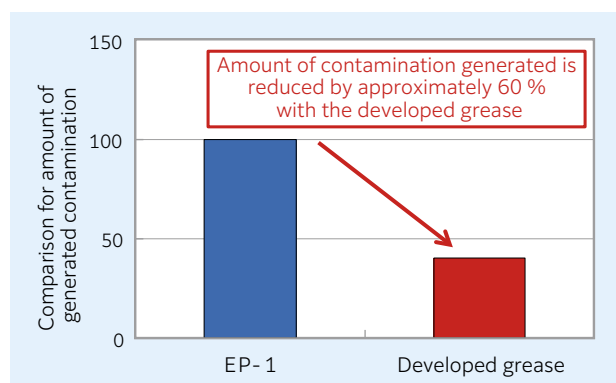
Fig. 9 Contamination generation test of the developed grease[*]

* The contamination generation test used a test machine that simulates a servo motor. A glass plate that simulated a rotation detector was used to measure the mass of oil that stuck to the glass plate.

3.2 Low Contamination Generation, Low Torque Seal

As described in section 3.1, in order to reduce contamination generated by the bearing, pressure increases inside the bearing should be prevented. To help prevent this internal bearing pressure, a contact seal can be installed on the control device side and a non-contact seal can be installed on the opposite side. This allows air intake/exhaust through the bearing and prevents pressure differential from occurring between the interior and exterior of the bearing.

In recent years, control devices are installed on both sides of the bearing, necessitating low contamination generation on both sides of the bearing. Furthermore, low bearing torque is required to increase servo motor power output.

The newly developed **NTN** contact seal adopts the following two points compared to a conventional contact seal **(Fig. 10)**.

---

① A slit is added to the seal outer diameter to allow air intake/exhaust through the bearing.
② The shape of the seal lip is changed.

To confirm the effect of this seal slit ① , a seal was installed on one side of a bearing and oil was injected into the opposite side to check whether oil seeped out of the slit. This indeed resulted in oil seeping through the slit and confirmed air intake/exhaust air through the bearing is possible **(Fig. 11)**.
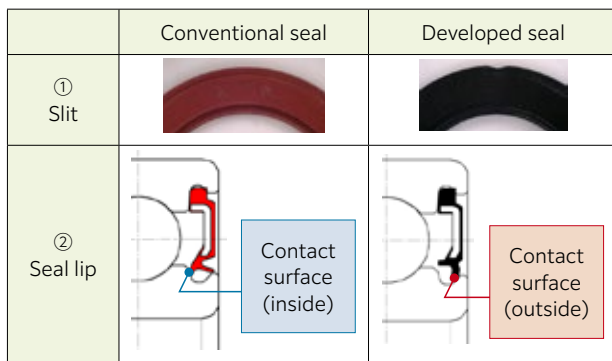
Fig. 10 Characteristics of the Developed Seal

Slit position   Enlarged view of slit (**after** injecting oil)

Fig. 11 Performance test of the seal slit

Furthermore, for conventional seals, the seal lip makes contact with the inside of the inner ring seal groove. In contrast, the lip of the developed seal makes contact with the outside of the seal groove. This ensures interference between the seal lip and inner ring seal groove and prevents contamination from exiting the bearing, even when the pressure inside the bearing increases and the seal lip deforms towards the outside

of the seal groove.

If the seal lip of a conventional seal that makes contact with the inside of the seal groove deforms towards the outside of the bearing, the seal/inner ring interference, tension force of the seal lip, and rotational torque will increase. The developed **NTN** seal prevents this seal lip tension force from increasing when interference increases due to the shape of the seal lip **(Fig. 12)**.

Table 4 and **Fig. 13** show the bearing rotational torque with usage of the developed seal. The developed seal reduces the rotational torque by approximately 60 % compared to the conventional seal.
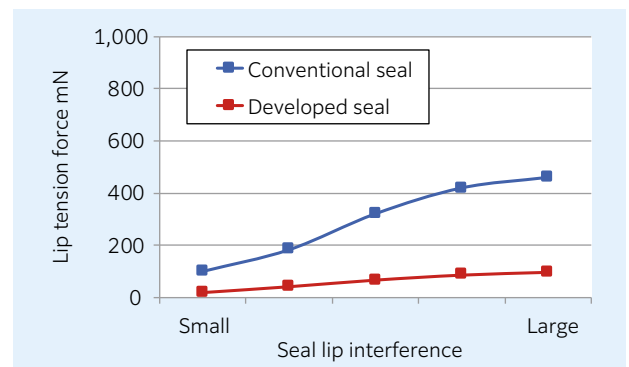
Fig. 12 Relation between seal lip interference and tension forth (FEM analysis)

Table 4 Conditions for Torque Test

Test bearing	6900 (φ 10 $\times$ φ 22 $\times$ 6) Each seal installed only on one side
Load condition	Fa = 39 N
Rotation speed	Constant 3,600 min^{-1}
Axis position	Vertical axis
Lubrication	Small quantity of VG32 oil applied
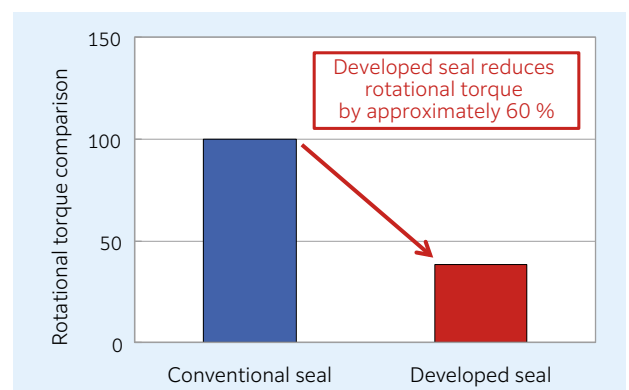
Fig. 13 Torque test of the developed seal

4. Evaluation Test

4.1 Test Conditions

Contamination generation and rotational torque tests were conducted to evaluate the performance of this **NTN** developed product. **Tables 5** and **6** show the specifications of the evaluated bearings and the test conditions for each evaluation.

Table 5 Specifications of Test Bearings

	Conventional product	Developed product
Bearing	6900 (ϕ 10 × ϕ 22 × 6)	
Seal	One side: Contact seal One side: Non-contact seal	Both sides: Contact seal (Developed seal)
Grease	EP-1	Developed grease
Amount of grease injected	Approximately 0.1 g	

Table 6 Condition for torque test

Test bearing	Same specifications as **Table 5**
Load condition	Fa = 39 N
Rotation speed	Constant 3,600 min^{-1}
Axis position	Vertical axis

4.2 Test Results

Figures 14 and **15** show the results of the contamination generation test while **Fig. 16** shows the results of the rotational torque test. The test results reinforced the conclusions drawn earlier in this report. This developed bearing both reduces the amount of contamination by approximately 90 % and reduces the rotational torque by approximately 50 % when compared with **NTN** conventional product.

The contamination generation test used a test machine that simulates a servo motor, the same as shown in **Fig. 9** in section 3.1. A glass plate was installed next to the bearing to measure contamination accumulation. **Fig. 14** shows a photo of the exterior view of the glass plate before and after the test. The cloudy section of the glass plate after the test is the result of oily substances generated by the bearing. The greater the amount of contamination generation, the thicker this cloudy section becomes. As shown in **Fig. 15**, the developed product has a lower amount of contamination generation than the conventional product.

Application of this developed bearing in a servo motor means that a sealed device is no longer necessary to prevent contamination generated from the bearing from sticking to the control device. It also enables servo motors to be more compact and results in higher power output by reducing the rotational torque of the bearing.

These factors enable further performance improvements for servo motors and can contribute towards productivity improvements for industrial robots.

Before test

After test (conventional product)　　After test (developed product)
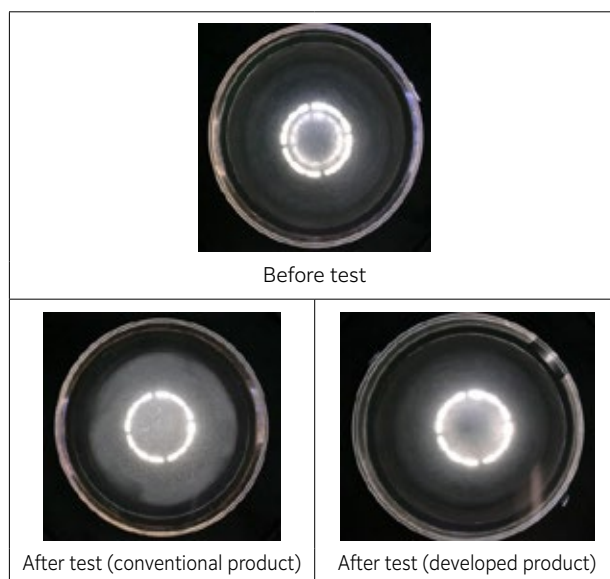
Fig. 14 Photo of Glass Plate After Testing

Amount of contamination generated is reduced by approximately 90 % with the developed product
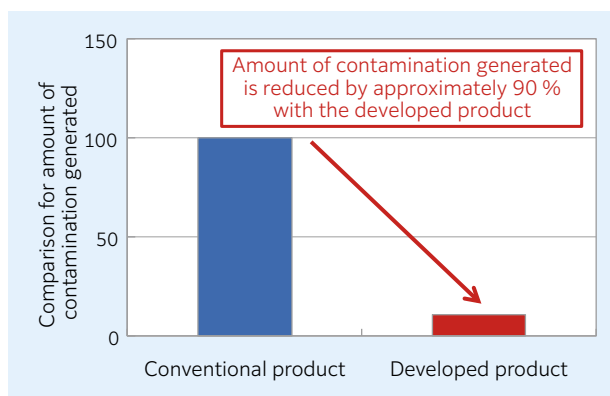
Fig. 15 Contamination Generation Test Results

Rotational torque is reduced by approximately 50 % with the developed product
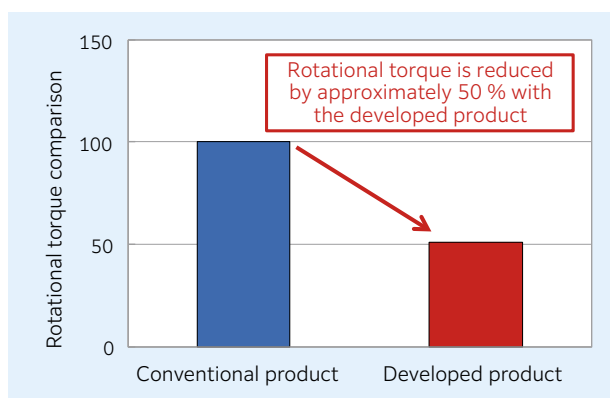
Fig. 16 Torque test of the developed bearing

5.Summary

With increasing demand for improved productivity and reduced labor costs against the backdrop of a diminishing working population, performance improvement is required for FA devices and motors, the power sources of devices such as machine tools and industrial robots.

NTN has developed the low contamination generation bearing for servo motors that significantly reduces rotational torque and generated bearing contamination to help make servo motors used in industrial robots more compact and provide higher power output.

NTN aims to further improve bearing performance and quality in the future and provide outstanding support for customer requests by strengthening its technical support and product proposals.

References

1) Hikaru Ishida, Technical Trend of Servo Motor Bearings, THE TRIBOLOGY, No.388, (2019) 42-44.
2) Chikara Katagiri, Kenichiro Naito, Next Generation Deep Groove Ball Bearing for High-Speed Servomotor, NTN TECHNICAL REVIEW, No.72, (2004) 46-51.
3) Hidenobu Mikami, Development of Long Life Grease for High Speed Application "ME-1" Grease for Motor Bearings, NTN TECHNICAL REVIEW, No.72, (2004) 20-25.
4) NTN ULTAGE Deep Groove Ball Bearings for High-speed Servo Motors, CAT.No.3103, 11. 05. 03, (2011).
5) Takayuki Kawamura, Masami Minami, Masakazu Hirata, Evaluation of Dust Generation Characteristics of Lubricating Oil due to Rolling Bearings, Japanese Society of Tribologists, Proceedings for Tribology Conference, (2000) 85-86.

Photo of authors

Araki TANAKA

Application Engineering Dept., Industrial Business Headquarters

Naoaki TSUJI

Product Design Dept., Industrial Business Headquarters

Hideyuki MITANI

Product Design Dept., Industrial Business Headquarters

Takayuki KAWAMURA

Advanced Technology R&D Center

Introduction of Composite Material Products for Industrial Machinery

Shinji KOMATSUBARA*
Norikazu MUNEDA**

Composite Material Products Division has developed and produced bearings, mechanical parts, and unit module products made of multi materials such as plastic, sintered metal, and magnetic material using tribology as a basic technology. In this article, we introduce composite material products used in various advanced fields of industrial machinery.

1.Introduction

New markets are emerging and growing for products equipped with advanced technology according market trends in the field of industrial machinery. Machine parts with tribological characteristics that are better than existing technologies are required for new products in this advanced field. Creating lightweight or low-friction parts to save energy and control CO_2 emissions are an example of this. The Composite Material Product Division has been using and developing materials such as plastics, sintered metal and magnetic material for products that meet these higher performance requirements, and has been proposing and supplying these products to our customers. This paper introduces examples of applications for composite material products in advanced fields.

2. Hydrodynamic BEARPHITE Bearing for Thin Cooling Fan Motors

There has been a rapid growth in demand for mobile devices such as laptops for use in teleworking and online courses. A superior quietness is required for cooling fans **(Fig. 1)** equipped in these types of devices that covers an extensive range of low to high rotational speed. **NTN**'s Hydrodynamic BEARPHITE **(Fig. 2)** has the reputation of achieving this quietness and reliability, and has been widely adopted in thin cooling fans.

Hydrodynamic BEARPHITE provides non-contact support for the shaft and bearing through oil-film pressure generated within the bearing clearance due to the hydrodynamic effect. Therefore, it is a bearing

an excellent quietness. Generally, oil-film pressure increases proportional to the rotational speed for hydrodynamic BEARPHITE bearings. Like when the bearing is rotating at high speeds, it is important to maintain the oil-film pressure required to provide non-contact support even at low speeds when the oil-film pressure drops. By improving the Hydrodynamic BEARPHITE material, we have maintained a quietness at low rotational speed, a requirement of cooling fans.
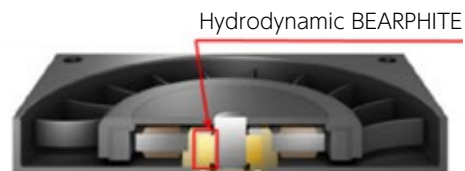

Fig. 1 Fan for cooling

Fig. 2 Hydrodynamic BEARPHITE

*   Hydrodynamic Bearing Engineering Dept., Composite Material Product Division
** Plastics Engineering Dept., Composite Material Product Division

2.1 Features

There are 2 types of Hydrodynamic BEARPHITE: the copper and iron based material EZ06 which is a standard material, and EZ17 with increased oil-film pressure. **Table 1** shows the material composition.

Table 1 Material composition

Chemical composition %		Material	
		EZ06	EZ17
	Cu	Remaining amount	Remaining amount
	Sn	1 - 3	1 - 3
	C	0.5 - 2.5	−
	Fe	38 - 42	38 - 42

Hydrodynamic BEARPHITE is a type of oil-impregnated sintered bearing manufactured using a powder metallurgy method. So it has pores on the bearing surface and interior. While the pores have an important function of maintaining and supplying lubricating oil, they can also be the cause of decreasing of generated oil-film pressure. In order to maintain a quietness at a low rotational speed of 1,000 min^{-1} required for thin cooling fans used in mobile devices, it is important to control the pores to maintain a high oil-film pressure.

In case of EZ17, the pores are micronized to improve the oil-film pressure by optimizing the particle distribution and shape of the material powder. **Fig. 3** shows a comparison of the bearing inner diameter surface. Pores on EZ17 are clearly micronized than EZ06.

Pore (black area)
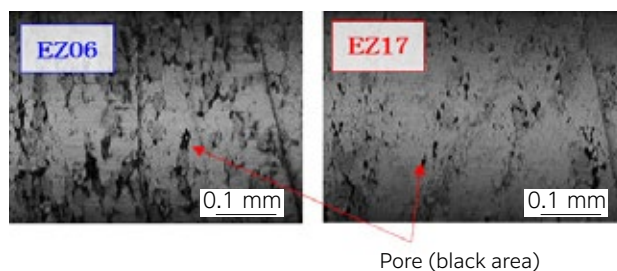
Fig. 3 Enlarged photo of inner surface
(Inner diameter 2 mm)

2.2 Performance

We compared the rotational speed at which EZ06 and EZ17 can provide non-contact support for the shaft by determining whether contact occurs between the shaft and Hydrodynamic BEARPHITE using an electrical resistance method. **Fig. 4** shows the results.

EZ17 can reduce the rotational speed at which non-contact support can be provided for the shaft by 30 % compared to EZ06. This shows that it is possible to provide non-contact support even at the low rotational speed of 1,000 min^{-1} required for cooling fans.

< Test conditions >
Shaft material SUS420J2
Bearing dimensions: Inner diameter 2 mm, outer diameter 4 mm, width 3 mm
Surface pressure 0.5 MPa, room temperature, test time of 2 min
Lubricating oil kinematic viscosity (40 ℃) 12 mm^2/s
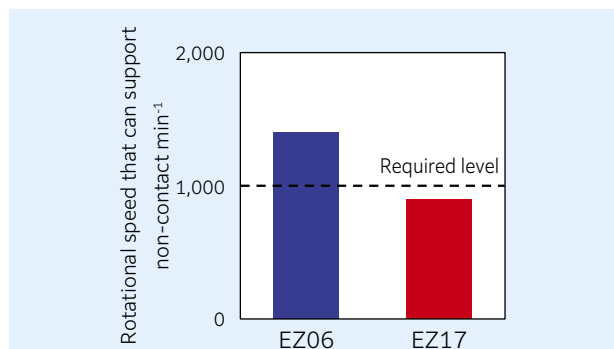
Fig. 4 Test result of contact of shaft and BEARPHITE
(Shaft outer diameter 2 mm)

3.Plastic Bearings for Electric Water Pump[1]

Heat pump water heaters using natural coolant, residential fuel cell cogeneration systems, and water-heated floors are some of the technology used for residential equipment to support ZEH (Net Zero Energy House). Electric water pumps are used for their circulation and cooling systems. **NTN**'s underwater plastic (BEAREE AS5704) sliding bearing is used in these electric water pumps.

3.1 Structure of Electric Water Pump

Fig. 5 shows the structure of a magnetic drive water pump as a typical electric water pump.
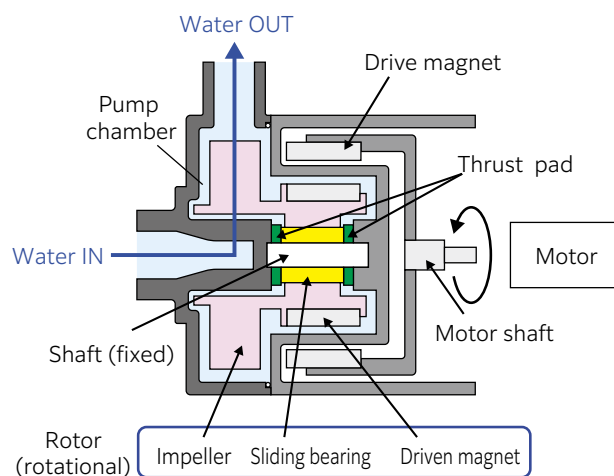
Fig. 5 Structure of magnetic drive electric water pump

A rotor integrated with a plastic impeller, driven magnet and sliding bearing is housed inside the pump chamber and supported by the shaft using a sliding bearing. The drive magnet installed on the motor shaft rotates the rotor by magnetic force to transfer water sucked by the impeller into the pump chamber. Since radial load and axial load occur when the rotor rotates, the bearing surface of inner diameter and shaft, and the bearing end surface and thrust pad slide underwater respectively. Generally, the bearing is inserted into a mold along with the driven magnet and the plastic impeller is integrated using an injection molded composite mold.

3.2 Required Performance and Bearing Material

Low-friction properties and high wear resistance in a liquid are required for bearings to achieve power saving and long-life electric water pumps.

Furthermore, chemical resistance and dimensional stability in water or acidic and alkaline liquids are also required. For magnetic drive water pumps, the bearing is integrated with the impeller using a composite mold, therefore the bearing outer diameter surface must be provided a retainer and rotation lock (D-shaped cut, protrusion, etc.) from the impeller. Therefore, the flexibility of the shape design is also important.

Due to the above requirements, electric water pumps use plastic bearing made of polyphenylene sulfide (PPS), polyether ether ketone (PEEK) and polytetrafluoroethylene (PTFE) or carbon bearing. Among plastic bearing, PPS bearing is less wear and longer operating life than PTFE bearing, and are cheaper than PEEK bearing. PPS bearing also has the benefit of a high flexibility of the shape design since it can be injection molded. Consequently, **NTN**'s "BEAREE AS5704 Bearing" for underwater **(Fig. 6)** which has excellent friction and wear properties, and chemical resistance by combining fillers such as solid lubricants and stiffeners with PPS, is used on electric water pumps.

10 mm

Fig. 6 BEAREE AS5704 bearings for using in water

3.3 Comparing BEAREE AS5704 Bearing with Other Bearings

PPS have high rigidity and excellent water, chemical and heat resistance, although it is comparatively low cost. PPS lacks the mechanical properties and friction and wear properties by itself, so it is combined with fillers. The friction coefficient and wear resistance change depending on the conditions of use like the environment (the atmosphere, oil, or water), the load, sliding speed, and mating material. Bearings for electric water pumps slide on a soft stainless steel mating material in fluid such as water.

Fig. 7 shows the results from a friction and wear test performed underwater on 4 types of bearings. These bearings are the BEAREE AS5704 bearing, and PPS combined with glass fiber (GF), carbon fiber (CF) and polytetrafluoroethylene (PTFE).

The CF combined bearing has a low specific wear amount but has high dynamic friction coefficient. The PTFE combined bearing has 30 to 40 % lower dynamic friction coefficient than both the GF and CF combined bearings but has less wear resistance. The BEAREE AS5704 bearing has a lower friction coefficient than the PTFE combined bearing and its specific wear amount is under 1/5 of the CF combined bearing.

The BEAREE AS5704 bearing is combined with fillers selected appropriately for using in electric water pumps, so the wear amount of the bearing and mating material is small, and it has excellent friction and wear properties underwater in comparison with PPS bearings combined with other fillers.

< Test conditions >
Ring on disc type testing machine
Mating material SUS304
Surface pressure 0.4 MPa, speed 25 m/min
Underwater, room temperature, test time 50 hours

Fig. 7 Results of friction and wear test of PPS bearings

Carbon bearing also used to use in electric water pumps. As shown in **Fig. 8**, the BEAREE AS5704 bearing has the same or greater friction and wear properties as carbon bearing, therefore adoption of BEAREE AS5704 bearing is increasing by replacing from carbon bearing.

Table 2 shows the comparison in performance of the BEAREE AS5704 bearing and carbon bearing.

Since carbon bearing is machined product made from molding material, so it is expensive and has a low flexibility of the shape design. Furthermore, it is fragile and easy to chip due to impact, so it is necessary to be taken care with handling during transportation and fixing them to rotors.

Meanwhile, BEAREE AS5704 bearing is an injection molded product, so the retainer, rotation lock and lubrication grooves on bearing inner diameter surface and end surface can be easily designed. Furthermore, it is cheaper compared to carbon bearing and easy to handle since it is difficult to chip.

< Test conditions >
Ring on disc type testing machine
Mating material SUS304
Surface pressure 1 MPa, speed 125 m/min
Underwater, room temperature, test time 10 hours
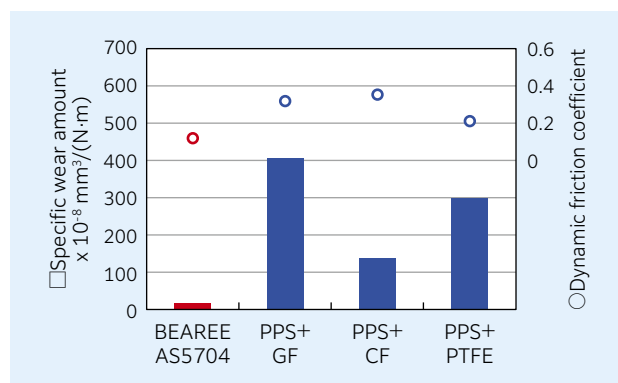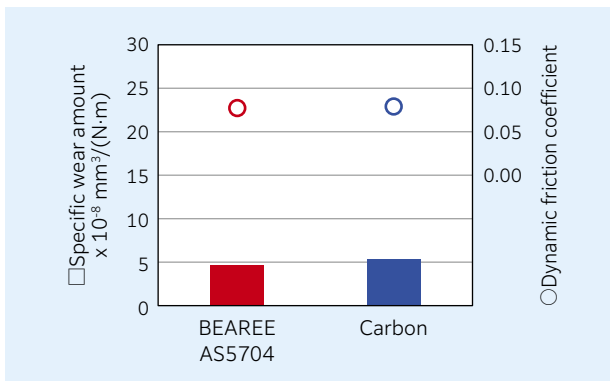

Fig. 8 Results of friction and wear test of BEAREE AS5704 bearing and carbon bearing

Table 2 Comparison between BEAREE AS5704 bearing and carbon bearing

Item	BEAREE AS5704 bearing	Carbon bearings
Processing method	Injection molded	Machined
Friction coefficient (underwater)	◎	◎
Wear resistance (underwater)	◎	○
Water and chemical resistance	◎	◎
Chip due to impact	○	△
Flexibility of shape design	◎	△
Cost	◎	△

◎：Excellent ○：Good △：Acceptable

4. Plastic Sliding Screws for Medical Devices Such as Eye Testers, Dialysis Machines and Anesthesia Apparatus[2]

Ball screw and sliding screw are available for feed screw that convert the rotational movement of the motor into linear motion, and these screws are used depending on their application and conditions of use. Ball screw have a high allowable load and excellent screw efficiency, but is not suitable for use in environments where grease cannot be used. Meanwhile, plastic sliding screw has a low allowable load but can be used without lubrication, produce low-noise, and is light and compact.

Due to these features, **NTN** plastic sliding screws are also adopted in inspection devices for COVID-19. In terms of other medical devices, these screws have been installed for eye testers, dialysis machines and anesthesia apparatus. In other fields, there are also adopted for such as substrate positioning on semiconductor manufacturing equipment.

4.1 NTN Plastic Sliding Screw Structure and Required Performance

Plastic sliding screw is assembled plastic nut and stainless steel screw shaft. During shaft rotation, the plastic nut and screw shaft slide, so low friction and wear properties are required for the plastic nut. As shown in **Fig. 9**, the plastic nut material of the "**NTN** Plastic Sliding Screw" is "BEAREE AS5000", which has combined with PPS and a special solid lubricant. **NTN** has a lineup of 16 standard types with a screw shaft outer diameter of 4 to 12 mm and leads of 1 to 36 mm.

Generally, polyoxymethylene (POM), polyamide, and PPS are used for the plastic nut material on the plastic sliding screw and are combined with a solid lubricant to provide low friction properties. The durability of plastic sliding screw depends on the wear resistance of the plastic nut which is improved through the use of a filler. However, combining fibrous filler increases the friction coefficient and generates sliding noise.

BEAREE AS5000 plastic nut
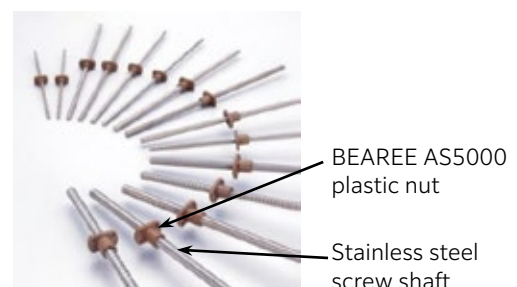
Stainless steel screw shaft

Fig. 9 NTN Plastic sliding screws

4.2 Comparison between NTN Plastic Sliding Screws and Other Sliding Screws

A special fibrous PTFE is combined to BEAREE AS5000 to produce a plastic nut that has low friction and wear properties. **Fig. 10** shows wear properties

without lubrication based on an element test for 3 types of sliding screws: BEAREE AS5000, PPS combined with a general granular PTFE, and PPS combined with granular PTFE and CF. The specific wear amount of BEAREE AS5000 combined with fibrous PTFE is 1/5 lower compared with that of PPS combined with granular PTFE, and half compared with that of PPS combined with granular PTFE and CF as stiffener.

< Test results >
Ring on disc type testing machine
Mating material S45C
Surface pressure 0.4 MPa, speed 25 m/min
Room temperature, no lubrication, test time 50 hours
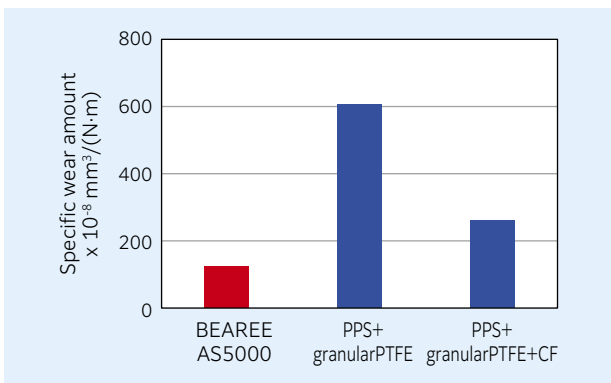
Fig. 10 Result of wear test of PPS

POM plastic sliding screw which is assembled an oil-impregnated POM plastic nut and a stainless steel screw is widely used in the market. **Fig. 11** shows the results of a wear test for this POM plastic sliding screw and the **NTN** plastic sliding screw. Generally, a sliding screw can be used as long as the amount of increase in axial clearance due to operation is 0.3 mm or less. In contrast, the POM plastic sliding screw which exceeds 0.3 mm for the amount of increase in axial clearance at a 60 km of sliding distance, the **NTN** plastic sliding screw is 0.15 mm even at 200 km, so it has a long operating life.

< Screw test conditions >
Screw specification: Shaft diameter 8 mm, lead 24 mm, 6 threads
Load 100 N, rotational speed 500 min^{-1}, room temperature, no lubrication
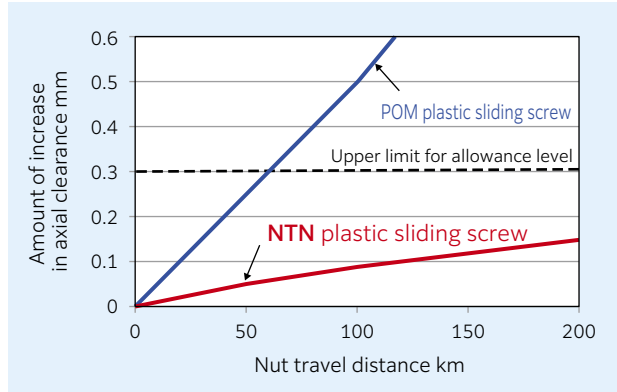
Fig. 11 Result of wear test of plastic sliding screws

5. Conclusion

This paper introduced examples of adopting bearing and element products made of plastics and sintered metal in various fields for the purpose of low-noise, energy-saving, compact design, lightweight and long operating life.

In future, societies will emerge driven by new technologies such as robotics, hydrogenation and IoT.

The Composite Material Product Division contributes developing the industrial machinery field by developing products to further improve functionality and making low friction and element products for growing markets.

References

1) Takuya Ishii, Ken Yasuda, Plastic Sliding Bearings for Electric Water Pumps in Hybrid Vehicles and Electric Vehicles, Latest Technology for Plastics Used in Automotive and Aircraft, (2016)167-176.
2) Naonari Tanigawa, Norio Itou, Tomomi Tonomura, Plastic sliding screws, NTN TECHNICAL REVIEW, No.84, (2016) 69-73.

Photo of authors

Shinji KOMATSUBARA
Hydrodynamic Bearing Engineering Dept., Composite Material Product Division

Norikazu MUNEDA
Plastics Engineering Dept., Composite Material Product Division

Activities and Achievements for Automotive Market Trends CASE

Koji KAMETAKA*

In this article, we explain our considerations and actions of research & technological development for fuel economy regulations, autonomous driving and car sharing, in the change of business conditions represented by "CASE". In other words, we introduce our development of technologies and products which meet the needs of the market.

Today, automobile industry is facing a great change. We are to develop in advance of the market trends, improving efficiency and accuracy with high speed. We also mention our CAE simulation technologies that support the research & technological development based on our core competence.

1. Introduction

Europe implements the strictest fuel efficiency regulations, and it will be necessary to further improve fuel efficiency by approximately 15 % in 2025 versus 2021 regulations. Automobile manufacturers will continue to improve fuel efficiency into the future by decreasing vehicle weight, improving aerodynamics, engine downsizing, and further shifting from mild hybrids to strong hybrids and fully electric vehicles. **(Fig. 1)**

Furthermore, as shown in **Table 1**, we know that the level of autonomous driving can be divided into 4 to 5 stages. Current mainstream autonomous driving systems are considered to be very effective in reducing traffic congestion at level 1, reducing road accidents due to human error at level 2, and reducing the environmental impact at level 3 due to the fact that they reduce the burden on the driver. However, it is necessary to closely monitor industrial trends for level 4 and 5 until transportation system management has been established a little further in the future.

Recently, car sharing has been increasing mainly in urban areas. The current utilization rate per hour for passenger cars is said to be around 5 %. If this utilization rate increases due to car sharing, there will be a demand to improve the durability of all parts, including **NTN** parts, or provide vehicles with various types of sensor functionality such as failure detection.
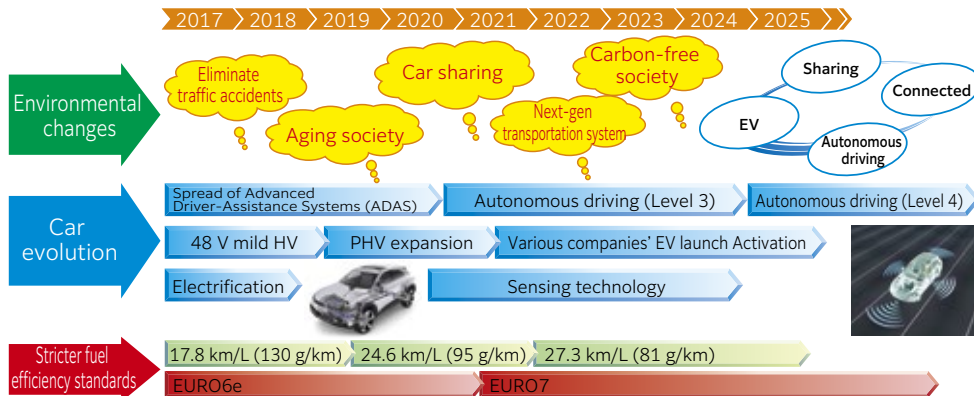

Fig. 1 Market trend of automobile

* Executive Officer, Deputy Corporate General Manager of Automotive Business Headquarters, Corporate General Manager of Electric Module Products Division

Table 1 Issues and measures for each level of autonomous driving

Level	Challenges	Measure
1	Reduce traffic congestion	Can reduce traffic congestion by managing the transportation system
2	Reduce traffic accidents	Reduce accidents due to human error by controlling the vehicle with a autonomous driving system
3	Reduce environmental impact	Reduce unnecessary acceleration or deceleration and reduce environmental impact by reducing traffic congestion
4	Movement assist for the elderly and disabled	Assisted movement for people who are unable to drive using autonomous driving vehicles
5	Labor-saving	Resolve driver shortages using unmanned driven vehicles

2. Market Needs and Responding to These Needs with NTN's Research and Development

There is a strong demand from the market to produce lighter and more compact bearings that have a lower friction and such from the perspective of reducing fuel consumption and saving energy **(Table 2)**. **NTN** has been making progress in developing high-performance products and deploying them to the market more than our competitors based on our accumulated technology and knowledge. We have also established the **NTN** Next Generation Research Alliance Laboratories at Osaka University (in 2017) to conduct research into next-generation technology that cannot be achieve through corporate research alone, and have continued to incorporate findings from this research into **NTN** technology.

For example, we took up the challenge of producing an axle bearing that has approximately 60 % lower friction than conventional products and achieved a product to meet this goal. Grease-filled bearings have a seal to prevent the grease from leaking and prevent muddy water from penetrating from outside the bearing. It was necessary to establish an optimal design for the sealing characteristics and friction characteristics, which was the root of the challenge concerning friction. We were also successful in reducing the friction of transmission ball bearings by 80 %. In the past, a contact-type seal was used to prevent hard foreign objects, such as gear debris generated inside the transmission, from entering the bearing. However, after coming up with a bold new design for the seal we achieved an 80 % reduction in friction.

The electrification of auxiliary equipment driven by the internal combustion engine is also making progress due to the electrification of drivetrains. Therefore, low friction, lightweight and compact bearings are required for the purpose of achieving further energy reduction. It is necessary to also respond to speed increases that accompany motors becoming faster. **NTN** has explored solutions for these issues as it has continued to do so in the past. Our core competencies lie in technologies that include multi-material technology, heat treatment technology,

high-precision machining technology, measurement technology, surface processing technology, and simulation technology. **NTN** has a dedicated team of researchers and engineers who excel in these core competencies in our Research and Engineering Division. We believe the time has come to contribute towards the automotive industry by using these core competencies and various human resources to further expand the playing field to meet market needs such as improved fuel efficiency.

We have also received many requests for high-performance module products, beginning with bearings, utilizing these core competencies. All of which have the goal of reducing traffic accidents, providing freedom of movement in a safe and secure manner, bringing convenience to users, and establishing environmental measures. **NTN** has been developing electric module products by integrating such things as motors and controllers through collaboration with other companies and in-house development. Some of these products have already entered the preliminary stage of mass production. More specifically, products such as electric oil pumps, electric water pumps, and electric parking locks for which demand is increasing. This also includes products such as Hub Bearing with Motor Generator Function (eHUB) and Hub Bearing with Steering Assist Function (sHUB™), which provide multi-functionality to the axle bearing, a bearing that has taken the top global share.

Table 2 Market trend and needs

	Market trend	Market needs
1	Environmental technology (Low fuel and power consumption)	· Electric module products · Lower friction · Higher speed · More compact and lightweight · Greater efficiency · Greater reliability
2	Car sharing	· Greater reliability · Durability
3	Comfort	· Low-noise profile
4	Safety and autonomous driving	· Sensors, control technology (linearity)

3. Developed Products

3.1 Electric Module and Actuator Development and Application Examples

We have developed an electric module and actuator constructed from a motor, sensor and mechanical body that utilizes such as motor design technology and bearing/ball screw product technology, which are some of our core competencies. More specifically, the BIII-series **(Fig. 2)** combines a hollow high power output brushless DC motor and a ball screw, with a linear motor mechanism arranged in the hollow section of the motor. The SP-series **(Fig. 3)** is also available for use in applications that require a thin and high torque rotational actuator by incorporating a reducer in the hollow section of the BIII-series.

The following are application examples proposed to the market, beginning with the electric module and actuator.

(1) Electric hydraulic brake (BIII-series)
Applying the coaxial type BIII-series with built-in ball screw to the master cylinder shaft can create a more compact electric hydraulic brake system.
(2) Electric variable valve timing control (SP-series)
Incorporating the SP-series into the camshaft can achieve a more compact and highly efficient electric variable valve timing mechanism.
(3) Electric oil pump (SP-series)
Incorporating a thin and highly efficient SP motor and integrating it with a controller can create a more compact electric oil pump.

・Compact design due to coaxial arrangement
・Optimized size, torque and output using a polymerized structure for the magnet and core
・Shares the magnet and coil, which are the main components of a motor
・Built-in non-contact linear position sensor

Fig. 2 BⅢ series

・Brushless DC motor series
・Hollow structure based on the motor unit from the BIII-series
・Can be applied as a thin and high torque rotational actuator by incorporating a reducer in the hollow section
・Built-in rotation angle sensor

Fig. 3 SP series

3.2 Axle Bearing Low Friction and Modular Products
3.2.1 60 % Reduction in Friction "Low Friction Hub Bearing III" (Fig. 4)

"Low Friction Hub Bearing III" is constructed with seals, grease and an internal bearing design in pursuit of lowering the friction, reduces the rotational torque by about 60 % when compared to conventional products, and has improved vehicle fuel efficiency by approximately 0.53 % **(Fig. 5)**. This product has already been proposed to several automobile manufacturers and is undergoing prototype evaluation and being ordered by customers.

(1) Low friction due to the seal
Approximately 50 % of rotational torque from a hub bearing is friction due to sliding with the seal. The seals ability to resist muddy water is an important characteristic and the following two points are challenges in maintaining this characteristic and lowering the friction. The friction was reduced for both the outer seal and inner seal making full use of each element test and simulation technology.
① Labyrinth structure, lip shape and material
② Optimal design for lip contact surface, lip application dedicated grease
(2) Low friction due to grease inside the bearing
The following 3 points are challenges present for resistance and friction that accompany grease agitation and such. Low friction was achieved by optimizing the thickening agent and additive and lowering the viscosity and friction of the base oil.
① Rolling viscous resistance between the rolling element and raceway surface
② Friction due to micro slips at the rolling contact zone of the rolling element and raceway
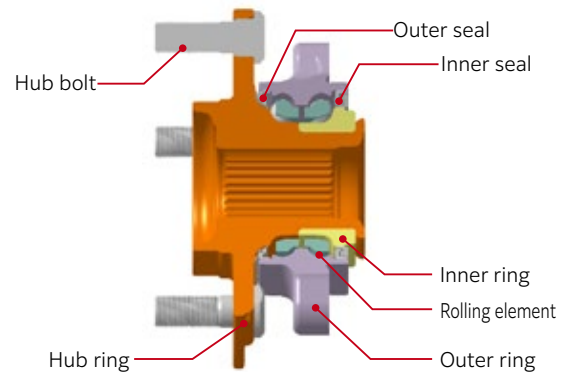③ Resistance due to grease shearing between the rolling element and cage pocket surface
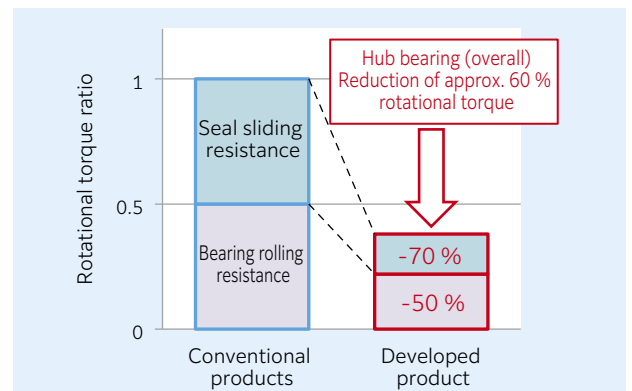

Fig. 4 Low Friction Hub Bearing Ⅲ

Fig. 5 Performance of Low Friction Hub Bearing Ⅲ

3.2.2 Hub Bearing with Steering Assist Function "sHUB ™" (Fig. 6)

Since the steering device arranged at the front wheels of a vehicle is mechanically connected to the tires on both sides (left and right) of the vehicle, the steering angle for the left and right tire is uniquely determined against the steering angle of the steering wheel. When making a large turn at low speed, the turning radius of the path through which each of the left and right wheel passes through is different. Therefore, it is necessary that Ackermann geometry (a setup in which the steering angle for the inside wheel is large and the outside wheel is small) is used for the left and right wheel to ensure the vehicle turns smoothly in theory. Furthermore, the turning center of a vehicle changes depending on the vehicle speed in a medium to fast speed range so the ideal left and right wheel angle will also change.

NTN developed the "Hub Bearing with Steering Assist Function" (hereafter, sHUB™), which grants the hub bearing with a function that can control steering geometry depending on the conditions.

sHUB™ achieves reliable and comfortable driving by controlling the angle of the left and right wheel separately according to the vehicle driving conditions. This product is a module system that improves straight running stability and driving reliability when cornering and also contributes towards avoiding dangers during an emergency such as when a vehicle wheel slips while driving on a low coefficient of friction road. It can also save energy when driving by reducing cornering drag when turning the vehicle normally. It is a module that achieves vehicle maneuverability and a comfortable driving experience with the aim of applying it to such things as avoidance operation in future autonomous driving technology. The following are its features.

(1) assembled on both left and right wheels to separately set the left and right steering angle
(2) Ideal angle control that matches driving conditions at each wheel separately
 ・Energy-saving driving with reduced cornering drag
 ・Stabilizes the vehicle attitude even during emergencies such as to avoid dangers
(3) Can be assembled regardless of the type of suspension system
 Can be assembled without significant modification to the existing vehicle's driven wheels (front and rear)
(4) Provides a compact and lightweight solution using an optimal internal bearing design

Furthermore, sHUB™ for the rear wheels described in this paper was designed for the purpose of further improving vehicle maneuverability and achieving safe, comfortable, and energy-saving driving by assembling it on the vehicle's rear driven wheels to control them. We have also received many inquiries about its application on front-wheel-drive vehicles.
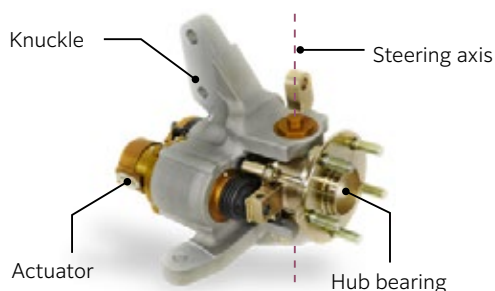

Fig. 6 Structure of sHUB™

3.3 Support for Next-Generation Mobility with World's Highest Level in Low Temperature Rise and Low Torque "Low Temperature Rise and Low Torque Tapered Roller Bearing" (Fig. 7)

Within this revolutionary period typified by CASE (Connected, Autonomous, Shared & Services, Electric) and against the backdrop of such things as the increase in vehicle travel distance due to vehicle electrification and car sharing, the move to higher efficiency power transmission devices is underway. Furthermore, due to reduction in the amount of lubricating oil in devices and the switch to low-viscosity oil, there has been a greater need for bearings to work under harsh lubrication conditions and for bearings with lower torque.

To fill this need, we developed the "Low Temperature Rise and Low Torque Tapered Roller Bearing" for automobile transmissions and differentials. By optimizing the newly designed plastic cage and the internal bearing design, we achieved the world's highest level in low temperature rise (capability for protecting against seizure) and low torque performance. The following are this product's features.

(1) Low temperature rise:
 10 times improvement in comparison with **NTN** standard type (world's highest level)
 ・Reduces temperature rise even under harsh lubrication conditions due to decreasing amount of lubricating oil and reducing lubricating oil viscosity
 ・The concave shape of the plastic cage enables oil to be supplied to the roller end face when there is insufficient lubrication to reduce temperature rise
 ・Reduces temperature rise with a design that improves the lubricity of sliding contacts between the roller end face and inner ring cone back face rib surface
(2) Low torque:
 66 % reduced torque compared to **NTN** standard type (world's highest level)
 ・Plastic cage reduces excessive lubricant inflow into the bearing, reduces rotational torque due to lubricant stirring resistance
 ・Smaller bearing size with longer operating life due to optimized internal bearing design and roller bearing design
 ・Reduces rotational torque due to reduction in rolling contact length between rolling elements (rollers) and raceway (inner and outer rings)

Since we were able to create a compact bearing size with this product, it contributes to making devices more compact and lightweight, and further increasing the amount of space inside the vehicle as well as improving driving comfort, in addition to providing greater efficiency for power transmission devices, and making vehicles more fuel and power efficient.

Fig. 7 Low Temperature Rise and Low Torque Tapered Roller Bearing

4. CAE Simulation Technology

In order to quickly launch competitive products on the market that meet market needs, it is essential to make research and technology development work more sophisticated and efficient. We have introduced CAE simulation technology as a means of this achievement. This technology allows to verify the performance of products including peripheral components at the design stage. This makes it possible to optimize design variables before creating a prototype, and reduce the number of prototype builds and tests. These factors can achieve improved work efficiency, reduce development costs, and shorten development lead times.

To ensure that designers can easily use CAE simulation technology required to develop products, we have been developing our own CAE system and program, and part of it is introduced here.

(1) FEM analysis automated system **(Fig. 8)**

FEM analysis is used when designing axle bearings to evaluate the stress and rigidity. In the past, this work was performed by dedicated CAE personnel but after developing a system that automates model creation, calculation, and results processing required for the analysis, it is now possible for designers to perform this analysis by themselves. This has enabled us to reduce the time needed to hold meetings between designers and dedicated CAE personnel and the time waiting for analysis to begin, and also speed up design changes influenced by the calculation results.

(2) Engineering calculation program for transmission bearings **(Fig. 9)**

Progress is being made for multi-stage and increasingly complex transmissions to respond to environmental requirements. To design bearings used in such products, we have developed an engineering calculation program that enables designers to easily create a model of the entire transmission and simulate it. This has enabled us to perform batch calculations for the bearing operating life and the load acting on each bearing's rolling element inside the transmission, a task that was traditionally performed using a combination of several programs. Further using a dynamic analysis system[1] for the bearing alone enables us to calculate stress generated at the cage as well[2][3]. Using these programs has enabled us to efficiently perform advanced optimal design for bearings that match the characteristics of transmissions.

Fig. 9 Simulation sample of transmission bearing

5. Conclusion

This paper describes **NTN**'s views and how the company will proceed concerning research and technology development with regards to fuel efficiency regulations, autonomous driving technology and car sharing amid environmental changes typified by CASE.

We believe that the information contained here has provided you with an understanding of our product development and market expansion that is superior to our competitors based on **NTN**'s accumulated technology and knowledge.

All developed products introduced here are the results of improving and incorporating elemental technology. We will continue to provide global proposals as specifications that can apply these products to next-generation mobility.

We sincerely hope that by providing products that resolve the various issues related to automobiles into the future will enable us to contribute to achieving a NAMERAKA smart mobility society.

References
1) Mariko Sekiya, Integrated Bearing Dynamic Analysis System (IBDAS), NTN TECHNICAL REVIEW,No.79, (2011)119-123.
2) Tomoya Sakaguchi, Kazuyoshi Harada, Sadatsune Kazama, Advancement of Cage Stress Analysis of Rolling Bearings, Tribology Congress Spring 2012 Tokyo, (2012) 233.
3) Tomoya Sakaguchi, Kazuyoshi Harada, Sadatsune Kazama, Advancement of Cage Stress Analysis of Rolling Bearings, NTN TECHNICAL REVIEW, No.80, (2012) 92.

Photo of authors

Koji KAMETAKA

Executive Officer,
Deputy Corporate General
Manager of Automotive
Business Headquarters,
Corporate General Manager of
Electric Module Products Division

Fig. 8 FEM analysis sample of axle bearing

Small and Lightweight CVJ for Rear Sub-axles

Tomoshige KOBAYASHI*

FF-based 4WD vehicles generally have a smaller rear torque distribution than the front, so small load capacity is applied to the constant velocity joints for the sub-axle.

There is a market demand for small-sized CVJs for rear sub-axles, similar to the "R series"; "R series is a compact and lightweight CVJ for rear of main axle, which is already in mass production and pursues miniaturization and weight reduction.

Introducing the features and performance of the developed "small and lightweight CVJ for rear sub-axles".

1. Introduction[1] [2]

Passenger cars are categorized by front-wheel drive (FF), rear-wheel drive (FR) or 4-wheel drive (4WD) driving methods, with 4WD vehicles further classified as being based on an FF layout or FR layout.

Constant velocity joints (CVJs) that are used as driveshafts for driving the front wheels of FF vehicles and 4WD vehicles have the role of transferring power from the engine or motor smoothly to the tires. These CVJs need to move with the tires steering and the suspension changing, and as such, consist of fixed type CVJs with a larger work angle used on the tire side, and sliding type CVJs that can slide in the axial direction used on the differential side

While rear driveshafts of FR vehicles and 4WD vehicles can actually use fixed axles (rigid axle with the left and right wheels connected in a line along the same axle), vehicles designed for ride comfort and driving stability require CVJs because they use suspension systems that allow the left and right axles to move up and down independently (independent suspension systems) **(Fig. 1)**. Yet they differ from the CVJs used for front wheels because the rear tires are not used for steering so a large operating angle is not needed.

NTN has developed a wide variety of CVJ types including fixed types and sliding types that provide different functions to suit specific applications. Furthermore, each type of CVJ is also available by load capacity in a range of sizes, from small (such as #75 for compact cars) to large (such as #113 for large vehicles).

Until recently **NTN** had used front wheel CVJs as rear wheel driveshafts, however as large operating angles are not required for rear wheel CVJs, **NTN** has developed the small and lightweight R Series[3] with a minimal operating angle. This product has been released in sizes with high load capacities and

marketed toward European automotive manufacturers for use as main axles in FR vehicles.

More recently, rear wheel CVJs have also been developed as small and lightweight CVJs in sizes with low load capacities for sub axle applications.
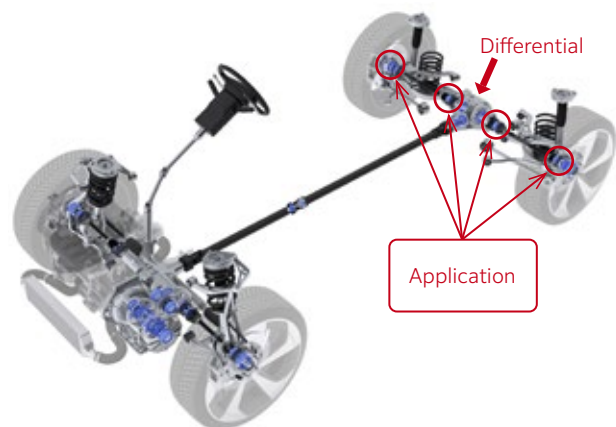
Fig. 1 Application of CVJ for rear

2. Developed Product Structure and Features

SUVs have been dominating the automotive market in recent years, and there are many models that are available with 4WD powertrains. C segment or smaller compact SUVs that are particularly popular in Japan and Europe also come in 4WD configurations based on an FF platform in order to maximize cabin space.

In general FF-based 4WD vehicles have a smaller torque distribution to the rear compared to the front, and in many cases small CVJs are used for the rear.

In light of this, **NTN** adapted its existing lightweight "R Series" rear driveshaft to develop the small size "Small and Lightweight CVJ for Rear Sub-axles."

A comparison of the developed "Small and Lightweight CVJ for Rear of Sub-axle" and the

---

* CVJ Development Dept., Automotive Business Headquarters

conventional product is shown in **Fig. 2**.

The developed product mass and outer diameter reduction rate from the conventional product is shown in **Table 1**. Compared to the conventional product, the fixed type CVJ is approximately 6.2 % lighter and the sliding type CVJ approximately 29 % lighter in weight.

This corresponds to a 429 g lighter weight per driveshaft for the #75 size, making each vehicle 858 g lighter when both left and right driveshafts are taken into account.

The outer diameter has also been reduced significantly, with an 8.5 mm smaller (12.3 %

reduction) diameter achieved on the sliding type CVJ in particular.

Note that as the vehicle mounting structure differs for each customer, the mass calculations shown in **Table 1** do not include the stem section (fitting shaft for vehicle mounting) in the shape shown in **Fig. 2**.

Fig. 2 Development product VS Conventional product (#75 size)

Table 1 Development product mass and outer diameter reduction rate (#75 size)

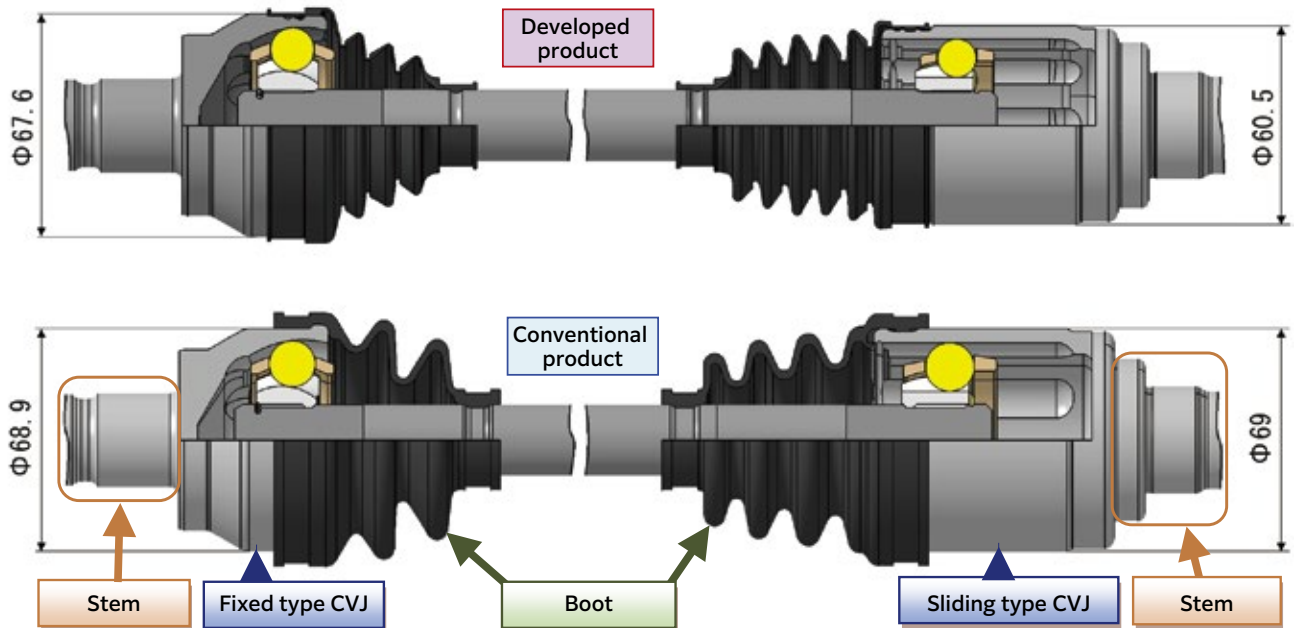| Developed Product	Mass Reduction Rate	Diameter Reduction Rate
Fixed type CVJ	6.2 %	1.9 %
Sliding type CVJ	29.0 %	12.3 %

3. Small and Lightweight Fixed Type CVJ for Rear Sub-axles

Fixed type CVJs for front wheels have a maximum operating angle of 47 to 50° as they need to cater to vertical movement of the suspension and turning of the wheels with steering.

In contrast, CVJs for rear wheels only need to cater to the vertical movement of the suspension, and as such an operating angle of 20° or less suffices on most vehicles when actual usage conditions are considered. As some vehicles may need an operating angle of 20° or more for mounting or handling requirements, the maximum operating angle of fixed type CVJs is 30°.

In the conventional product, the internal parts (inner ring, cage, ball) of the existing 47° design were adopted together with the 30° design, where the outer ring is shorter in the axial direction to achieve a lighter weight. To make the developed product even lighter in weight, each part was shortened in the axial direction, as well as a shorter design incorporated in the radial direction.

3.1 Features

A comparison of the lighter weight #75 size developed product and the conventional product is shown in **Table 2**.

Table 2 Comparison of development product and conventional product

Item	Developed Product	Conventional Product
Maximum operating angle [°]	30	30
Outer diameter [mm]	φ 67.6	φ 68.9
No. of balls	6	6
Mass [g]	834 Compared to conventional product - 6.2 %	889
SUB-ASSY		

The conventional product was based on the CVJ for front wheels, with the maximum operating angle limited to 30° and only the outer ring shortened in the axial direction. However, there was excess thickness in the material of each part designed with a maximum operating angle of 47°.

The developed product was designed for rear wheels so the maximum operating angle was made smaller, which results in a smaller maximum input load and allows each part to have thinner material. Smaller

diameter balls could also be used to successfully make the outer ring outer diameter and cage smaller, which helped achieve a small size and light weight **(Fig. 3)**.
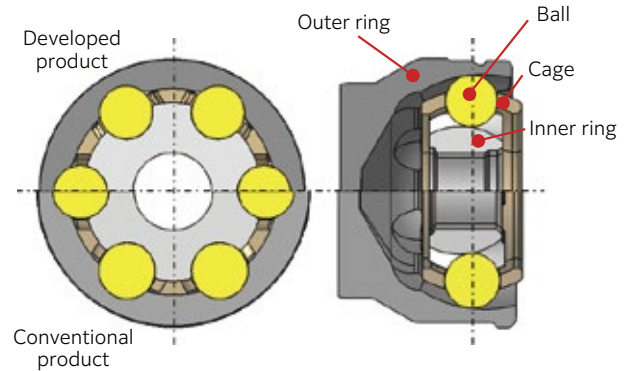
Fig. 3 Comparison of outer dia. and axial length

3.2 Functional Evaluation

The functional requirements are as outlined below.
① Strength: equivalent to conventional product (at maximum angle)
② Durability: equivalent to conventional product

Examples of strength test results for the developed product are shown in **Fig. 4**, and durability test results in **Fig. 5**.

The developed product meets the development targets set based on past test data for the conventional product, and was verified as having equivalent strength and durability as the conventional product.
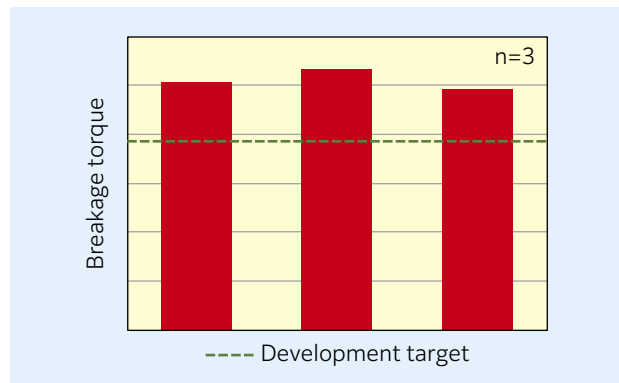
Fig. 4 Static torsion strength test result of developed product (θ=20°)
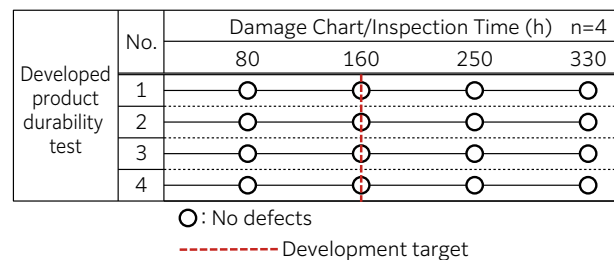
Fig. 5 Durability test result of developed product (θ=6°)

4. Small and Light Sliding Type CVJ for Rear Wheels[4)]

While there are many variations of sliding type CVJs available, FF vehicles and the front wheels of 4WD vehicles use either tripod or ball type CVJs. Tripod type CVJs have a low sliding resistance to limit engine vibrations being transmitted to the tires, steering and other parts of the vehicle body via the CVJs, while ball type CVJs are able to reduce rattle in the drivetrain.

For a long time, **NTN** had been using ball type sliding double offset joints (DOJ) as small CVJs for the rear wheels, but had been using the CVJs outlined above for front wheels.

The developed product was also applied to the DOJ to develop a new small and lightweight sliding type CVJ for rear wheels by limiting the maximum operating angle (23° → 20°) for the rear wheels only.

4.1 Features

A comparison of the lighter weight #75 size developed product and the conventional product is shown in **Table 3**.

Table. 3 Comparison of development product and conventional product

Item	Developed Product	Conventional Product
Maximum operating angle [°]	20	23
Outer diameter [mm]	φ 60.5	φ 69
No. of balls	8	6
Mass* [g]	910 Compared to conventional product - 29 %	1,284
SUB-ASSY		

* Slide amount: calculated at 45 mm

The conventional DOJ was designed with 6 balls, however the developed product was designed with 8 balls with the goal of reducing size and weight considerably.

Using 8 smaller diameter balls for transmitting torque helps to better disperse the load acting on each ball to achieve a smaller size and lighter weight. Limiting the maximum operating angle and using a smaller ball PCD decreases the range of movement of balls in the axial direction and reduces the groove length of the inner and outer rings. The result is that the inner and outer rings, and the axial length of the cage, can be reduced to achieve a more compact size as well as a lighter weight **(Fig. 6)**.
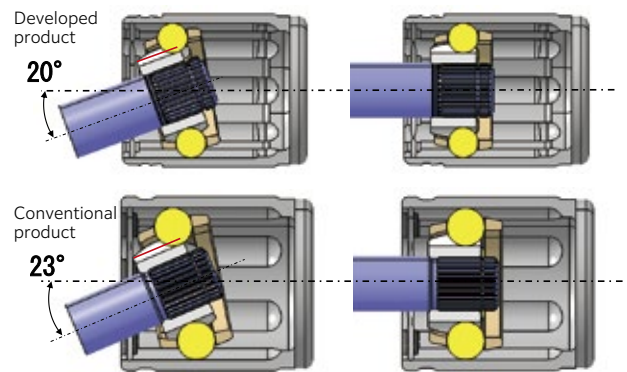
Fig. 6 Comparison of ball groove length (red line)

As the balls have a smaller diameter than the conventional product, the width of the cage window, and thus the width of the cage, could be reduced. Limiting the maximum operating angle and using a smaller ball PCD also decreases the range of motion of balls within the cage window, thus the length of the cage could be made shorter. Limiting the operating angle also allows for a smaller taper angle to be used for the outer diameter, which makes it easier to achieve the thickness for the cage and a smaller size in the radial direction **(Fig. 7)**.
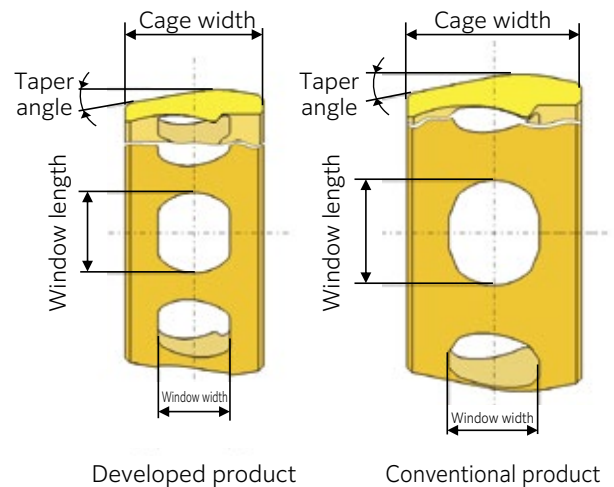
Fig. 7 Comparison of development product cage and conventional product cage

As the width of the cage and inner ring can be shortened, the length of the outer ring cup can be reduced while ensuring the same slide amount (L1 < L2 in **Fig. 8**), thereby making it shorter in the axial direction than the conventional DOJ.

Smaller diameter internal parts also mean the outer ring can be a smaller outer diameter.
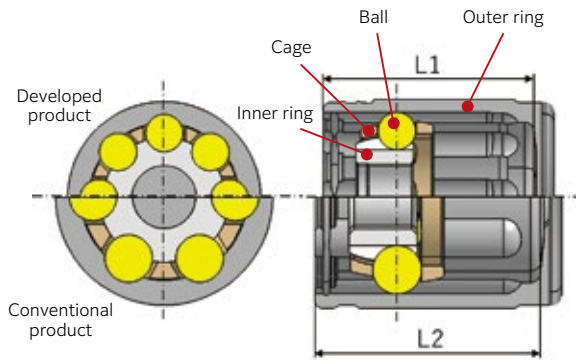
Fig. 8 Comparison of outer dia. and axial length

4.2 Functional Evaluation

The functional requirements are as outlined below.
① Strength: equivalent to conventional product (at maximum angle)
② Durability: equivalent to conventional product

Examples of strength test results for the developed product are shown in **Fig. 9**, and durability test results in **Fig. 10**.

The developed product meets the development targets set based on past test data for the conventional product, and was verified as having the equivalent strength and durability as the conventional product.

Fig. 9 Static torsion strength test result of developed product (θ=20˚)

Fig. 10 Durability test result of developed product (θ= 6˚)

5. Boot and Amount of Grease

Limiting the maximum operating angle also allowed for a small and lightweight boot to be used. Furthermore, the amount of injected grease could also be reduced due to the smaller size of the CVJ and boot.

Small and lightweight boot designs for fixed type CVJs and sliding type CVJs are being developed with the aim of reducing the weight of driveshafts even more.

## 6. Conclusion

This article outlined the features and performance of the "Small and Lightweight CVJ for Rear Sub-axles" developed for use with the sub-axle rear wheels of FF-based 4WD vehicles.

With the growing demand for small SUVs, there has been an increase in models designed using FF-based 4WD vehicles. The developed product can also be used for rear-wheel drive vehicles that need small size CVJs. With more environmentally friendly designs an essential requirement of recent vehicle development, this significantly lighter weight developed product is anticipated to meet a range of market requirements.

References

1) Shin Tomogami, Technical Trends in Constant Velocity Universal Joints and the Development of Related Products, NTN TECHNICAL REVIEW, No. 75, (2007) 10-15.
2) Shinichi Takabe, History of Constant Velocity Joints, NTN TECHNICAL REVIEW, No. 85, (2017) 40-45.
3) Tomoshige Kobayashi, Light Weight Drive Shaft for FR vehicle "R series," NTN TECHNICAL REVIEW, No. 85, (2017) 78-83.
4) Hiroshi Tone, Kenji Terada, Masamichi Nakamura, Summary of E Series, High Efficiency Constant Velocity Joints, NTN TECHNICAL REVIEW, No. 70, (2002) 18-23.

Photo of authors

Tomoshige KOBAYASHI

CVJ Development Dept.,
Automotive Business
Headquarters

Hub Bearing Module with Steering Function for Rear Wheel

Yusuke OHATA*
Atsushi ITO*

We have developed a hub bearing module, 'Ra-sHUB' with steering function incorporating the steering angle adjustment mechanism in the hub bearing. This product can be attached to rear driven wheels, by controlling the right and left wheel with separate actuators, we can control the angle of the right and left wheel independently. Therefore, the dynamic performance of the vehicle is significantly improved.

1. Introduction

There are Systems available that improve turning capabilities at low driving speeds and enhance vehicle stability at medium to high driving speeds by making corrections to the steering angle of the wheels to suit the vehicle's driving conditions.

NTN developed the "Hub Bearing Module with Steering Adjust Function[2)-4)](sHUB[TM])" that turns the front wheels by incorporating a steering function into the "Hub Bearing[1)]" of which **NTN** has the leading global market share.

NTN has verified in a number of actual driving tests that independently correcting the steering angle of the left and right front wheels can improve the driving performance of vehicles in a range of situations, from ordinary driving to harsh driving conditions, as well as from very low driving speeds up to high speeds.

The shape and configuration of each part has now been modified so that this system can be assembled to the rear wheels. This report covers the basic performance test and actual driving test that were conducted.

Conventional rear wheel steering systems have been limited to suspension structures such as multi-link systems, and large operating angles were difficult to achieve due to the structure of the system. The Hub Bearing Module with Steering Function for Rear Wheel (hereafter, Ra-sHUB) incorporates a steering shaft in the hub bearing for an integrated steering angle adjustment mechanism, with its compact design meaning it can be assembled in the same way as conventional hub bearings.

The result can be applied as a rear wheel steering system capable of large operating angles that can even be assembled to rigid axle systems such as torsion beams, regardless of the suspension structure.

2. Background

Rear wheel steering systems first became available in mass-produced vehicles in the 1980s, however many commented on the unnatural way the vehicle behaved with the driver's steering operation. The advances that have been developed to control technology prove this unnatural feeling can be minimized, and such systems have increasingly been used in luxury cars and sports cars in recent years.

Rear wheel steering systems have the following advantages.

● Low-speed cornering
Turning the rear wheels in the opposite direction (reverse phase) to the front wheels reduces the turning radius, allowing tighter turns to be made in the same way as a vehicle with a shorter wheelbase.

● High-speed cornering
Turning the rear wheels in the same direction (same phase) as the front wheels and controlling the centrifugal force to reduce the yaw moment achieves the same level of stability as vehicles with a longer wheelbase.

● Better fuel efficiency
Vehicles generally have rear wheels set to toe-in to increase stability during braking, however this increases running resistance and in turn reduces fuel efficiency. Reducing running resistance with the tires parallel to the driving direction during ordinary driving, and changing to toe-in when braking can help achieve both safety and low-fuel consumption driving.

* New Business Search and Development Dept., New Product and Business Strategic Planning Headquarters

3. Concept

The aim of control with Ra-sHUB assembled to the rear wheels is to increase the dynamic performance of the vehicle, as well as achieving safe, comfortable and energy-efficient driving. The system is also anticipated to be used with future automated driving technologies. The main concepts are as outlined below.

① Assembled on the left and right rear wheels for independent control of steering angles. This allows each wheel to be controlled at the optimum angle to suit driving conditions
  ・Energy-efficient driving with minimal cornering drag
  ・Excellent response and stable vehicle stance even during emergency situations like hazard avoidance
② Can be assembled to existing vehicles without requiring any modifications, regardless of the type of suspension system
③ Small and lightweight due to optimized internal design
④ Assembled within wheels to maintain vehicle design flexibility

Fig. 1 shows Ra-sHUB assembled to a vehicle's rear wheels. The Ra-sHUB controller separately calculates and controls the target angle of the left and right Ra-sHUB based on vehicle information such as speed and angle of the steering wheel.
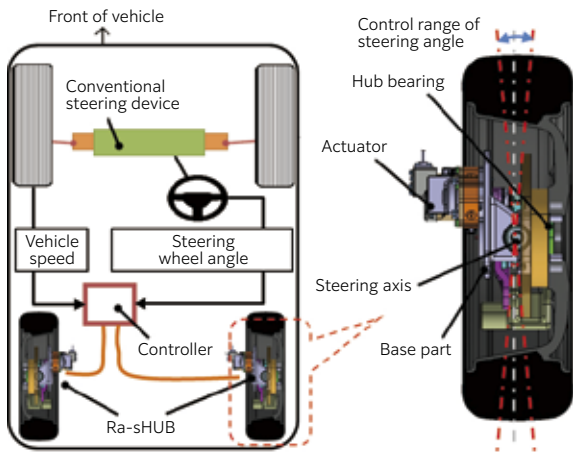
Fig. 1 Vehicle image with Ra-sHUB (Attached to rear wheels)

Fig. 2 shows the layout with Ra-sHUB assembled to an ordinary rigid axle (torsion beam). Turning the rear wheels when a rigid axle is used generally requires movement of the entire rigid axle, however, a rear wheel steering system can be achieved easily by attaching Ra-sHUB to the hub bearing mounting face of the torsion beam.
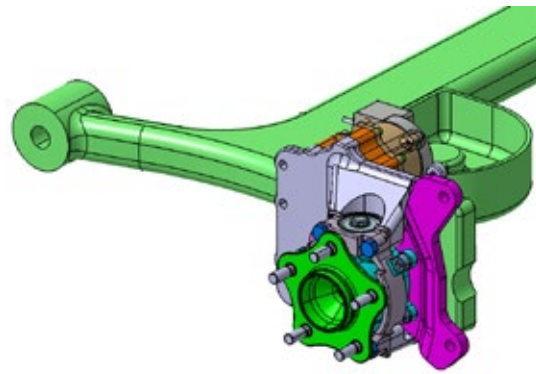
Fig. 2 Ra-sHUB attached to rigid axle

The basic layout of the rear wheel with Ra-sHUB assembled is shown in **Fig. 3**. When all four wheels of the vehicle are in equal contact with the ground, the steering axis is slightly behind the point of contact between the tire and ground. This results in ground contact point located forward of the steering axis, so when the reverse input load from the ground contact point acts on the outside tire of the turn when cornering, the large load applied to the outside tire forces it toward a natural toe-in direction, which increases the cornering limit performance for more stable driving.
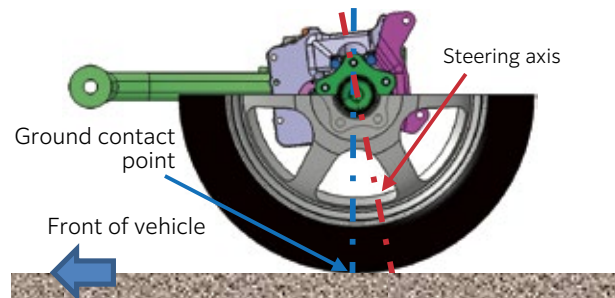
Fig. 3 Layout of rear wheel with Ra-sHUB

4. Configuration and Specification

4.1 Components

Fig. 4 shows the components of Ra-sHUB. Ra-sHUB is comprised of three core components: an actuator, base part, and hub bearing. The role of each component is as follows.
  ・Actuator : fixed to the base part, and consists of a motor, reducer and trapezoidal screw for steering the hub bearing.
  ・Base part : connects to the suspension system of the vehicle.
  ・Hub bearing : supports the base against rotation around the rotation axis and around the steering axis of the wheel.
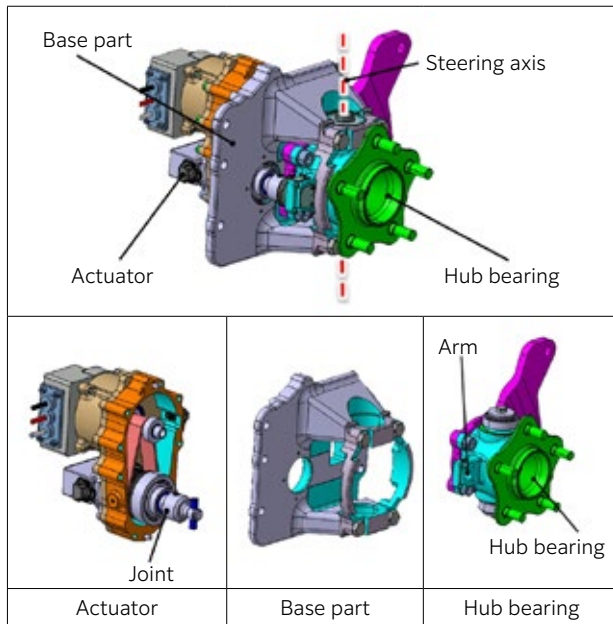
Fig. 4 Components of Ra-sHUB

The motor of the actuator is controlled at the best tire angle by the controller based on the input such as the vehicle speed and steering wheel angle. The rotation from the motor is converted to linear motion by the trapezoidal screw via the reducer, and the screw drives the end of the arm via the joint to steer the hub bearing around the steering axis.

The reverse input load from the tires is also blocked by the self-lock mechanism of the trapezoidal screw, which helps to reduce motor power consumption.

4.2 Specifications

Fig. 5 shows the appearance of the developed product designed for the rear wheels of a front-wheel drive C segment vehicle (with torsion beam rear suspension structure). The specifications of the developed product are shown in **Table 1**.
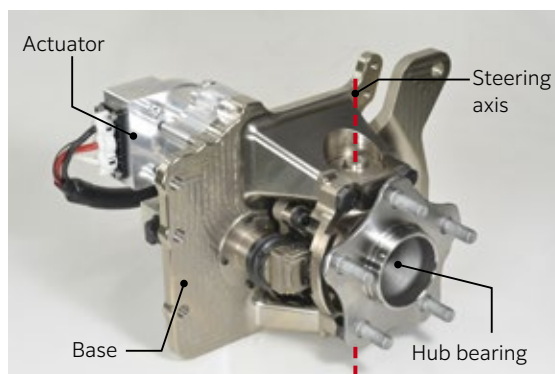
Fig. 5 Prototype of the Ra-sHUB (Left rear wheel use)

Table 1 Specifications of the Ra-sHUB prototype

Item	Values
Maximum steering torque	350 Nm
Power supply voltage	24 V
Maximum steering angle	± 3.5 deg
Maximum steering angular speed	16 deg/s

5. Basic Performance Test

The basic characteristics of the developed product required for assembling it to vehicles were verified.

5.1 Frequency Response

A frequency response characteristics test was conducted with the wheels of a test vehicle (in a stationary state) assembled with Ra-sHUB placed on a turntable. The response of the actual steering angles was verified by applying a steering angle command in the form of a 0.5 degree amplitude sinusoidal wave to Ra-sHUB and changing the frequency.

The test results are shown in **Fig. 6**. At frequencies of 4 Hz or less, the amplitude gain (shown as the log of the ratio between the amplitude value of the actual steering angle and the command value, **Fig. 6** (a)) and the absolute value of the phase difference (**Fig. 6** (b)) were small, and deemed to be at a level that can be used to control the stance of the vehicle without any issues.

(a) Gain

(b) Phase difference
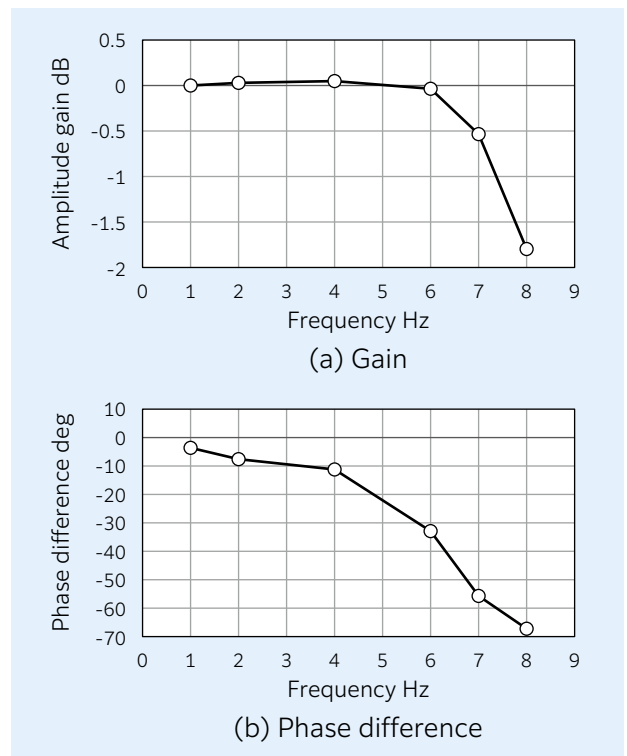
Fig. 6 Frequency response characteristic

5.2 Small Steering Angle Durability Test

Many repeated minor adjustments around the central steering position are expected during actual driving, so the durability was verified under the conditions shown in **Table 2**. **Fig. 7** shows the comparison of response characteristics before and after the durability test. There was no change in response characteristics with respect to commands before and after the test, and there was no difference in the response waveform. This verified that there was no decrease in performance even after repeated minor steering adjustments.

Table 2 Durability test condition

Steering Angle	± 0.5 deg
Steering frequency	5 Hz (sinusoidal wave)
Load from road surface	3.8 kN (equivalent to vehicle weight acting on each wheel)
No. of repeated steering cycles	10^7 cycles
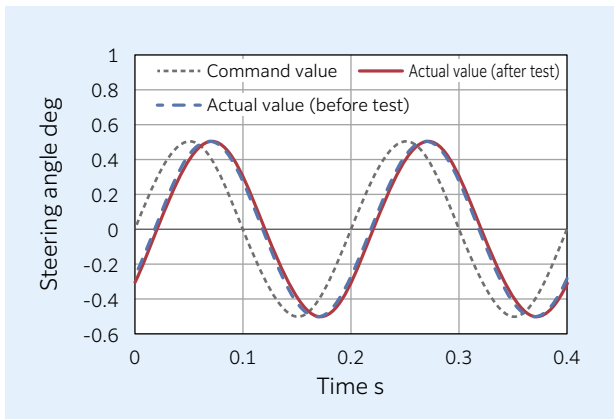
Fig. 7 Comparison of response characteristic

5.3 Temperature Characteristics

The usage temperature of the Ra-sHUB was set at the same temperature as hub bearings in ordinary vehicles at -40 to +120 ℃ . The change in steering speed within environment temperature ranges was checked. The test involved immersing the controller and sample into a constant temperature bath and kept at a set temperature for one hour before testing operation. **Fig. 8** shows the measured waveforms of steering speed at each environmental temperature.
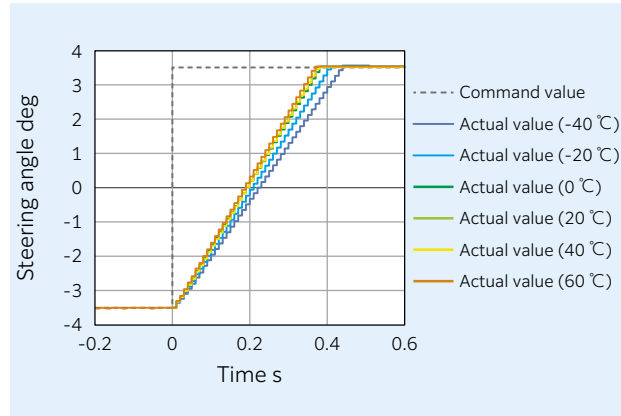
Fig. 8 Waveform of steering speed

The steering speed was determined from the actual steering angle inclination of the Ra-sHUB when applied with stepped steering commands (-3.5 ⇒ +3.5 deg (**Fig. 8** dotted line)).

Fig. 9 shows the relationship between the steering speed and environmental temperature. While a decrease in steering speed that is thought to be caused by an increase in internal resistance at low temperature ranges was observed, the design meets specifications and has minimal impact on vehicle control.
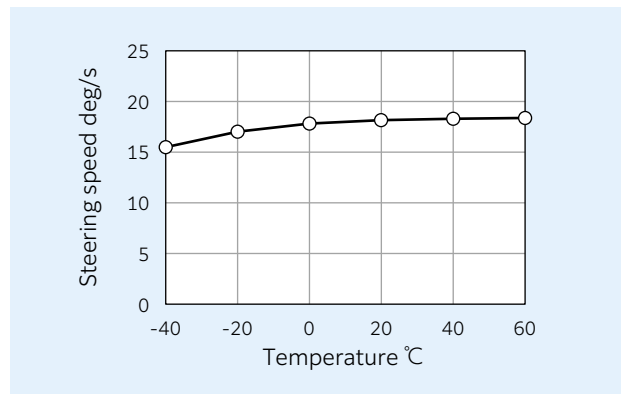
Fig. 9 Relations of temperature and steering speed

5.4 Rigidity and Strength Tests

The rigidity and strength when mounted to the vehicle was verified for factoring in external forces from the road surface when driving, by individually applying loads in the vertical direction (z direction) and the longitudinal direction (x direction), and moments around the x axis. The XYZ directions are shown in **Fig. 10**.

Fig. 11 shows the relationship between the load from each direction and displacement. There were no major differences in rigidity in the vehicle's vertical and longitudinal directions. **Fig. 12** shows the relationship between the moment load in the camber (x axis) direction and the flange inclination. No deformation or damage was observed after removing the load under all conditions.
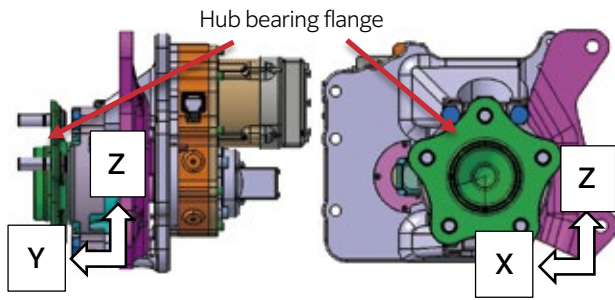
Fig. 10 Axis direction of the product
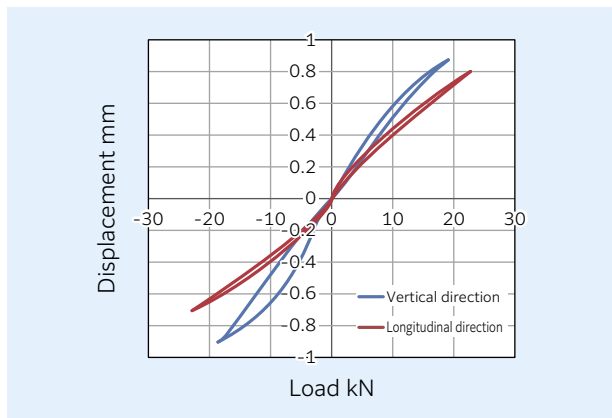
Fig. 11 Wheel rigidity
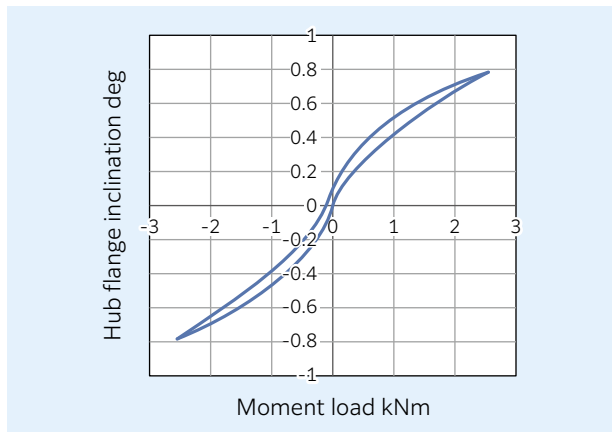
Fig. 12 Moment rigidity

6. Verification of Effective Ra-sHUB Rear-wheel Steering

To verify the improvement in vehicle cornering performance with Ra-sHUB steering, Ra-sHUB was assembled to the rear wheels (torsion beam) of a C segment test vehicle and actual driving tests conducted.

The rear wheel steering angle was changed with Ra-sHUB to suit driving conditions to control the vehicle's slip angle.

Fig. 13 shows the layout of the course on a compacted snow road used for driving tests. The test compared differences in vehicle behavior with or without Ra-sHUB steering operation while following

the same line.

Data at points A to E in **Fig. 14 to 16** correspond to each of the positions A to E in **Fig. 13**.
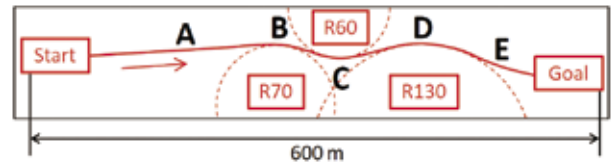
Fig. 13 Course layout

Fig. 14 shows the vehicle speed and steering wheel angle during the test, and **Fig. 15** shows the longitudinal and lateral acceleration. When driving at the same speed (84 km/h) at position B and following the same line at the tight radius position C, steering control with Ra-sHUB made cornering possible without exceeding the grip limit (0.4 G) of the tires on compacted snow roads, and there was also a 7 % rate of decrease in speed. Compared to driving without Ra-sHUB steering, the vehicle could drive through the whole course approximately 2 seconds faster.

(a) Vehicle speed

(b) Steering wheel angle
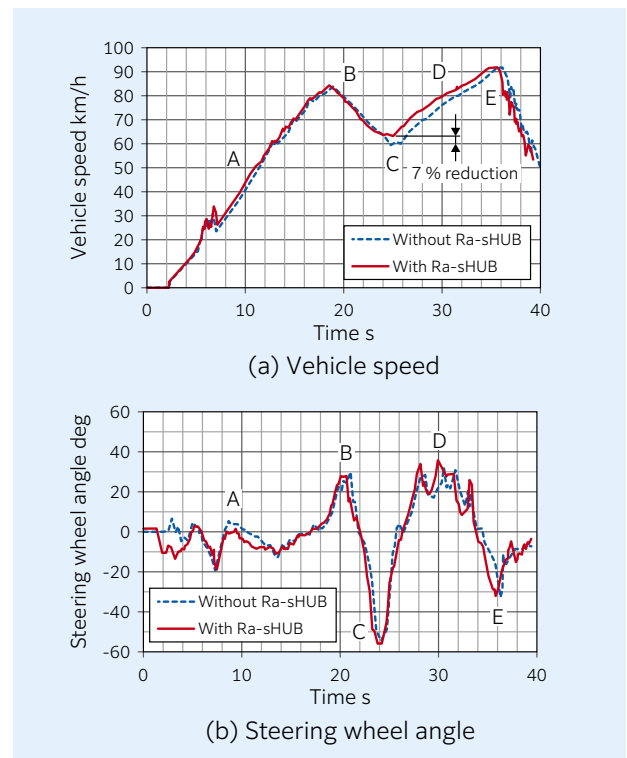
Fig. 14 Test results (Speed, Steering Angle)
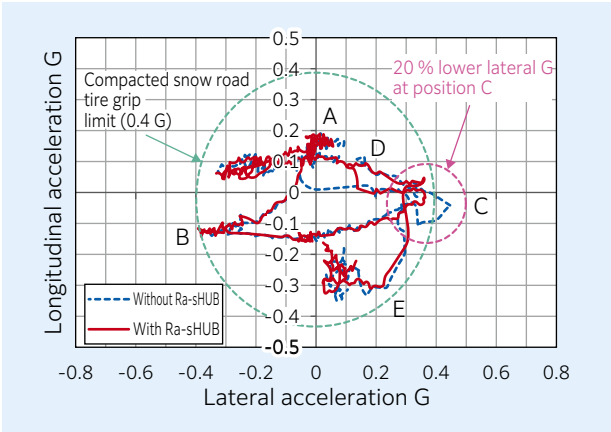
Fig. 15 Test results (Longitudinal acc, Lateral acc)

As shown in **Fig. 16**, there is a closer linear relationship between the yaw rate and steering wheel with Ra-sHUB steering compared to without Ra-sHUB steering, and the improvement in vehicle operation is clear.
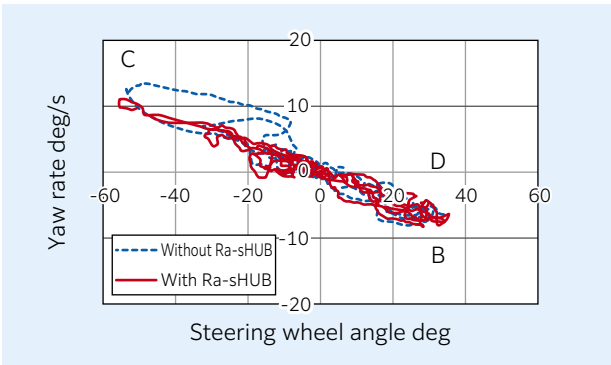
Fig. 16 Test results (Steering angle, Yaw rate)

The command value and actual angle match during this Ra-sHUB operation as shown in **Fig. 17**, and operation was observed to be in line with the command value without any delay.
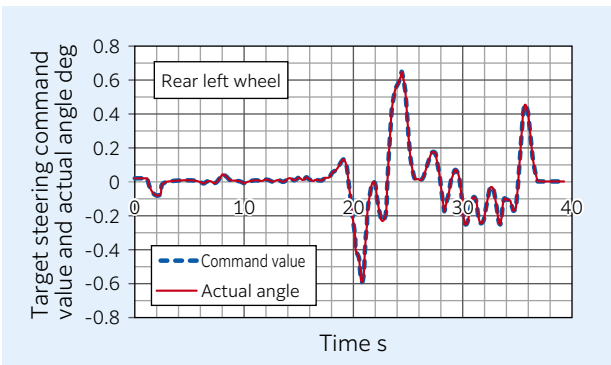
Fig. 17 Ra-sHUB command value and actual angle

The driver's workload was also estimated using the steering entropy method[5], which calculates the driver's workload from how smooth the steering angle changes.

The difference (prediction error) between the target steering angle and actual steering angle at each measurement position is calculated, with the steering entropy corresponding to the 90th percentile of absolute values of the prediction error distribution. This means that if 90 % of the data lies within the range of prediction error $\pm \alpha$ margin, the steering entropy is α. A smaller value here indicates that steering is close as possible to the ideal smoothness.

Fig. 18 shows the prediction error distribution calculated from the results of driving tests, and **Table 3** shows the values for steering entropy. This table shows that the steering entropy value is lower with Ra-sHUB steering compared to without Ra-sHUB steering, indicating that the vehicle is easier to drive by the driver and that smoother operation is possible.
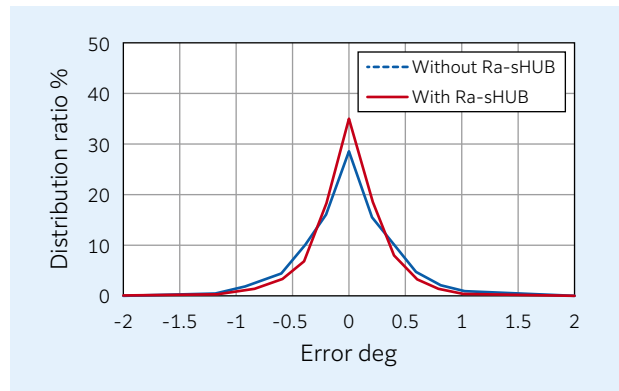
Fig. 18 Prediction error

Table 3 Steering entropy (90 percentile)

Without Ra-sHUB	With Ra-sHUB
0.73 deg	0.56 deg

7. Conclusion

This article outlines the configuration, specifications and basic performance of the "Hub Bearing Module with Steering Function for Rear Wheel."

Ra-sHUB is a system that allows rear wheel steering with large operating angles that can be assembled to rigid axle systems such as torsion beams, regardless of the suspension structure. The article outlines how Ra-sHUB is effective for improving vehicle dynamic performance and operation in driving tests conducted on compacted snow roads.

Practical applications for Ra-sHUB will be developed in the future, including compatibility with various suspension systems and further improvements in functionality.

References

1) NTN Corp. Hub Bearings Catalog, NTN homepage, https://www.ntn.co.jp/japan/products/catalog/ja/4601/index.html
2) Norio Ishihara, Mitsunori Ishibashi, Hirokazu Ooba, Atsushi Ito, Makoto Yamakado, Yoshio Kano, Masato Abe, Hub Bearing with Integrated Active Front Steering Function that Improves Vehicle Dynamic Performance, Proceedings of Society of Automotive Engineers of Japan, (2018) 20185263.
3) Norio Ishihara, Mitsunori Ishibashi, Hirokazu Ooba, Atsushi Ito, Makoto Yamakado, Yoshio Kano, Masato Abe, Hub Bearing with Integrated Active Front Steering Function that Improves Vehicle Dynamic Performance [2nd Report], Proceedings of Society of Automotive Engineers of Japan, (2019) 20191269.
4) Satoshi Utsunomiya, Norio Ishihara, Yusuke Ohata, Atsushi Ito, Hub Bearing Module with Steering Adjust Function (sHUB™), NTN TECHNICAL REVIEW, No. 87, (2019) 18-23.
5) Takayuki Kondoh, Tomohiro Yamamura, Nobuyuki Kuge, Perez Miguel, Takashi Sunda, Development of a Real-time Steering Entropy Method for Quantifying Driver's Workload, Transactions of the Society of Automotive Engineers of Japan, Volume 46 Issue 1, (2015) 167-172.

Photo of authors

Yusuke OHATA

New Business Search and Development Dept., New Product and Business Strategic Planning Headquarters

Atsushi ITO

New Business Search and Development Dept., New Product and Business Strategic Planning Headquarters

Creepless Ball Bearing

Hayato KAWAGUCHI*   Toshiki MASUDA*
Marina NAGATA**   Toshiki KAWAI***

As housings and bearing rings are made thinner to accommodate downsizing or reduced weight transmissions for improved fuel consumption in automobiles, outer ring creep is more likely to occur.

NTN has developed a "Creepless ball bearing" capable of preventing creep during single direction load conditions. This article introduces the features and performance capabilities of the Creepless ball bearing.

1. Introduction

Deep groove ball bearings are frequently used as gear support bearings in automotive transmissions. These bearings are often configured with a loose fit between the outer ring and housing, which could result in the outer ring experiencing creep depending on factors such as bearing specifications, loose fit conditions or load conditions. Creep of the outer ring causes wear on the fitting surfaces of the outer ring and housing, and increases misalignment or inclination of the shaft which results in problems like abnormal noises or vibrations in the apparatus[1].

The growing demand for greater fuel efficiency in recent years has led to motors being developed with more gears or more compact and lightweight designs. To achieve this, housings and bearing raceways tend to be designed with thinner raceways; however, this can result in outer ring creep occurring more often. As such, there has been increasing demand for creep-resistant bearings in recent years.

The creepless ball bearing developed here is able to prevent creep when a load is applied from a specific direction as in the case of progressive wave type creep[2], where the outer ring slips in the same direction as the rotation of the inner ring.

This article provides an outline of a newly developed product that is easy to assemble as it features the same components as standard bearing types.

2. Features

The features of the developed Creepless Ball Bearing (hereafter, developed product) are as follows.

Superior creep resistance* : prevents creep
                             No creep wear
                             (under **NTN** test
                             conditions)
Ease of assembly   : equivalent to standard
                             type
Durability   : equivalent to standard
                             type (under **NTN** test
                             conditions)

* Under conditions with load applied in a specific direction

3. Structure and Performance

3.1 Types of Bearing Creep[2]
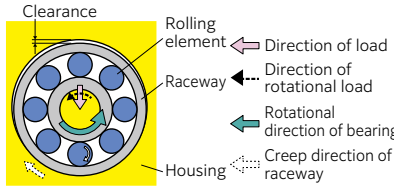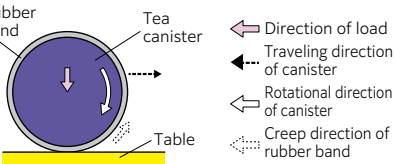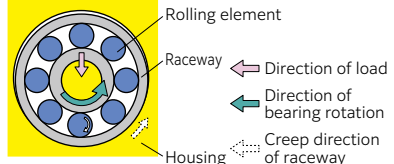
There are two main types of bearing creep depending on the direction of rotation and phenomena. **Table 1** outlines the various types of outer ring creep. Outer ring creep in the opposite direction of rotation occurs when there is clearance between the outer ring and housing, or elastic deformation and slippage of the outer ring. Outer ring creep in the same direction as rotation occurs when there is outer ring distortion due to the rolling element load being applied in progressive waves. **NTN** calls this "progressive wave type creep" (which occurs when load is applied to the bearing in one specific direction).

*   Automotive Engineering Dept., Automotive Business Headquarters
**   CAE R&D Center
*** Automotive Testing Dept., Automotive Business Headquarters

Table 1 Types of outer ring creep[2]

Type	Illustration
Creep (opposite direction of rotation)	① Loose fit for outer ring and housing Clearance, Rolling element, Raceway, Housing — Direction of load, Direction of rotational load, Rotational direction of bearing, Creep direction of raceway · Occurs with rotating load · Caused by clearance between the outer ring outer diameter and housing inner diameter ② Interference fit for outer ring and housing (example of tea canister with rubber band around it) Rubber band, Tea canister, Table — Direction of load, Traveling direction of canister, Rotational direction of canister, Creep direction of rubber band · Occurs with rotating load · Caused by elastic deformation and slippage of the raceway
Creep (same direction as rotation) → Progressive wave type creep	 Rolling element, Raceway, Housing — Direction of load, Direction of bearing rotation, Creep direction of raceway · Occurs when load is in one direction · Caused by outer ring distortion

3.2 Mechanism of Progressive Wave Type Creep[2]

Details of the mechanism are shown below **(Fig. 1)**.
(1) Rolling element load acts on the outer ring
(2) Outer ring material immediately below is displaced
(3) Outer ring surface becomes wavy up to several microns depending on the magnitutde of the rolling element load
(4) When inner ring rotates, the rolling elements also move
(5) Surface waves become progressive waves and cause outer ring creep

Load of rolling element, Rotation direction of rolling element, Creep direction of raceway, Traveling direction of rolling element, Elliptic motion of surface, Raceway elongation, Raceway contraction, Rolling element, Raceway, Housing
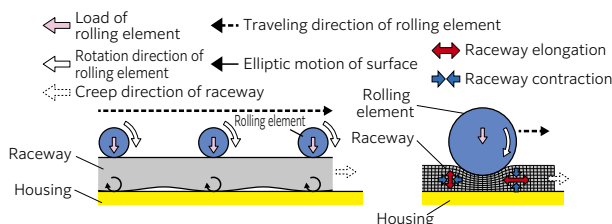
Fig. 1 Creep by strain

Progressive wave type creep only occurs when the load on the bearing is in one direction. By using the following formula, progressive waves can be prevented. However, extremely thick sections are required for standard bearings, which makes preventing progressive wave type creep difficult in reality **(Fig. 2)**.

Raceway thickness t / pitch interval between rolling elements w > 0.6

Rolling element, Raceway, w, t
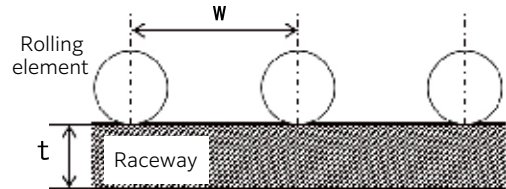
Fig. 2 Thickness of bearing ring and rolling elements

3.3 Overview of Developed Product
3.3.1 Aim of Design

The gear support sections of transmissions often suffer from progressive wave type creep due to the bearing fit and load conditions. By focusing on the mechanism of progressive wave type creep, **NTN** developed a product to stop creep by blocking progressive waves in the outer ring.

3.3.2 Appearance

The components are the same as the standard type bearing, but the developed product features an arc-shaped undercut across the full width of part of the outer diameter of the outer ring **(Fig. 3, 4)**.

The size of the new product is interchangeable with standard bearings, and does not impact assembly into the housing.

Undercut
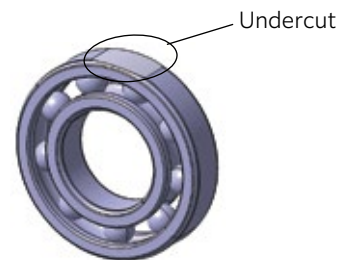
Fig. 3 Appearance of developed product

Undercut, Outer ring outer diameter
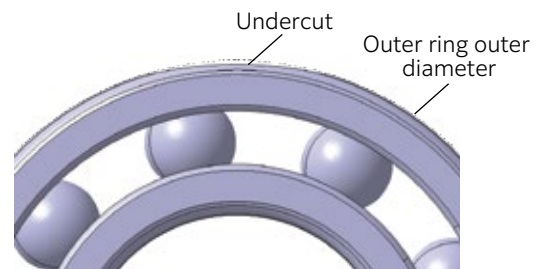
Fig. 4 Structure of developed product

3.3.3 Mechanism to Prevent Creep

Standard type bearings transmit progressive waves in the load region if the outer diameter surface of the outer ring deforms and makes contact with the housing, causing creep in the same direction. The developed product however, avoids contact with the housing in the region of the undercut, which blocks progressive waves and stops creep from occurring.

An image of the mechanism that prevents creep is described below and shown in **Fig. 5**.
(1) Bearing load acts on outer ring after passing through the inner ring and rolling elements
(2) Outer ring outer diameter surface deforms in the radial direction due to the load from the rolling elements
(3) Undercut used to avoid contact with the housing
(4) Progressive waves caused by distortion on outer ring outer diameter surface are blocked, which prevents creep

(a) Standard type   (b) Developed product
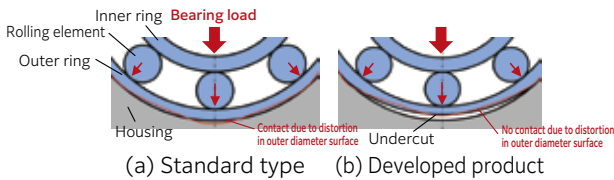
Fig. 5 Mechanism image for creep stop

Outer ring creep is prevented when the undercut is positioned in the load zone; even when the undercut is positioned outside of the load zone, creep is prevented when the outer ring undercut enters the load region as a result of creeping. Accordingly, there is no need to factor in phase when installing the developed product into the housing.

3.3.4 Creep Speed

Tests were conducted to verify the speed at which the developed product would creep. The test conditions are shown in **Table 2** and test results shown in **Fig. 6**.

Four types of samples were tested alongside the developed product, including standard type bearings, **NTN**'s conventional creep prevention AC bearings[3], and bearings with coated outer ring outer diameters.

Creep speed in the standard type bearings and AC bearings increased as the load was increased. However, there was no creep in the developed product even with high loads verifying that progressive waves in the outer ring were blocked and creep was prevented by the new design.

Table 2 Test condition

Bearing number	6208
Load Fr (P/C)	4 standards from 0.1 to 0.4
Inner ring rotational speed min⁻¹	6,000
Lubricant	CVT fluid
Bearing outer ring temperature ℃	50
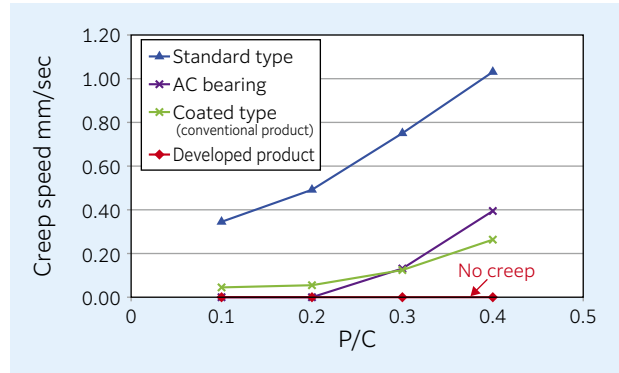
Fig. 6 Creep speed test results

The order of creep speed at high loads was as follows.

High   ←   Creep speed   →   Low

Conventional product > AC bearing > Coated type > Developed product

3.3.5 Impact on Outer Ring Undercut Strength

Tests were conducted using FEM analysis to verify the stress on the outer ring outer diameter surface of the developed product.
The analysis conditions are shown in **Table 3** and analysis results shown in **Fig. 7**.

While the developed product generated around 10-times the tensile stress compared to the standard type, this was not at a level that could cause failure and had several times the safety factor for allowable tensile stress of bearing steel (SUJ2).

Table 3 Strength analysis condition

	Standard Type	Developed Product
Bearing number	6208	
Undercut	No	Yes (immediately below load region)
Load Fr (P/C)	0.4 * (top of ball)	
Bearing fits	Clearance fit (outer ring outer diameter / housing inner diameter)	
Analysis model image		

* The rolling element load distribution of the developed product differs from the standard type due to the undercut.
  As indicated in these analysis conditions, the maximum rolling element load of the developed product is lower than the standard type when the undercut is immediately below the load region. To consider the worst case scenario, the same rolling element load as the standard type has been used for the analysis.

(a) Standard type   (b) Developed product
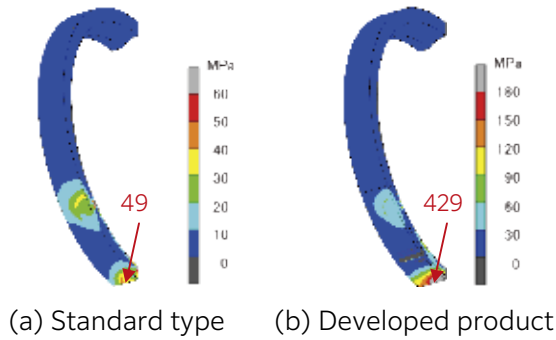
Fig. 7 Strength analysis result

3.3.6 Impact on Operating Life

The load distribution on the rolling elements in the developed product differs from standard bearings due to the position of the undercut in relation to the load direction. As such, the impact on the rolling fatigue life was calculated theoretically.

To understand how the undercut affects the developed product, the balance of forces was calculated by factoring in both the elastic deformation of the outer ring and housing as well as the amount of elastic contact between the balls and raceway due to Hertzian contact.

Table 4 shows a list of the analysis results.

Table 4 Calculation result

	Standard Type	Developed Product	
		Undercut 45° position	Immediately below undercut
Bearing number	6208		
Undercut	No	Yes (45° position)	Yes (immediately below)
Load Fr (P/C)	0.4		
Illustration		Undercut position	Undercut position
Rolling fatigue life L_{10} (compared to standard type)	1	0.95	1.06

When the undercut is at a 45° position with respect to the load direction, the rolling fatigue life decreases (around 5 %) compared to the standard type; however when the undercut is immediately below the load, it actually increases (around 6 %). This is due to the change in the maximum rolling element load as compared to the standard type. As such, the impact on the rolling fatigue life due to the undercut is small.

3.4 Evaluation Result of Developed Product
3.4.1 Outer Ring Crack Test (static)

A static crack test was conducted to verify the strength of the outer ring outer diameter surface undercut included in the developed product.

The test jig is shown in **Fig. 8**. The undercut of the developed product was simulated with a load using a special jig, with one rolling element positioned in the load region to concentrate the load at the undercut. A precision universal testing machine was used as the tester to apply a static load from the inner ring, with the cracking load deemed to be the point when the load decreased suddenly.
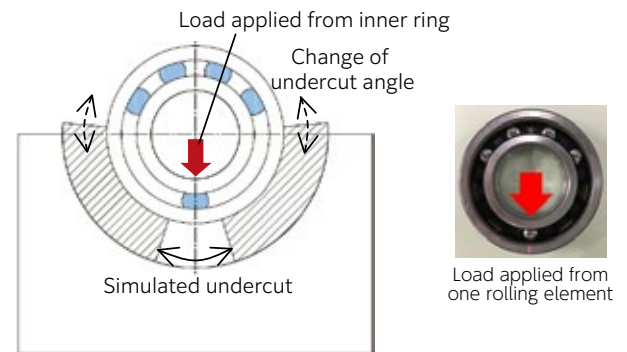
Fig. 8 Outer ring crack tester

The test results are shown in **Fig. 9**.

The cracking load was determined to have a safety factor of two times or more against the basic static load rating C_0, and as such was deemed acceptable with respect to static destruction.
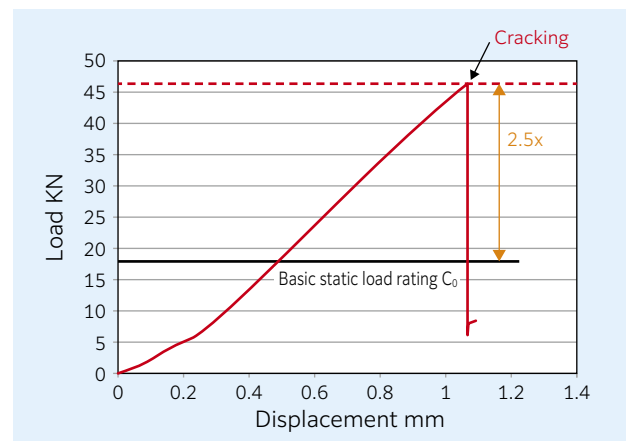
Fig. 9 Crack test results

3.4.2 Outer Ring Crack Test (dynamic)

A dynamic crack test was conducted to verify the strength of the outer ring outer diameter surface undercut included in the developed product.

To evaluate the fatigue strength, a load exceeding the basic dynamic load rating was applied for more than 10^7 cycles. The test conditions and results are shown in **Table 5**.

Table 5 Test condition and result

Test conditions	Bearing number	6208
	Load Fr (P/C)	1.2
	Inner ring rotational speed min^{-1}	2,500
	Lubricant	CVT fluid
	Bearing outer ring temperature ℃	Natural temperature rise
	Operating time	Suspended at double the 1×10^7 cycles passed by the rolling element (equivalent to 3-times or more the rolling fatigue life)
Test result		No failure in standard type or developed product

Under these conditions, the developed product was deemed acceptable with respect to dynamic destruction.
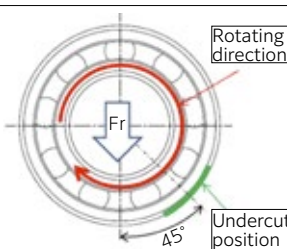
3.4.3 Durability Test

The rolling fatigue life was verified with a durability test. The test conditions are shown in **Table 6**. The undercut was positioned at 45° from the direction of the applied load where the rolling element load is the highest. The operating time was set to be suspended at 10-times the calculated operating life.

From the results shown in **Table 6**, the developed product was deemed acceptable with respect to rolling fatigue life under these conditions.

* This durability test used a high-rigidity housing to ensure that there was no creep.

Table 6 Test condition and result

Test conditions	Bearing number	6208
	Load Fr (P/C)	0.6
	Inner ring rotational speed min^{-1}	3,000
	Lubricant	CVT fluid
	Bearing outer ring temperature ℃	Natural temperature rise
	Operating time h	$L_{10h} \times 10$
	Undercut position	Test configured at position with highest rolling element load
Test result		No failure in standard type or developed product (suspended at 10-times calculated operating life)

4. Conclusion

This article provided an outline of the Creepless Ball Bearing. The developed product features an undercut in part of the outer diameter surface of the outer ring to successfully prevent outer ring creep caused immediately below the load when the bearing rotates in a specific direction. Creep is traditionally restricted by using external parts or applying a coating; however the developed product completely prevents all creep by including a simple modification to the outer ring without any changes to the internal components or envelope dimensions of the standard type bearing and without affecting assembly to the housing.

The Creepless Ball Bearing is anticipated to contribute to making automotive transmissions smaller, more lightweight and more fuel efficient, and will be actively released in various markets. Efforts will also be made to promote product development with the aim of further increasing performance.

References

1) Takayuki Teramoto, Yutaka Sato, Prediction Method of Outer Ring Creep Phenomenon of Ball Bearing Under Bearing Load, Transactions of the Society of Automotive Engineers of Japan, Volume 46 Issue 2 March, (2015) 355.
2) Tsuyoshi Niwa, A Creep Mechanism of Rolling Bearings, NTN TECHNICAL REVIEW, No. 81, (2013) 100-103.
3) NTN "Ball and Roller Bearings Catalog" CAT. No. 2203/J, (2020) B-15.

Photo of authors

Hayato KAWAGUCHI
Automotive Engineering Dept., Automotive Business Headquarters

Toshiki MASUDA
Automotive Engineering Dept., Automotive Business Headquarters

Marina NAGATA
CAE R&D Center

Toshiki KAWAI
Automotive Testing Dept., Automotive Business Headquarters

Low Temperature Rise and Low Torque Tapered Roller Bearing

Yasuhito FUJIKAKE*
Takanori ISHIKAWA*

Power transmission devices such as automobile transmissions and differentials are becoming smaller due to environmental regulations, and the use of low-viscosity oil and reduced oil quantity are advancing for high efficiency and power savings. The tapered roller bearings used in such power transmission devices are required to withstand severe conditions and to have low friction. In order to meet these demands, **NTN** has developed a tapered roller bearing with a new shape resin cage and incorporated design technology for low torque improvement and low temperature rise, thus attaining the world's highest level for both low torque performance and high seizure resistance. This paper introduces the structure and performance of the developed product "Low Temperature Rise and Low Torque Tapered Roller Bearing".

1. Introduction

The automotive industry is facing major changes[1] such as the transition to Connected, Autonomous, Shared, Electric (CASE) and smart mobility.

As companies boost their social responsibility toward the environment with measures such as Corporate Average Fuel Economy (CAFE) regulations[2], increasingly stringent CO_2 regulations means companies are focusing on electrification as a viable solution.

With the growing need for safety and comfort while driving, efforts are not only focusing on automated driving and collision safety, but also on achieving a greater freedom of layout design and more cabin space with the use of compact power transmission units.

The background to this shift in mobility is that automotive power transmission devices like the transmission and differential use an internal lubricant with lower viscosity and reduced quantity because such devices are becoming more compact with lower torque performance.

Tapered roller bearings that have a high load capacity are used in power transmission devices. However, these bearings have a higher rotational torque compared to ball bearings and as such suffer from sudden temperature increases under severe lubrication conditions. To achieve a longer operating life and lower temperature rises, **NTN** released the "ULTAGE Tapered Roller Bearing for Automotive Application"[3] in 2017.

Tapered roller bearings that support the power transmission devices mounted in vehicles required even lower torque and greater protection against

seizure, so efforts into enhancing these technologies were continued with the development of a new resin cage shape to meet such demands. This was combined with lower torque and lower temperature rise design technologies to develop the "Low Temperature Rise and Low Torque Tapered Roller Bearing" that achieves the world's highest level in low torque performance and protection against seizure. This article outlines the structure and features of this bearing.

2. Structure

An overview of the structure of the developed Low Temperature Rise and Low Torque Tapered Roller Bearing is shown in **Fig. 1**. The features ① to ④ shown in **Fig. 1** correspond to the following explanations of the structures in the developed product.

● New resin cage shape
① The inner diameter on the small side of the cage has been reduced for a smaller clearance with the inner ring small side rib outer diameter surface. This suppresses the amount of lubricant inflow into the bearing, which reduces stirring resistance due to the lubricant to achieve a lower torque.
② An open concave shape has been applied to the inner diameter side of the cage pocket large side edge. The corners within the concave shape retain lubricant inside the concave shape due to surface tension, and feed lubricant to the roller end face after operation starts, thus limiting any sudden temperature increases.

---

* Automotive Engineering Dept., Automotive Business Headquarters

● Optimal design between the roller end face and inner ring large side rib
  ③ An optimal design has been used to improve lubricity of the sliding contact between the roller end face and inner ring large side rib.

● Optimized design of rollers
  ④ A more compact roller design and smaller roller pitch circle diameter design have been used. The former decreases the rolling contact line between the rollers and the inner and outer rings. Reducing the rolling contact line decreases the rolling viscosity resistance, which achieves a lower torque. The latter reduces the circumferential speed of the rolling contact between the rollers and the inner and outer rings, which limits rolling resistance to achieve a lower torque.
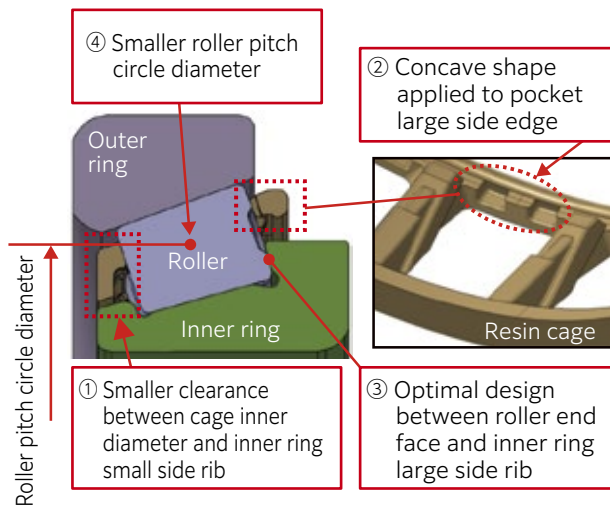
Fig. 1 Structure of "Low Temperature Rise and Low Torque Tapered Roller Bearing"

3. Features

The features of the Low Temperature Rise and Low Torque Tapered Roller Bearing (hereafter, the developed product) compared to conventional tapered roller bearings (conventional product)[4] are as shown below.
  (1) World's highest level in low torque performance
    : reduces rotational torque by 66 % compared to conventional product
  (2) World's highest level in protection against seizure
    : up to 10-times protection against seizure compared to conventional product

3.1 Reduced Rotational Torque
3.1.1 Reduced Lubricant Stirring Resistance
The raceway of tapered roller bearings is inclined with respect to the center of rotation, which creates a phenomenon called pumping action where lubricant flows from the small side to the large side of the developed product when it is rotating. To prevent more lubricant than is necessary flowing into the bearing due to pumping action, the developed

product uses the cage shape in **Fig. 1** ① , which limits torque loss caused by lubricant stirring resistance and thus achieves a lower torque.

3.1.2 Bearing Internal Optimal Design
The internal design for a longer operating life used in **NTN**'s proprietary "ULTAGE Tapered Roller Bearing for Automotive Application" technology, as well as an optimal design[5] of factors affecting the bearing load rating (such as outer ring angle, and angle and length of rollers), have been used to limit the decrease in bearing rated life while allowing for smaller size, and as a result achieving lower torque.

Table 1 shows an example of tests conducted on the small and lightweight design with load conditions expected to be acting on transmission support bearings of medium size passenger vehicles. The developed product test example has a 25 % reduction in bearing width dimension and 44 % lighter weight compared to conventional tapered roller bearings. This results in a shorter rolling contact length as well as a smaller roller pitch circle diameter, which helps to achieve low torque.

In contrast, the smaller size results in a reduction in the bearing dynamic load rating and operating life, so carbonitriding treatment was used to maintain the operating life.

Table 1 Study example of downsizing and weight reduction by applying the development specification

	① Conventional Product	② Developed Product
	Tapered roller bearing 32007X[4]	Tapered roller bearing
Scale drawing of bearing cross-section		
Size	φ 35 × φ 62 × 18	φ 34 × φ 58.5 × 13.5 (width reduced by 25 %)
Mass (kg)	0.223	0.125(44 % lighter weight)
Dynamic load rating (N)	46,000	28,500
Material heat treatment	Carburized case-hardened steel	Carbonitrided bearing steel
Operating life	Meets standards	Meets standards
Contact stress	Meets standards (with edge stress)	Meets standards (without edge stress)

3.2 Greater Protection Against Seizure
3.2.1 Concave Shape Applied to Pocket Large Side Edge

The effectiveness of the lubricant retention function that the concave shape applied to the cage pocket large side edge achieves was verified using flow analysis of the lubricant. The analysis conditions were as shown below.

<Lubricant flow analysis conditions>
・Model conditions **(Fig. 2)**: the analyzed cage pocket was positioned at the bearing top (12 oʼclock) to simulate supporting a horizontal shaft
(selected the position with the worst lubricant retention)
・Lubricant: ATF (120 ℃)
・Analysis conditions: unsteady flow analysis of multi-phase flow (VOF)
・Analysis step 1 : rotate bearing in lubricant until lubricant flow within bearing is steady
・Analysis step 2 : stop rotation of bearing. Stop supplying lubricant
・Analysis step 3 : analysis ends when outflow (movement) of lubricant within bearing stops
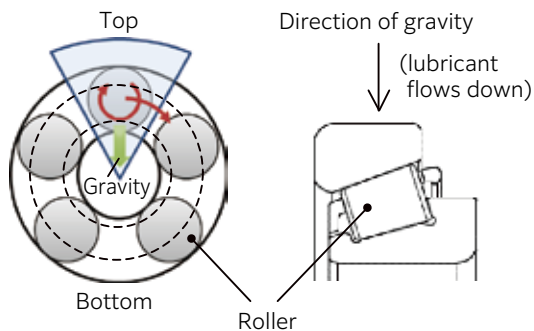
(a) Analysis model image of bearing front

(b) Direction of gravity and bearing top position cross-sectional image

Fig. 2 Definition of oil flow analysis

The analysis results are shown in **Fig. 3**. Lubricant was observed being retained in the concave shape of the cage pocket large side edge. This analysis helped determine the optimum shape within the concave section for retaining an amount of lubricant that can be supplied to the roller end face.
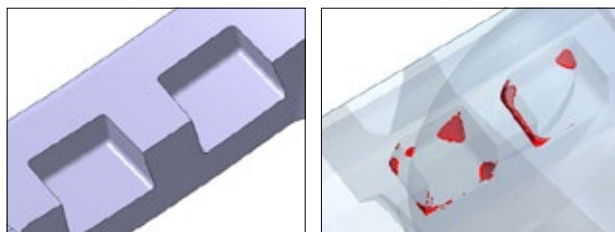
(a) Cage concave shape (same view as **Fig. 3** (b))

(b) Lubricant flow analysis results(red parts: lubricant)
(bearing shown as semi-transparent)

Fig. 3 Oil flow analysis results (Enlarged view of large diameter end face recessed shape of cage pocket)

3.2.2 Optimized Shape of Tapered Rollers

The inner ring large side rib and roller end face of tapered roller bearings make sliding contact with each other, leading to concerns over sudden temperature increases due to the lack of oil film formation when there is insufficient lubricant or low-viscosity lubricant is used. As such, the lubricity (oil film formation) needs to be improved on the sliding contact components to ensure greater protection against seizure.

The inner ring large side rib uses a straight shape to make this sliding contact more steady, and the roller end face uses an optimal rounded design to improve lubricity (oil film formation).

Fig. 4 shows the results of seizure protection tests of the development specifications with a rounded roller end face used to check the effectiveness of this design. The test conditions were set to abundant lubricant conditions (oil rich) and extremely low lubricant (oil poor). Better lubricity (oil film formation) was achieved under both conditions for the development specifications with a rounded roller end face, thus indicating better protection against seizure compared to the conventional standard specifications.
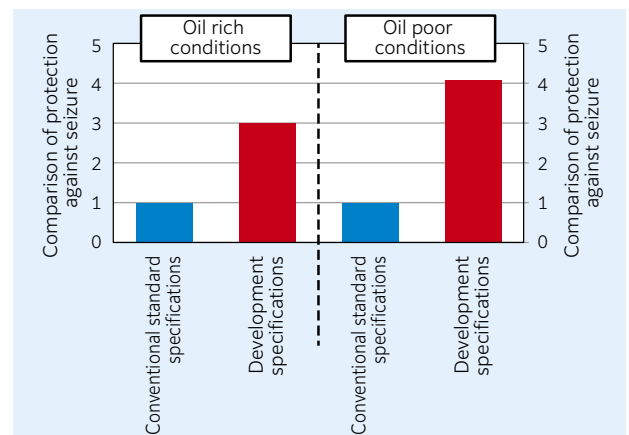
Fig. 4 Seizure resistance evaluation results for development specification roller end face radius
(Comparison result when the seizure resistance of the conventional standard specification is set to 1)

4. Bearing Performance

4.1 Rotational Torque Test

A rotational torque test was conducted on the bearing itself to check the effectiveness of reduced torque of the developed product.

The test results are shown in **Fig. 5**. As outlined in the previous section, the developed product was found to have a significant 66 % reduction in torque compared to the conventional product due to the effects of lower rolling friction and lower stirring resistance of the lubricant.

<Test conditions>
・Tested bearing size: Conventional product ø35 × ø62 × 18 (**Table 1** ① bearing)
Developed product ø34 × ø62 × 16
(same internal structure as **Table 1** ② bearing, with different dimensions for outer diameter and assembled width)
・Axial load   : 3,000 N
・Rotational speed   : 5,000 min^{-1}
・Lubricant conditions : oil bath lubrication, ATF (50 ℃)
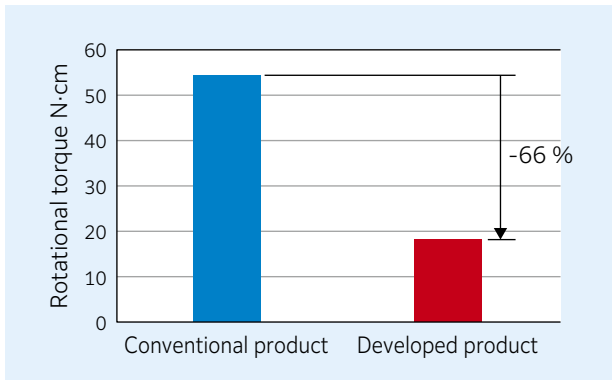
Fig. 5 Bearing rotational torque test results

4.2 Protection Against Seizure Evaluation Test

An evaluation test under the following conditions was conducted to check the effects of protection against seizure of the developed product. Test conditions were set with a low amount of lubricant based on the assumption of using a low-viscosity lubricant in power transmission devices or simulating the quick acceleration of electric vehicles. The bearing was applied with a set miniscule amount of lubricant, and then operated at room temperature in a non-lubricated state to test the time taken until the temperature of the bearing outer ring reached 100 ℃.

The test results are shown in **Fig. 6**. The conventional product standard steel plate cage has no lubricant retention function, and the rib between the inner ring and rollers is the standard design, and thus the bearing reached 100 ℃ in 72 seconds. In contrast, the developed product features the new resin cage shape outlined in the previous section, and in this test the initial amount of adhered lubricant increased 1.3 times compared to the conventional product. With the optimized roller end face and inner ring large rib, the test duration was approximately 10 times longer at 710 seconds, which is an immense improvement to protection against seizure.

<Test conditions>
 ・Tested bearing size: Conventional product ø35 × ø62 × 18 (**Table 1** ① bearing)
       Developed product ø34 × ø62 × 16
(same internal structure as **Table 1** ② bearing, with different dimensions for outer diameter and assembled width)
 ・Lubricant   : ATF (25 ℃)
 ・Rib contact stress : approx. 200 MPa
 ・Rib sliding speed : approx. 2.5 m/s
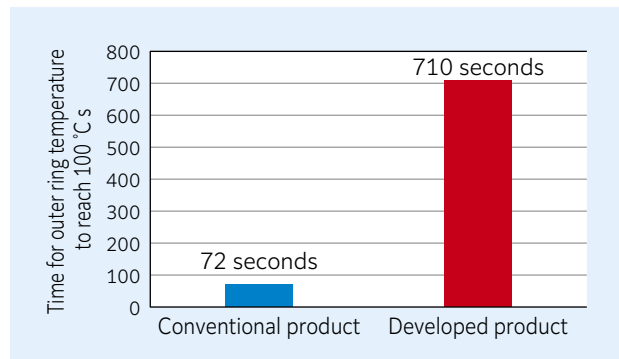
Fig. 6 Seizure resistance evaluation test results

4.3 Longer Operating Life Under Lubrication Conditions that Contain Contaminants

An operating life test was conducted on the developed product under lubrication conditions containing hard contaminants. The operating life of power transmission devices may be affected if hard contaminants are mixed in with lubricant. While there are various conditions of hard contaminants contained in the lubricant of power transmission devices, this test assessed the operating life under the following conditions.

The test results are shown in **Fig. 7**. Under the contaminant conditions of this test, the developed product was deemed to have an ample effective operating life with respect to the rated operating life. Furthermore, no deformation or other wear was observed in the new plastic cage shape after the test.

<Test conditions>
 ・Tested bearing
 ➤Developed product : carbonitrided bearing steel
 ➤Size   : ø30 × ø65 × 22
 ➤Dynamic load rating : 47,500 N
 ・Load conditions   : 42 % of dynamic load rating
 ・Rotational speed   : 2,000 min^{-1}
 ・Lubricant   : ATF (approx. 70 ℃)
 ・Contaminant average : ① 20 μm, ② 90 μm
  particle diameter   (tested with a mix of ①
          and ② contaminants)
 ・Total amount of contaminants : 0.1 g/L
 ・Rating life (L$_{10h}$)   : 149 h
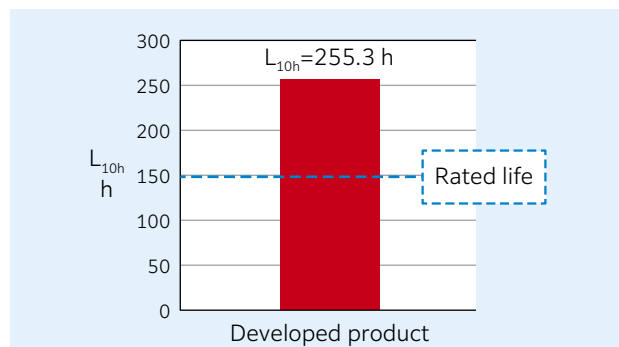
Fig. 7 Life test results under contamination lubrication condition

4.4 Comparison with Tandem Type Double Row Angular Contact Ball Bearing

In recent years during the bearing selection stage, there have been cases where ball bearings are selected to achieve lower torque instead of tapered roller bearings. With this in mind, a functional comparison was made between the developed product and the Tandem Type Double Row Angular Contact Ball Bearing **(Fig. 8)** that is used to support differential pinion shafts.
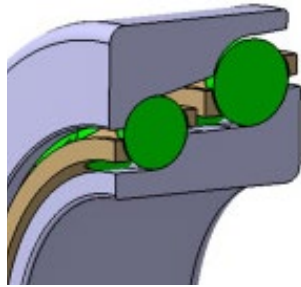
Fig. 8 Structure example of tandem type double row angular contact ball bearing

Table 2 Study example of "Low Temperature Rise and Low Torque Tapered Roller Bearing" with the same calculation life as tandem type double row angular contact ball bearing

	① Ball Bearing	② Developed Product	③ Conventional Product
	Tandem type double row angular contact ball bearing	Tapered roller bearing	Tapered roller bearing 33108U[4]
Scale drawing of bearing cross-section			
Size	$\varphi\,40 \times \varphi\,95 \times 40$	$\varphi\,40 \times \varphi\,77.1 \times 21$	$\varphi\,40 \times \varphi\,75 \times 26$
Mass (kg)	1.06	0.423 (60 % lighter weight compared to ① Ball bearing)	0.498 (53 % lighter weight compared to ① Ball bearing)
Dynamic load rating (N)	Large side: 50,000 Small side: 42,500	83,500	88,000

The sizes of the ① Ball bearing and the ② Developed product in **Table 2** were selected to simulate operating life under load and rotational speed conditions expected when used as a rear differential pinion shaft support bearing for large size passenger vehicles. As a reference comparison, the ③ Conventional tapered roller bearing (33108U) is shown, as it has the same inner diameter as the ② Developed product and a similar outer diameter and dynamic load rating. The results of this bearing comparison revealed that the ② Developed product was 60 % lighter weight than the ① Ball bearing.

For the bearings shown in **Table 2**, rotational torque was calculated at conditions based on the rotational speed expected with large size passenger vehicles. The calculation results are shown in **Fig. 9**.

The ③ Conventional product is shown with the highest rotational torque, and while the ② Developed product had a higher torque than the ① Ball bearing up to a vehicle speed of 5 km/h, it was observed with a lower torque than the ① Ball bearing at speeds over 5 km/h.
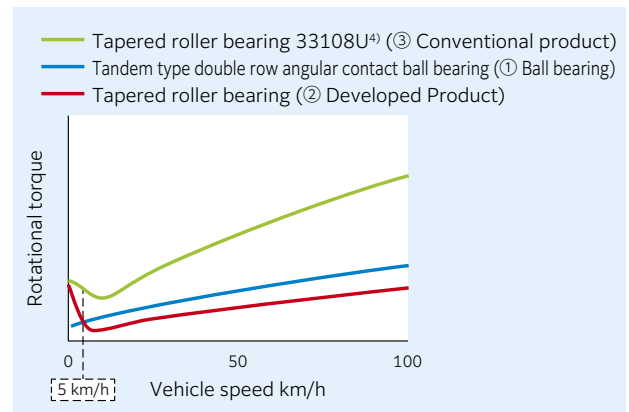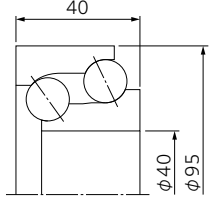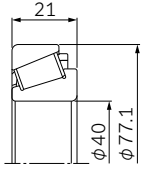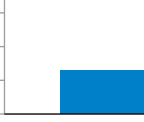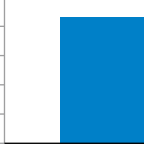
Fig. 9 Bearing rotational torque calculation results

Comparisons of the calculation results of bearing rigidity with applied load in both the radial and axial directions are shown in **Table 3**. Although the ② Developed product has a smaller size than the ① Ball bearing, both radial rigidity and axial rigidity were verified as equivalent or better.

Table 3 Bearing rigidity calculation results

	① Ball Bearing	② Developed Product
	Tandem type double row angular contact ball bearing	Tapered roller bearing
Scale drawing of bearing cross-section	40 / φ40 / φ95	21 / φ40 / φ77.1
Radial rigidity		2.6-times higher rigidity ⇒
Axial rigidity		Equivalent ⇒

5. Conclusion

The automotive industry is said to be facing a once-in-a-100-year period of change, and while usage conditions of bearings will become even more stringent than before, they will be expected to have an even higher level of reliability. The "Low Temperature Rise and Low Torque Tapered Roller Bearing" featured in this article is a new product that is sure to help vehicles achieve a higher mechanical efficiency and better electrical efficiency, as well as contribute to increased uptake of electric vehicles. **NTN** will focus on technical innovation of the new technologies attained through this development and continue contributing to a smooth "smart mobility society" with the release of this new product.

References

1) Ministry of Economy, Trade and Industry, Ministry of Land, Infrastructure, Transport and Tourism, "Smart Mobility Challenge" project https://www.mobilitychallenge.go.jp/
2) Ministry of Land, Infrastructure, Transport and Tourism, "Report on New Fuel Efficiency Standards for Passenger Vehicles" https://www.mlit.go.jp/report/press/jidosha10_hh_000217.html
3) Yasuhito Fujikake, Takanori Ishikawa, Susumu Miyairi, ULTAGE Tapered Roller Bearing for Automotive Application, NTN TECHNICAL REVIEW, No. 85, (2017) 51-55.
4) NTN "Ball and Roller Bearings Catalog" CAT. No. 2203/J
5) Daisuke Imada, Tsuyoshi Niwa, Takashi Ueno, Tomohisa Uozumi, Development of a System for Rolling Bearing Design Optimization, NTN TECHNICAL REVIEW, No. 79, (2011) 98-102.

Photo of authors

Yasuhito FUJIKAKE

Automotive Engineering Dept., Automotive Business Headquarters

Takanori ISHIKAWA

Automotive Engineering Dept., Automotive Business Headquarters

Initiation Mechanism of Peeling in Rolling Bearings, and Its Life Estimation Method

Naoya HASEGAWA*   Takumi FUJITA*
Michimasa UCHIDATE**   Masayoshi ABO***
Hiroshi KINOSHITA***

Peeling, which consists of spalls and cracks of about 10 μm in size, is one of the common failure modes of rolling bearings. Peeling is known to occur under poor lubrication conditions which result in direct contact of surface roughness asperities. However, the initiation mechanism of peeling is not yet completely understood. In this study, we investigated the peeling formation mechanism by observation of rolling contact surfaces, surface topography measurements, residual stress measurements, and contact analysis. These results clarified that initial peeling cracks arose from notches which formed due to plastic contact of surface roughness asperities.

We also developed a peeling life estimation method based on the above formation mechanism. The method can estimate peeling life under pure rolling and boundary lubrication conditions.

1. Introduction

In order to reduce friction, the recent trend has been towards the use of low viscosity oil lubrication. The chance that rolling bearings (hereafter, "bearings") are used in thin lubricating conditions is therefore increasing. Thus, clarifying the damage mechanism of bearings under such conditions has become an important engineering task.

Peeling is one type of failure experienced by bearings operating under thin lubricating conditions and is indicated by dense area of spalls and cracks approximately 10 μm in size[1]. Peeling is likely to occur when the surface roughness is high and the oil film parameter Λ (ratio between the minimum oil film thickness obtained from the EHL Theory and the square root of the square sum of the root-mean-square roughness of two surfaces) is low[2]. Therefore, repeated stress applied on the direct contact area (hereafter, "real contact area") of the surface roughness is the cause of peeling. Although, the peeling mechanism is roughly understood, the details remain unclear[3][4]. The authors studied the formation mechanism of peeling in detail by reproducing peeling with a two-cylinder type testing machine, observing the rolling contact surface, and conducting various analyses[5]. In addition, the mechanism of crack formation during peeling was quantitatively examined by estimating the repeated stress applied to the real contact area using the surface topography and the measurement of residual stress[6]. Chapter 2 of this paper explains the peeling formation mechanism obtained from this study.

In order to examine the reliability of bearings under thin lubricating conditions, a tool to estimate peeling life is also required. The authors developed a life estimation method based on the above peeling mechanism[7]. Chapter 3 of this paper describes this method for estimating peeling life.

2. Peeling formation mechanism

2.1 Two-cylinder test

The two-cylinder type tester shown in **Fig. 1** was used to reproduce peeling. A driving cylinder attached to a motor is put in contact with a driven cylinder, both of which are rotated under a pure rolling condition without slippage. Lubrication was provided through an oil saturated felt pad in contact with the test pieces. The test pieces were both 40 mm OD and 12 mm in length, with a 60 mm crown radius placed axially along the outer diameter surface of the driving cylinder. The material of the test pieces is JIS-SUJ2 with ordinary quenching and tempering. A ground finish was applied to the outer diameter of the driving cylinder while superfinishing was applied to the driven cylinder. Two types of driving cylinders were prepared, one with black oxide treatment (Test No. 2) and the other without such treatment (Test No. 1). The purpose is to examine how the reduction of surface roughness (hereafter, "running-in")[8] progresses due to black oxide treatment affects the formation of peeling. The condition of the black oxide treatment was set based on DIN 50938[9]. **Table 1** shows the surface roughness, hardness and thickness of the black oxide layer and **Table 2** shows the test conditions. The test was interrupted after each loading cycle, with analysis to be described later taking place, then the test continued until the total number of loading cycles reached 5.0 x 10^5.

*   Advanced Technology R&D Center
**   Faculty of Science and Engineering, Iwate University
*** School of Engineering, University of Hyogo
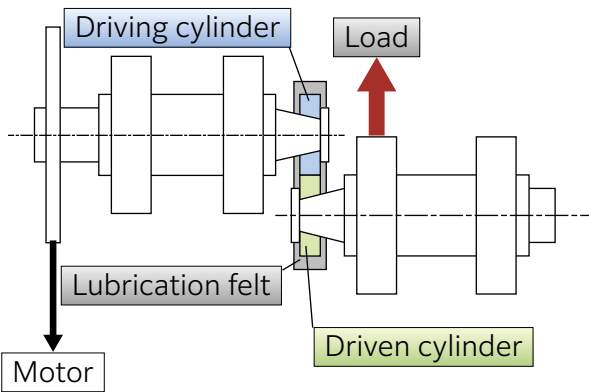
Fig. 1 Two-cylinder type rolling contact fatigue tester

2.2 Observation of rolling contact surface, measurement of shape and analysis of surface roughness

Under the conditions shown in **Table 1**, peeling is likely to form on the driven cylinder with lower surface roughness. Therefore, peeling formation was examined by observing the rolling contact surface of the driven cylinder with an optical microscope and scanning electron microscope (hereafter, "SEM"). For observation of the crack section of peeling, a focused ion beam (FIB) system was used to prepare the test pieces.

Topography of the rolling contact surface of both cylinders was measured by confocal laser scanning microscopy and used in the estimation of repetitive stress on the rolling contact surface, as described later. In addition, the relationship between the change of surface topography on the driven cylinder and formation of peeling was investigated. Furthermore, to study the relationship between the degree of running-in and the formation of peeling, two types of 3-dimensional roughness parameters on the surface topography of the driving cylinder (standard deviation σ^* of height of protrusions and arithmetic mean curvature S_{pc}) were analyzed. Based on the theory of rough surface contact of Greenwood, etc.[10], the severity of contact at the real contact area decreases as the product of σ^* and S_{pc} ($\sigma^* \cdot S_{pc}$) is reduced. In section 2.5.2, the relationship between $\sigma^* \cdot S_{pc}$ and the progress of peeling will be discussed.

2.3 Estimation of repeated stress of rolling contact surface

Triaxial stress components of contact stress that act on the real contact area were estimated during the test by elastic analysis using the boundary element method[11]. In this analysis, the oil film parameter during the test was low ($\varLambda \approx 0.10$), so we assumed there was no load supported by the oil film. The subject area of the analysis was set to the area surrounding the center of the contact ellipse where the apparent contact pressure is relatively large. The details of the analysis are discussed in reference 6).

Furthermore, under the condition that the oil film parameter is low, plastic deformation occurs in the contact region and residual stress is produced on the rolling contact surface. In this study, triaxial stress components of the residual stress on the driven cylinder were measured with the X-ray stress measuring method[12] and the area detector method.

The triaxial stress components that actually acted on the rolling contact surface can be estimated with the following equation (1) by adding the results from the above contact analysis and X-ray stress measurement.

$$\hat{\sigma} = \sigma_{con} + \sigma_{res} \tag{1}$$

Where, the subscripts 'con' and 'res' indicate contact stress and residual stress, respectively. As discussed later, plastic deformation of the rolling contact surface is involved in the formation of the initial cracks in peeling. Therefore, in the study of the formation mechanism of peeling, the discussion uses von Mises stress (hereafter, "Mises stress") which indicates the yield condition of the material. Mises stress σ_{vm} can be obtained by the following equation (2) by using the triaxial stress components obtained in equation (1).

$$\sigma_{vm} = \sqrt{\frac{1}{2}\left\{(\sigma_x - \sigma_y)^2 + (\sigma_y - \sigma_z)^2 + (\sigma_z - \sigma_x)^2 + 6(\tau_{xy}^2 + \tau_{yz}^2 + \tau_{zx}^2)\right\}} \tag{2}$$

Table 1 Surface roughness, hardness and thickness of the black oxide layer for test cylinders

Test No.	Surface roughness (R_a) μm		Hardness		Thickness of black oxide layer μm	
	Driving cylinder	Driven cylinder	Driving cylinder	Driven cylinder	Driving cylinder	Driven cylinder
1	0.75	0.02	61.5 HRC		-	-
2	0.70				2.0	

Table 2 Test conditions of the RCF testing

Items	Conditions
Lubricant	poly- α -olefin, VG5
Rotational speed min^{-1}	2,000
Load kN	2.25
Maximum contact pressure GPa	2.3
Oil film parameter Λ	0.09 - 0.11 (at 40 ℃)
Total number of loading cycles	5.0×10^5

2.4 Results of experiment and analysis
2.4.1 Observation of rolling contact surface of the driven cylinder

Fig. 2 shows optical micrographs of the rolling contact surface on the driven cylinder. Test No. 1 shows crack-like damage at 0.1×10^5 loading cycles. At 2.5×10^5 loading cycles, the damage increased, then at the 5.0×10^5 cycles, several small spalls approximately 10 μm in size are also observed. On the other hand, no damage formed on No. 2 even after 5.0×10^5 loading cycles.

Fig. 3 shows the topography of the rolling contact surface on the driven cylinder. **Fig. 3** (a) shows the pre-test surface topography created by superfinishing. In **Fig. 3** (b) Test No. 1 at the 1.0×10^5 loading cycles, the wavy pattern indicates a larger amplitude and period than before the test, as well as multiple small protrusions. These protrusions matched the location of the damage seen in **Fig. 2** (b). On the other hand, **Fig. 3** (c) Test No. 2 at 1.0×10^5 loading cycles shows a wavy pattern, however, its amplitude is small and no small protrusions are observed.

Rolling direction ➡

(a) No. 1, 0.1×10^5 rev.   (b) No. 1, 2.5×10^5 rev.

(c) No. 1, 5.0×10^5 rev.   (d) No. 2, 5.0×10^5 rev.
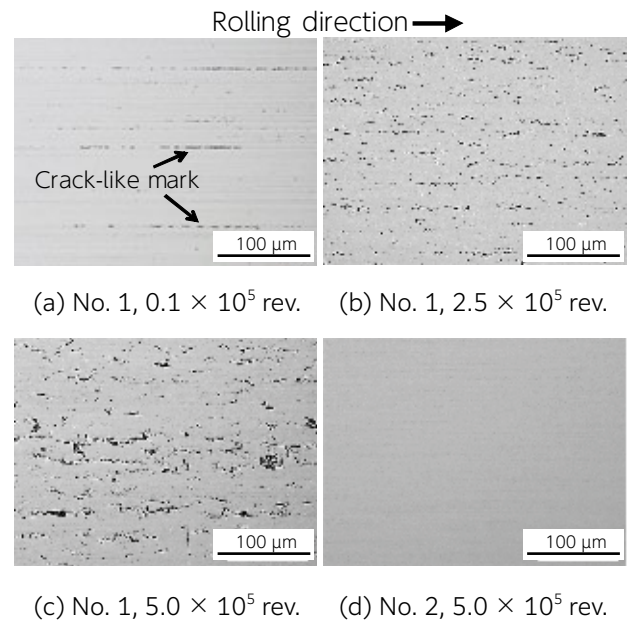
Fig. 2 Optical micrographs of rolling contact surfaces for driven cylinders

(a) No. 1, Before testing   (b) No. 1, 1.0×10^5 rev.   (c) No. 2, 1.0×10^5 rev.
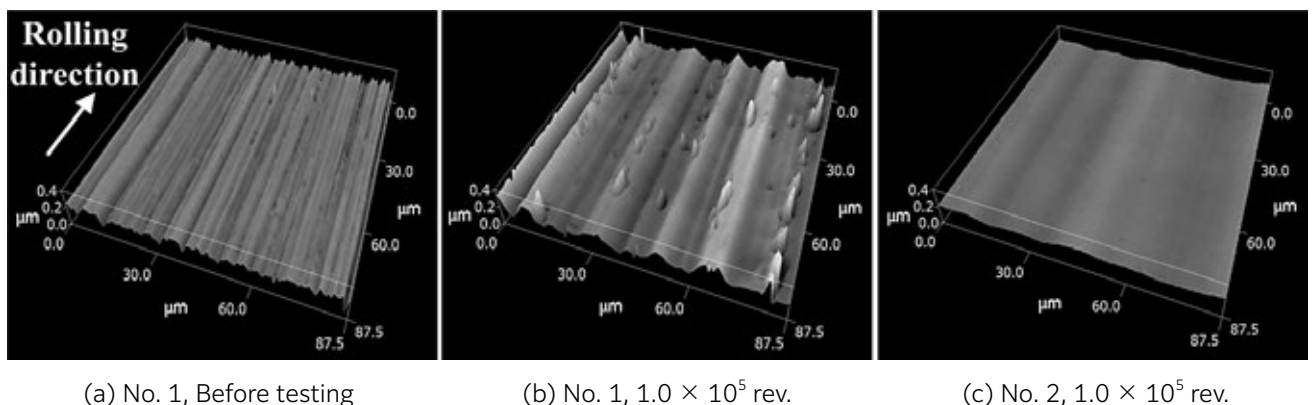
Fig. 3 Surface topographies of driven cylinders measured by laser microscopy
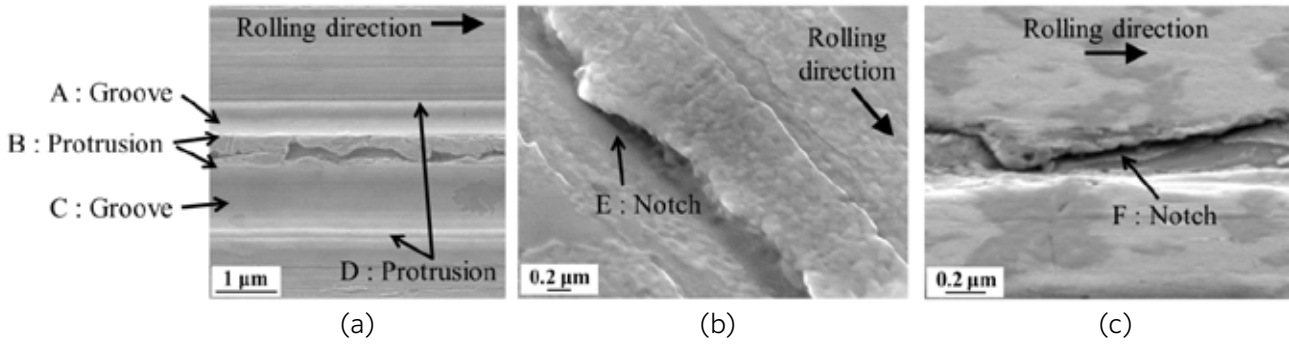
Fig. 4 SEM images of the crack-like marks on the driven cylinder of test No. 1 at 0.1×10^5 rev.

Fig. 4 shows the damage seen on the Test No. 1 driven cylinder at 0.1×10^5 loading cycles observed by SEM. **Fig. 4** (a) - (c) show higher magnification views from different observation points. In **Fig. 4** (a), protruded areas (B and D in the figure) exist adjacent to grooves on both sides (A and C in the figure). This means the aforementioned wavy pattern was formed by plastic deformation. In **Fig. 4** (b), the protruded area of the wave is deformed as if pressed in the vertical direction, from which a notch (E in the figure) was formed. A notch (F in the figure) was also formed in **Fig. 4** (c), however, it was folded down along the slope of the adjacent groove.

Fig. 5 shows the damage on the Test No. 1 driven cylinder at 5.0×10^5 loading cycles observed by SEM from the axial direction. A crack which propagated from the notch (area enclosed by dotted line in the figure) can be seen.
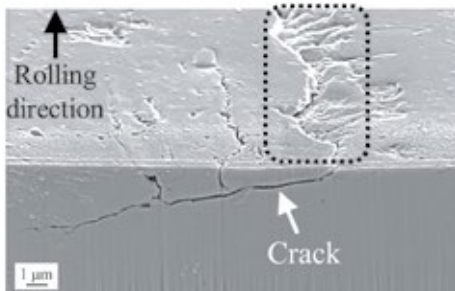
Fig. 5 Cross-section SEM image of the crack-like mark on the driven cylinder of test No. 1 at 5.0×10^5 rev.

2.4.2 Measurement result of residual stress

Fig. 6 shows the relationship between the residual stress on the rolling contact surface of the driven cylinder and number of loading cycles. The value of the vertical axis $\sigma_{vm,res}$ is the Mises stress calculated from the triaxial stress components. The inserted graph in the figure is an enlarged view during the early loading cycles. $\sigma_{vm,res}$ of Tests No. 1 and No. 2 stabilized at 1,050 - 1,100 MPa after 0.1×10^5 loading cyles.

The rate of increase of $\sigma_{vm,res}$ was slightly slower for No. 2. **Table 3** shows the triaxial stress components of

the residual stress of the driven cylinder at 0.5×10^5 loading cycles, at which point there was almost no difference in residual stress between Tests No. 1 and No. 2.
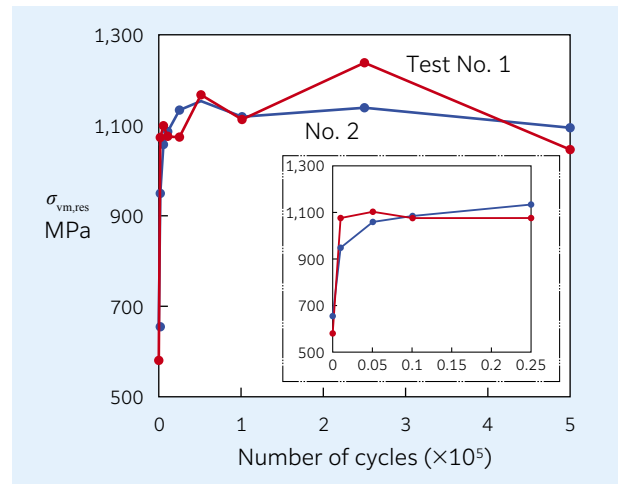
Fig. 6 Relationship between residual stresses at rolling contact surfaces of driven cylinders and loading cycles

Table 3 Tri-axial stress components of residual stresses for driven cylinders at 0.5×10^5 rev.

Test No.	Residual stress GPa					
	σ_x	σ_y	σ_z	τ_{xy}	τ_{yz}	τ_{zx}
1	-1.53	-1.34	-0.37	-0.02	-0.01	0.00
2	-1.52	-1.43	-0.41	-0.01	0.02	0.00

2.4.3 Surface roughness parameters of driving cylinder

Fig. 7 shows the relationship between the surface roughness of the driving cylinder and the loading cycles. In each test, $\sigma^* \cdot S_{pc}$ decreased immediately after the start of testing, however, Test No. 2 decreased more than Test No. 1. This means that the

severity of contact due to running-in is much lower in Test No. 2 when compared to Test No. 1.
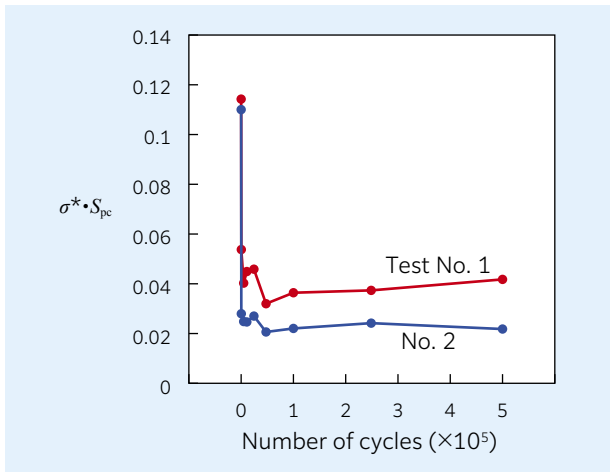
Fig. 7 Relationship between the surface roughness of driving cylinders and loading cycles
(σ^* : Standard deviation of peak height,
S_{pc} : Arithmetic mean peak curvature)

2.4.4 Estimation result of repeated stress applied to rolling contact surface

Fig. 8 shows the pressure distribution of the real contact area on the rolling contact surface obtained by contact analysis. On the rolling contact surface of Tests No. 1 and No. 2 before testing, contact pressure of more than 10 GPa was observed. Areas of more than 10 GPa were found on Test No. 1 at 0.5×10^5 loading cycles, however most areas on the rolling contact surface were less than 10 GPa for Test No. 2.

Fig. 9 shows the distribution of Mises stress acting on the rolling contact surface of the driven cylinder, in the depth direction, at 0.5×10^5 loading cycles. In the figure, Mises stress that considered the residual stress $\overline{\hat{\sigma}_{vm}}(z)$ and Mises stress that did not consider residual stress $\sigma_{vm, con}(z)$ are both plotted. The stress values on the vertical axis indicate the mean values of Mises stresses at points where the stresses are the largest among the neighboring stress values (within a square area of 6.25 μm centered on the own points) on the x-y plane of depth z. The area enclosed by a dotted line in the figure shows the yield stress of the bearing steel (1.8 - 2.0 GPa[13]). $\overline{\hat{\sigma}_{vm}}(z)$ in Tests No. 1 and No. 2 exceeded the yield stress in all the areas up to 5 μm of depth. $\overline{\hat{\sigma}_{vm}}(z)$ in Test No. 2 was smaller than Test No. 1 at all depths. In addition, the maximum value of $\overline{\hat{\sigma}_{vm}}(z)$ occurred at about 0.5 μm for both tests. The stress value for Test No. 2 at this depth was about 40 % smaller than for Test No.1. In all tests, $\overline{\hat{\sigma}_{vm}}(0.5)$ was about 10 % smaller than $\sigma_{vm, con}(0.5)$.
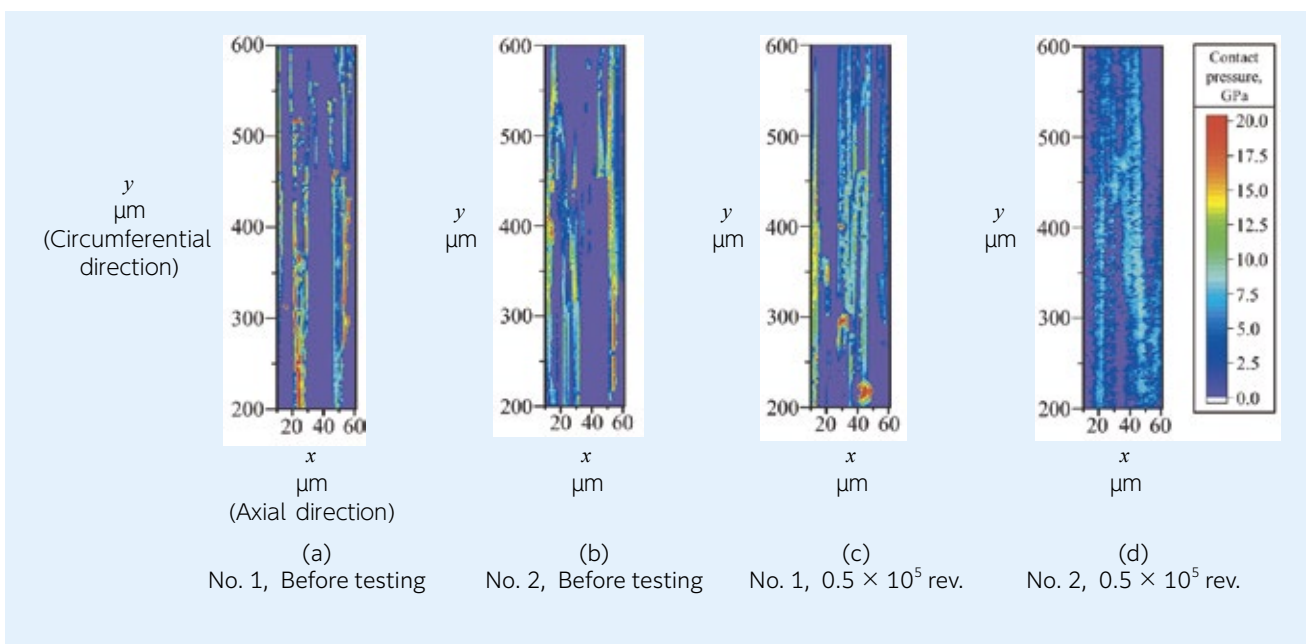
Fig. 8 Contact pressure distributions at real contact area on rolling contact surfaces
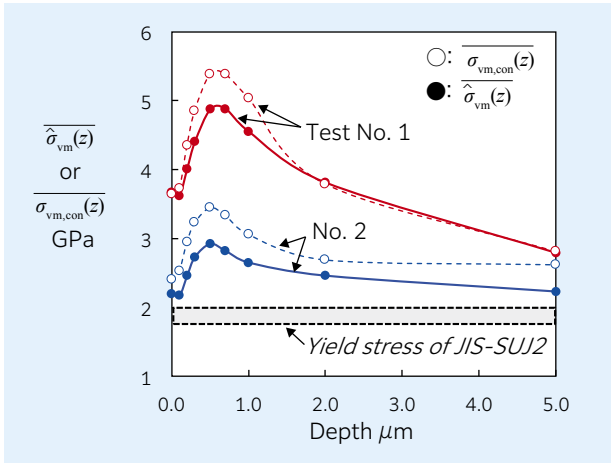
Fig. 9 Depth dependence of von Mises stress on the rolling contact surface of the driven cylinder at 0.5×10^5 rev.

2.5. Discussion

2.5.1 Crack formation mechanism in peeling

From observation with the optical microscope in **Fig. 2**, small peeling spalls formed on the driven cylinder in Test No. 1 which seem to be a result of propagation of the damage that initiated from small cracks at 2.5×10^5 loading cycles (hereafter, "initial cracks"). Also, it is assumed that the initial cracks were formed from micro-scaled plastic deformation originating on the driven cylinder during rotation, based on measurement of the surface shape in **Fig. 3** and observation by SEM in **Fig. 4**. Based on these results, **Fig. 10** shows a schematic diagram of the formation mechanism of peeling cracks. Initially, asperity on the rough surface of the driving cylinder contacts the rolling contact surface of the driven cylinder, which creates a wrinkle-like pattern of plastic deformation on the driven cylinder (Steps 1-2). Subsequent asperities, contact the plastically deformed surface of the driven cylinder, flattening the protrusions. Additional rolling creates notch folding which leads to stress concentrations and initial cracking (Steps 3-4). A similar phenomenon is also observed in a study of micro-pitting of gears by Mallipeddi, etc[14]. Based on the above mechanism, it can be assumed that the risk of peeling crack formation will be larger when plastic deformation on the rolling contact surface is high. In fact, the plastic deformation of the driven cylinder in Test No. 1, where peeling formed, was more significant than on the driven cylinder of Test No. 2 where peeling did not form.

2.5.2 Relationship between repeated stress of rolling contact surface and peeling formation

It is assumed that a stress of $\overline{\hat{\sigma}_{vm}(z)}$ over the yield stress was applied to the driven cylinders in Tests No. 1 and No. 2 and plastic deformation continued even after "running-in" and stabilization of residual stress (after 0.5×10^5 loading cycles) . It is also understood that the plastic deformation of the driven cylinder was more significant on Test No. 1 than Test No. 2 because $\overline{\hat{\sigma}_{vm}(z)}$ up to 5 μm of depth was larger . From the above, it seems that peeling life (formation of initial cracks and degree of progress) should be shorter as the repeated stress on the rolling contact surface is larger and the degree of plastic deformation is greater.

Both cylinders in Tests No. 1 and No. 2, $\overline{\hat{\sigma}_{vm}(z)}$ was approximately 10 % smaller than $\overline{\sigma_{vm, con}(z)}$ at the same depth. This indicates that the Mises stress acting on the rolling contact surface was reduced due to the impact of the residual stress, so the residual stress must affect the peeling life. However, as shown in **Table 3**, there was no difference between the residual stresses in Tests No. 1 and No. 2, so the impact of residual stress was not apparent.

In test No. 2 where black oxide treatment was applied to the driving cylinder, the Mises stress acting upon the rolling contact surface at 0.5×10^5 loading cycles was smaller than No. 1. This is due to the lower $\sigma* \cdot S_{pc}$ on the driving cylinder in Test No. 2, indicating better "running-in", was the main reason that peeling did not occur on the driven cylinder in Test No. 2.

Fig. 10 Formation mechanism of a crack in peeling on the driven cylinder

3. Development of peeling life estimation

3.1 Overview of life estimation method

We have developed a peeling life estimation method based on the findings of the mechanism described in Chapter 2[7]. **Fig. 11** shows an overview of the life estimation method. First, conduct rolling contact fatigue tests under various operating conditions to obtain a 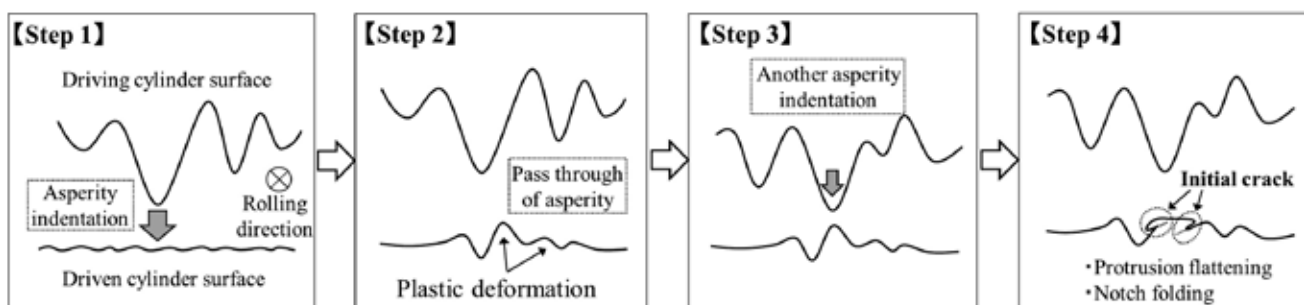peeling life and a history of repeated stresses acting on the rolling contact surface. (hereafter, "stress history") for each test (Step 1). The stress history changes depending on running-in and change of residual stress. Therefore, estimation must be done based on the contact analysis using the actual measured surface topography and residual stress measurement. Then, obtain peeling *S-N* curves (Stress – Number of cycles to failure) by regression analysis by applying Miner's rule to the data obtained in Step 1 (Step 2). Finally, estimate the peeling life under any conditions using this *S-N* curve. At this time, conduct a preliminary test simulating operating conditions of the subject of estimation, obtain stress history under those conditions (Step 3) and estimate the life using the *S-N* curve from the obtained stress history and Miner's rule (Step 4). *S-N* curves must be prepared for each steel type and thermal treatment of the rolling elements. The preliminary tests can be conducted up to the loading cycles where running-in and residual stress become stable. In our experience, running-in and residual stress stabilize by 10^4 loading cycles, under the condition that the oil film parameter is lower than 1.5.

Currently, it is difficult to accurately simulate running-in and change in residual stress of rolling elements used in various conditions. In this estimation method, the impact of running-in and change of residual stress can be considered based on preliminary test that simulates the actual operating conditions. Impact of the materials can also be considered if *S-N* curves for each steel type and thermal treatment are prepared.
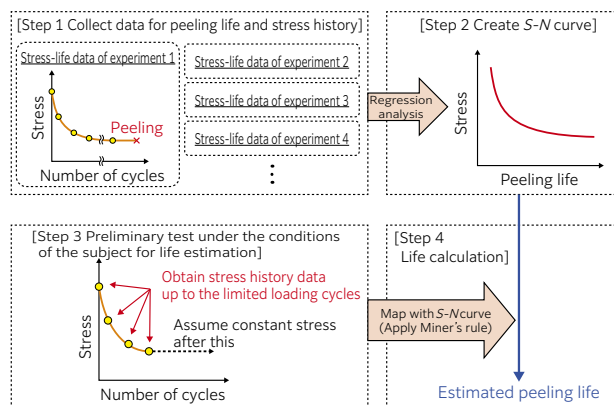
Fig. 11 Flow of the estimation method of peeling life

3.2 Various assumptions for this life estimation method

It must be noted that the following are assumed in this life estimation method.

1) Repeated stress that produces peeling (dominant stress) is Mises stress.
2) The relationship between peeling life and repeated stress follows Miner's rule.
3) Loss of fatigue layer of the surface layer due to wear is negligible.
4) The relationship between peeling life L_{th} and repeated stress $\overline{\hat{\sigma}_{vm}(z)}$ can be expressed by the *S-N* curve of the double logarithmic model in the following equation (3).

$$\log L_{th} = -A \log (\overline{\hat{\sigma}_{vm}(z)} - S_f) + \log B \quad (3)$$

Where, A, B and S_f are constants specific to the materials.

Using Mises stress as the dominant stress of peeling in 1) should be appropriate considering that formation of peeling is affected by the magnitude of plastic deformation of the rolling contact surface. Use of Miner's rule and the *S-N* curve of the double logarithmic model in 2) and 4) is generally adopted in other research involving rolling fatigue life estimation[15) 16)] and this method also followed that practice. The assumption of 3) impact of wear, should be considered appropriate under the conditions that the depth of wear on the rolling contact surface is relatively small. It should be noted that the scope of application of this life estimation method is currently limited to pure rolling and boundary lubrication conditions.

3.3 Validation of life estimation accuracy

The accuracy of this life estimation method was examined by conducting two - cylinder type tests similar to **Fig. 1** under various test conditions. **Table 4** shows the test conditions and **Fig. 12** shows the relationship between the estimated peeling life (L_{est}) and the actual life (L_{act}). *S-N* curves were generated with the test data from Test No. 1 - 7 and the estimated life of each test was obtained from the stress history of up to 10^4 cycles. In the figure, the median, minimum and maximum values of the life ratio (L_{act}/L_{est}) are indicated. These statistics values within the range of this test condition was 0.89, 0.49 and 1.82, respectively. This accuracy is the same or higher than other life estimation methods[17)] (90 % reliability interval of L_{act}/L_{est} under thin lubrication condition is 0.98-4.3), therefore, this life estimation method should be applicable as one of the peeling life estimation methods. The tests of No. 8 and No. 9 were additionally conducted after generating the *S-N* curves. The life ratios of these tests were 0.61 and 1.07, respectively, thus, the validated life estimate of the same accuracy as those in Test No. 1 - 7.

Moving forward, we plan to develop methods applicable to conditions with slippage and mixed lubrication, in order to expand the scope and application of this life estimation method.

Table 4 Test conditions of the RCF testing for validation of the life estimation accuracy

Test No.	Surface roughness (R_a) μm		Rotational speed min^{-1}	Maximum contact Pressure GPa	Oil film parameter Λ
	Driving cylinder	Driven cylinder			
1	0.75				0.11
2	0.40				0.21
3	0.35		2,000	2.3	0.24
4	0.30				0.28
5	0.75	0.02	500		0.06
6	0.75		2,000	1.6	0.12
7	0.40		1,000		0.17
8	0.50		2,000	2.3	0.17
9	0.75				0.11
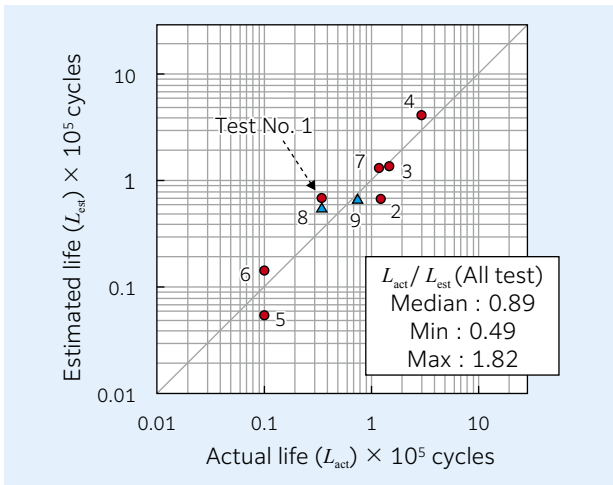
Fig. 12 Relationship between estimated peeling lives and actual peeling lives

4. Summary

In this paper, we examined the formation mechanism of peeling based on experiments and analysis. We also introduced a life estimation method based on the peeling formation mechanism.
1) Initial peeling cracks are produced from the notches which are formed by plastic deformation of protrusions on the rolling contact surface.
2) The developed life estimation method can estimate peeling life under pure rolling and boundary lubrication conditions with the same or better accuracy than other life estimation methods. Moving forward, we also plan to develop life estimation methods applicable to conditions with slippage and mixed lubrication.

References

1) Noriyuki Tsushima, Hirokazu Nakashima, Hiroshi Kashimura, Typical Failures of Bearings, NTN TECHNICAL REVIEW, No. 57 (1990) 59.
2) Y. Akamatsu, et. al., SAE Paper, 891909, (1989).
3) K. Maeda, N. Tsushima & H. Muro, The Inclination of Cracking in the Peeling Failure of a Ball Bearing Steel and its Relationship to the Inclination of the Principal Residual Stress, Wear, 65, (1980) 175.
4) A. Oila, B. A. Shaw, C. J. Aylott & S. J. Bull, Martensite Decay in Micropitted Gears, Proc. IMechE. Part J. J. Eng. Trib., 219, (2005) 77.
5) Naoya Hasegawa, Takumi Fujita, Michimasa Uchidate, Masayoshi Abo, Mechanism for Initiation of Peeling in Rolling Contact and the Effect of Black Oxide Treatment on the Suppression of Peeling (Part 1), The Tribologist, 63, 8, (2018) 551.
6) Naoya Hasegawa, Takumi Fujita, Michimasa Uchidate, Masayoshi Abo, Mechanism for Initiation of Peeling in Rolling Contact and the Effect of Black Oxide Treatment on the Suppression of Peeling (Part 2), The Tribologist, 63, 9, (2018) 618.
7) N. Hasegawa. T. Fujita, M. Uchidate, M. Abo & H. Kinoshita, Estimation Method of Micropitting Life from *S-N* Curve Established by Residual Stress Measurements and Numerical Contact Analysis, Tribology Online, 14, 3, (2019) 131.
8) V. Brizmer, K. Sradler, M. V. Drogen, B. Han, C. Matta & E. Piras, The Tribological Performance of Black Oxide Coating in Rolling/Sliding Contacts, STLE Tribol. Trans., 60, 3, (2017) 557.
9) DIN 50938, (2003).
10) J. A. Greenwood & J. B. P. Williamson, Contact of Nominally Flat Surfaces, Proc. Roy. Soc. London, A295, (1966) 300.
11) M. Uchidate, Comparison of Contact Conditions Obtained by Direct Simulation with Statistical Analysis for Normally Distributed Isotropic Surfaces, Surface Topography, Metrology and Properties, 6, 3, (2018) 034003.
12) Toshihiko Sasaki, Shun-ichi Takahashi, Katsunari Sasaki, Yuichi Kobayashi, A Study on Improvements in Multiaxial Stress Analysis with Area Detector Type Diffraction Method, Transactions Vol. A of The Japan Society of Mechanical Engineers, 75, 750 (2009) 219.
13) E. Yhland, Static Load-Carrying Capacity, Ball Bearing Journal, SKF, 211, (1982) 1.
14) D. Mallipeddi, M. Norell, M. Sosa & L. Nyborg, Influence of running-in on surface characteristics of efficiency tested ground gears, Tribology Int., 115, (2017) 45.
15) L. Houpert & F. Chevalier, Rolling Bearing Stress Based Life-Part I, Calculation Model, Journal of Tribology, 134, 2, (2012) 021103, 1.
16) S. Shimizu, Fatigue Limit Concept and Life Prediction Model for Rolling Contact Machine Elements, Tribology Transactions, 45, 1, (2002) 39.
17) J.Gnagy, L. Houpert & F. Chevalier, Rolling Bearing Stress Based Life-Part II, Experimental Calibration and Validation, Journal of Tribology, 134, 2, (2012) 021104, 1.

Photo of authors

Naoya HASEGAWA
Advanced Technology R&D Center

Takumi FUJITA
Advanced Technology R&D Center

Michimasa UCHIDATE
Faculty of Science and Engineering, Iwate University

Masayoshi ABO
School of Engineering, University of Hyogo

Hiroshi KINOSHITA
School of Engineering, University of Hyogo

Development of a Machine Learning Algorithm to Improve Defect Detection Accuracy for Rolling Bearings

Masashi KITAI*   Yoshinobu AKAMATSU**

Ken-ichi FUKUI***

Detection of rolling bearing defects is important for machine maintenance. Previous studies by the authors attempted to detect artificial defects of various sizes on the outer ring raceway surface of a rolling bearing, and found that key features for successful detection depend on the defect size. This study shows an improvement in accuracy of the defect detection process by using a size-based feature selection approach coupled with a two-step outlier detection method.

1. Introduction

Rolling bearings are indispensable elements for many rotating machines and their use spans across many industries such as automotive, aircraft, and industrial plants. When rolling bearings suffer damage, it may not only affect the accuracy and operating efficiency of rotating machines but may also have serious consequences for the machines themselves if the damage propagates and expands. Therefore, it is important to accurately detect any damage in rolling bearings.

A frequently used diagnostic approach for rolling bearings is analysis on vibration acceleration or vibration data of Acoustic Emission (AE). The reason for this is because measurement of the data is easy and can be conducted while the target machines are in operation. Methods of detecting damage on rolling bearings using vibration data include, for example, condition monitoring by analyzing changes in trends of different statistical data such as effective value and peakedness calculated from vibration acceleration[1], condition monitoring by tracking changes of characteristic frequency peaks after FFT process[2] and detecting formation of initial cracks using AE[3]. However, these methods require an understanding of vibration characteristics of rolling bearings and signal processing for analysis. Therefore, a simpler diagnostic approach is desirable.

On the other hand, an approach using machine learning has recently been attracting attention as a method to evaluate damage conditions of rotating machines as it does not require an understanding of analysis and signal processing. We can see some examples in faulty symptom detection of hydraulic power plants[5] using the One Class Support Vector Machine (OC SVM)[4], faulty vibration detection of driving machines[7] using Nearest Neighbor Data

Description[6] and fault detection of wind turbines[9] using the tandem connection approach of the Deep Neural Network/Gaussian Mixture Model[8].

We also attempted fault detection by OC SVM, creating artificial faults of different sizes on outer raceways of rolling bearings, and found that small defects could not be detected depending on the rotational speed of the main shaft[10]. After examining various feature quantities (considering domain, frequency filter, and measurement direction of vibration acceleration), we verified that variations in defect size change feature quantities that are useful for defect detection[11]. Therefore, it is necessary to conduct feature selection against different defect sizes to improve the accuracy of defect detection.

In this study, we propose a new defect detection method combining feature selection against various artificial defect sizes and the two-step outlier detection method. As a preliminary test, we selected Local Outlier Factor (LOF)[12] as a method to achieve the highest defect detection accuracy, after comparing the defect detection accuracy of various outlier detection methods. Additionally, as a result of investigation into classification accuracy of normal bearings and bearings with small defects by Random Forest (RF)[13], it was determined that RF was appropriate to capture features of vibration due to defects as it could achieve high classification accuracy. Therefore, RF was adopted for feature selection against bearings with artificial defects of different sizes and normal bearings, after which the effect of feature selection by LOF on defect detection accuracy was examined.

Finally, the proposed method considering preliminary test results and the original method were compared to evaluate the defect detection performance of the proposed method. By conducting feature selection according to defect sizes and two-

*   Product and Business Strategic Planning Dept., New Product and Business Strategic Planning Headquarters
**   New Product and Business Strategic Planning Headquarters
***   The Institute of Scientific and Industrial Research, Osaka University

step outlier detection, it was shown that the defect detection accuracy was improved compared to the existing research results[10] [11].

In the following section, relevant research regarding fault detection of rolling bearings using machine learning will be reviewed. In Section 3, the outlier detection method and feature selection method that are used in this research are discussed. In Section 4, the evaluation test and results of the proposed method are presented along with the final conclusion.

2. Relevant research

Recently, diagnostic approaches using machine learning and a combination of machine learning and vibration analysis have been attracting attention as diagnostic approaches for rolling bearings and rotating machines that involve rolling bearings.

For example, Li et al. succeeded in determining a fault location for rolling bearings with higher accuracy than the existing methods, targeting rolling bearings with defects set on surfaces of the inner and outer ring raceways and rolling elements[18], by feature extraction with Local Mean Decomposition[14] and Multiscale Permutation Entropy[15], feature selection with Laplacian Score (LS)[16], and finally by classification with Improved SVM-BT, which is their own unique improvement of the Support Vector Machine based of Binary Tree (SVM-BT)[17]. Also, Bugharbee et al. improved detection accuracy of faults on surfaces of inner and outer ring raceways and rolling elements of bearings under different rotational speeds by analysis of main components using Singular Spectrum Analysis[19] and the creation of a fault detection threshold based on Mahalanobis' Distance, using vibration data of normal bearings[20]. Shao et al. classified defects using Deep Belief Network[22] which optimizes the number of neurons in each hidden layer by Particle Swarm Optimization[21] targeting rolling bearings with defects of different sizes on the outer and inner ring raceways and rolling elements. Additionally, they showed its advantage of classification accuracy over other classification methods such as SVM and Bayes' estimation[23].

However, Bugharbee et al. target bearings with only one type of defect in each part of the outer and inner raceway and rolling element surfaces and do not state the impact of the size of defects on detection accuracy[20]. Li and Shao classify defects by supervised learning as the method of defect detection and do not discuss defect detection accuracy under unsupervised learning[18] [23].

3. Proposed method

3.1 Overview

The proposed method takes the input data v, which is the feature vector calculated from measured vibration acceleration data of rolling bearings, and calculates the anomaly score a by feature selection using the classification method and two-step outlier detection method. **Fig. 1** shows a flow diagram of defect detection using the proposed method. The defects to be detected are divided into 3 stages based on their status. The importance of each feature is calculated using the classification method for each defect status, after which the feature selection is performed (Feature Selection in **Fig. 1**).
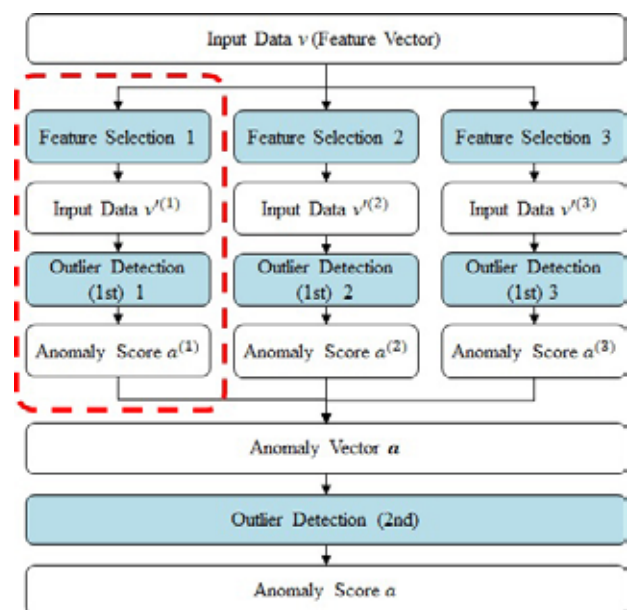
Fig. 1 Flow of defect detection

The calculation of importance by the classification method is only done during training. During testing, feature selection is directly performed using the importance calculated during training. After feature selection, each outlier detection method is trained and tested individually for each input data $v'^{(M)}$, $M \in \{1\ 2\ 3\}$ and the respective anomaly score $a^{(M)}$ is calculated (Outlier Detection (1st) 1 to Outlier Detection (1st) 3 in **Fig. 1**). The input data after feature selection $v'^{(M)}$ are targeting different defect statuses, respectively, and therefore defect statuses other than their target may not be detectable. Therefore, multiple anomaly scores $a^{(M)}$ obtained from input data $v'^{(M)}$ are handled as one vector (anomaly vector a in **Fig. 1**) for corresponding measured data. A final anomaly score a is calculated by outlier detection against the anomaly vector a (Outlier Detection (2nd) in **Fig. 1**). In this research, after the anomaly score is calculated based on the proposed method on all the input data obtained from the measured data of the target to be tested. The ratio of input data for which the anomaly score exceeds the defect detection threshold determined in advance is evaluated as an anomaly

ratio. The presence of any defect in the target data is determined based on the magnitude of the anomaly ratio.

3.2 Input/output data

The input data v are the vectorized statistics of the measured vibration acceleration data divided into segments at a fixed time interval considering domain (time, frequency, and quefrency), band pass filter (BPF), and the direction of sensor measurement. The output data is the anomaly score a obtained by the outlier detection method of the second step.

3.3 Evaluation metrics

Anomaly Ratio (AR) and Area Under Curve Score (AUC Score)[24] are used as metrics to evaluate defect detection accuracy using the proposed method. The calculation method of AR and AUC Score is shown in the following:

3.3.1 Anomaly ratio

The anomaly ratio AR is calculated using the following equation based on anomaly score a which is calculated by the proposed method against the input data v that can be obtained from consecutive multiple segments in the measurement data. $a_{\text{threshold}}$ is a defect detection threshold to be predetermined and set as the average of the anomaly score against the normal data + 5 × standard deviation of the anomaly score against the normal data. In addition, N_{DS} indicates the number of segments included in the measurement data of the evaluation target.

$$U_i = \begin{cases} 1(a_i \geq a_{\text{threshold}}) \\ 0(a_i \leq a_{\text{threshold}}) \end{cases} \qquad (1)$$

$$AR = \frac{1}{|N_{DS}|} \sum_{i \in N_{DS}} U_i \qquad (2)$$

3.3.2 Area Under Curve Score

As evaluation metrics of identification performance, when positive is correctly identified as positive, it is called True Positive (TP); when negative is correctly identified as negative, it is called True Negative (TN); when negative is incorrectly identified as positive, it is called False Positive (FP); and when positive is incorrectly identified as negative, it is called False Negative (FN). The False Positive Rate (FPR) and True Positive Rate (TPR) are given in the following equations, respectively:

$$FPR = \frac{FP}{FP + TN} \qquad (3)$$

$$TPR = \frac{TP}{TP + FN} \qquad (4)$$
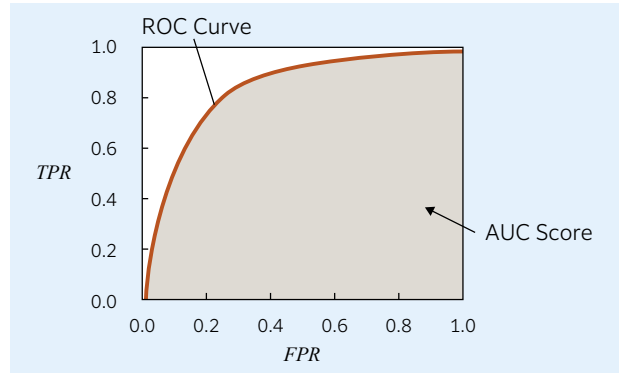
Fig. 2 ROC Curve and AUC Score

By setting FPR at a certain defect detection threshold on the horizontal axis and TPR on the vertical axis and plotting the relation of FPR and TPR in the graph when the defect detection threshold is changed, the Receiver Operating Characteristic Curve (ROC Curve) is obtained. An example of ROC Curve is shown in **Fig. 2**. AUC Score is defined as the area below the ROC Curve. If the normal data and anomaly data can be completely separated, the AUC Score becomes 1.0. On the other hand, in random identification, the AUC score will be 0.5. This means that, if the AUC Score is close to 1.0, then the created machine learning model has a high identification performance.

3.4 Machine learning method

For the outlier detection method, OC SVM, LOF, and Isolation Forest (IF)[25] were used and for the feature selection method, RF and LS were used. The following is a discussion of each of these methods. For implementation of the machine language method, Python 2.7 and Scikit-learn 0.19.0 were used.

3.4.1 One Class Support Vector Machine

OC SVM is a method to determine the identification boundary that classifies normal data and anomaly data by mapping normal data to a certain feature space and obtaining the radius and center of the hypersphere where normal data is preferably included in the feature space. When unknown data is obtained and mapped to the feature space, if it is mapped outside the radius of the hypersphere, the target data is regarded as an anomaly. By selecting the kernel function used for mapping into feature space, non-linear problems can be handled. In this research, Gaussian kernel was used for the kernel function.

3.4.2 Local Outlier Factor

LOF is an outlier detection method based on the density of the feature space. Outliers are based on an assumption that they distribute in a range with low density in the feature space. For each point on the feature space, the marginal density is calculated. When the marginal density of the target point and neighboring points are almost the same, the target point is regarded as normal. On the other hand, when

the marginal density of the target point is lower than the marginal density of the neighboring points, the target point is regarded as an anomaly.

3.4.3 Isolation Forest

IF is a method to calculate the anomaly score based on the average number of splits until certain data is isolated from the other data by random selection of feature quantities and split points. Since normal data have similar characteristics to other normal data, the average number of splits for each normal data to become isolated will be large. On the other hand, since anomaly data have different characteristics from normal data, the average number of splits for each normal data to become isolated will be small. Leveraging these characteristics, target data is regarded as an anomaly when the average number of splits required to isolate from certain data is smaller than other data.

3.4.4 Random Forest

RF is a classification method based on ensemble learning using decision trees. Multiple training sets are generated from the input data by sampling with replacement, and then each training set is classified based on a decision tree. Importance of the feature quantity is also calculated based on the information obtained from the training stage of RF. In this research, the importance calculated by RF was used in effective feature selection according to defect status.

3.4.5 Laplacian Score

LS is a method to create a neighborhood graph, taking input data as nodes, and perform feature selection based on the graph Laplacian for each neighboring node in the graph. In this research, values of Laplacian score calculated for each feature quantity were used in effective feature selection according to defect status.

4. Evaluation Test

4.1 Test equipment

Fig. 3 shows an outline diagram of the test equipment used for evaluation of defect detection accuracy and **Table 1** shows shapes and sizes of artificial defects created on the test bearings. Rolling bearings (angular contact ball bearing, model No. 7216) were used for the test, with cylindrical holes of different sizes (2b to 8b in **Table 1**) and a rectangular groove sufficiently larger than the cylindrical holes (RG in **Table 1**) created on the outer ring raceway surface. The size of the cylindrical holes was set as 2 to 8 times the minor axis radius (b) of the elliptic elastic contact area of ball and outer ring raceway surface. For example, 2b means the diameter of the cylindrical hole is twice the size of b. These artificial defects assume flaking produced as a result of rolling fatigue, with the cylindrical holes simulating the initial stage of flaking and the rectangular groove simulating the progressed state of flaking.

The test was conducted with a normal bearing without artificial defects (ND in **Table 1**) and bearings with artificial defects of different sizes discussed above, attached to the test equipment. The main shaft of the test equipment was operated at the rotational speeds of 1,000, 1,500 and 2,000 min^{-1} and vibration acceleration in the radial, horizontal, and axial directions was measured and used for evaluation. Evaluation was made individually for each rotational speed of the main shaft. One measurement data of vibration acceleration of a specific direction $X^{(D)} = [x_1 \ x_2 \cdots x_i \cdots x_N], D \in$ {Axial, Radial, Horizontal} involved 33 times of measurement for each artificial defect size with sampling frequency of 50 kHz and sampling time of 20 sec. Where, index i indicates an order of time sequence and x_i indicates an instantaneous value of vibration acceleration amplitude of index i. In addition, considering the impact of bearing recombination on vibration, bearings were recombined after 3 measurements.
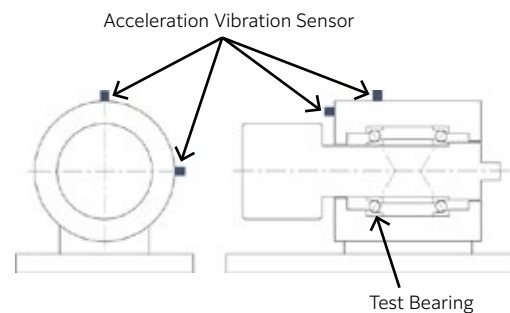
Fig. 3 Test equipment

Table 1 Shape and size of artificial defect

Symbol	Shape of Defect	Size mm
ND	None	-
2b	Hole	$\phi0.32$
4b	Hole	$\phi0.64$
6b	Hole	$\phi1.02$
8b	Hole	$\phi1.36$
RG	Rectanguler Groove	Width 2, Height 10, Depth 1

4.2 Calculation of input data v_j

The measurement data of vibration acceleration $X^{(D)}$ was divided into segments at an interval of 5 rotations of the main shaft, and one segment data $y_j^{(D)}$ = $[x_{(j-1)n+1} \, x_{(j-1)n+2} \cdots x_{(j-1)n+k} \cdots x_{(j-1)n+n}]$ was taken for each segment. Where, n is the number of data points included in the segment data, $j = 1,2,3,\cdots, \lfloor N/n \rfloor$ is the segment number and index k indicates the order of time series. Therefore, the total number of segment data $y_j^{(D)}$ which are obtained from a measurement data $X^{(D)}$ is as shown in **Table 2**.

Table 2 Number of segment data y_i in each measurement data X

Rotation Speed	Number of Segment Data
1,000 min^{-1}	66
1,500 min^{-1}	100
2,000 min^{-1}	133

Table 3 Kind of band-pass filter

Filter	Frequency Range(Hz)
Raw	None
Low1	20-200
Low2	20-1,000
Mid1	200-2,000
Mid2	1,000-5,000
High1	2,000-20,000
High2	5,000-20,000

The amplitude data after BPF processing on each segment data $y_j^{(D)}$ in each frequency range shown in **Table 3** was defined as time domain data $y_j^{(D,TIME)}$. In addition, the amplitude data in frequency domain obtained by envelope processing[26] and FFT processing on time domain data $y_j^{(D,TIME)}$ was defined as frequency domain data $y_j^{(D,SPEC)}$ and the amplitude data obtained by another FFT processing on frequency domain data $y_j^{(D,SPEC)}$ was defined as quefrency domain data $y_j^{(D,CEPS)}$. For feature quantities, for $y_j^{(D,R)}$, $R \in \{\text{TIME}, \text{SPEC}, \text{CEPS}\}$, statistics such as modulation value (MOF) was used in addition to effective value (OA), maximum value (MAX), crest factor (CF), Kurtosis (KS) and skewness (SKN), which are frequently used, in general, in the diagnosis of rolling bearings. The following shows the calculation method of effective value, maximum value, crest factor, Kurtosis and skewness:

$$OA_j^{(D,R)} = \sqrt{\frac{1}{n}\sum_{k=1}^{n}(y_{j,k}^{(D,R)})^2} \qquad (5)$$

$$MAX_j^{(D,R)} = \max_{1 \le k \le n} y_{j,k}^{(D,R)} \qquad (6)$$

$$CF_j^{(D,R)} = MAX_j^{(D,R)}/OA_j^{(D,R)} \qquad (7)$$

$$KS_j^{(D,R)} = \frac{1}{n}\sum_{k=1}^{n}\frac{(y_{j,k}^{(D,R)} - \bar{y}_j^{(D,R)})^4}{(\sigma_j^{(D,R)})^4} \qquad (8)$$

$$SKN_j^{(D,R)} = \frac{1}{n}\sum_{k=1}^{n}\frac{(y_{j,k}^{(D,R)} - \bar{y}_j^{(D,R)})^3}{(\sigma_j^{(D,R)})^3} \qquad (9)$$

Where, D is the direction of measurement, R is domain, j is the segment number, $y_{j,k}^{(D,R)}$ is the element of index k, $\bar{y}_j^{(D,R)}$ is mean of $y_j^{(D,R)}$, $\sigma_j^{(D,R)}$ is standard deviation of $y_j^{(D,R)}$. Modulation value was defined as the effective value of $y_j^{(D,R)}$ after envelope processing. Also, input data v_j was set as a vectorized feature quantities from different measurement directions and domains in segment data y_j. **Table 4** summarizes the number of parameters included in domain, BPF, statistics and direction of sensor measurement to be considered for calculation of feature quantities. Each input data v_j is composed of total of 378 feature quantities considering domain (3), BPF (7), statistics (6), direction of sensor measurement (3).

Table 4 Number of parameters included in each input data v_j

	Regions	BPFs	Statistics	Sensors	Features
Number of Parameters	3	7	6	3	378

4.3 Selection of feature quantities by variation coefficient

Among various feature quantities included in input data v_j, some quantities exhibit larger variation due to the recombination of bearings rather than variation due to the different sizes of artificial defects. Therefore, variation coefficient (standard deviation divided by mean) was calculated for each feature quantity calculated from segment data y_j of normal bearings, which was used for training, and quantities which variation coefficient exceeded 0.3 were excluded from the target of training and testing, as preprocessing. Approximately 20-40 % of feature quantities, among all the feature quantities calculated in Section 4.2 are excluded by this processing, by the selection of measurement data X used for training. These feature quantities, selected by variation coefficient, were used for training and testing, calculating Z Score for each feature quantity based on the input data v_j of artificial defect size ND, which was used for training described later.

4.4 Selection of training data and test data

Considering the impact of recombination of bearings on defect detection accuracy, a combination of measurement data X was randomly changed for learning and evaluation of the proposed method. **Fig. 4** shows the details of the combination of measurement data X, when feature selection is conducted on artificial defect sizes ND and 2b, which is indicated by the red dotted lines in **Fig. 1**. During training, from 33 measurement data X for each artificial defect size, 24 measurement data X were selected for artificial defect sizes ND and 2b, respectively, then the importance of feature quantity was calculated and features were selected by the classification method based on each of the input data v_j. The input data after feature selection obtained by this process was set as $v'_j{}^{2b}$. The superscript 2b indicates that the input data after feature selection v'_j uses a set of feature quantities configured for the artificial defect size 2b. Then, the input data $v'_j{}^{2b}$ of artificial defect size ND was used for the training outlier detection method, and hyperparameters were selected, so that the specificity is the highest by 10-fold cross validation, and anomaly score $a_j{}^{2b}$ was calculated.

During the test, anomaly score $a_j{}^{2b}$ was calculated using the outlier detection method against the input data $v'_j{}^{2b}$ obtained from 9 measurement data X for each artificial defect size.

Similarly, feature selection was conducted for the combination of artificial defect sizes of ND and 4b, as well as ND and 6b and anomaly scores $a_j{}^{4b}$ and $a_j{}^{6b}$ were calculated from the input data after feature selection $v'_j{}^{4b}$ and $v'_j{}^{6b}$. In addition, anomaly score $a_j{}^{(S)}$ against input data after feature selection $v'_j{}^{(S)}$, $S \in \{2b, 4b, 6b\}$, which can be obtained by this processing, was set as one anomaly score vector $a_j = (a_j{}^{2b}, a_j{}^{4b}, a_j{}^{6b})$ for each corresponding segment. The anomaly score vector a_j against input data $v'_j{}^{(S)}$ for training/testing was used for training/testing of the second-stage outlier detection method. In addition, we made sure that the measurement data X to be used for training were not duplicated with those for testing.
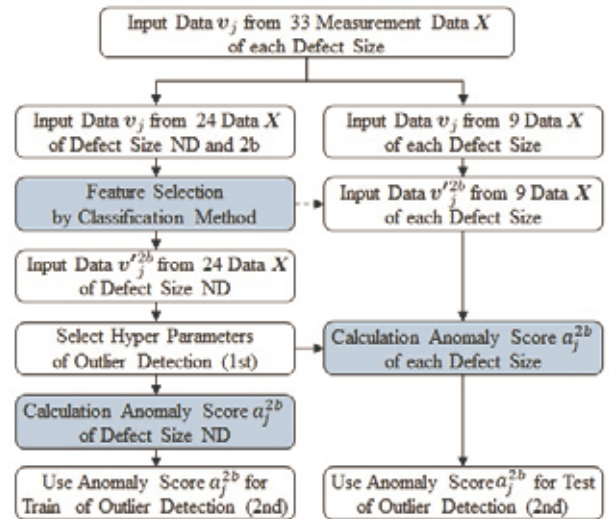
Fig. 4 Selection of measurement data X for train and test

4.5 Testing defect detection accuracy

Defect detection accuracy was tested by calculating the anomaly ratio of each defect size using equation (1) from the anomaly score obtained by the outlier detection method against the measurement data X of the test target. When rotational speed of 1,500 min^{-1} is set as a target, there are 9 measurement data X for test targets of each defect size and 100 segment data y_j obtained from each measurement data, for a total of 900 segment data y_j for the test target of each defect size. The anomaly ratio for each artificial defect size was calculated by using the anomaly score calculated by the outlier detection method against input data v_j, $v'_j{}^{(S)}$ or anomaly score vector a_j from each segment data y_j. Measurement data X used for training was randomly changed 50 times and defect detection accuracy was tested by mean and variation of anomaly ratios on differences among the training data.

4.6 Preliminary test
4.6.1 Comparison of outlier detection methods

Fig. 5 shows the relation between artificial defect size and anomaly ratio when feature selection is not made, at rotational speeds of 1,000, 1,500 and 2,000 min^{-1}, for each outlier detection method. In addition, **Fig. 6** shows the result of calculation of AUC Score from different outlier detection methods for artificial defect sizes of ND and 4b, and **Table 5** shows mean, maximum value, minimum value, and standard deviation of hyperparameters obtained by cross validation of different training data. In the table, v indicates the lower limit of support vector ratio in OC SVM, γ indicates hyperparameter of Gaussian kernel, n-neighbors indicates neighborhood number in calculation of marginal density of LOF, and n-estimators indicates number of estimators in ensemble learning of IF.

(a) Rotation speed: 1,000 min^{-1}

(b) Rotation speed: 1,500 min^{-1}

(c) Rotation speed: 2,000 min^{-1}

Fig. 5 Comparison of outlier detection methods

Fig. 6 AUC Score for each method

Table 5 Variation of hyper parameters for difference of train data

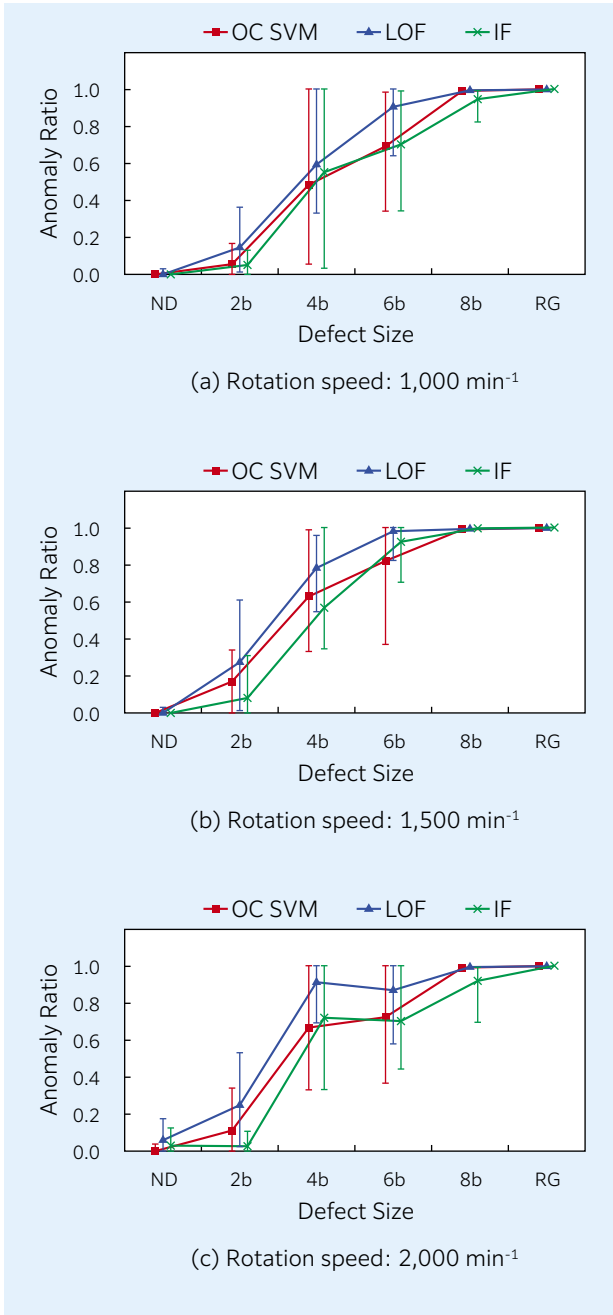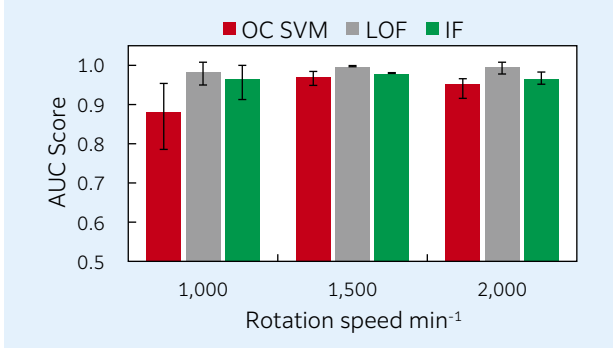| Method	Hyper Parameter	Rotation Speed	Average	Max	Min	Standard Deviation
OC SVM	ν	1,000 min^{-1}	2.0×10^{-3}	5.6×10^{-3}	1.8×10^{-4}	2.0×10^{-3}
		1,500 min^{-1}	1.1×10^{-3}	2.0×10^{-3}	4.5×10^{-4}	6.7×10^{-4}
		2,000 min^{-1}	1.6×10^{-3}	5.6×10^{-3}	1.8×10^{-4}	1.5×10^{-3}
	γ	1,000 min^{-1}	2.8×10^{-4}	1.0×10^{-3}	1.0×10^{-4}	2.8×10^{-4}
		1,500 min^{-1}	2.7×10^{-4}	1.0×10^{-3}	7.9×10^{-5}	2.8×10^{-4}
		2,000 min^{-1}	1.6×10^{-4}	3.1×10^{-4}	7.9×10^{-5}	1.1×10^{-4}
LOF	n-neigbors	1,000 min^{-1}	13.3	24	2	8.0
		1,500 min^{-1}	9.8	25	2	8.6
		2,000 min^{-1}	8.4	29	2	8.3
IF	n-estimators	1,000 min^{-1}	33.0	60	17	15.1
		1,500 min^{-1}	32.7	59	23	11.1
		2,000 min^{-1}	71.7	96	35	20.0

Fig. 5 reveals that the average anomaly ratio of artificial defect sizes 2b - 6b is the highest in LOF. **Fig. 6** shows that LOF gives the highest defect detection accuracy for AUC Score also. However, in any method, the average anomaly ratio of artificial defect size 2b is 0.3 or lower, which is lower than the artificial defect size 4b or larger. From **Table 5**, it was estimated that the variation of anomaly ratio was produced along with variation of hyperparameter values depending on different training data. Therefore, feature selection with RF was performed to improve defect detection accuracy.

4.6.2 Calculation of feature importance by Random Forest

Classification accuracy of artificial defect size 2b, which was difficult to detect by the outlier detection method of the previous section, was tested using RF. Initially, in order to confirm the influence of hyperparameter of RF, the number of decision trees of RF at the rotational speed of 1,500 min^{-1} was changed to 100, 1,000 and 10,000, and the maximum depth of decision trees to 10, 100 and 1,000. However, there was no difference in significance level in the influence of artificial defect sizes of ND and 2b on classification accuracy. Therefore, we set the number of decision trees to 1,000 and the maximum depth of decision trees to 100 and conducted evaluation of classification accuracy and feature selection for each rotational speed. **Fig. 7** shows classification accuracy of artificial defect sizes ND and 2b, at rotational speeds of 1,000, 1,500 and 2,000 min^{-1}. **Table 6** shows an example of extracting 10 feature quantities, which are selected based on difference in training data, after feature selection by RF, against artificial defect sizes of ND and 4b;ND and 6b; and ND and 2b at rotational speed of 1,500 min^{-1}. Feature quantities of high importance common to classification of artificial defect sizes ND and 2b and classification of artificial defect sizes ND and 4b are indicated in bold font. Feature quantities of high importance common to classification of artificial defect sizes ND and 4b and classification of artificial defect sizes ND and 6b are indicated in bold font with an underline. Feature quantities are expressed by statistics - domain - BPF (direction of measurement) in the table.

Fig. 7 reveals that artificial defect size 2b can be

classified with very high accuracy by RF regardless of rotational speed. In addition, **Table 6** reveals that 2 feature quantities are common in classification of artificial defect size ND and 2b and classification of ND and 4b, and only 1 feature quantity is common to classification of artificial defect sizes ND and 4b and classification of ND and 6b, while no feature quantity is common to classification of artificial defect sizes ND and 2b and classifications of ND and 6b. Therefore, all the defect sizes cannot be tested with the same feature quantity.
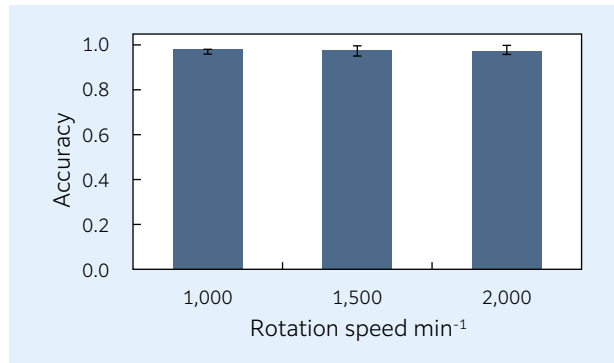

Fig. 7 Classification accuracy by Random Forest

Table 6 Features with high importance to defect size (Rotation speed 1,500 min^{-1})

	Comparison ND and 2b	Comparison ND and 4b	Comparison ND and 6b
1	OA-TIME-LOW1(Radial)	OA-TIME-LOW1(Radial)	OA-TIME-LOW2(Radial)
2	OA-TIME-LOW1(Horizontal)	OA-CEPS-LOW1(Radial)	MOF-TIME-LOW2(Radial)
3	MAX-TIME-LOW1(Horizontal)	OA-CEPS-MID1(Radial)	OA-SPEC-LOW2(Radial)
4	OA-TIME-LOW1(Horizontal)	MAX-CEPS-MID2(Radial)	MOF-SPEC-LOW2(Radial)
5	OA-CEPS-LOW1(Horizontal)	OA-TIME-LOW1(Axial)	OA-CEPS-LOW2(Radial)
6	CF-CEPS-LOW1(Horizontal)	MAX-TIME-LOW1(Axial)	MOF-TIME-MID1(Radial)
7	MOF-TIME-LOW1(Axial)	MAX-SPEC-LOW1(Axial)	OA-SPEC-MID1(Radial)
8	OA-SPEC-LOW1(Axial)	SKN-SPEC-LOW1(Axial)	MOF-SPEC-MID1(Radial)
9	MAX-SPEC-LOW1(Axial)	OA-CEPS-LOW1(Axial)	OA-CEPS-MID1(Radial)
10	MOF-SPEC-LOW1(Axial)	KS-CEPS-LOW1(Axial)	MAX-CEPS-MID1(Radial)

4.6.3 Defect detection accuracy by input data $v'_j{}^{(S)}$ after feature selection

Feature vector composed of the selected 10 feature quantities of high importance with respect to each artificial defect size was set as input data $v'_j{}^{(S)}$, and defect detection accuracy by LOF was tested. **Fig. 8** shows the relation between artificial defect size and anomaly ratio against input data $v'_j{}^{(S)}$ after feature selection. Anomaly ratios calculated from input data $v'_j{}^{2b}$, $v'_j{}^{4b}$ and $v'_j{}^{6b}$ which selected feature quantities of high importance to the classification of artificial defect sizes ND and 2b, ND and 4b, and ND and 6b are shown in the figure as Feature(2b), Feature(4b) and Feature(6b), respectively. In the same figure, anomaly ratios directly calculated from input data v'_j before feature selection using LOF for each defect size are shown as the original method (Original). The results from input data v_j before feature selection are the same as **Fig. 5**. In addition, **Table 7** shows the mean, maximum values, minimum values, and standard deviation of neighborhood numbers in the marginal density calculation of LOF, obtained by cross validation for input data $v'_j{}^{(S)}$ after feature selection.

(a) Rotation speed: 1,000 min^{-1}

(b) Rotation speed: 1,500 min^{-1}

(c) Rotation speed: 2,000 min^{-1}
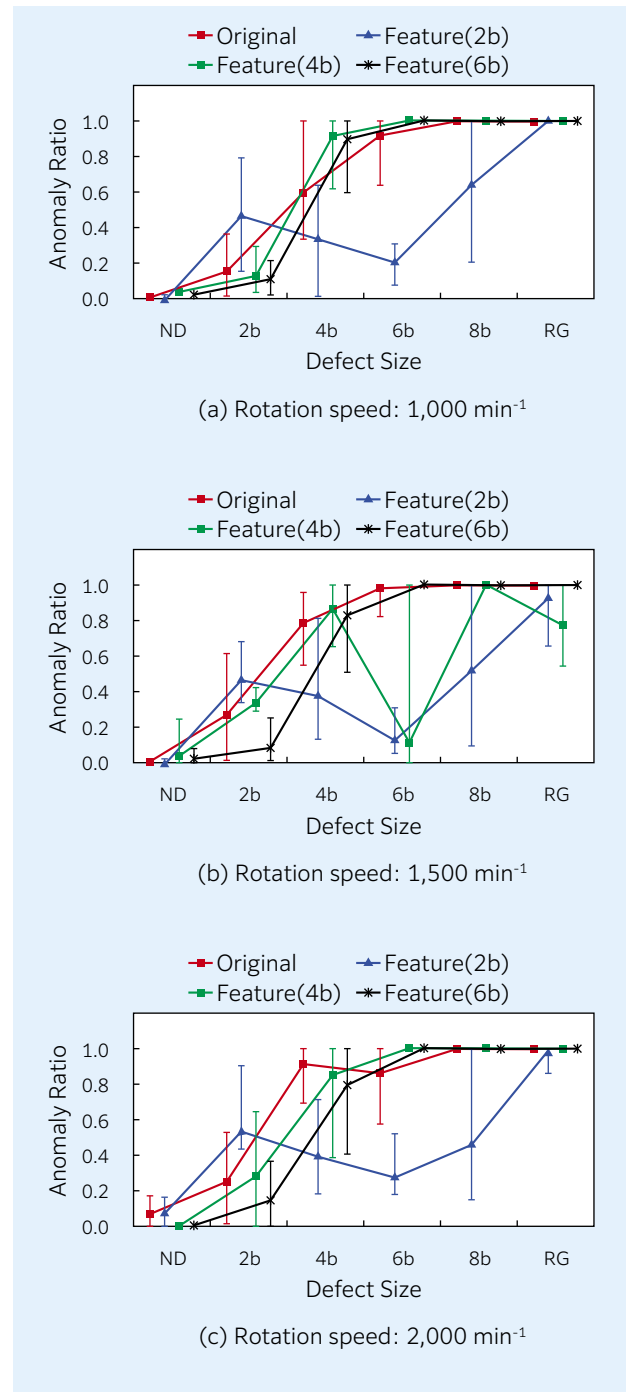
Fig. 8 Anomaly ratio for each input data $v'_j{}^{(S)}$

Fig. 8 reveals that, when feature quantities of high importance are selected for artificial defect size 2b, anomaly ratio of artificial defect size 2b increases compared to the case when feature quantities of high importance for artificial defect sizes 4b and 6b are selected.

On the other hand, when the above feature quantities are selected, anomaly ratios for artificial defect sizes 4b and 6b are lower than anomaly ratios for artificial defect size 2b, and the detection accuracy decreases for those other than the targeted artificial defect size. In addition, **Table 7** shows that variation of the neighborhood number does not

change depending on the different training data. Therefore, defect detection accuracy for each input data $v'_j{}^{(S)}$ after feature selection must be evaluated comprehensively.

Table 7 Variation of the neighborhood numbers of Local Outlier Factor for the difference of train data

Feature Vector	Rotation Speed	Average	Max	Min	Standard Deviation
Original	1,000 min⁻¹	13.3	24	2	8.0
	1,500 min⁻¹	9.8	25	2	8.6
	2,000 min⁻¹	8.4	29	2	8.3
Feature(2b)	1,000 min⁻¹	16.0	28	3	7.5
	1,500 min⁻¹	14.0	28	5	6.4
	2,000 min⁻¹	24.4	29	16	4.0
Feature(4b)	1,000 min⁻¹	23.1	28	14	4.9
	1,500 min⁻¹	14.4	28	2	8.9
	2,000 min⁻¹	18.1	27	2	7.2
Feature(6b)	1,000 min⁻¹	15.2	28	2	7.8
	1,500 min⁻¹	17.2	27	5	7.0
	2,000 min⁻¹	24.4	29	15	4.6

4.6.4 Outlier detection accuracy by 2-step LOF and impact of number of feature quantities used for feature selection

In order to resolve the problem of reduction of anomaly ratio other than artificial defect size targeted for feature selection, the proposed method uses anomaly score for input data $v'_j{}^{(S)}$ after feature selection as the input data on the second stage of LOF as one vector (anomaly score vector a_j) for each segment corresponding to the original measurement data. Then the proposed method compares the defect detection accuracy again. Therefore, defect detection accuracy of the proposed method varies depending on the number of feature quantities in feature selection of input data $v'_j{}^{(S)}$. **Fig. 9** shows the relation between the number of feature quantities in feature selection of input data $v'_j{}^{(S)}$ and the mean and variation of anomaly ratios of artificial defect sizes ND, 2b, 4b and 6b in the proposed method at the rotational speeds of 1,000, 1,500 and 2,000 min⁻¹. In addition, **Table 8** shows the relation between the number of feature quantities in feature selection and the mean, maximum values, minimum values, and standard deviation of the neighborhood number.

Fig. 9 shows that the number of feature quantities to improve defect detection accuracy varies depending on the rotational speed. In any rotational speed, the anomaly ratio of artificial defect sizes 2b and 4b decreases when the number of feature quantities is 5 or less. In addition, the anomaly ratio of artificial defect size 2b increases at the rotational speed of 1,500 min⁻¹ when the number of feature quantities is 30 or more, however, the anomaly ratio of artificial defect sizes 2b and 6b decreases at the rotational speed of 2,000 min⁻¹ and the average anomaly ratio of artificial defect size ND increases up to 0.2. **Table 8** shows no difference in the neighborhood number for different numbers of feature quantities.

In the practice of defect detection methods, misjudgment of anomaly for normal bearings should be avoided. Also, the larger the difference of anomaly ratios between normal bearings and bearings with small defects, the easier the defect detection will be. Therefore, selection criterion for number of feature quantities adequate for defect detection was determined as the anomaly ratio of artificial defect size ND to be 0.2 or lower and the margin between artificial defect sizes ND and 2b to be large. Furthermore, when the margin between artificial defect sizes of ND and 2b is about the same, features with less numbers of feature quantities should be selected. Based on the above criterion, the number of feature quantities adequate for defect detection was determined to be 30 for rotational speed of 1,000 min⁻¹, 150 for rotational speed of 1,500 min⁻¹ and 10 for rotational speed of 2,000 min⁻¹.
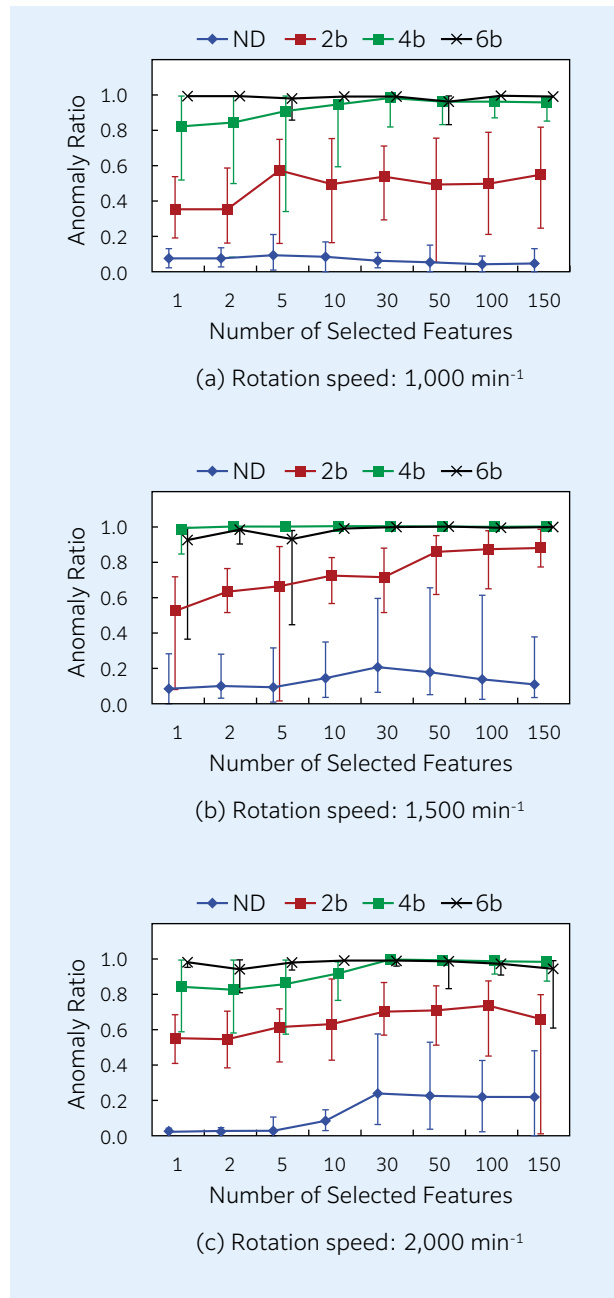

(a) Rotation speed: 1,000 min⁻¹

(b) Rotation speed: 1,500 min⁻¹

(c) Rotation speed: 2,000 min⁻¹

Fig. 9 Influence of number of features on feature selection

Table 8 Comparison of the neighborhood numbers of Local Outlier Factor for the number of features

Number of Features	Rotation Speed	Average	Max	Min	Standard Deviation
1	1,000 min⁻¹	11.2	24	3	7.4
	1,500 min⁻¹	14.9	24	6	7.0
	2,000 min⁻¹	16.9	29	8	7.8
2	1,000 min⁻¹	21.5	29	4	8.3
	1,500 min⁻¹	21.3	27	11	5.8
	2,000 min⁻¹	16.2	24	8	7.0
5	1,000 min⁻¹	16.0	25	5	6.5
	1,500 min⁻¹	17.8	29	2	7.9
	2,000 min⁻¹	17.7	29	9	6.7
10	1,000 min⁻¹	16.3	29	6	8.5
	1,500 min⁻¹	18.0	25	3	6.6
	2,000 min⁻¹	22.0	29	16	4.2
30	1,000 min⁻¹	16.9	28	3	10.5
	1,500 min⁻¹	18.1	28	6	6.7
	2,000 min⁻¹	21.8	29	13	5.9
50	1,000 min⁻¹	20.7	29	8	7.4
	1,500 min⁻¹	21.5	29	2	9.4
	2,000 min⁻¹	16.6	28	2	8.5
100	1,000 min⁻¹	15.6	23	8	5.5
	1,500 min⁻¹	16.1	29	2	9.4
	2,000 min⁻¹	21.3	29	2	8.1
150	1,000 min⁻¹	16.6	29	5	7.2
	1,500 min⁻¹	15.6	26	9	5.1
	2,000 min⁻¹	17.7	29	8	7.1

## 4.7 Defect detection accuracy of the proposed method

Fig. 10 shows the relation between artificial defect size and anomaly ratio by the proposed method (Proposed) which uses the appropriate number of feature quantities for defect detection selected by the previous section at rotational speeds of 1,000, 1,500 and 2,000 min⁻¹. As a comparison, anomaly ratios directly calculated from input data v_j before feature selection using LOF for each artificial defect size are shown as the original method (Original). Results of the original method are the same as **Fig. 5**. Also, the anomaly ratio for each artificial defect size using Laplacian Score[16] as the feature selection method is depicted in the figure as the comparison method (Comparison). **Fig. 11** shows the comparison of AUC Score among the proposed method, original method and comparison method against artificial defect sizes ND and 2b. In the anomaly ratio of **Fig. 10** and AUC Score of **Fig. 11**, * is marked on the difference of significance level of 5 % between the original method and the proposed method, and the comparison method and the proposed method, and ** is marked on the difference of significance level of 1 %. **Table 9** shows the mean, maximum value, minimum value, and standard deviation of the neighborhood numbers of the proposed method and original method.

Fig. 10 indicates that the anomaly ratios of artificial defect size 6b or more by the proposed method are almost 1 regardless of rotational speed and even those for artificial defect size 2b significantly increased compared to the original method and comparison method. Also, for artificial defect size 4b, the anomaly ratio by the proposed method significantly increased at rotational speeds of 1,000 and 1,500 min⁻¹ over the original method, and regardless of rotational speed over the comparison method. From **Fig. 11**, AUC Score can be improved by using the proposed method at any rotational speed over the original and comparison methods. At rotational speeds of 1,000 min⁻¹ and 1,500 min⁻¹, although the anomaly ratio of artificial defect size ND shows significant difference between the original method and the proposed method, AUC Score also significantly improved with the proposed method. Therefore, use of the proposed method improved the defect detection accuracy.
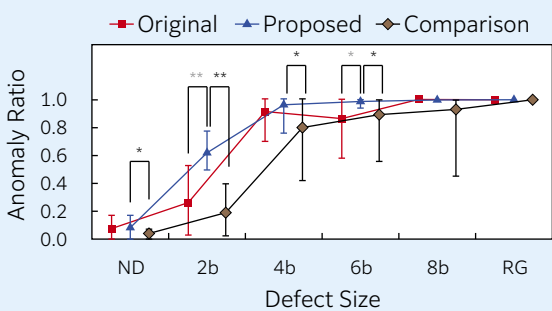
Table 9 reveals no difference in variation of neighborhood number of LOF between the original and the proposed methods.
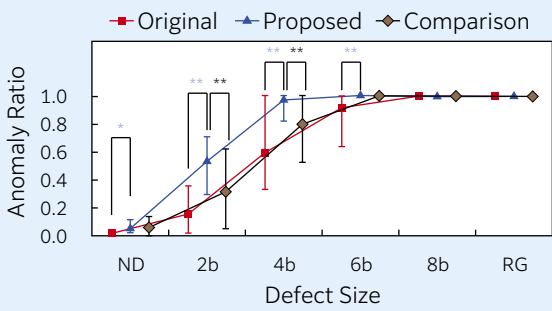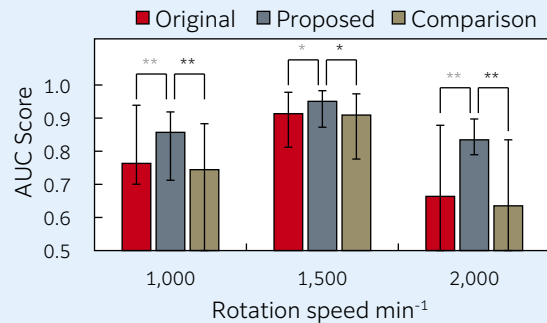
(a) Rotation speed: 1,000 min^{-1} (30 Features)
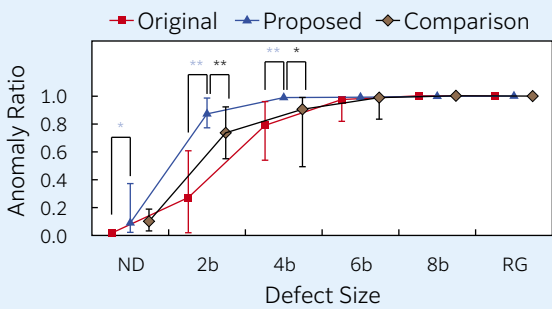
(b) Rotation speed: 1,500 min^{-1} (150 Features)

(c) Rotation speed: 2,000 min^{-1} (10 Features)

   * : Significance level 5 %
  ** : Significance level 1 %

Fig. 10 Comparison of anomaly ratios between original, comparison and proposed method

   * : Significance level 5 %
  ** : Significance level 1 %

Fig. 11 Comparison of AUC Score between original, comparison and proposed method

Table 9 Comparison of the neighborhood numbers of Local Outlier Factor between original and proposed method

Method	Rotation Speed	Average	Max	Min	Standard Deviation
Original	1,000 min^{-1}	13.3	24	2	8.0
	1,500 min^{-1}	9.8	25	2	8.6
	2,000 min^{-1}	8.4	29	2	8.3
Outlier Detection (2nd) (Proposed)	1,000 min^{-1}	16.3	29	6	8.5
	1,500 min^{-1}	18.0	25	3	6.6
	2,000 min^{-1}	22.0	29	16	4.2

5. Future challenges

The test equipment used for this evaluation showed large variation due to recombination of bearings. It is considered that recombination has some impact on the test environment. For validation of the proposed method, evaluation with completely different test equipment is necessary. Currently, data collection using new test equipment is underway, with a plan to validate the proposed method moving forward.

In the proposed method, feature selection with supervised learning is conducted for calculating anomaly score in the first stage of LOF and vibration data of bearings with defects are used as supervised data. However, in practice, it is almost impossible to obtain vibration data of bearings with defects. As a solution to this problem, for example, a method to improve defect detection accuracy by extracting features which do not depend on rotational speed or equipment can be considered, using vibration analysis methods such as Persistent Homology[27] and Dynamic Mode Decomposition[28]. Or using data obtained from a theoretical analysis model instead of measurement data from the actual equipment as the supervised data can be considered, by using the theoretical analysis model[29] such as Dynamic Analysis in feature

selection by Random Forest. Or, using Transfer Learning, data from test equipment or a theoretical analysis model may be used for diagnosis of other equipment as supervised data. We will study these possibilities for improvement.

6. Summary

Various anomaly detection methods were compared for defect detection accuracy against vibration acceleration data of bearings with artificial defects. Insights obtained from this study are as follows:

- When 3 types of outlier detection methods, One Class Support Vector Machine, Local Outlier Factor and Isolation Forest, were compared for defect detection accuracy, Local Outlier Factor provided the highest defect detection accuracy. However, in all methods, defect detection accuracy of artificial defect size 2b was lower than artificial defect size 4b or larger.
- Evaluation of classification accuracy of artificial defect size by Random Forest revealed that feature quantities of high importance for classification of bearings with and without defects are different depending on the size of artificial defects. In addition, feature selection by Random Forest for micro artificial defect size improved the defect detection accuracy of the targets.
- The proposed defect detection method successfully provided a significant improvement of defect detection accuracy for small artificial defect size without reducing detection accuracy of larger defect size, compared to the cases of no feature selection by Random Forest.

Acknowledgment

References

1) Akio Igarashi, Banda Noda, Eichi Matsushima, A Study on Fault Prediction of Rolling Bearings (1st Report), Journal of Japan Society of Lubrication Engineers, Vol. 24, No. 2, (1979) 122–129.

2) Akio Igarashi, Hiroyoshi Hamada, Research on Vibration and Sound of Defective Rolling Bearings (1st Report), Transactions (C) of The Japan Society of Mechanical Engineers, Vol. 47, No. 422, (1981) 1327-1336.

3) Hiroki Mano, Atsushi Korenaga, Diagnosis for rolling bearing using acoustic emission and vibration technique, Proceedings of JSPE Spring Conference of The Japan Society for Precision Engineering, (2014) 683-684.

4) Schölkopf, B., Platt, J.C., Taylor, J.S., Smola, A.J., and Williamson, J., Estimating the Support of a High Dimensional Distribution, Neural Computation, Vol. 13, (2001) 1443–1471.

5) Takashi Onoda, Norihiko Ito, Hideaki Koreeda, Data Indicating Malfunction Sign of Hydroelectric Power Plants, The transactions of the Institute of Electrical Engineers of Japan. D, Vol. 131, No. 4, (2011) 448–457.

6) Tax, D.M.J., One Class Classification, Ph.D thesis, Delft University of Technology (2001).

7) Minoru Kondo, Tatsuro Takashige, Shin'ichi Manabe, Hiroshi Kanno, Abnormality Detection in a Contaminated Diesel Engine by a Vibration Monitoring Method, RTRI Report, Vol. 30, No. 4, (2016) 47–52.

8) Hermansky, H., Ellis, D.P. and Sharma, S., Tandem Connectionist Feature Extraction for Conventional HMM Systems, IEEE International Conference on Acoustics, Speech, and Signal Processing. Proceedings, Vol. 3, (2000) 1635–1638.

9) Takanori Hasegawa, Jun Ogata, Masahiro Murakawa, Tetsuji Ogawa, Advancement of anomaly detection technology for wind turbine system based on representation learning for normal and faulty classification, 39th Symposium on Wind Energy Application (2017)

10) Masashi Kitai, Hideyuki Tsutsui, Anomaly Diagnosis of Angular Ball Bearings using One Class Support Vector Machine, Proceedings for Tribology Conference 2017 Fall (2017) C41.

11) Koma Kato, Ryoji Tani, Hideyuki Tsutsui, Relationship between defect size and various vibration features in angular contact ball bearings, Proceedings for Tribology Conference 2017 Spring (2017) F33.

12) Breunig, M.M., Kriegel, H.P., Ng, R.T., and Sander, J., LOF, Identifying Density-Based Local Outliers, Management of Data, Vol. 29, (2000) 93–101.

13) Breiman, L., Random Forests, Machine Learning, Vol. 45, (2001) 5–32.

14) Smith, J.S., The Local Mean Decomposition and Its Application to EEG Perception Data, J.R.Soc. Interface, Vol. 2, (2005) 443-445.

15) Aziz, W. and Arif, M., Multiscale Permutation Entropy of Physiological Time Series, 9th International Multitopic Conference, (2005) 1-6.

16) He, X., Cai, D. and Niyogi P., Laplacian Score for Feature Selection, Adv.Neural Inform. Process. Syst., (2005) 16.

17) Cheong, S., Sang, H.O. and Lee, S.Y., Support Vector Machines with Binary Tree Architecture for Multiclass Classification, Neural Inform. Process. -Lett. Rev., Vol. 2, (2004) 47-51.

18) Li, Y., Xu, M., Wei,Y., and Huang, W., A New Rolling Bearing Fault Diagnosis Method Base on Multiscale Permutation Entropy and Improved Support Vector Machine Based Binary Tree, Measurement, Vol. 77, (2016) 80-94.

19) Kilundu, B., Chiementin, X. and Dehombreux, P., Singular Spectrum Analysis for Bearing Defect Detection, Journal of Vibration and Acoustics, Vol. 133, No. 5, (2011) 051007.

20) Bugharbee, H.A. and Trendafilova, I., A New Methodology for Fault Detection in Rolling Element Bearings using Singular Spectrum Analysis, The International Journal of Condition Monitoring, Vol. 7, No. 2, (2018) 26-35.

21) Zhu H., Wang Y., and Wang K., Particle Swarm Optimization (PSO) for the Constrained Portfolio Optimization Problem, Expert System, Vol. 38, (2006) 10161-10169.

22) Hinton G. E. and Osindero S., A Fast Learning Algorithm for Deep Belief Nets, Neurocomputing. Vol. 18, (2006) 1527-1554.

23) Shao, H., Jiang, H., Zhang, X., and Niu, M., Rolling Bearing Fault Diagnosis Using an Optimization Deep Belief Network, Measurement Science and Technology, Vol. 26, (2015) 1-17.

24) Tsuyoshi Ide, Masashi Sugiyama, Anomaly Detection and Change Detection, Kodanshsa, (2015) 11–12.

25) Liu, F.T., Ting, K.M. and Zhou, Z.H., Isolation Forest, Eighth IEEE International Conference on Data Mining, (2008) 413–422.

26) Toshio Toyota, Procedure of anomaly diagnosis of rotating machines, Japan Institute of Plant Maintenance, (1991) 94–96.

27) Umeda Y., Time Series Classification via Topological Data Analysis, Transactions of the Japanese Society for Artificial Intelligence, Vol. 32, No. 3, (2017) 1-12.

28) Kota Dohi, Naoya Takeishi, Takehisa Yairi, Koichi Hori, Anomaly detection of acoustic data using dynamic mode decomposition, 32nd National Conference of the Japanese Society for Artificial Intelligence, 1P2-02, (2018).

29) Gupta, P.K., Advanced Dynamics of Rolling Elements, Springer-Verlag, (1984).

Photo of authors

Masashi KITAI

Product and Business Strategic Planning Dept., New Product and Business Strategic Planning Headquarters

Yoshinobu AKAMATSU

New Product and Business Strategic Planning Headquarters

Ken-ichi FUKUI

SANKEN (The Institute of Scientific and Industrial Research), Osaka University

"ETFA" Bearings Strengthened by Fine Microstructure Design

Masahiro YAMADA*   Naota YAMAMOTO**
Chikara OHKI*

NTN designed a special heat treatment to improve bearing properties by resulting in a fine microstructure of steel. The resulting fine microstructure consists of homogeneous martensite blocks and precipitations of a refined size. Testing shows specimens with fine microstructure had high impact strength and wear resistance. Fine microstructure test bearings also showed superior rolling contact fatigue lives under both clean and contaminated lubrication conditions. **NTN** calls these bearings "ETFA". In this paper, we explain the details of ETFA bearings.

1. Introduction

With a shift toward lower fuel consumption of automobiles and increasing compactness of industrial machinery, there is a trend toward increasingly severe bearing operating conditions. Typically these include higher contact surface pressure and lower viscosity of lubricating oils. These increasingly harsh use environments may promote problems such as flaking that originates from an indentation and shorten bearing life. Therefore, there is a need for higher bearing strength.

To achieve higher bearing strength, it is crucial to strengthen the steel material. There are a number of methods for strengthening steel and one of these involves refinement of crystal grains[1]. This can be regarded as a strengthening method that hinders dislocation motion due to the increase in grain boundaries and changes the plastic properties of steel. There has previously been discussion of the effects of the size of prior austenite grains (referred to hereafter as "prior γ grains") on strengthening by the refinement of crystal grains in quenched steel. However, there are few examples of comparative examination of the size of martensite grains actually formed due to quenching[2]. In recent years, it has been thought that the size of martensite blocks (referred to hereafter as "blocks") that are the effective crystal grains is the dominant factor in determining the strength of steel. Therefore, to strengthen steel through crystal grain refinement, it is necessary to produce a more refined martensite structure rather than refining the prior γ grains[3)-6)].

The authors have already developed long-life, high-strength bearings made of JIS SUJ2 in which blocks were refined through special heat treatment[7]. These through hardened bearings had blocks strengthened through refinement, and were enhanced with improved anti-wear performance through nitriding[7)-9)].

Recently, we have used the aforementioned heat treatment technology to develop new bearings made of low-carbon steel with refined blocks for longer life and higher strength. **NTN** calls these newly developed bearings "ETFA," and we are currently moving toward practical application.

This article describes the details of these ETFA bearings.

2. Fine microstructure of ETFA

2.1 Material and state of precipitation formation

The material used is low-carbon steel containing Cr and Mo. The fine microstructure of low-carbon steel is controlled by applying carbonitriding treatment and grain refinement treatment. **Table 1** shows a comparison of ETFA characteristics with the characteristics of conventional carbonitriding treated bearings (referred to hereafter as the "conventional product")[10]. Compared to the conventional product, the prior γ grains, blocks, and precipitations of ETFA are finer than the conventional product, and the number density of precipitations is high.

Fig. 1 shows a typical example of the depth distributions of carbon and nitrogen concentrations in ETFA measured with an Electron Probe Micro Analyzer (EPMA). Multiple sharp rises in concentration attributable to precipitations were confirmed in the surface layer. It is evident that carbides, nitrides, and carbonitrides are present at high density and with high refinement.

Fig. 2 shows a scanning electron microscope (SEM) image of prior γ grain boundaries and precipitations in the raceway surface layer. The crystal grains of ETFA are fine and precipitations are homogeneously dispersed.

*   Advanced Technology R&D Center
** Application Engineering Dept., Industrial Business Headquarters

Table 1 Feature of the developed bearings

| Item	Conventional product	ETFA
Heat treatment	Carbonitriding quenching	Carbonitriding quenching Grain refinement treatment
Carbon concentration	Standard	Standard
Nitrogen concentration	Standard	Standard
Residual γ amount	Standard	Standard
Size of precipitations	Standard	Fine
Number of precipitations	Standard	Numerous
Size of prior γ grain	Standard	Fine
Size of martensite blocks	Standard	Fine
Hardness	Standard	Standard
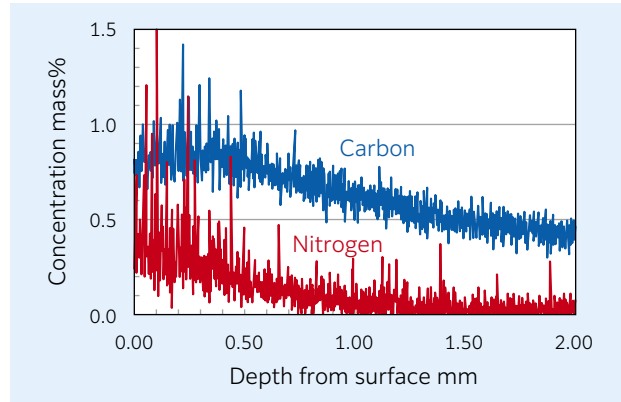
Fig. 1 Typical depth profiles of C and N concentrations of the developed bearings

2.2 Condition of block formation

Fig. 3 shows images of prior γ grains and blocks in the raceway surface layer. The block images are inverse pole figure crystal orientation maps measured using the electron backscatter diffraction (EBSD) method. The prior γ grains and blocks of ETFA are fine compared to the conventional product. **Fig. 4** shows the {011} pole figure for blocks. The block crystal orientation density is lower overall than that of conventional products and crystalline orientation is low.

Fig. 5 shows the average grain size of these blocks and their average aspect ratio. These values were calculated for blocks corresponding to a specific area ratio. That is, blocks within the field of observation are added together in order of their area, and this is the average value for those grains when their total area corresponds to 30, 50, or 70 % of the block total area. The difference in block diameter compared to the conventional product increases as the area ratio decreases, and a similar trend is event for the aspect ratio as well.
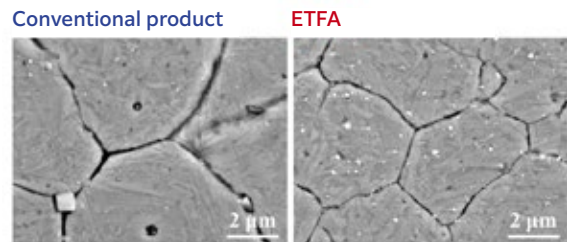

Fig. 2 SEM-micrographs of prior austenite grain boundary and precipitations near race surfaces of the bearings

As indicated above, the formation of precipitations and blocks is refined and homogeneous on the raceway surfaces of ETFA bearings.
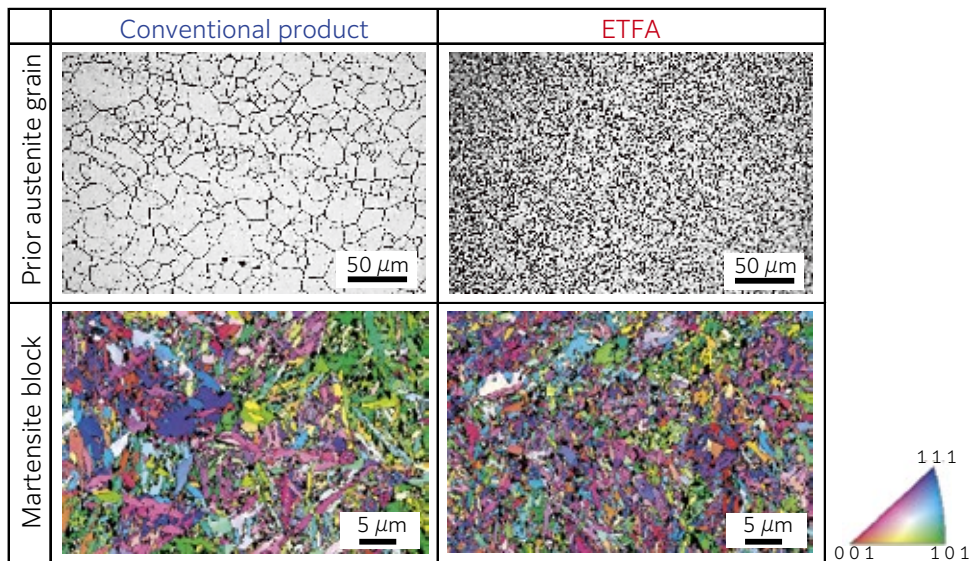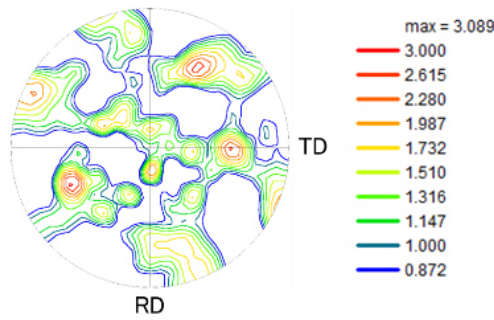

Fig. 3 Observation images of prior austenite grain and martensite block near race surfaces of the bearings
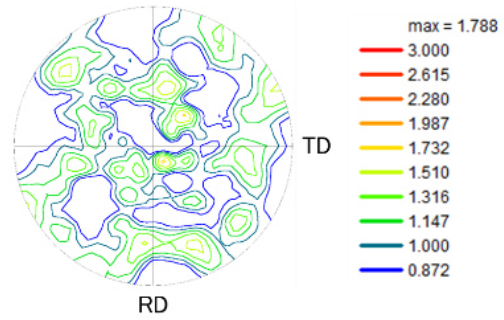
Fig. 4 {011} pole figure of martensite block near race surfaces of the bearings
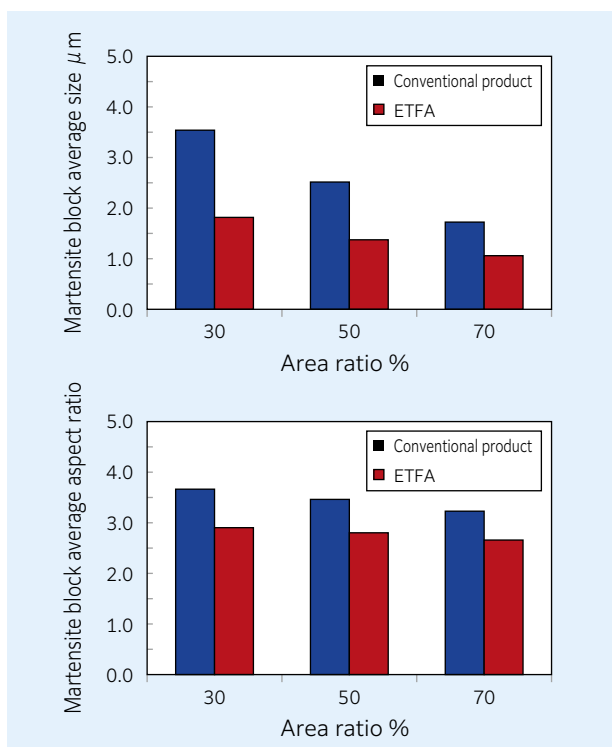

Fig. 5 Martensite block size and aspect ratio near race surfaces of the bearings

3. Rolling fatigue life of ETFA bearings

3.1 Rolling fatigue life test conditions

Rolling fatigue life testing was carried out under both clean and contaminated lubrication conditions. **Fig. 6** shows a schematic drawing of the test rig, and **Table 2** shows the test conditions[7]. The test bearing used in the life test was a tapered roller bearing. The life test with clean lubrication was carried out with N=5 for bearing A (inner diameter 30 mm × outer diameter 62 mm × width 17.25 mm). To improve the reliability of evaluation results in the life test with contaminated lubrication, testing was carried out with N=6–9 for bearings A and B in two sizes (inner diameter 85 mm × outer diameter 165 mm × width 56–58 mm). To increase contact surface pressure of the raceway in testing of bearing B, the number of rolling elements was reduced from the standard 17 to 5.
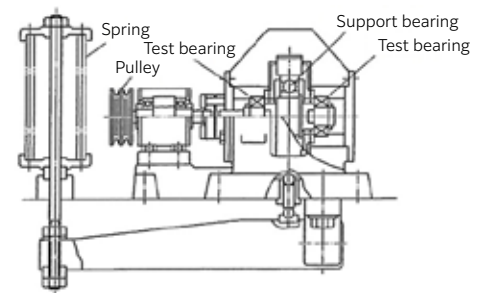

Fig. 6 Schematic drawing of the life test rig

Table 2 Conditions of the life test

Item	Bearing A	Bearing B
Basic dynamic radial load rating	48.5 kN	Conventional product: 150 kN ETFA: 168 kN (Number of rolling elements: 5)
Radial load	17.64 kN	53.9 kN
Axial load	1.47 kN	29.4 kN
Max. contact surface pressure	2.5 GPa	Conventional product: 2.9 GPa ETFA: 2.8 GPa
Inner ring rotational speed	2,000 min^{-1}	500 min^{-1}
Lubricating oil viscosity	ISO VG 56	ISO VG 100
Contaminant type	High speed tool steel dust	High speed tool steel dust
Contaminant size	100 - 180 μm	100 - 180 μm
Contaminant hardness	700 - 800 HV	700 - 800 HV
Amount of contaminant in lubricating oil	1.0 g/L	0.4 g/L

3.2 Rolling fatigue life under clean lubrication conditions

After operation for 10,000 h or more in all cases, the ETFA bearings were stopped in undamaged condition. Therefore, life under clean lubrication conditions was clearly longer than the basic rating life under these test conditions (L_{10h} = 243 h).

3.3 Rolling fatigue life under contaminated lubrication conditions

Fig. 7 shows results of the test under contaminated lubrication conditions. Rolling fatigue life of the ETFA bearing under contaminated lubrication conditions is roughly 2 times or more greater than that of the conventional product.

Flaking due to rolling fatigue can be broadly divided into two types depending on differences in the point of damage origin: surface originated and subsurface originated[11]-[13]. In both cases, the magnitude of stress concentration due to rolling has an effect on life. Therefore, it is conjectured that ETFA has some effectiveness in easing stress concentration during rolling.

In flaking under contaminated lubrication conditions, the damage originates at the margin of an indentation formed by a hard foreign body. This sort of indentation-originated flaking is thought to occur due to application of repeated normal stress at the surface normal to the raceway tangent direction[14]. The fatigue strength of low-carbon steel after carburizing improves with greater refinement of prior γ grain[15]. Therefore, rolling fatigue life of the developed product under contaminated lubrication conditions is thought to improve due to block refinement.
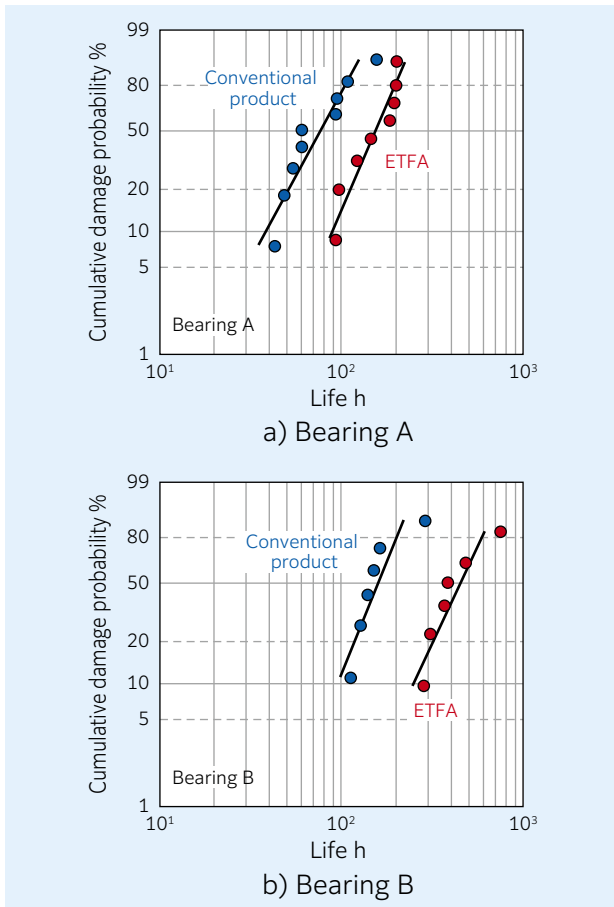

a) Bearing A

b) Bearing B

Fig. 7 Results of the life tests under contaminated lubrication conditions

4. ETFA impact strength

4.1 Impact test conditions

A Charpy impact test was carried out at room temperature and low temperature (-20 ℃). The test specimen was the U-notch type with dimensions of 55 mm × 10 mm × 10 mm. The test method conformed to JIS Z 2242.

4.2 Impact strength

Table 3 shows the results of the Charpy impact test. Impact strength of ETFA was roughly 1.8 times that of conventional material.

Table 3 Charpy impact values of the specimens at room temperature and – 20 ℃

[J/cm^2]

Test temperature \ Test material	Conventional material	ETFA
Room temperature	5.3	9.8
Low temperature (-20 ℃)	5.0	9.5

4.3 Reason for improving toughness

Fig. 8 shows observation images of the fracture surface near the notch bottom of the impact test specimen, and Cr mapping images of the fields of observation. A SEM was used for observation, and energy-dispersive X-ray spectroscopy (EDX) was used for Cr mapping. Enlargements of the observed fields a) and d) are given in b) and e). Mapping images were obtained for observed fields b) and e). In addition, the region of ductile crack formation prior to fracture is indicated with a dotted line in the images for observed fields a) and d)[16].

The main fracture morphology of the conventional material was grain boundary fracture at prior γ grain boundaries. The width of the ductile crack formation region was about 5 μm. Also, dispersion of Cr-based precipitations was confirmed at the prior γ grain boundary surface, and the size of the precipitations was roughly 500 nm or less.
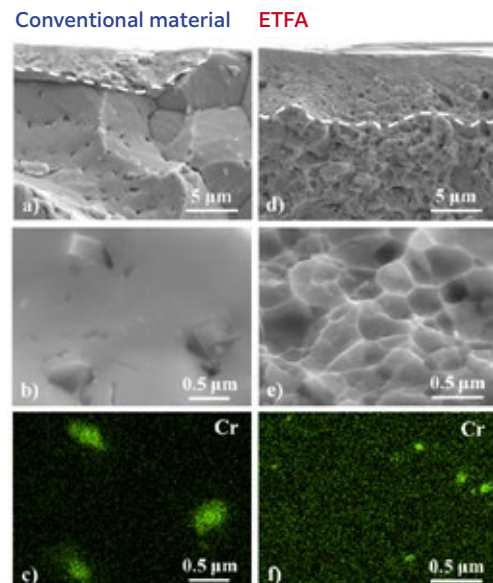

Fig. 8 SEM-micrographs and EDX-mappings of the fracture surfaces near the U-notch after impact test

On the other hand, the main fracture morphology of ETFA was transgranular fracture. Width of the ductile crack formation region was about 10 μm. Numerous dimples were confirmed at the fracture surface, and their size was roughly 50 – 500 nm. Dispersion of Cr-based precipitations was also confirmed at the fracture surface. Their size was roughly 100 nm or less.

For the above reasons, it is thought that grain boundary segregation of precipitations containing Cr is suppressed in ETFA, and prior γ grain boundaries are strengthened[17]. Also, the region where ductile cracking forms expands, and thus it is likely that fracture stress has been increased due to transgranular plastic deformation[18)-20]. Improved toughness likely occurred due to refinement of blocks and precipitation structure.

5. ETFA wear resistance

5.1 Wear test conditions

A Savin type wear test was conducted at room temperature[21]. **Fig. 9** shows a schematic drawing of the test rig, and **Table 4** gives the test conditions. The test specimen was sheet-shaped with dimensions 15 mm × 6 mm × 3 mm. The rotating circular plate serving as the opposing material has an outer diameter of 40 mm, and a subcurvature of R 60.
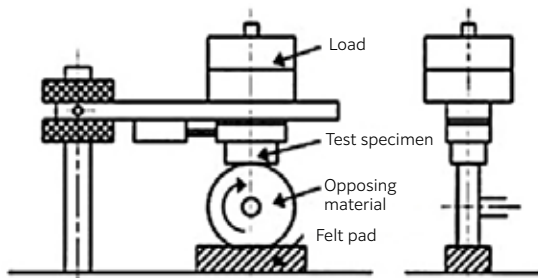

Fig. 9 Schematic drawing of Savin type wear test rig

Table 4 Condition of the wear test

Item	Setting conditions
Load	50 N
Initial max. contact surface pressure	0.49 GPa
Sliding speed	0.05 m/s
Sliding time	60 min
Lubricating oil viscosity grade	ISO VG 2
Lubrication type	Felt pad lubrication
Opposing material diameter	40 mm
Opposing material sub-curvature	R 60
Opposing material surface roughness	Ra 0.01 μm

5.2 Wear resistance

Table 5 shows the specific wear rate obtained from the wear test. The specific wear rate of ETFA was compared with that of the conventional material, and it was about 1/2 or less. Based on the order of the specific wear rate, it is conjectured that the main wear mode is adhesive wear[22].

Table 5 Specific wear rate of the specimens

[× 10^{-10} mm^3/(N·m)]

Test material / Opposing material	Conventional material	ETFA
Conventional material	701	120
ETFA	357	166

5.3 Reason for improved wear resistance

Fig. 10 shows optical microscope images, SEM images, and oxygen mapping images obtained through EDX, of the test specimen wear traces. The wear traces of the conventional material form a number of streaks due to wear scratching in the sliding direction (vertical direction). ETFA, on the other hand, exhibits wear scratches with a fine line width over a wide range. Oxidation was evident in the region where these wear scratches occurred.

Compared with conventional material, ETFA has high toughness, and hard, fine precipitations are dispersed homogeneously over the surface, and those precipitations and high toughness are thought to raise the shear resistance of the direct contact surface. As a result, it is likely that severe wear was suppressed, and high surface pressure was maintained at the contact surface, so that oxidation at the wear surface was promoted[23)24].
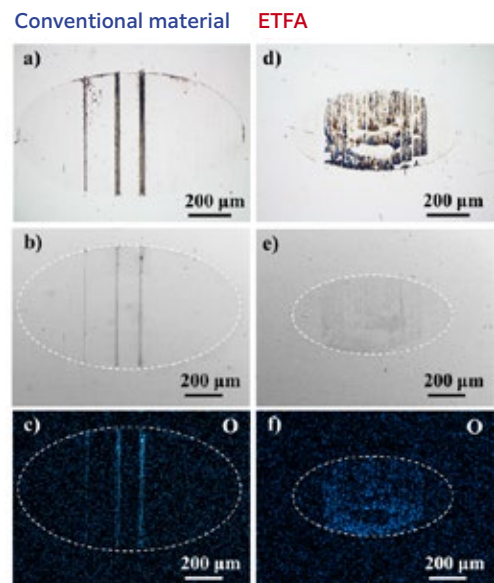

Fig. 10 Optical micrographs, SEM-micrographs and oxygen mappings of the wear traces for the specimens

6. Conclusion

This article has described in detail "ETFA" roller bearings strengthened through fine microstructure design. The rolling fatigue life and strength characteristics of these bearings greatly surpass conventional bearings, and thus ETFA can cope with the increasing severity of roller bearing use environments.

We at **NTN** will continue improving our heat treatment and material technologies, and contributing to the development of roller bearings.

References

1) R. A. Grange, ASM Trans Quart., 59, (1966) 26.
2) G. Krauss, Deformation and Fracture in Martensitic Carbon Steels Tempered at Low Temperatures, Metallurgical and Materials Transactions A, (2001) 861.
3) Tadashi Maki, Imao Tamura, Morphology and Substructure of Lath Martensite in Steels, Tetsu-to-Hagane (Iron and Steel), 67, (1981) 852.
4) Yuuji Kimura, Kaneaki Tsuzaki, Trends in Technology for Refinement of Martensite Structure, The Special Steel, 52, (2003) 12.
5) S. Morito, H. Yoshida, T. Maki and X. Huang, Effect of Block Size on the Strength of Lath Martensite in Low Carbon Steels, Materials Science and Engineering A, 438-440, (2006) 237.
6) Akinobu Shibata, Martensite in Iron-based Alloy —the Formation Mechanism of Microstructure and the Origin of Mechanical Property —, Materia Japan, Bulletin of the Japan Institute of Metals, 50, (2011) 254.
7) Chikara Ohki, Improving Rolling Contact Fatigue Life of Bearing Steels Through Grain Refinement, SAE Tech. Paper Series, (2004) 01-0634.
8) Nobuyuki Mouri, Improvement of Carburized Steel Wear Resistance by Heat Treatment, Tribology Conference Proceedings, 2008, Fall, Nagoya.
9) Nobuyuki Mouri, Kazuhiko Taguchi, Improvement of Carburized Steel Wear Resistance by Heat Treatment, NTN TECHNICAL REVIEW, No. 76, (2008) 17.
10) Kikuo Maeda, Hirokazu Nakashima, Hiroshi Kashimura, Development of Long Life TAB and ETA Bearings and Their Automotive Applications, NTN TECHNICAL REVIEW, No. 65, (1996) 17.
11) W. E. Littmann and R. L. Winder, Propagation of Contact Fatigue from Surface and Subsurface Origins, Transactions of ASME, D, 88, (1966) 624.
12) T. E. Tallian and J. I. McCool, An Engineering Model of Spalling Fatigue Failure in Rolling Contact, Wear, 17, (1971) 447.
13) Y. P. Chiu, T. E. Tallian and J. I. McCool, An Engineering Model of Spalling Fatigue Failure in Rolling Contact, Wear, 17, (1971) 433.
14) Toru Ueda, Takashi Sakaguchi, Naoya Seno, Shigeru Okita, Nobuaki Mitamura, Flaking Morphology in a Contaminated Lubrication Environment — Effects of Tangential Force on Indentation-Originated Flaking —, NSK Technical Journal, 685, (2012) 58.
15) C. A. Apple and G. Krauss, Microcracking and Fatigue in a Carburized Steel, Metallurgical Transactions, 4, (1973) 1195.
16) Toshiro Kobayashi, Evaluation of Impact Fracture Characteristics of Metal Materials at Low Temperatures using the Instrumented Charpy Test Method, Bulletin of the Japan Institute of Metals, (1973) 546.
17) Riichi Murakami, Yunhe Kim, Kazuhiro Kusukawa, Fundamentals of Material Strength and Fracture, Nishinihonhouki Shuppan, (2005) 62.
18) Seiichi Karashima, Metal and Alloy Strength, Japan Institute of Metals and Materials, (1972) 134.
19) Toshiro Kobayashi, Koichi Takai, Evaluation of Mechanical Fracture Behavior of Metal Materials at Low Temperature, Fuji Electric Journal, 46, (1973) 235.
20) T. Hanamura, F. Yin and K. Nagai, Ductile-Brittle Transition Temperature of Ultrafine Ferrite/Cementite Microstructure in a Low Carbon Steel Controlled by Effective Grain Size, ISIJ International, 44, (2004) 610.
21) Makio Mizuno, Measurement of Abrasion Loss, Journal of Japan Society of Lubrication Engineers, 25, (1980) 801.
22) Mechanical Engineers Handbook B1, Japan Society of Mechanical Engineers, (1985) 61.
23) Tadashi Sasada, Wear, Yokendo, (2008) 48.
24) Yuji Yamamoto, Motohiro Kaneta, Tribology 2nd Edition, Ohmsha, (2010) 195.

Photo of authors
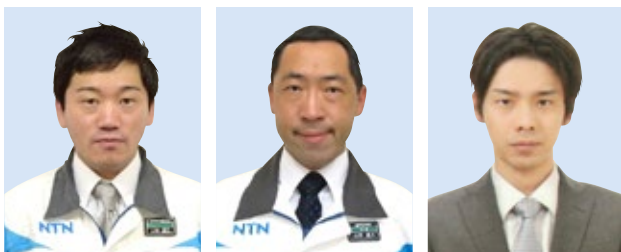
Masahiro YAMADA
Advanced Technology R&D Center

Naota YAMAMOTO
Application Engineering Dept., Industrial Business Headquarters

Chikara OHKI
Advanced Technology R&D Center

Application Examples and Function Improvements of the Wrist Joint Module "i-WRIST™"

Keisuke KAZUNO* Hiroshi ISOBE*
Masaki KAGAMI* Jun MIDOMAE*
Yuki SHIMURA* Seigo SAKATA**
Yukihiro NISHIO** Naoki MARUI**

NTN developed an angle control device that uses a parallel link mechanism which is a type of constant velocity joint[1-7] and started mass production under the product name " i-WRIST™" in August 2018[8].

Since then, we received many inquiries for improved automation, labor savings, improved appearance, improved inspection process and acquired more advanced needs for product specifications. We have just developed the upgraded product to meet these needs and have significantly improved its functions. We would like to introduce the upgraded product.

1. Introduction

The use of industrial robots is expanding at a tremendous rate as a means of boosting productivity due to increasing demand for automation and labor-saving methods. The shortage of labor is becoming a serious issue in Japan due to its shrinking population, and installation of industrial robots is gaining traction as a means of overcoming this issue.

In 2012, **NTN** announced its angle control equipment based on its proprietary parallel link mechanism. It was marketed for greasing and cleaning applications that require fast and precise changes in position that industrial robots have difficulty with. After changing the name to "i-WRIST™" Wrist Joint Module from 2018 (product registration in 2019), **NTN** began mass-production with the aim of targeting visual inspection applications of automotive and electronic components that had relied on manual labor in the past.

This article focuses on visual inspection applications developed by **NTN**, as well as the features, functionality and examples of compatible systems for the further enhanced i-WRIST™ "IWS Series."

2. i-WRIST™ Overview

Fig. 1 shows a conceptual diagram of i-WRIST™, which identifies the parallel link mechanism and drive mechanism that control its positioning. The three motors mounted on the drive mechanism are under synchronous control to achieve two-degree of freedom angular positioning (bending angle, swing angle).

Controlling two of the three rows of link systems (1st to 3rd link systems) of i-WRIST™ can be used for unique angular positioning, however motors mounted to the link systems of all three rows eliminate backlash in the drive mechanism and achieves greater positioning accuracy.
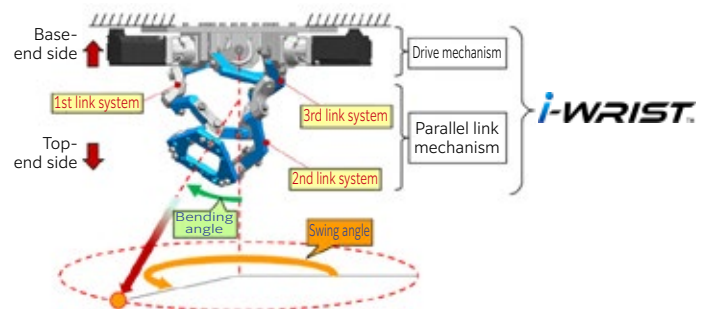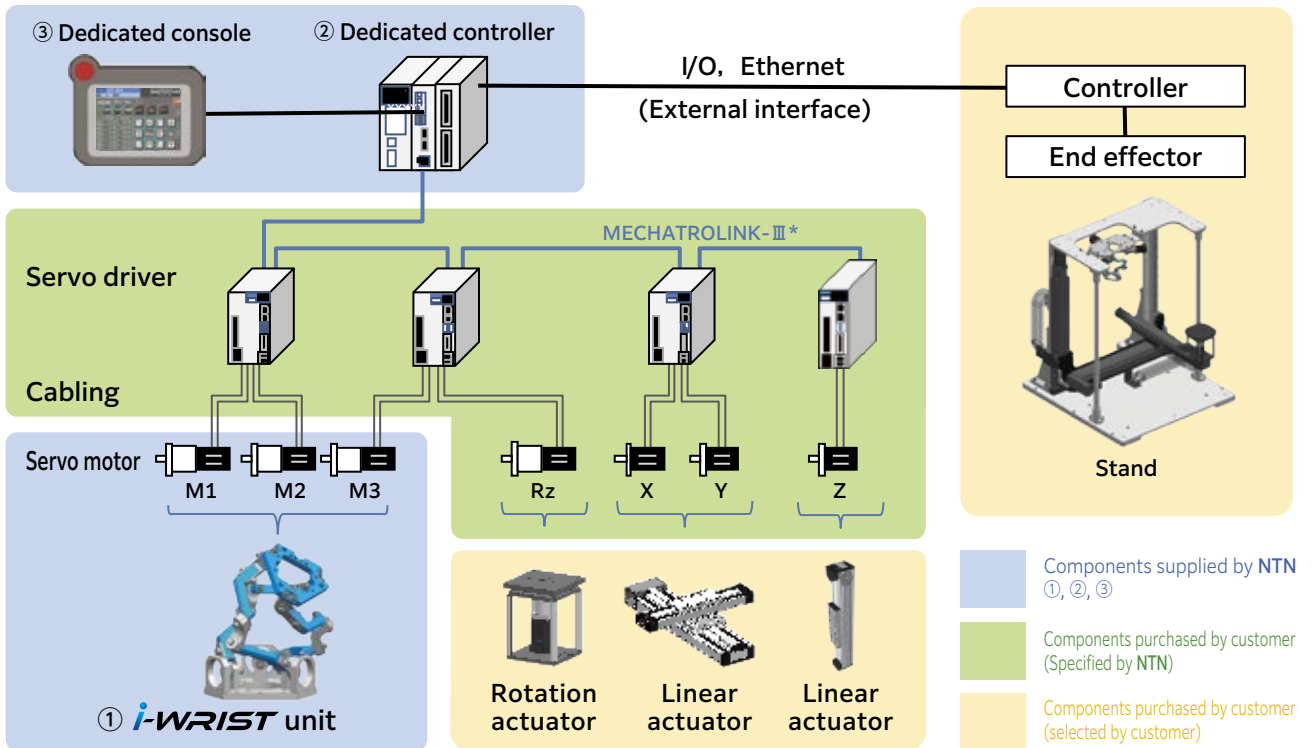

Fig. 1 Schematic of i-WRIST™

---

* Industrial Business Headquarters
** New Business Search and Development Dept., New Product and Business Strategic Planning Headquarters

* MECHATROLINK-III is a registered trademark of MECHATROLINK Members Association

Fig. 2 Configuration example of automation equipment

Components supplied by NTN
①, ②, ③

Components purchased by customer
(Specified by NTN)

Components purchased by customer
(selected by customer)

Fig. 2 shows a basic configuration example of automation equipment that includes i-WRIST™. i-WRIST™ is incorporated into the equipment with a combination of linear actuators and rotation actuators. **NTN** supplies ① i-WRIST™, ② Dedicated controller and ③ Dedicated console as a set, while the overall equipment is designed and made by the user or a system integrator.

2.1 i-WRIST™ Features

Production sites are implementing more methods that use automation and labor-saving technologies based on robots. Yet as robots are not perfect and suffer from a range of issues, user's automation and labor-saving efforts often do not go as planned, which required more time and cost to develop dedicated devices.

i-WRIST™ provides three main features that can resolve these issues faced by production sites.

1) High-speed operation

Conventional wrist joint modules with pan and tilt mechanisms move slowly when approaching workpieces from many directions for visual inspections of complex shapes, which meant there was a limit in the reduction of takt time. i-WRIST™ controls minute changes in position at high speed, making it possible to achieve further reductions in takt time.

A comparison of i-WRIST™ with pan and tilt mechanisms is shown by the movement required for approaching the four points in **Fig. 3**. The operating

pattern was set as ① → ② → ③ → ④ → ① → ④ → ③ → ② → ① . The results show that i-WRIST™ completed the pattern in 1.4 seconds compared to the pan and tilt mechanism at 4.0 seconds, verifying that i-WRIST™ moved 2.8-times faster.
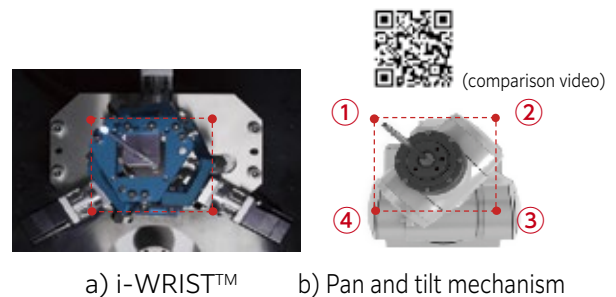

(comparison video)

a) i-WRIST™   b) Pan and tilt mechanism

Fig. 3 Operation pattern for comparison with view from the end effector side

2) Ease-of-use

The majority of industrial robot manufacturers generally use their own proprietary robot language, which required specialist knowledge for the programming when changing over or teaching the robots.

In contrast, changing configuration parameters or teaching i-WRIST™ can be performed on the dedicated console screen, eliminating the need for any specialist programming language expertise. Operating patterns are created using the dedicated console screen shown in **Fig. 4** to enter each coordinate

directly for the i-WRIST™ or associated linear actuators. Another method involves moving i-WRIST™ or linear actuators to their desired positions using JOG operations and then registering the coordinates. **NTN** also provides software **(Fig. 5)** for creating operating patterns efficiently using a computer. These i-WRIST™ operations can be acquired by simply taking a half-day course.

Fig. 4 Operation screen of dedicated console

Input area for position coordinates and operating direction

3D model

Operating screen
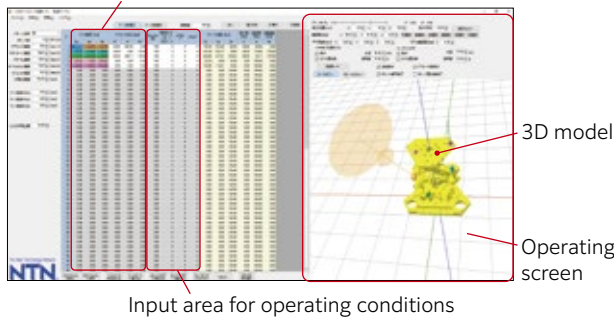
Input area for operating conditions

Fig. 5 Point data edit software

3) Space efficiency

The problems with using robots to achieve automation is the installation space or the major changes required to existing production lines.

i-WRIST™ is designed to be used with a combination of linear actuators and rotation actuators. The configuration of the system that rotates workpieces requires around half the stroke of the linear actuator (XY stage), which makes the overall system size more compact. To operate on a workpiece around ⌀100 mm and a height of 100 mm in size, **NTN** managed to design a system size with a width of 800 mm and a depth of 850 mm, meaning automation equipment can be installed in the space where manual labor is performed **(Fig. 6)**.

Fig. 7 also shows an example image comparing the installation size when building automation equipment using a conventional robot (multijoint robot) or i-WRIST™. This example illustrates how using i-WRIST™ means a system can be built using around half the space.

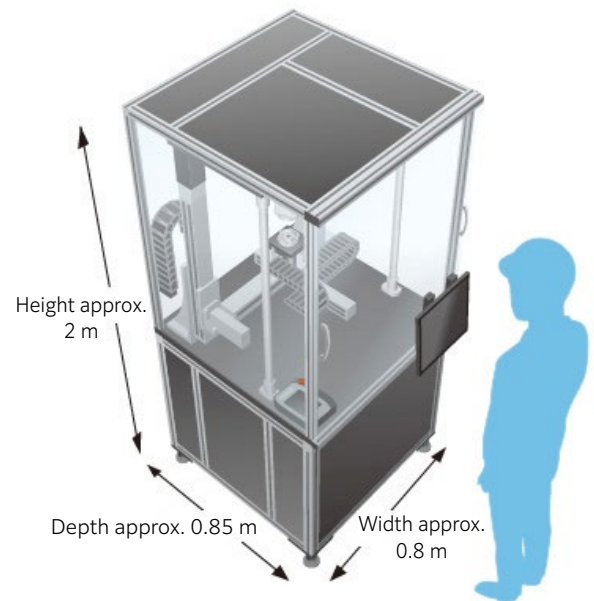As such, i-WRIST™ can help resolve problems such as insufficient space at a production site.

Height approx. 2 m

Depth approx. 0.85 m

Width approx. 0.8 m

Fig. 6 Compact equipment (image)

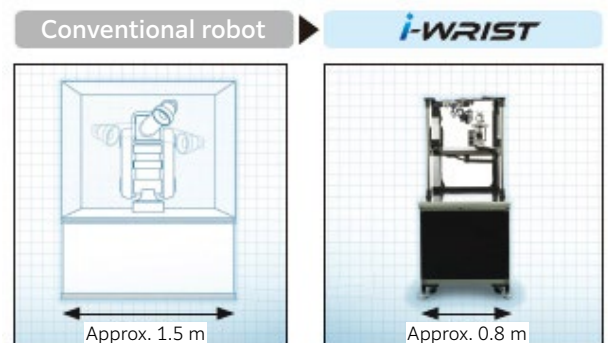Conventional robot

i-WRIST

Approx. 1.5 m

Approx. 0.8 m

Fig. 7 Installation size comparison example of automation equipment (image)

3. Example Application of Visual Inspection System

Since beginning mass-production of i-WRIST™ in 2018, **NTN** has mainly marketed it for visual inspection applications. In particular, it has been praised for its capability of approaching workpieces with complex shapes from many directions at a high speed. Specific examples of target workpieces include aluminum diecast components, forged parts, pressed moldings and resin moldings.

3.1 Example of Off-line System Configuration

Fig. 8 shows an example configuration of a visual inspection system designed as an off-line system. In this configuration, i-WRIST™ is installed on a stand in a downward attitude, and a camera and lighting unit are mounted to the end of i-WRIST™. The workpiece is moved and rotated with linear actuators (XYZ stage) and a rotation actuator.

This configuration allows workpieces to be approached from multiple directions with angle changes of i-WRIST™ and workpiece movement/rotation, which means the linear actuator (XY stage) stroke can be shortened for a more compact overall system size.
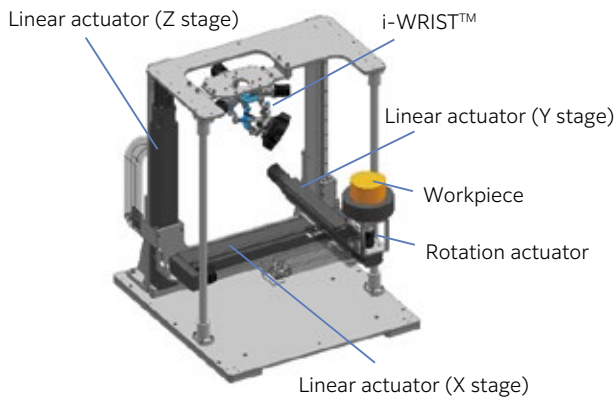

Fig. 8 Configuration example of off-line system

3.2 Example of In-line System Configuration

Fig. 9 shows an example configuration of a visual inspection system designed as an in-line system. In this configuration the i-WRIST™ with a camera and lighting unit is mounted in a downward attitude to the linear actuator (XYZ stage). This allows it to approach workpieces from many directions while they are moving along an existing conveyor belt.
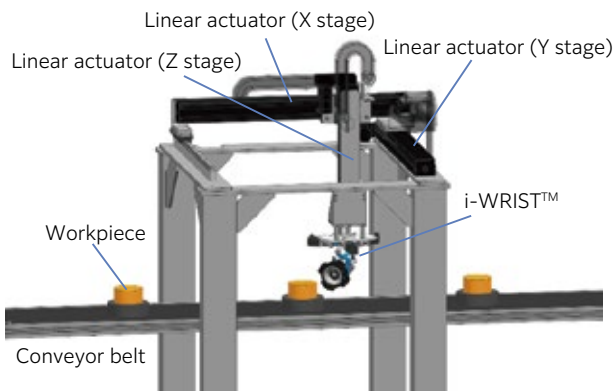

Fig. 9 Configuration example of in-line system

4. i-WRIST™ "IWS Series"

While the product had been marketed toward visual inspection applications until now, the i-WRIST™ "IWS Series (hereafter, IWS Series)" has been developed to address new needs.

The main functions of the IWS Series are as below.

4.1 i-WRIST™ Installation Direction

Fig. 10 shows the typical installation directions and definitions of coordinates for the bending angle and swing angle.

When mass-production began in 2018, the installation direction was limited to that shown in **Fig. 10** a).

The IWS Series has extended functionality for calculating the i-WRIST™ angle and coordinates of associated actuators that are used, to also enable installation in the upward **(Fig. 10** b)**)** and vertical **(Fig. 10** c)**)** directions.

a) Downward
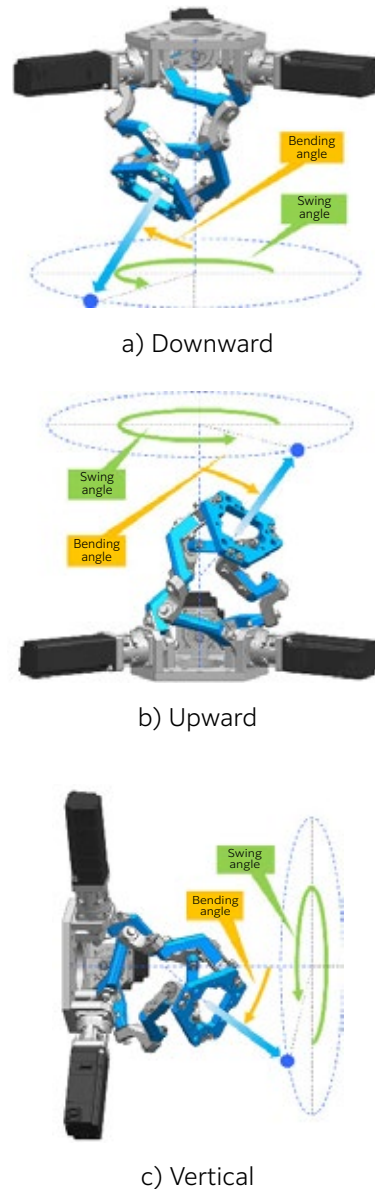

b) Upward

c) Vertical

Fig. 10 Installation direction

4.2 Compatible System Configurations

The IWS Series significantly expands on the various possible system configurations of i-WRIST™ and the associated linear actuators and rotation actuator that can be used.

Devices that can be mounted to i-WRIST™ had been limited to the end effector (camera and lighting unit for visual inspection applications), however with the IWS Series, workpieces can now be mounted. This gives users a much broader range of system configuration options to select from.

There are two i-WRIST™ coordinate systems: a "base coordinate system" based on the orthogonal coordinates of the entire system, which defines the angle of the i-WRIST™ and rotation actuator as well as the position coordinates of the linear actuators; and a "work coordinate system" based on the orthogonal coordinates of the workpiece that defines the position and working direction of the workpiece. Similar to the previous designs, the system has been developed using the software included in the dedicated controller for calculating the coordinates of the entire system. This allows coordinates to be calculated for the system without the need for users or system integrators to develop and test complex coordinate calculations.

Fig. 11 shows typical examples of system configurations compatible with the IWS Series. Users can select a configuration to suit their desired application.

Configuration examples (1) and (2) are system configurations that are compatible with the previous system, and correspond to the configurations shown in **Fig. 8** and **Fig. 9** above.

Configuration examples (3), (4) and (5) are extended system configurations that are now available with the IWS Series. Configuration example (3) rotates i-WRIST™ with the rotation actuator so that the direction of the end effector can be adjusted to suit the position of i-WRIST™. Example (4) is a configuration for handling workpieces and is suited to visual inspections of small, lightweight workpieces like resin molded parts. Configuration example (5) has i-WRIST™ installed on a rotation actuator at an inclined angle, where the rotation actuator is actually mounted on a linear actuator to enable positioning in the XYZ stage directions. This configuration means workpieces can be viewed from a lower angled approach, and in visual inspection applications, means inspections can be performed around almost the entire workpiece.
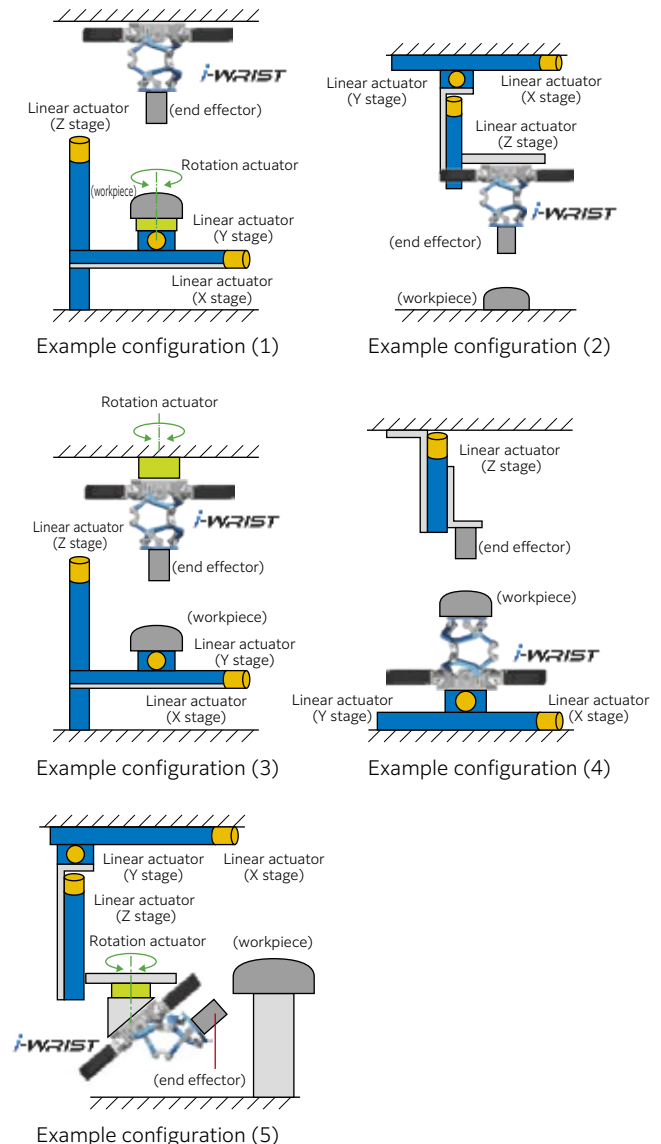

Example configuration (1)

Example configuration (2)

Example configuration (3)

Example configuration (4)

Example configuration (5)

Fig. 11 Typical examples of system configurations

4.3 Compliance with Safety Standards

IWS Series has been designed with specifications that meet 'ISO10218-1 (JIS B 8433-1)' standards for the safety of industrial robots.

The first area of compliance with the IWS Series is the addition of a motor with a brake for the servo motor that acts as the i-WRIST™ drive mechanism. In the event of a power outage or an unexpected alarm being triggered, the brake stops the motor from rotating so there is no unexpected movement.

Operating modes have also been defined clearly as "Auto mode," "Manual low-speed mode" and "Manual high-speed mode" to comply with safety standards for industrial robots. An example of this is when users switch from auto mode to manual mode to perform teaching—operation will be forced to manual low-speed mode. The dedicated controller software has been updated to ensure that the movement speed of the linear actuator is 250 mm/s or less as specified in the safety standards.

As i-WRIST™ is a module product (embedded

system) that forms part of automation equipment, users or system integrators are expected to install appropriate safety and protective devices stipulated in ISO10218.

4.4 External Interface

The IWS Series helps to boost convenience and versatility with greater support for external interfaces.

The external interface of the previous i-WRIST™ only included a parallel input/output (I/O) for connecting with the user's controller. Operating patterns created in advance via teaching using the dedicated console can be specified with I/O signals from the user's controller, which provides compatibility with sequential control that issues commands to begin automated operation. The I/O provides faster communication speeds than serial communications such as "Ethernet" and other industry networking protocols and enables control using relatively simple signals, a feature that has always been highly regarded by users.

In addition to the existing I/O, the IWS Series also includes "Ethernet" to significantly increase the amount of possible data communications such as connecting to user controllers from multiple FA equipment manufacturers. This means point data (coordinates) of operating patterns can be loaded and written to the dedicated controller from user's controllers to increase the flexibility of operating commands. For instance, after a workpiece is loaded onto visual inspection equipment and scanned with image processing, the coordinates and angles for approaching the workpiece can be changed before automatically starting inspection operations. Another practical example is completing visual inspections with a specific sequence of operating patterns, and then performing additional inspections at a desired coordinate or angle.

5. Summary

Since the development of the angle control equipment in 2012 based on the proprietary parallel link mechanism, **NTN** has been marketing it for greasing and cleaning applications. To take full advantage of its capabilities, i-WRIST™ was developed and started being mass-produced in 2018 for visual inspection applications. Feedback received after mass-production has now been included as standard specifications and developed as the IWS Series.

With further declines in the working population in the future, demand for automation is expected to grow even more for applications like visual inspections that had previously relied on manual work. In addition to visual inspection applications, **NTN** is also focusing more on development of robotic products that can help enhance automation and labor-saving technologies at worksites as well as increase productivity and quality as a way of contributing to society.

References

1) Keisuke Sone, Hiroshi Isobe, Koji Yamada, Wide Angle Active Link Equipment, NTN TECHNICAL REVIEW, No. 71, (2003) 70-73.
2) Hiroshi Isobe, Yukihiro Nishio, Parallel Link High Speed Angle Control Equipment (PHACE), NTN TECHNICAL REVIEW, No. 80, (2012) 42-47.
3) Hiroshi Isobe, Yukihiro Nishio, Keisuke Sone, Hiroyuki Yamada, Yoshio Fujikawa, Parallel Link High Speed Angle Control Equipment, Proceedings of the Japan Society for Precision Engineering Spring Meeting in 2013, (2013) 809- 810.
4) Hiroshi Isobe, Yukihiro Nishio, Seigo Sakata, Naoya Konagai, Hiroyuki Yamada, Yoshio Fujikawa, Parallel Link High Speed Angle Control Equipment - Implementation on Grease Application Equipment -, Proceedings of the Japan Society for Precision Engineering Spring Meeting in 2014, (2014) 1087-1088.
5) Naoya Konagai, Hiroshi Isobe, Seigo Sakata, Kenzou Nose, Hiroyuki Yamada, Yoshio Fujikawa, Parallel Link High Speed Angle Control Equipment, Proceedings of the Japan Society for Precision Engineering Spring Meeting in 2015, (2015) 605-606.
6) Kenzou Nose, Hiroshi Isobe, Seigo Sakata, Naoki Marui, Naoya Konagai, Parallel Link High Speed Angle Control Equipment - Enhancement of Performance by Improvement, Proceedings of the Japan Society for Precision Engineering Spring Meeting in 2016, (2016) 483-484.
7) Kenzou Nose, Hiroshi Isobe, Seigo Sakata, Speeding Up of Parallel Link Angle Control Equipment, NTN TECHNICAL REVIEW, No. 84, (2016) 96-101.
8) Keisuke Kazuno, Hiroshi Isobe, Jun Midoumae, Yuuki Shimura, Masayuki Ohara, Development of "i-WRIST™" Wrist Joint Module, NTN TECHNICAL REVIEW, No. 86, (2018) 22-27.

Photo of authors (Representative)

Keisuke KAZUNO

Industrial Business
Headquarters

Deployment and Improved Reliability of the Condition Monitoring System for Wind Turbines

Katsuyoshi SUZUKI*

NTN is providing information services using condition monitoring system for wind turbines. This article introduces market trends of the CMS and gives some future prospects of the CMS service for wind turbines.

1. Introduction

Unparalleled natural disasters and abnormal weather are frequently occurring all over the world. Urgent action is needed to reduce CO_2 emissions and other greenhouse gases, that are an underlying cause of these phenomena, and to achieve a low-carbon society. Therefore, renewable energy is garnering a great deal of attention; as solar and wind power generation is increasing worldwide.

Wind power in Japan has been trailing behind Europe and the U.S., but is currently expanding due to national policies such as a Feed-in-Tariff (FIT) system. Due to Japan's location, it faces a harsher climatic environment than Europe, caused by factors such as sudden squalls, turbulence, typhoons, and winter lightning, making problems with wind turbines not unusual. Accelerated steps are being taken to help achieve stable operation, by accurately assessing the equipment's condition, and conducting appropriate and efficient maintenance to reduce downtime, which includes emergency shutdowns.

2. NTN's vision

In wind power sector, **NTN** supplies special-purpose bearings, these bearings play a vital role in ensuring wind turbines achieve higher performance and a larger size. We also help improve the efficiency of wind turbine maintenance by offering a wind turbine Condition Monitoring System (CMS) and CMS services employing that system.

CMS services is aimed at monitoring and diagnosing the condition of wind turbines based on data such as vibration and rotational speed, gathered from the wind turbines. In addition to the high-quality manufacturing ("*monodzukuri*") that **NTN** has cultivated over many years, we are focusing efforts as part of our "service and solution business" strategy of providing intangible products such as information and proposals beneficial to our users.

NTN's CMS has a track record of adoption in over 200 wind turbines, with the number of installations increasing year after year. We are highly regarded by power producers as a top supplier in Japan, in part due to our CMS services.

3. CMS for wind turbines

3.1 History of CMS for wind turbines

Full-fledged adoption of CMS for wind turbines began in Europe around 2000 with the goal of detecting drivetrain problems, caused by sporadic malfunctions. With the dissemination of on-shore wind throughout Europe and the growth of off-shore wind primarily in Northern Europe, the CMS is increasingly being used as a standard tool for condition based maintenance (CBM).

On the other hand, Japan's domestic wind industry has focused on conventional time based maintenance (TBM). Until recently, maintenance procedures such as replacing parts, diagnosing equipment, checking for abnormal noise, and analyzing grease and lubricating oil, have only been carried out periodically. However, there were also cases of overtreatment or over-servicing, where parts that had not reached their service life were repaired to prevent malfunction, and cases where entire units were replaced due to risk management concerns. Additionally, when identifying problem points, we often relied on the heuristics of skilled maintenance workers. Although the dissemination and growth of the CMS in Europe was well known in Japan, one factor which delayed adoption in Japan were the features of the CMS — i.e., data analysis capability, accuracy of information, and cost effectiveness — which had not been fully verified.

Recently, the importance of CMS adoption and data analysis have been increasingly recognized for wind turbines in Japan, due to the increase in active use of IoT and big data in various fields.

* Industrial Business Headquarters

3.2 Needs of wind power producers

Wind power producers aim to increase their availability factor, and lower running costs by reducing downtime from inspections, repair, and emergency shutdown. With that goal in mind, power producers use the following criteria for maintenance.

1) Beginning in early autumn and continuing into early spring, when wind conditions are stable, the top priority is power generation, and unplanned maintenance is avoided.
2) Large-scale maintenance is concentrated in the summer.
3) To minimize shutdown time, investigating failures and resolving problems such as abnormal noise or vibration, analysis and repairs must be done quickly and efficiently.
4) Faulty parts and equipment must be accurately identified and necessary parts obtained in a planned manner.

3.3 Advantages of CMS for wind turbines

Wind turbines are built based on meticulous surveys of wind conditions, stringent environmental assessments, and consent from the local area. Construction sites are often difficult to access, as they typically include remote areas, such as mountaintops, or offshore locations far from population. Additionally, the nacelle, which houses the wind turbine drivetrain, is located 60–80 m above ground, preventing servicemen from climbing the tower in cases where strong winds or lightning is present. Furthermore, when identifying issues, it is best to directly check for vibration or abnormal noise during operation. However, due to safety, work cannot be performed during the power generation operation. Therefore, the usual approach is to carry out inspection while in an operation shutdown condition or during low-speed rotation, where there is a risk of missing signs of malfunction.

In response to the concerns above, adoption of the CMS enables remote monitoring of the drivetrain of wind turbines even during the power generation operation. The CMS also enables identification of problem points and early detection of malfunction by identifying slight changes in conditions from data. These condition changes are difficult to pick up, despite the skilled maintenance workers. The CMS has made it possible to determine whether maintenance is needed, and gauge the urgency, so that replacement parts can be obtained and replaced at periodic inspection or other planned shutdowns. This efficiency helps reduce shutdown periods and lost profits.

3.4 Configuration of Wind Doctor™ system

In 2012, **NTN** marketed Wind Doctor™, a CMS for wind turbines. Since then, we have offered monitoring results and condition information, derived from the gathered data, to power producers, wind turbine manufacturers, and showcased the effectiveness of the CMS through discussion of wind turbine events.

The system configuration is shown in **Fig. 1**. Data gathered from wind turbines is recorded and stored in a cloud server. Through various types of signal processing and analysis inside the server, the system detects problems with the components of the drive train, and automatically notifies a preset point of contact (automatic first decision).

If signs of damage or changes are identified from additional diagnosis by our engineers, that information is communicated through a report with recommendations to the service subscriber.
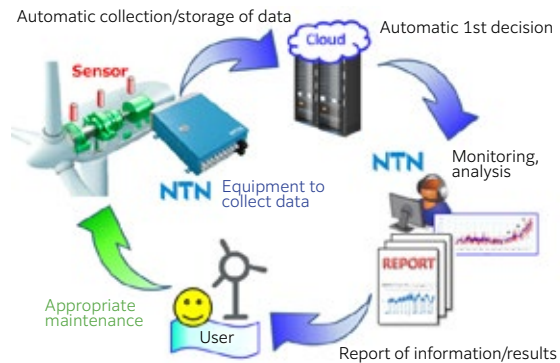

Fig. 1 System configuration of Wind Doctor™

When monitoring changes or trends in mechanical equipment, it is best to conduct measurements while the equipment is running at constant speed. However, wind turbines interact with nature, wind speed and direction is constantly changing, leading to an unavoidable decline in monitoring accuracy. In order to minimize the effects of the operating conditions, the Wind Doctor™ records those conditions together with sensor signals. We then focus on similar conditions within the data set, extract applicable data, and use that for diagnosis.

3.5 The uniqueness of Wind Doctor™

In addition to providing standard CMS functions, we strive to differentiate Wind Doctor™ from other products. Examples of this are described in 3.5.1 to 3.5.3.

3.5.1 Event recording function

Normally, the CMS performs measurements with a fixed sampling cycle. When monitoring trends of a wind turbine with no problems, sampling a few times a day is sufficient. On the other hand, it is best to shorten the measurement intervals in order to evaluate changes and record sudden events caused by worsening conditions on wind turbines experiencing issues. Setting the interval to zero and acquiring data continuously is ideal; however, this increases the operating load on the CMS unit, and causes an enormous increase in the amount of recording done by the server, increasing difficulty.

Thus, the Wind Doctor™ is equipped with an additional event recorder function. If an external signal trigger or a preset internal threshold is exceeded, then the function automatically records measurement

data for a certain time before and after, taking that moment as a starting point. This enables data to be captured when a sudden disturbance or malfunction occurred during the interval, and use of the data in analysis. A specific application example is described in section 4.

3.5.2 CMS dedicated communication unit

There are two methods of sending the CMS data: using the wind turbine LAN, or installing an additional CMS dedicated line with a separate channel. The former can use the existing communication environment of the wind turbine; however, a robust network security must be provided to prevent unauthorized access and viruses. In contrast, when a CMS dedicated line is installed, it is completely isolated from the wind turbine LAN. In the event of unauthorized access to the wind turbine or the CMS, the effects will not spill over to the other side. The CMS dedicated communication unit in **Fig. 2** is a data communication tool employing a mobile phone line and router, and self-checking functions are better than the commercial communication modules called IoT gateways. More specifically, the unit is equipped with a function for automatic recovery if malfunctions occur such as a communication error or communication freeze due to a drop in electromagnetic wave strength.

The unit is also linked with a data acquisition module, and setting can be done to force a reboot of the data acquisition module when issues arise in the measurement operation.

Fig. 2 Communication Unit

3.5.3 Improved analysis accuracy

A wind turbine is composed of multiple drive units and parts, and operates under conditions exposed to the natural environment. Various types of noise inevitably occur inside the nacelle, and superposition of this noise on the sensor signal is unavoidable. Specifically, there is a mixture of noise from various directions around the main shaft, which is fastened solidly to the nacelle frame. Examples include transmitted vibration from the hub, operation vibration from the motor for yaw drive, squeaking due to wind gusts and stress, operation vibration of hydraulic pumps, and so forth. Additionally, the rotational speed of the main shaft is low, at about

15 min^{-1}; therefore, the issue of vibrational energy due to damage is small, and the S/N ratio is extremely low. To improve analysis accuracy with Wind Doctor™, we've incorporated the technique of identifying disturbance noise using the spectrogram shown in **Fig. 3**.
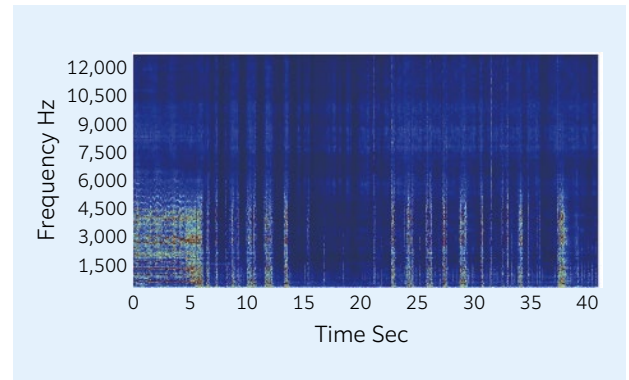

Fig. 3 Spectrogram

To conduct high-accuracy vibration analysis of the rotor, ideally data is measured while rotating at a constant speed, but as mentioned above, a wind turbine interacts with natural unpredictable wind, and thus fluctuations in rotational speed inevitably arise, as indicated in **Fig. 4**. Analysis accuracy declines due to these fluctuations, and in some cases it becomes challenging to detect abnormalities.
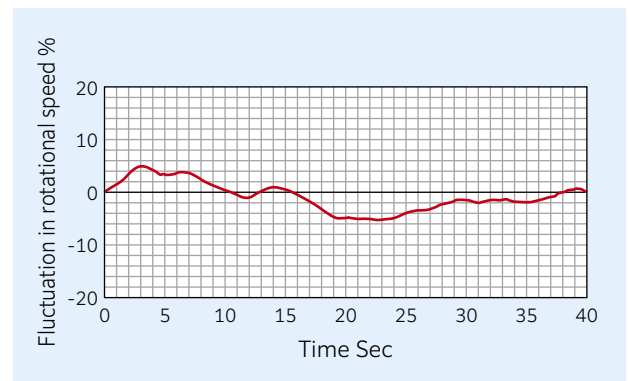

Fig. 4 Rotation fluctuation

As a countermeasure, Wind Doctor™ has a function to correct fluctuations in rotational speed. **Fig. 5** shows the raw frequency spectrum before correction, and **Fig. 6** shows the frequency spectrum after correction. The corrected graph clarifies the frequency peaks and shows the effectiveness of the correction.
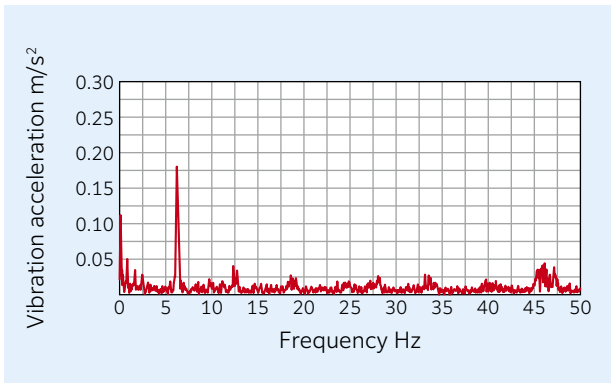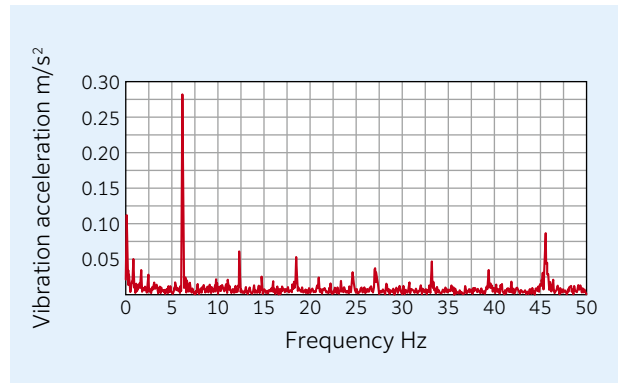
Fig. 5 Raw frequency spectrum

Fig. 6 Corrected frequency spectrum

4. Event recording function applications

This section describes applications of the event recording function in 3.5.1.

Presently, the New Energy and Industrial Technology Development Organization (NEDO) is engaged in a research and development project on technology for more sophisticated management of wind turbines. The goal of this project is to raise the availability factor of wind turbines to 97 % or higher, with the support of the University of Tokyo, National Institute of Advanced Science and Technology (AIST), and Chubu University to establish the necessary technology.

Chubu University is working to achieve more sophisticated wind turbine management by organically linking lightning detection technology with wind turbine issues, and developing an understanding of lightning strike characteristics. They are specifically using a lightning detection system exemplified by the Rogowskii coil in **Fig. 7** to analyze the effects of lightning strikes. This involves comprehensive comparative examination of: ① Lightning strike data such as current wave crest values and electric charge, ② Lightning damage data such as malfunction points and conditions, and ③ SCADA and CMS data.

Winter lightning, a peculiar phenomenon in Japan, has become the catalyst for these efforts. The coasts of Hokuriku and Tohoku regions of Japan are suitable sites for wind turbines due to their favorable wind conditions. However, extremely high energy lightning, strikes the wind turbines frequently during the winter in these regions. These frequent strikes lead to constant accidents, where the blades of wind turbines become damaged. To prevent secondary damage in the surrounding area from fragmented pieces falling from lightning strikes, it becomes necessary to shut down operations, and promptly carry out an inspection, either visual or using other techniques, before resuming operations. Decline in the availability factor due to lightning issues and the associated response is 4-5 %. Therefore, there is a demand for operation improvements that help raise the availability factor, such as enabling remote decision-making to determine whether to operate or shutdown based on data analysis.
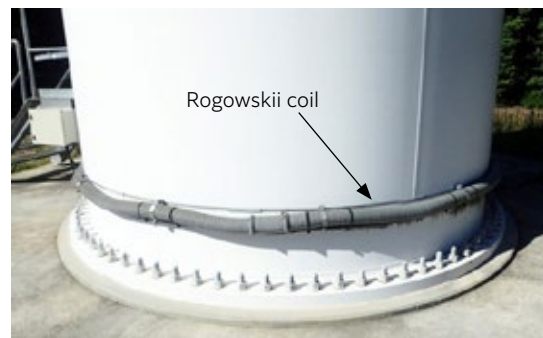

Fig. 7 Rogowskii coil

NTN is not a direct participant in this NEDO project, but we are assisting by using the event recording function of Wind Doctor™ to acquire and accumulate data during normal conditions and lightning strikes, and making that information available to the project.

The configuration of the system is shown in **Fig. 8**. A lightning detection system at the base of the tower detects the high current that flows during a lightning strike, and sends out a lightning strike signal. This is transmitted to a signal repeater in the nacelle, via optical fibers installed inside the tower, and input as a trigger signal to the data acquisition module. The event recorder function inside the Wind Doctor™ activates, and records vibration data for a specified time before and after the lightning strike.

We have installed this system in multiple wind turbines in the Hokuriku region, and are continuing to gather data.
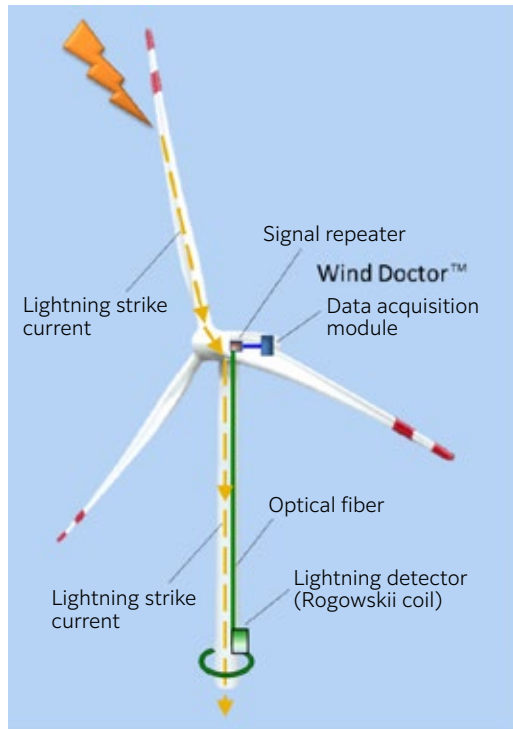
Fig. 8 CMS with Lightning detection system

5. Issues for the future

As previously noted, it is difficult to detect problems due to the low signal level at parts which rotate at low speed such as the main shaft and gearbox input. Maintenance costs are high for these components, and there is a pressing need to accurately assess their status. Therefore, as a provider of the CMS services, we need to establish highly accurate problem detection technology. Another important issue is detecting indications of parts missing or falling out, which may lead to sudden accidents. Users have high expectations from more sophisticated CMS.

Additionally, further evolution of the entire system is needed, including improvements to the malfunction detection performance, implementing machine learning and other types of AI, suited for cutting-edge technical innovation, and linking with prediction of damage magnitude and progression.

6. Conclusion

This article has covered market trends, efforts by **NTN**, and future prospects relating to CMS for wind turbines.

Broader use of renewable energy is the key to protecting the environment and achieving a low-carbon society. Therefore, we need to discover equipment issues, detect malfunctions early, and carry out proper maintenance. We are convinced that the CMS and its associated services will play an increasingly important role in this sector.

Going forward, we will continue advancing by integrating tangible and intangible assets through IoT, and contribute to society through a variety of services.

References

1) Wataru Hatakeyama, The Recent Applications of the Condition Monitoring Systems for Wind Turbines, THE TRIBOLOGY, No. 356, (2017) 38- 41.
2) Makoto Miyazaki, Wataru Hatakeyama, Application of Condition Monitoring System (CMS) for Wind Turbines, NTN TECHNICAL REVIEW, No.86, (2018) 40-44.
3) NEDO Fiscal 2019 Result Report Meeting, "Research and Development on Technology for Wind Power Generation, etc. / Research and Development for Sophisticated Practical Application of Wind Power / Research and Development on More Sophisticated Technology for Wind Turbine Management"

Photo of authors

Katsuyoshi SUZUKI

Industrial Business
Headquarters

Hub Bearing Module with Steering Adjust Function "sHUB™"

Hirokazu OHBA* Satoshi UTSUNOMIYA* Norio ISHIHARA* Yusuke OHATA* Atsushi ITO*

1. Introduction

In order to tackle environmental challenges and create a society free of traffic accidents, new vehicles are being developed incorporating self-driving and electric propulsion to help improve automobile safety and reduce energy consumption.

sHUB™ assists in achieving safety, comfort, and energy-efficient driving in internal combustion engine vehicles, electric vehicles, and self-driving vehicles, by properly applying correct control to the tire angles to suit any situation, with varying speeds.

In recognition of the details stated above, sHUB™ received the Nippon Brand Award of the 2019 "CHO" MONODZUKURI Innovative Parts and Components Award.

2. Structure

This hub bearing components include a steering shaft and an actuator incorporating a linear motion mechanism, fastened to a knuckle, and tires are steered by the actuator's power, with the steering axis of the hub bearing as the center.
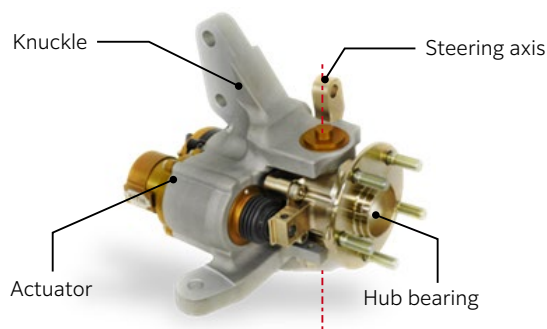

Fig. 1 Structure of the sHUB™

3. Features

The following characteristics of the vehicle shown in **Fig. 2** have been improved by providing control using sHUB™ for the vehicle's front wheels:
1) Improved vehicle stability when driving straight
2) Cornering performance
3) Safe control of tire angle before tires slip while maneuvering
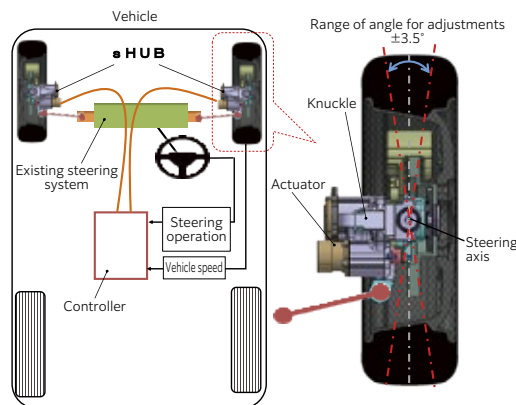4) Reduction of running resistance and improved fuel consumption

Fig. 2 Vehicle with sHUB™ installed (on front wheels)

4. Summary

We are currently moving toward commercialization and testing is taking place for this product in test vehicles. As indicated in another article in this review we are also working on creating sHUB™ for rear wheels, and we expect to increase automobile safety through the development of new automotive products.

References

1) Norio Ishihara, Hirokazu Ohba, Atsushi Ito, Mitsunori Ishibashi, Makoto Yamakado, Yoshio Kano, Masato Abe, Hub Bearing with Steering Function that Improves Vehicle Dynamic Performance, NTN TECHNICAL REVIEW, No. 86, (2018) 84-90.
2) Satoshi Utsunomiya, Norio Ishihara, Yusuke Ohata, Atsushi Ito, Hub Bearing Module with Steering Adjust Function (sHUB™), NTN TECHNICAL REVIEW, No. 87, (2019) 18-23.

Photo of authors (Representative)

Hirokazu OHBA*

* New Business Search and Development Dept., New Product and Business Strategic Planning Headquarters

Micro Hydro Turbine

Hiroki MUKAI* Fumihiko MATSUURA* Takashi ITO* Tomoya KAWAI** Yasunari KANAMURA*

1. Introduction

Micro Hydro Turbine **(Fig. 1)** received the New Energy Foundation Chairman Award at the 2019 New Energy Awards hosted by the New Energy Foundation. The New Energy Awards commends products that are outstanding in promoting adoption and raising awareness of new energy. Micro Hydro Turbine generates power by simply placing it in an existing water channel with a flowing current. It is very friendly to the global environment and is contributing to SDGs on a global scale. It is highly regarded because it helps to reduce maintenance costs of irrigation facilities by supplying and selling power at locations without electrical infrastructure.

Fig. 1 Micro Hydro Turbine

2. Product Design

Micro Hydro Turbine is shown in **Fig. 2**. The turbine consists of high-efficiency blades connected to a generator that is mounted on a frame for installation on water channels. There are two types of controllers for power generation; one for charging batteries as an independent power source and the other for connecting to the grid so that generated power can be sold. This versatility allows the product to respond to broad market requirements for power generation.
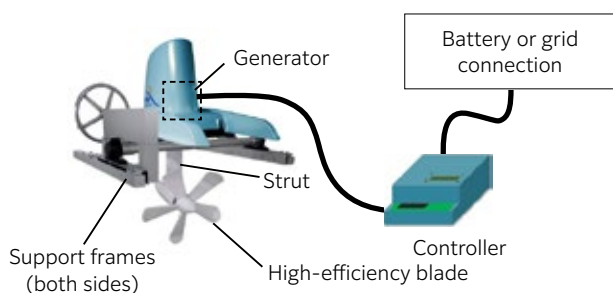

Fig. 2 Configuration of Micro Hydro Turbine

3. Product Specifications of Typical Model

The model with a blade diameter of 90 cm achieves a rated output of 1 kW when the flow rate is 2 m/s **(Table 1)**.

Table 1 Product Specifications of Typical Models

Turbine	Propeller hydro turbine for flowing water
Generator	Permanent magnet synchronous generator
Blade diameter	60 cm, 90 cm, 130 cm
Rated power output	1 kW (90 cm model at flow rate of 2 m/s)
Recommended water channel	At least 100 cm width and depth
Size/weight	H190 cm × W230 cm* × D170 cm, 170 kg

*Varies depending on the width of the water channel.

4. Summary

Ordinary hydro turbines require major construction work to create different water levels. The issue with major construction is its cost and damage to the environment. Micro Hydro Turbine can be installed by simply placing the unit on an existing water channel with the beams fitted to the width of the water channel, with little to no construction costs and environmental impact.

References
1) Tomoya Kawai et al., Micro Hydro Turbine, NTN TECHNICAL REVIEW No. 84, (2016) 28-33.
2) Takashi Ito et al., Grid Connectable NTN Micro Hydro Turbine, NTN TECHNICAL REVIEW No. 86, (2018) 102-107.

Photo of authors (Representative)

Hiroki MUKAI*

*   Engineering Department, Green Energy Products Division
** Business Development Dept., Green Energy Products Division

Mechanism for Initiation of Peeling in Rolling Contact and the Effect of Black Oxide Treatment on the Suppression of Peeling (Part 1, Part 2)

Naoya HASEGAWA   Takumi FUJITA   Michimasa UCHIDATE   Masayoshi ABO

1. Introduction

Papers[1][2] submitted to the *Tribologist*, the Journal of the Japanese Society of Tribologists, received the society's Encouragement Award for FY2019. The following provides an overview of these papers.

2. Overview

This research examined the initiation mechanism of peeling, a type of roller bearing failure which occurs under poor lubrication conditions, and the effect of black oxide treatment on the rolling contact surface to suppress peeling. In the first paper[1], a peeling simulation test (RCF test) was carried out with a two - cylinder type tester. The mechanism of initial crack initiation of peeling was investigated based on observation of the rolling contact surface and various analysis results. In the second paper[2], the repeated stress acting at the true contact point was estimated by examining the rolling contact surface and measurement of residual stress. The relationship with progression of peeling was also investigated. As a result of the above efforts, the following findings were obtained.

① The initial crack of peeling originated at a notch formed due to plastic contact by roughness asperity of the rolling contact surface.

② At the rolling contact surface, maximum shear stress acts in a direction inclined by about 45° from the radial direction. It is likely that the initial crack of peeling progressed due to the action of this maximum shear stress.

③ When black oxide treatment was applied to the rolling contact surface, it promoted a drop in surface roughness (running-in), and the repeated stress acting at the true contact point was lessened. As a result, there was a reduction in the formation of notches due to plastic deformation, and it became more difficult for peeling to occur.

④ In the black oxide product, running-in is promoted by phenomenon where the surface roughness become smaller with black oxide treatment and only the protrusions of the black oxide layer wear during rolling **(Fig. 1)**.
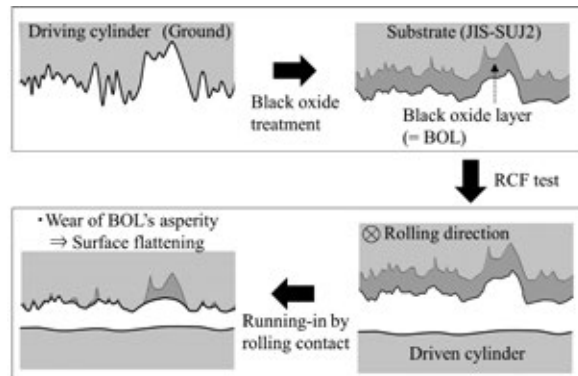

Fig. 1 Mechanism of running-in on rolling contact surface with the black oxide layer [1]

3. Future development

The findings obtained in this research will contribute to guidelines for the development of life enhancements for roller bearings. Going forward, we hope to make use of these findings to offer users bearings with higher reliability.

References

1) Naoya Hasegawa, Takumi Fujita, Michimasa Uchidate, Masayoshi Abo, Mechanism for Initiation of Peeling in Rolling Contact and the Effect of Black Oxide Treatment on the Suppression of Peeling (Part 1) — Discussion of Crack Initiation Based on Experimental Results, Tribologist, 63, 8, (2018) 551-562.

2) Naoya Hasegawa, Takumi Fujita, Michimasa Uchidate, Masayoshi Abo, Mechanism for Initiation of Peeling in Rolling Contact and the Effect of Black Oxide Treatment on the Suppression of Peeling (Part 2) — Relationship between Progression of Peeling and Stress Under the Rolling Contact Surface, Tribologist, 63, 9, (2018) 618-628.

Photo of authors

Naoya HASEGAWA
Advanced Technology
R&D Center

Takumi FUJITA
Advanced Technology
R&D Center

Michimasa UCHIDATE
Faculty of Science and
Engineering,
Iwate University

Masayoshi ABO
School of Engineering,
University of Hyogo

Inch Series, SAFC/SAFD Plummer Blocks

High-strength plummer blocks with a new design, resistant to shock and vibration

X bar shape on bottom for reinforcement

Features

① **High strength**   X bar shape on bottom to help reinforce base, greater thickness of top and side parts for reinforcement

② **Dust and moisture resistant**   Prevents ingress of water, mud, and debris by using labyrinth seals

③ **Improved ease of handling**   Use of alignment pins in the base for easier mounting and removal of outer housing halves

④ **Multi-purpose**   Enables mounting of accessory parts (taconite seal, closing cover, etc.) to suit various environmental needs
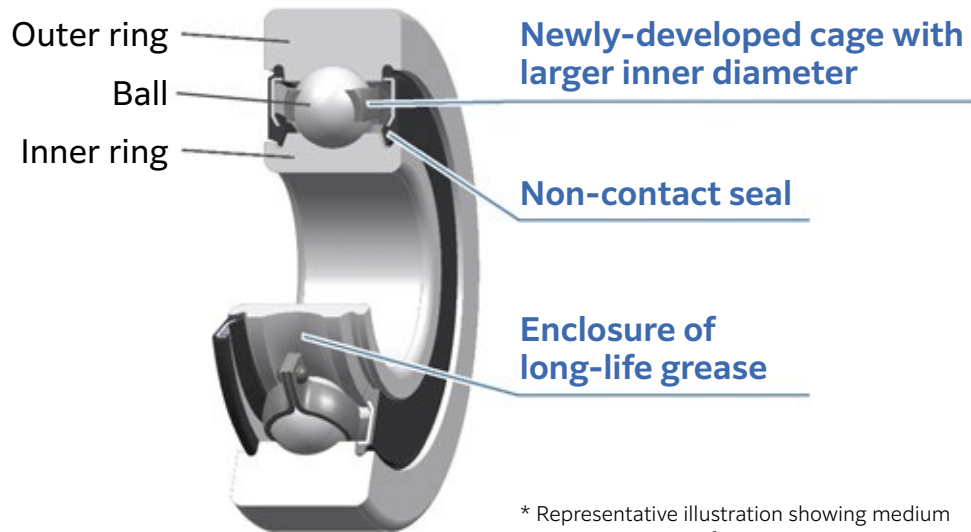
Specifications

Material	Gray cast iron (SAFC series) Ductile cast iron (SAFD series) 15 % increase in static fracture strength (compared to SAFC)
Size	SAFC/SAFD509 – SAFC/SAFD544
Shaft diameter	ϕ1-7/16 inch (ϕ36 mm) – ϕ7-15/16 inch (ϕ202 mm)

Application

Steel facilities, mine facilities, transportation port facilities, etc.

Tenter Clip Bearings for Film Stretching Machine

Low torque and high durability, while dramatically improving grease leak resistance

Outer ring

Ball

Inner ring

Newly-developed cage with larger inner diameter

Non-contact seal

Enclosure of long-life grease

* Representative illustration showing medium temperature specifications

Features

① **High reliability** Grease leakage reduced by 70 % (compared to conventional product)

② **High durability** Seizure resistance improved by 40 % (compared to conventional product)

③ **Low torque** Bearing rotational torque 1/4 that of a contact seal bearing

Applications

Guide rollers for tenter clips of film stretching machines
Lineup includes:
1) Medium-temperature specifications for bearing temperatures up to 230 ℃*
2) High-temperature specifications for bearing temperatures up to 300 ℃

Stretching and transfer of plastic film

Tenter clip movement

Tenter clip

Clips film

Rail
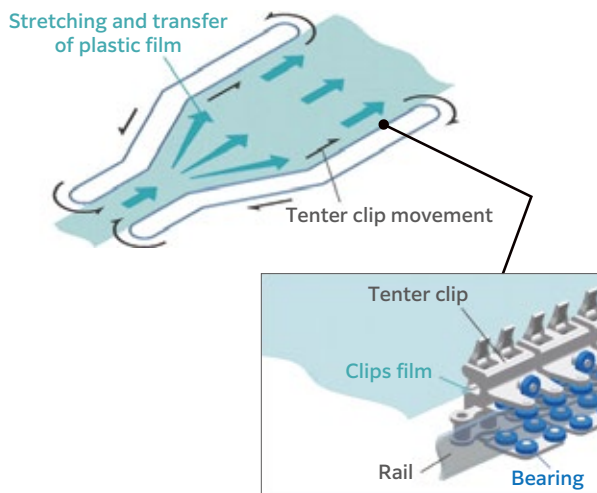
Bearing

Structure

By using a newly-developed cage with larger inner diameter and long-life grease, together with a non-contact seal bearing, this product achieves both low torque and grease leakage resistance, and improved seizure resistance

Developed product

Clearance between cage and inner ring
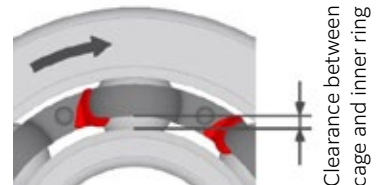
Movement of grease to the outer diameter side of the inner ring is suppressed and flow to the outside is prevented by optimizing clearance between the cage and inner ring.

Conventional product

Grease scraped from the ball surface by the cage may accumulate on the inner diameter surface of the cage, move to the outer diameter surface of the inner ring, continue on to the seal groove, and flow to the outside.